Elif Ağcakoca, Civil Engineering, Sakary Apllied Science University (Turkey)

Elif Eker Kahveci, Mechanical Engineering, Sakarya University (Turkey)

Erman Aslan, Mechanical Engineering, Kocaeli University (Turkey)

Fahrettin Horasan, Computer Engineering, Kırıkkale University (Turkey)

Faruk Fırat Çalım, Civil Engineering, Alparslan Türkeş University (Turkey)

Feyza Gurbuz, Industrial Engineering, Erciyes University (Turkey)

Francesco de Paulis, Electrical and Electronics Enginering, University of L'Aquila (Italy)

Gökhan Dok, Civil Engineering, Sakary Apllied Science University (Turkey)

Grazyna S Martynkova, Nanotechnology Centre, VŠB-Technical University of Ostrava · Nanotechnology Centre (Czech Republic)

Grzegorz Jaworski, Physics, Heavy Ion Laboratory, University of Warsaw (Poland)

H. F. Nied, Department of Mechanical Engineering and Mechanics, Lehigh University (U.S.A.)

Hakan Alp, Geophysical Engineering, Cerrahpaşa University (Turkey)

Hatice Esen, Industrial Engineering, Kocaeli University (Turkey)

Hüseyin Aksoy, Biology, Sakarya University (Turkey)

Issa Al-Harty, Civil and Architectural Engineering, Sultan Qaboos University (Oman)

İbrahim Bahadır Başyiğit, Electrical and Electronics Engineering, Isparta Apllied Science University (Turkey)

İsmail Hakkı Demir, Architecture, Sakarya University (Turkey)

Kamaruzzaman Sopian, Renewable Energy, Universiti Kebangsaan Malaysia (Malaysia)

Khalifa Al-Jabri, Civil and Architectural Engineering, Sultan Qaboos University (Oman)

Kevser Ovaz Akpınar, Computer Engineering, Rochester Institute of Technology of Dubai (Dubai)

Luan Thach Hoang, Mathematics, Texas Tech University (U.S.A.)

Luis A. Materon, Biology, The University of Texas Rio Grande Valley (USA)

M. Hilmi Nişancı, Electrical and Electronics Engineering, Sakarya University (Turkey)

Mahmud Tokur, Metallurgical and Materials Engineering, Sakarya University (Turkey)

Mehmet Emin Aydın, Industrial Engineering, University of Bedfordshire (UK)

Mehmet Uysal, Metallurgical and Materials Engineering, Sakarya University (Turkey)

Mesut Baran, Electrical and Computer Engineering, FREEDM Systems Center, North Carolina State University (U.S.A.)

Miraç Alaf, Metallurgical and Materials Engineering, Bilecik Şeyh Edebali University (Turkey)

Mohammad Sukri bin Mustapa, Faculty of Mechanical & Manufacturing Engineering, Universiti Tun Hussein Onn Malaysia (Malaysia)

Muhammed Fatih Adak, Computer Engineering, Sakarya University (Turkey)

Muhammed Maruf Öztürk, Computer Engineering, Süleyman Demirel University (Turkey)

Murat Güzeltepe, Mathematics, Sakarya University (Turkey)

Murat Sarduvan, Mathematics, Sakarya University (Turkey)

Technical Editor

Hatice Vural, Electrical and Electronics Enginering, Amasya University (Turkey)

Editorial Assistant

Ahmet Erhan Tanyeri, Sakarya University (Turkey)

Evrim Yüksel, Sakarya University (Turkey)

RESEARCH ARTICLES

Potential Health Risks of Chloroacetanilide Herbicides: An In Silico Analysis	Ahmet Ali BERBER, Şefika Nur DEMİR, Nihan AKINCI KENANOĞLU	865-871
A Novel Machine Learning-based Diagnostic Algorithm for Detection of Onychomycosis through Nail Appearance	Serkan DÜZAYAK, Muhammed Kürşad UÇAR	872-886
Characterization of Polyphenol Oxidase from Eruca sativa	Negin SHABNAM, Sibel KAHRAMAN	887-894
Experimental and Numerical Investigation of Flexural Properties of Solid Wood Materials Reinforced with Various FRP	Şemsettin KILINÇARSLAN, Yasemin ŞİMŞEK TÜRKER	895-901
Bibliometric Profile of Global Scientific Research on Monitoring and Assessment of Aquatic Toxicology (2015-2019)	Ayşen Nil BERBER, V. Zülal SÖNMEZ, Ceyhun AKARSU, Nüket SİVRİ	902-911
The Effect of Royal Jelly on Irisin in Experimentally Diabetic Rats	Selcen ÇAKIR	912-919
Survay Study of Antimicrobial Activities of Different Region Honeys in Turkey	Mehtap USTA	920-929

Sakarya University Journal of Science
SAUJS

Title: Analysis of Occupational Health and Safety Risks in Beekeeping with FMEA Method

Authors: Mustafa ÖZDEMİR, Serhan KÖKHAN

How to cite
Mustafa ÖZDEMİR, Serhan KÖKHAN; (2023), Analysis of Occupational Health and
Safety Risks in Beekeeping with FMEA Method. Sakarya University Journal of
Science, 27(4), 708-723, DOI: 10.16984/saufenbilder.1228959
Access link
https://dergipark.org.tr/en/pub/saufenbilder/issue/79486/1228959

Analysis of Occupational Health and Safety Risks in Beekeeping with FMEA Method

Mustafa ÖZDEMİR [1] , Serhan KÖKHAN*[1]

Abstract

Contrary to popular belief, beekeeping, which dates back to prehistoric times and is one of the most important plant and animal production branches today, is not an innocent profession in terms of occupational health and safety. In this study, in order to determine the occupational health and safety risk factors in the beekeeping profession, Interviews with beekeepers were conducted in 10 apiaries operating in Bayburt, where especially wandering beekeeping is practiced. In light of the data obtained from the danger hunt applied by the occupational health and safety specialist, ergonomic, physical, biological, and chemical risks were revealed using the FMEA risk analysis method. The effect, probability, and detection values were found for each failure mode, and then Risk Priority Number values were calculated. As a result of the study, for the five basic stages of beekeeping, 15 processes, 39 failure modes, 72 potential effects, and 39 failure causes were determined. Failure modes with a Risk Priority Number value of 100 and above were evaluated as "situations where urgent action and axiom should be taken," and preventive axioms were proposed for each relevant failure mode. The number of studies on the risk factors in the beekeeping profession is very limited in the literature. For this reason, it is predicted that this study will fill an important gap in the related field and make significant contributions to the literature.

Keywords: Beekeeping, FMEA, occupational health and safety, risk management

1. INTRODUCTION

Beekeeping is a production activity that includes producing bee products such as honey, royal jelly, bee venom, pollen, and propolis by combining plant resources, bees, and labor, as well as producing queen bees, swarms, and pack bees, which constitute an essential source of income [1]. In Turkey, which is at a high level in terms of natural conditions, it is seen that the profession of beekeeping is carried out quite intensively. This has made Turkey the 3rd in the world with 8,179,000 hives after India and China in terms of the number of hives, according to 2020 data [2]. Although the profession of beekeeping is defined in the "Dangerous" profession class with the code 01.49.01 NACE (EU Economic Activities Nomenclature) according to the Workplace Hazard Classes List published in the Official Gazette dated 27.2.2017 and numbered

* Corresponding author: serhankokhan@bayburt.edu.tr (S. KÖKHAN)
[1] Bayburt University
E-mail: mozdemir@bayburt.edu.tr
ORCID: https://orcid.org/0000-0002-6067-2007, https://orcid.org/0000-0001-6691-6271

29992, both those who practice this profession and the institutions and organizations that provide beekeeping education do not show sufficient sensitivity about the occupational health and safety risks in the beekeeping profession. Studies on occupational health and safety reveal that occupational accidents, work-related diseases, and occupational diseases can be significantly prevented if conscious, effective, and adequate health and safety measures are taken. In order to prevent or minimize occupational health and safety risks, it is important to control the hazards while they are at the source, to plan the working systems, and to prefer less dangerous processes instead of dangerous ones. In addition, it is necessary to create an occupational health and safety culture by using less dangerous machinery or equipment and personal protective equipment and by adopting occupational health and safety issues by both management and employees [3, 4]. In the studies carried out in this context, it is important to investigate the occupational health and safety risks in the beekeeping profession, defined in the dangerous class, and to determine what precautions should be taken against these risks. In the literature, very few studies examine the beekeeping profession's occupational health and safety risk factors. The information about these studies is presented in Table 1 below.

Table 1 Literature

References	Results
[5]	As a result of the examination of 45 bibliographic sources, it was concluded that beekeepers generally face risks such as mechanical and physical difficulties, environmental and climatic conditions, stress, insomnia, irregular diet, and occupational accidents.
[6]	In the risk analysis made with the FMEA method, especially in terms of food safety, in a honey production unit in Tunisia, it was determined that 56% of the non-compliances were caused by not applying good hygiene and good farming practices.
[7]	In the study conducted with Fine-Kinney Risk Assessment Method on some beekeepers in Turkey, serious chemical, biological, physical, and ergonomic risk factors were determined in beekeepers.
[8]	In the study carried out in Turkey, it was concluded that allergy testing for bee stings is very rare in beekeepers, they stay in tents or barracks, traffic accidents, scorpion, snake bites, tick bites, and fire incidents are common in bee sting transportation, and sometimes bear and pig damages are seen.
[9]	In the study conducted on 3 beekeepers in Australia, it was determined that beekeepers are exposed to ergonomic risks, bee stings, and chemical risks due to heavy loads such as hives.
[10]	In the study on beekeepers' health problems and bee allergy, it was determined that beekeepers have health risks such as bee venom and propolis allergies (including anaphylaxis) and Lyme borreliosis associated with tick bites.

The profession of beekeeping involves significant health and safety risks, and reducing these risks is crucial. However, only considering certain risk factors can lead to ignoring all the other risks and failing to take necessary precautions. Therefore, it is necessary to examine all risk factors in beekeeping and take measures accordingly. This is important not only for the health and safety of beekeepers but also for the sustainability of this profession. Thus, scientific research and studies are needed to consider all risk factors in beekeeping and reduce them.

As far as it has been examined, studies on occupational health and safety risk factors in beekeeping only focus on ergonomics, animal attack, etc. focuses on specific risk factors. In addition, existing risk analysis studies do not offer effective solutions. In this study, all possible risk factors (ergonomic, physical, biological, and chemical) are examined and solutions are offered for permanent and migratory beekeepers.

This study primarily aims to investigate what kind of risks can be associated with beekeeping applications throughout all stages (settlement in the selected apiary, spring maintenance and works, harvest works, autumn maintenance and works, winterization) in terms of occupational health and safety. Subsequently, it seeks to identify the measures that can be taken to minimize these identified risks.

In this respect, it can be said that this study has an original quality.

2. MATERIAL AND METHODS

2.1. Material

This research has been planned as a cross-sectional study to determine the occupational health and safety risks in the beekeeping profession and the urgent and non-urgent measures to be taken against these risks. The materials used in the research consist of the data obtained from the interviews with the beekeepers and the danger hunt applied by the occupational health and safety specialist in 10 apiaries, including the fixed and itinerant beekeepers operating in Bayburt province. The Failure Mode Effects Analysis (FMEA) method was used in the analysis, and studies were carried out to determine occupational health and safety risks in terms of ergonomic, physical, biological, and chemical aspects. Coordinate and map information of the study apiaries are given in Figure 1 and Table 2.

Figure 1 Representation of apiaries included in the study on the map

Bayburt province is among the newly developing regions in beekeeping and according to the data of the Agricultural Economy and Policy Development Institute Tepge Beekeeping 2022 Product Report. There are 75,088 hives in the province, and 500 tons of honey were produced in the same year [2].

Table 2 Coordinate information of apiaries included in the study

Place Names	Coordinates
Akşar	40° 21' 02" N 39° 58' 26" E
Çiğdemtepe	40° 19' 57" N 40° 08' 07" E
Demirözü	40° 09' 43" N 39° 53' 35" E
Kavakyanı	40° 17' 24" N 40° 30' 45" E
Kitre	40° 18' 41" N 39° 51' 55" E
Kop	40° 03' 54" N 40° 26' 14" E
Aslandağı	40° 13' 51" N 40° 13' 48" E
Sırakayalar	40° 05' 51" N 40° 15' 38" E
Taht	40° 17' 18" N 40° 25' 39" E
Yukarı Kırzı	40° 23' 16" N 40° 05' 20" E

2.2. FMEA Method

Reliability is the probability that a component or system will perform its intended function for a specified period of time under specified operating conditions [11]. Reliability analysis also aims to measure and analyze a system to eliminate or reduce its failures, probabilities, and security risk. Commonly used reliability analysis techniques are fault tree analysis (FTA) [12–14], failure mode and effect analysis (FMEA) [15, 16], root cause analysis (RCA) [17, 18], and event tree analysis (ETA) [19, 20]. Unlike other reliability management, FMEA is a proactive method to prevent system failures. Its main purpose is to identify, prioritize and act on known or potential system failure modes before they occur. The FMEA stages are shown in Figure 2 [21, 22].

There are different effect, probability, and detection scales in the literature. The scale values recommended and widely used in the study are in Table 3-5 [23-32].
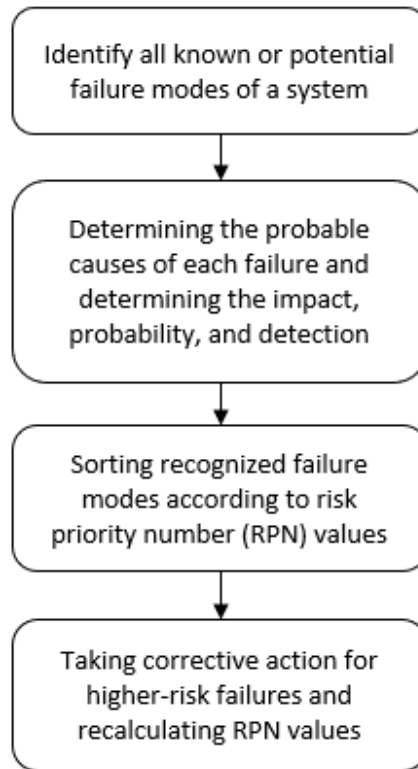
Figure 2 FMEA stages

Table 3 Effect of error mode, intensity of impact, and scale values

Effect (E)	Error Mode	Score
Dangerous without warning	Potential failure mode death without warning	10
Dangerous with warning	Death by warning of a potential failure mode	9
Very high	Serious injury at the disability level	8
High	Incapacity level injury	7
Temperate	Improvement with a break of one month or more	6
Low	Improvement with a one-week break	5
Very low	Improvement with a one-day break	4
Small	Improvement with a short break	3
Very small	Recovery with rapid intervention	2
None	No effect	1

Table 4 Probability expression, number of errors, and scale values of the error mode

Probability of Errors (P)	Error Number	Score
Very High: Failure is almost inevitable	>1 in 2	10
	1 in 3	9
High: Repeated errors	1 in 8	8
	1 in 20	7
	1 in 80	6
Moderate: Occasional errors	1 in 400	5
	1 in 2,000	4
Low: Relatively few errors	1 in 15,000	3
	1 in 150,000	2
Remote: Failure unlikely	<1 in 1,500,000	1

Table 5 Detection of fault mode, detection probability, and scale values by process control

Detection (D)	Detection Probability with Process Control	Score
Absolute Uncertainty	Cannot detect error	10
Very far	It is doubtful that it will detect the error	9
Far	It is unlikely that it will detect the error	8
Very low	Very low chance of detecting the error	7
Low	Low probability of detecting the error	6
Temperate	Medium probability of detecting the error	5
Moderately high	The probability of detecting the error is above medium	4
High	High probability of detecting the error	3
Very high	The probability of detecting the error is very high	2
Almost certain	Detects error	1

While calculating the RPN value, according to Table 3-5, the effect (E), probability (P), and detection (D) values determined by the occupational health and safety experts in line with the data obtained in the face-to-face interviews with the beekeepers are multiplied by each other (RPN = E * P * D). In the evaluation of RPN scores in the study; It has been determined by occupational safety experts that if the RPN score is below 40, there is no need to take any precautions, if $40 \leq RPN \leq 100$, precautions can be taken, and if it is above 100, it is necessary to take precautions and improve it.

3. RESULTS

In the FMEA tables created in the study, error modes were determined for each process. These error modes were classified in terms of their potential effects, and possible causes of errors were determined. Impact, probability, and detection values were determined for each potential impact in line with expert opinions, and RPN values were calculated. By the determined classification, priority axioms have been determined for error effects with RPN values above 100. In addition to these axioms, In the FMEA tables created in the study, error modes were determined for each process. These error modes were classified in terms of their potential effects, and possible causes of errors were determined. Impact, probability, and detection values were determined for each potential impact in line with expert opinions, and RPN values were calculated. By the determined classification, priority axioms have been determined for error effects with RPN values above 100. In addition to these axioms, axiom suggestions are also presented for all potential error effects with RPN values between 40 and 100. The analyzes made are given in Tables 6-10. Examples of some failure modes identified in FMEA tables before and after improvement are presented in Figure 3-12.

Table 6 Risk assessment reports 1

Stage	Process	Potential Failure Mode	Potential Effect(s) of Failure	Probable Cause(s) of Failure	E	P	D	RPN	Suggested Axioms	After The Axiom			
										E	P	D	RPN
Settlement in the Selected Apiary	Transfer of Hives to the Selected Apiary	Traffic accident	Death	C1	9	3	8	216	A1	9	2	7	126
			Injury		8	3	8	192		8	2	7	112
			Minor Injury		5	3	8	120		5	2	7	70
		Bee sting	Death	C2	9	5	2	90	A2	9	4	2	72
			Loss of Workforce		4	5	2	40		4	4	2	32
	Transport	Incorrect Transport	Short-Term Muscle and Joint Traumas	C3	5	6	5	150	A3	5	4	5	100
			Permanent Muscle and Joint Disorders		7	4	5	140		7	2	5	70
			Injury		5	5	5	125		5	3	5	75
		Trips, Slips, and Falls in the Field	Minor Injury	C4	3	5	5	75	A4	3	4	3	36
			Serious Injury		4	4	5	80		4	3	3	36
			Death		9	3	5	135		9	2	3	54
Spring maintenance and works	Cleaning of Hive Flight Holes, Ventilation	Bee sting	Death	C5	9	6	2	108	A2	9	3	2	54
			Loss of Workforce		4	6	2	48		4	3	2	24
	Nutritional Supplementation If There Is Not Enough Food For Bees	Bee sting	Death	C6	9	6	2	108		9	3	2	54
			Loss of Workforce		4	6	2	48		4	3	2	24
		Fire	Minor Injury	C7	5	4	2	40	A5	5	2	2	20
		Incorrect Transport	Short-Term Muscle and Joint Traumas	C3	5	5	5	125	A6	5	4	5	100
			Permanent Muscle and Joint Discomfort		7	3	5	105		7	2	5	70
	Spraying	Inhalation Poisoning	Loss of Workforce	C8	5	6	6	180	A7	5	4	5	100
		Contact / Skin Poisoning			5	6	6	180		5	4	5	100
		Chemical Burns	Injury and Loss of Work		7	6	3	126		7	4	2	56
		Oral Poisoning	Loss of Workforce	C9	5	5	5	125		5	3	4	60

Table 7 Risk assessment reports 2

Stage	Process	Potential Failure Mode	Potential Effect(s) of Failure	Probable Cause(s) of Failure	E	P	D	RPN	Suggested Axioms	After The Axiom			
										E	P	D	RPN
Harvest works	Honey Harvest	Bee sting	Death	C5	9	6	2	108	A2	9	3	2	54
			Loss of Workforce		4	6	2	48		4	3	2	24
		Incorrect Transport	Short-Term Muscle and Joint Traumas	C3	5	5	5	125	A6	5	4	5	100
			Permanent Muscle and Joint Discomfort		7	3	5	105		7	2	5	70
		Sunburn and Sunstroke	Loss of Workforce	C10	5	5	5	125	A8	5	4	4	80
			Short-Term Loss of Workforce		3	4	5	60		3	3	4	36
		Working in the Sun	Sun Spots on the Skin		3	5	5	75		3	3	5	45
		Non-Ergonomic Working Type	Permanent Muscle and Joint Discomfort (Varicocele etc.)	C11	7	7	6	294	A9	7	4	5	140
		Fire	Loss of Workforce		6	6	3	108	A10	5	5	2	50
	Transport	Incorrect Transport	Short-Term Muscle and Joint Traumas	C3	5	6	5	150	A6	5	4	5	100
			Permanent Muscle and Joint Discomfort		7	4	5	140		7	2	5	70
			Injury		5	5	5	125		5	3	5	75
		Stuck in the Field, Slip, and Fall	Minor Injury	C4	3	5	5	75	A4	3	4	3	36
			Serious Injury		4	4	5	80		4	3	3	36
			Death		9	3	5	135		9	2	3	54
		Unequipped Transport	Hand Cut	C15	5	6	4	120	A11	5	4	4	80
	Honey Straining Process	Improper Honey Harvesting	Hand Cut		5	5	4	100	A12	5	4	4	80
		Strainer Accidents	Injury Due to Entrapment of the Limbs (Hand-Arm) into the Machine	C16	6	6	3	108	A13	6	4	3	72
				C17	6	6	3	108		6	4	3	72
			Injury of Limbs (Hand-Arm) Due to Electric Shock	C18	6	7	3	126	A14	6	5	1	30
	During the Harvest Process	Wild Animal Attack	Death	C19	9	5	6	270	A15	9	3	3	81
			Long-Term Loss of Workforce		6	5	6	180		6	3	3	54
			Short-Term Loss of WorkforcE		5	5	6	150		5	3	3	45

Table 8 Risk assessment reports 3

Stage	Process	Potential Failure Mode	Potential Effect(s) of Failure	Probable Cause(s) of Failure	E	P	D	RPN	Suggested Axioms	After The Axiom			
										E	P	D	RPN
Autumn maintenance and works	Colony Consolidation	Bee sting	Death	C5	9	6	2	108	A2	9	3	2	54
			Loss of Workforce		4	6	2	48		4	3	2	24
		Incorrect Transport	Short-Term Muscle and Joint Traumas	C3	5	5	5	125	A6	5	4	5	100
			Permanent Muscle and Joint Discomfort		7	3	5	105		7	2	5	70
		Bellows Fire	Loss of Workforce	C12	6	6	3	108	A10	5	5	2	50
	General cleaning	Injury	Hand Cut	C13	5	5	4	100	A11	5	4	4	80
		Incorrect Transport	Short-Term Muscle and Joint Traumas	C3	5	5	5	125	A6	5	4	5	100
			Permanent Muscle and Joint Discomfort		7	3	5	105		7	2	5	70
	Disease and Parasite Treatment	Inhalation Poisoning	Loss of Workforce	C8	5	6	6	180	A16	5	4	5	100
		Contact / Skin Poisoning	Loss of Workforce		5	6	6	180		5	4	5	100
		Chemical Burns	Injury and Loss of Workforce		7	6	3	126		7	4	2	56
		Oral Poisoning	Loss of Workforce	C9	5	5	5	125		5	3	4	60
Winterization	Transfer of Hives to the Wintering Site	Traffic accident	Death	C1	9	3	8	216	A1	9	2	7	126
			Injury		8	3	8	192		8	2	7	112
		Hive Fire in Vehicle	Death	C14	9	4	5	180	A17	9	2	5	90
			Injury		8	4	5	160		8	2	5	80
		Bee sting	Death	C2	9	5	2	90	A2	9	4	2	72
			Loss of Workforce		4	5	2	40		4	4	2	32
	Transport	Incorrect Transport	Short-Term Muscle and Joint Traumas	C3	5	6	5	150	A6	5	4	5	100
			Permanent Muscle and Joint Discomfort		7	4	5	140		7	2	5	70
			Injury		5	5	5	125		5	3	5	75
		Stuck in the Field, Slip, and Fall	Minor Injury	C4	3	5	5	75	A18	3	4	3	36
			Serious Injury		4	4	5	80		4	3	3	36
			Death		9	3	5	135		9	2	3	54
	Narrowing the barrel holes	Bee sting	Death	C2	9	5	2	90	A2	9	4	2	72
			Loss of Workforce		4	5	2	40		4	4	2	32

Table 9 Probable cause(s) of failure

Code	Probable Causes
C1	Insomnia, Inattention, Inattention, Fatigue, Rushing, Bee Sting
C2	Bee Sting by a Venom Susceptible Person
C3	Non-Ergonomic Transport Methods, Unsuitable Body Position, and Vehicleless Cargo Transport
C4	Working on Rough Terrain, Carelessness, Insufficient Lighting, Slippery Ground
C5	The sting of a Person Sensitive to Bee Venom by a Bee Due to Not Using Protective Equipment during Cleaning
C6	The sting of a Person Sensitive to Bee Venom by Bee Due to Not Using Protective Equipment during Nutritional Supplementation
C7	Failure to Extinguish the Fire Burned During the Preparation of the Nutritional Supplement (Sherbet) After the Process
C8	Incorrect Spraying, Not Using Personal Protective Equipment (Mask, Gloves, etc.)
C9	Medicated Cake Consumption
C10	Long-Term Unprotected Working in the Sun
C11	Working for a long time while standing
C12	Leaving the bellows used during the honey harvest in the apiary without being extinguished
C13	During the cleaning of the hive, not using a protector and contacting the hand with the cutting metal on the cover
C14	Late Detection of the Fire Caused by the Carriage of the Unextinguished Bellows in the Vehicle and Exposure to the Fire in the Vehicle
C15	Carrying a Hive with One Person, Holding the Hive from Inappropriate Places
C16	Inserting the Limbs into the Machine while the Manual Honey Extractor is Working
C17	Inserting the Limbs into the Machine while the Electric Honey Extractor is Working
C18	Electric Leakage in Electric Honey Extractor
C19	Animal Attack That Comes To Apiary To Meet Its Nutritional Needs (Bear, Pig, etc.)

Table 10 Suggested axioms

Code	Axioms
A1	Should not go out in traffic tired and sleepless. Excessive speed should be avoided. Transportation should not be done during the periods when the bees are actively working.
A2	Bee suits, gloves, etc., and protective equipment should be used. Perfume, etc., that bees will perceive as a threat should not be used. Bananas, etc., should not be eaten, which bees are sensitive fruits. Light-colored clothing should be worn. Sudden and harsh movements should be avoided while cleaning and airing. Allergy medication should be available for reactions that may occur after a bee sting.
A3	Prolonged standing work should not be done. Pay attention to ergonomic carrying positions while carrying loads. If possible, the hives should be carried with two people, or a wheelbarrow should be used.
A4	Care should be taken to choose less rough terrain in selecting an apiary. Before settling in the apiary, a detailed land exploration should be made. An adequate lighting system should be installed. In case of excessive fatigue, transportation should be avoided.
A5	The fire lit to prepare sherbet should be burned in places far from grassy and wooded areas. There is always a fire extinguisher in the apiary, a bucket filled with water, a shovel, etc., for firefighting. Fire equipment must be available.
A6	Do not work standing up for long periods. Attention should be paid to ergonomic carrying positions. Transportation should be done with two people if possible; if not, handcart, etc., tools should be used.
A7	Spraying should not be done without learning the technical spraying methods. Learning the medication dosages Use of personal protective equipment and equipment Paying attention to MSDS labels on drugs
A8	Do not work under the sun for a long time. Hats, scarves, gloves, etc., and, protective equipment should be used. An alternating working system should be established.
A9	Periodic rest breaks should be given while working. An alternating working system should be established.
A10	The bellows used during honey harvest should be burned and extinguished in places far from grassy and wooded areas. There is always a fire extinguisher in the apiary, a bucket filled with water, a shovel, etc., for firefighting. Fire equipment must be available.

Table 10 Suggested axioms (continue)

Code	Axioms
A11	If possible, the hives should be carried by two people. Work gloves should be used in transportation operations.
A12	Work gloves should be used.
A13	The machine should not be intervened before the honey filtering process is completed. A lid system should be installed on the honey extractor, which opens when the filtering process is finished.
A14	The machine should not be intervened before the honey filtering process is completed. A lid system should be installed on the honey extractor, which opens when the filtering process is finished. A leakage current relay should be used.
A15	Electric fence and strobe light should be used. Systems with motion-sensitive sensors should be used. If legal conditions are met, he must have a licensed weapon.
A16	Technical spraying methods should be learned. Education should be given about appropriate periods and appropriate dosages for medication. Personal protective equipment (mask, gloves, etc.) must be used during spraying. The safety information (MSDS) written on the drugs used should be respected.
A17	Do not rush while moving; the bellows should be entirely deflated before putting them in the vehicle. Combustible and combustible materials and bellows should never be placed side by side.
A18	Care should be taken to choose less rough terrain in selecting an apiary. Before settling in the apiary, a detailed land exploration should be made. An adequate lighting system should be installed. In case of excessive fatigue, transportation should be avoided.

Figure 3 Working without gloves

Figure 4 Working with gloves

Figure 5 Unsafe intervention during the honey extraction process

Figure 8 Putting the bellows safely

Figure 6 Safe position during the honey extraction process

Figure 9 Incorrect hive handling

Figure 7 Improper placement of the bellow

Figure 10 Ergonomic hive handling

Figure 11 Sunburn Caused by Working Without Gloves

Figure 12 Working with Gloves Against Sunburn

4. DISCUSSION

This study was conducted to determine the risk factors in occupational health and safety in the beekeeping sector; Face-to-face interviews and in-depth interviews were conducted with the employees of 10 apiaries operating in Bayburt, one of the regions of Turkey with significant potential in beekeeping. Then, with the collected data, occupational health and safety risks related to ergonomic, physical, biological, and chemical factors were analyzed with the FMEA risk analysis method, and axiom plans were created against these risks. It has been predicted that if the axioms recommended for each process with a high-risk value, such as permanent muscle and joint disorders, respiratory, contact poisoning, death, and

injury that may occur due to wild animal attack and after beehive fire in the vehicle are implemented, there may be significant decreases in RPN values.

It is thought that the study will fill an essential gap in the literature and will also be a reference study in terms of content and method for future academic and field studies. It is recommended that researchers who will work on a similar subject should consider especially bee breeds, climate, geographical conditions, beekeepers' occupational health and safety awareness level, and cultural codes.

Authors' Contribution
The authors contributed equally to the study.

The Declaration of Conflict of Interest/ Common Interest
No conflict of interest or common interest has been declared by the authors.

The Declaration of Ethics Committee Approval
This study does not require ethics committee permission or any special permission.

The Declaration of Research and Publication Ethics
The authors of the paper declare that they comply with the scientific, ethical, and quotation rules of SAUJS in all processes of the paper and that they do not make any falsification on the data collected. In addition, they declare that Sakarya University Journal of Science and its editorial board have no responsibility for any ethical violations that may be encountered, and that this study has not been evaluated in any academic publication environment other than Sakarya University Journal of Science.

REFERENCES

[1] Ç. Fıratlı, F. Genç, M. Karacaoğlu, H. Gençer, "Türkiye arıcılığının karşılaştırmalı analizi, sorunlar-öneriler," Türkiye Ziraat Mühendisliği V. Teknik Kongresi, Ankara, 2000, pp. 811-826.

[2] V. Burucu, Ürün Raporu – Arıcılık: Ankara Tarımsal Ekonomi ve Politika Geliştirme Enstitüsü–TEPGE, Report no. 351, pp. 39, 2022.

[3] İ. Kılkış, İş Sağlığı ve Güvenliği. Sosyal Politika: Fourth Edition. Dora Basın Yayın, 2014.

[4] Y. Kim, J. Park, M. Park, "Creating a Culture of Prevention in Occupational Safety and Health Practice," Safety and Health at Work, vol. 7, no. 2, pp. 89-96, 2016.

[5] E. Topal, M. Strant, C. Pocol, M. Kösoğlu, "Critical Point in Beekeeping: Beekeepers' Health," Bulletin UASVM Food Science and Technology, vol. 1, pp. 76, 2019.

[6] S. Jrıbı, N. Hanafi, D. Hajer, H. Ismaıl, "Application of Failure Mode and Effect Analysis and Cause and Effect analysis for honey production in Tunisia: A case study," International Journal of Innovative Approaches in Agricultural Research, vol. 5, no. 4, pp. 434-444, 2021.

[7] K. Karakuş, İ. Aslan, "Occupational Health and Safety In Beekeeping Enterprises: Bingöl Example," Idrc International Disaster and Resilience Congress, Eskişehir, 2019, pp. 623-626.

[8] Z. Sengül, "Ege Bölgesinde Arıcılık Yapan İşletmelerin Sürdürülebilirlik Yönünden Değerlendirilmesi," Ph.D. dissertation, Ege University, Tarım Ekonomisi Anabilim Dalı, İzmir, 2020.

[9] D. Fels, A. Blackler, "Cook D, Foth M. Ergonomics in apiculture: A case study based on inspecting movable frame hives for healthy bee activities," Heliyon, vol. 5, pp. 1-9, 2019.

[10] J. Stanhope, S. Carver, P. Weinstein, "Health outcomes of beekeeping: a systematic review," Journal of Apicultural Research, vol. 56, no. 2, pp. 100-111, 2017.

[11] C. Ebeling, An İntroduction to Reliability and Maintainability Engineering: Third Edition. Tata McGraw-Hill Education, 2004.

[12] S. Bhattacharyya, A. Cheliyan, "Optimization of a subsea production system for cost and reliability using its fault tree model," Reliability Engineering and System Safety, vol. 185, no. 213, pp. 9, 2019.

[13] P. McNelles, G. Renganathan, Z. Zeng, M. Chirila, L. Lu, "A comparison of fault trees and the dynamic flowgraph methodology for the analysis of FPGA-based safety systems part 2: theoretical investigations," Reliability Engineering and System Safety, vol. 183, pp. 60–83, 2019.

[14] E. Ruijters, D. Reijsbergen, PT. de Boer, M. Stoelinga, "Rare event simulation for dynamic fault trees," Reliability Engineering and System Safety, vol. 186, no. 220, pp. 31, 2019.

[15] M. Catelani, L. Ciani, M. Venzi, "Failure modes, mechanisms and effect analysis on temperature redundant sensor stage," Reliability Engineering and System Safety, vol. 180, pp. 425–33, 2018.

[16] K. Kim, M. Zuo, "General model for the risk priority number in failure mode and effects analysis," Reliability

Engineering and System Safety, vol. 169, pp. 321, 2018.

[17] S. Woo, M Pecht, D. O'Neal, "Reliability design and case study of the domestic compressor subjected to repetitive internal stresses," Reliability Engineering and System Safety, pp. 193, 106604, 2020.

[18] H. Mohammadnazar, M. Pulkkinen, H. Ghanbari, "A root cause analysis method for preventing erratic behavior in software development: PEBA," Reliability Engineering and System Safety, pp.191, 106565, 2019.

[19] C. Queral, J. Gómez-Magán, C. París, J. Rivas-Lewicky, M. Sánchez-Perea, J Gil, "Dynamic event trees without success criteria for full spectrum LOCA sequences applying the integrated safety assessment (ISA) methodology," Reliability Engineering and System Safety, vol. 171, pp. 152–68, 2018.

[20] S. Rahman, D. Karanki, A. Epiney, D. Wicaksono, O. Zerkak, V. Dang, "Deterministic sampling for propagating epistemic and aleatory uncertainty in dynamic event tree analysis," Reliability Engineering and System Safety, vol. 175, pp. 62–78, 2018.

[21] D. Stamatis, Failure Mode and Effect Analysis: FMEA From Theory to Execution: Second Edition. ASQ Quality Press, 2003.

[22] H. Liu, FMEA Using Uncertainty Theories and MCDM Methods. Springer, 2016.

[23] D. Chang, K. Sun, "Applying DEA to enhance assessment capability of FMEA," International Journal of Quality and Reliability Management, vol. 26, pp. 629–643, 2009.

[24] K. Chang, "Evaluate the orderings of risk for failure problems using a more general RPN methodology," Microelectronics Reliability, vol. 49, pp. 1586–1596, 2009.

[25] K. Chang, C. Cheng, "A risk assessment methodology using intuitionistic fuzzy set in FMEA," International Journal of Systems Science, vol. 41, pp. 1457–1471, 2010.

[26] K. Chang, T. Wen, "A novel efficient approach for DFMEA combining 2-tuple and the OWA operatör," Expert Systems with Applications, vol. 37, pp. 2362–2370, 2010.

[27] K. Chang, C. Cheng, Y. Chang, "Reprioritization of failures in a silane supply system using an intuitionistic fuzzy set ranking technique," Soft Computing, vol. 14, pp. 285–298, 2010.

[28] Ford Motor Company, "Potential failure mode and effects analysis (FMEA) reference manual," 1995, [Online]. Available: https://www.lehigh.edu/~intribos/Resources/SAE_FMEA.pdf

[29] F. Franceschini, M. Galetto, "A new approach for evaluation of risk priorities of failure modes in FMEA," International Journal of Production Research, vol. 39, pp. 2991–3002, 2001.

[30] H. Liu, L. Liu, N. Liu, L. Mao, "Risk evaluation in failure mode and effects analysis with extended VIKOR method under fuzzy environment," Expert Systems with Applications, vol. 39, pp. 12926–12934, 2012.

[31] N. Sankar, B. Prabhu, "Modified approach for prioritization of failures in a system failure mode and effects analysis," International Journal of

Quality and Reliability Management, vol. 18, pp. 324–336, 2001.

[32] S. Seyed-Hosseini, N. Safaei, M. Asgharpour, "Reprioritization of failures in a system failure mode and effects analysis by decision making trial and evaluation laboratory technique," Reliability Engineering and System Safety, vol. 91, pp. 872-881, 2006.

Title: Mathematical Modelling of Shear Cutting Process of Grain Oriented Electrical
Steels Using Regression Modelling

Authors: Nihat ÇELİK, Alaaddin TOKTAŞ

Mathematical Modelling of Shear Cutting Process of Grain Oriented Electrical Steels Using Regression Modelling

Nihat ÇELİK [*1] , Alaaddin TOKTAŞ[1]

Abstract

This article proposes a regression model for the shear-cutting process of grain-oriented electrical steel magnetic cores of transformers made from different gages and magnetic properties of steels. In the experimental runs, 3 levels for thickness (230, 270, and 300 μm) and 4 levels for magnetic features of electrical steels are considered. Core steels are supplied as foils and slit to designed lengths in slitting machinery along the rolling direction of coils. The best magnetic features rely on the rolling direction of the coil and the transverse direction of the coil is subject to the shear-cutting process. The result of cutting operations, discontinuities, and degradations in magnetic properties may occur because of deterioration in crystallography and strain gradation on laminated sheets. Shear-cutting process factors have a strong influence on magnetic degradation even the magnitude of the no-load loss of the transformer core. In this study, the mathematical relation between shear cutting factors sheet thickness ST, counts of hits $CH,$ and the response burr length BL is determined using regression modeling. For this purpose, the process parameters of GEORG TBA 400 cut-to-length machinery in use core production is studied. The calculated coefficient of determination is close to almost 1.00 i.e., $R^2 = 0.9896$ which means the factors are sufficient to model the response, and the model is obtained with a good prediction performance. The aim of the present study is building up a useful process control tool for the machinery and raise a discussion alike process in industry.

Keywords: Shearing, regression, burr, deformation, modelling

1. INTRODUCTION

The cut-to-length process is an important part of the core manufacturing of transformers because of plastic deformations and discontinuities that emerged along the transverse direction (TD) of steel. Length of burrs BL can indicate that plastic deformation occurred during shear cutting. BL levels of the cutting process are subject to be under a limited level. Such that, no-load losses, EDDY and stray loses can be kept under the desired level for stacked cores regarding IEC 60604-02. No-load losses are an important part of the total operation cost calculation of a transformer during at least 30 years life span, especially operated in partly loading conditions of a transformer in a grid. Transformer cores are made by stacking grain-oriented electrical steel laminations,

Nihat ÇELİK, Alaaddin TOKTAŞ

Mathematical Modelling of Shear Cutting Process of Grain Oriented Electrical Steels Using Regression ...

before stacking a few mechanical processes like slitting, and mitering must be applied. Advanced magnetic properties show up on the rolling (i.e., easy magnetization) direction of core steels because of the grain orientation pattern of laminations. Thicknesses are equal to or under 300 microns because of descending EDDY losses in AC magnetic field. The mitering process is very important because some of the magnetic features of steel are disappeared because of the mechanism of the cutting process and emerged plastic deformations on the near-cut surface. Some of the variances in the shearing process like cutting speed, diving angle of the upper tool, sharpness of tools, length of burr, thickness, hardness of sheet, cutting clearances, etc., have an influence on the deterioration magnetic properties of steel.

There are some published studies about statistical analysis and modeling of the shear-cutting process for transformer core steel. Wadi et al. [1] considered different blanking parameters such as neural network methodology and regression analysis in 1999. Baudion et al. [2] studied magnetic degradation on non-oriented electrical steels and blanking parameters in 2003. Peksoz et al.[3] proposed another experimental model for the degradation of magnetic properties of non-oriented electrical steels from the cutting line between grain size and silicon content of materials in 2008. Al-Momami et al. [4] created their statistical data from finite element modeling of the cutting process and implemented a neural network and multiple regression analysis in 2012. Multiple regression analysis was applied, and models were proposed [5] by Bashah et al. for die designers to estimate the spring-back effect in relation to design variables called die radius, punch radius, depth, and weight in 2012.

Models evaluated as capable to predict the spring-back response with high R^2 predicted values and supported by the results of the validation procedure. In another research for regression analysis and modeling, an adaptive response surface modeling was proposed by

Karaoglan et al. [6] and regression coefficients were calculated by supporting of consonant process parameters based on an experimental setup in 2014. A regression model proposed in 2017 by Park et al. [7] for the reconfigurable cold-forming process of thin steel sheets. The effects of clearance, blanking forces, and sheet thickness on burr length were also studied, and a regression model by Cavusoglu et al. [8] was proposed in 2017. Multiple regression analysis and finite element simulation were studied by Badgujar et al. [9] for sheet forming in 2017, also Bohdal et al. [10] studied slitting process parameters and made graphical modeling between process parameters and magnetic properties in 2020.

Another research was issued by Zhao et al. [11] about the usage of nonlinear regression modeling between process parameters in the monitoring of the turning process in 2020. Neseli et al. [12] experienced DOE and RSM for surface roughness and vibration level optimization on cylindrical grinding machinery in 2012. Potanai et al. [13] predicted the temperature of human being buildings by MLR modeling in 2022 and Hanief et al. [14] researched the turning process by process parameters via MLR and ANN in 2016. Lee et al. [15] researched optimized CNC turning processes with DOE, RSM, and ANN tools. The authors presented several regression models for different machine types in 2010. Patel et al., [16] established linear and non-linear multiple regression models on image processing systems to optimize the detection error of surface roughness in 2020.

Guided by previous research, to control the emerging of burr on the mitering process of grain-oriented electrical steels, a simply applicable regression model proposed for burr levels to keep under desired level for the aim of preventing magnetic degradation of electrical steels. Even, the supposed regression model can be useful in process control applications. The presented regression model in this research is useful for

Nihat ÇELİK, Alaaddin TOKTAŞ

Mathematical Modelling of Shear Cutting Process of Grain Oriented Electrical Steels Using Regression ...

keeping burr length which is an indicator of plastic deformation level in the shear cutting process, to keep within limited length thus preventing excessing plastic deformation and magnetic degradation at lower degrees on mitered edges to produce more efficient magnetic cores of transformers. This paper is part of research about building lower no-load loss cores with decreasing shear cutting degradation and recurring them with annealing after cutting.

Materials and methods are presented in the next section, data acquiring methodology is expressed, a quadratic regression analysis is implemented with acquired data for the blanking process, and a model is proposed for process control activities as a conclusion.

2. MATERIALS AND METHODS

Author of this article improved a regression model for shear-cutting process like as some of referenced researcher have already done but only 2 of shear cutting process predictors included and left non-measurable and controllable process parameters out for this specific process.

Sample groups are defined as five different types of industrial GO codes as shown in Table 1. These codes are generic and used for manufacturing the transformer cores in BEST TRANSFORMER COMPANY.

Table 1 Main GOES types used in core production in BEST Transformer

Type Number	Nominal Thickness (μm)	Well-known descriptions
Type1	300	(M5 – 0.30)
Type2	230	(MoH – 0.23)
Type3	270	(NV27S)
Type4	270	(MoH – 0.27)
Type5	300	(M4 – 0.30 PH110)

It is seen in Table 1 that the most frequently consumed steel thickness are 0,23 and 0,30 mm. Additionally, the chemical composition of Fe-Si 3,09% is given in Table 2.

Table 2 Chemical composition of GO steels

Atom.	Si	C	Mn	S	Cu	P	Al	Fe
W%	3.09	0.054	0.072	0.018	0.075	0.015	0.010	Bal.

Typical GOES consist of at most 3.00 - 3.25 Si%, very little C, and other elements, and the rest is ferritic Fe. Typical mechanical properties of GOES blanked in this project are presented in Table 3.

Table 3 Mechanical properties of grain-oriented steel cut samples

Type	Thickness (μm)	Tensile Strength (MPa)	Yielding Strength (MPa)	Elongation (%)	Hardness (Hv1)
Type1	300	361	336	12	205
Type2	230	352	330	12	200
Type3	270	358	333	13	204
Type4	270	358	333	13	204
Type5	300	361	336	12	205

Grain-oriented electrical steel foils are provided as in Table 1 and slit to designed lengths. The slitting process is also very precious and valuable for plastic deformation evaluation and has an important influence on the magnetic properties of the stacked core. For the current study, slitting is not in scope. Slitted foils loaded to mitering machinery to get mitered laminations. Both ends of laminations are mitered such that α is 45º and symmetrically as shown in Figure 1. The dimensions of laminations are defined as $L_1 = 300$ mm, $L_2 = 180$ mm, and $W = 60$ mm. Because the diving angle of the upper blade changes about ($2.0 \approx 2.5º$), thorough W emerged BL may show gradient. So, 3 different BL measuring points were selected for each cutting side and the maximum value was considered to represent the BL value of ends.
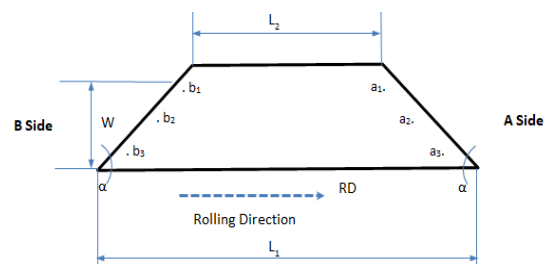
Figure 1 Main size of thin sheet GO lamination mitered at GEORG TBA400

Nihat ÇELİK, Alaaddin TOKTAŞ

Mathematical Modelling of Shear Cutting Process of Grain Oriented Electrical Steels Using Regression ...

The shear-cutting process executed in GEORG TBA 400 tried to be modeled with some of the process variances. Classical shear-cutting process parameters as the hardness of the steel sheet, the kinematic energy level of the upper blade (i.e., the velocity of upper blades), cutting forces occurring during diving of blades into the sheet, applied forces by upper blade holder, diving angle of upper blades, stroke of blades and a vertical clearance of blades are omitted in the model because of these process parameters are not possessing control ability or strictly kept as constant by machinery producer. Instead of these physical shear-cutting process parameters, direct or indirect process variables are chosen for modeling the critical output of the process.

BL is very critical in core building and expected that should be kept under crucial limits to ensure total no-load losses of the core as calculated level, this could be by minimizing of magnetic degradation of steel during mitering. Figure 2 shows how burr formed in shear cutting process.
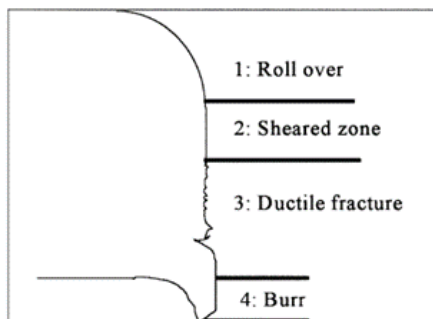
Figure 2 Surface profile after shear cutting process

Magnetic degradation is resulting from plastic deformation on mitered corners where flux movement is subject to change in vectorial direction in the core structure. Because of that, *BL* is considered a conclusive dependent variable of this special blanking process.

As shown in Figure 3 horizontal clearance of blades between the upper blade and lower blades is also another important parameter of the blanking process. In this case, as a main

setting parameter of machinery, horizontal clearance of blades is always kept under limited values
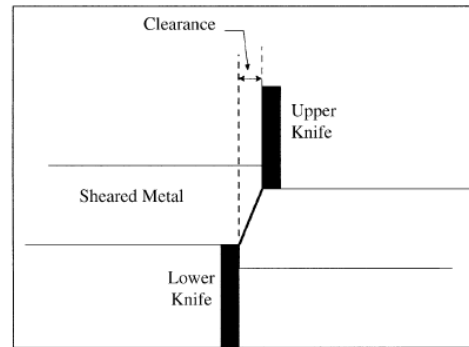
Figure 3 Simple presentation of horizontal clearance between blades

with Go & NoGo gages; preset values of the machine were 10 µm shims might be Go but 20 µm might be NoGo gages. Because of the very narrow adjustment gap and, not having any fine-tuning ability in the setup of machinery, horizontal clearance of blades is accepted as a constant parameter of the process. Although, the thickness of sheet lamination may vary regarding the chosen type of steel. As shown in Table 1, there are three different thicknesses of sample groups that show different effects regarding the horizontal clearance of blades. This means, all other conclusions accepted as immeasurable results of the process alike morphology of cut surface, plastic strains achieved during cutting, length of DAZ, and dislocation gradient near cut surface, all would be admissible that count on sheet thickness. Direct control of the horizontal clearance ratio of blades is not possible because of machinery stationary setup, but indirect effects can be representable by changing sheet thicknesses. Because of that, another independent variable of the shear-cutting process is chosen as Sheet Thickness *ST*.

The last independent variable would have been indicator of wearing oof blades. All blades are expected to have a sharp edge profile initially. By the time, after a working period, blades can get worn. During the process, there is no possibility for direct

measuring of the blunting level of blades. When a sharpened or original blade is fixed to the blade holders, fixing dates are recorded and counts of hits can be recorded automatically. So, the researcher can get the count of hits CH to show the blunting level of blades till than initial fixing date to the measuring day. In this study, CH values represent the wearing level of blades and accepted an independent variable CH_A for A side blade and CH_B for B side of blades.

Mitered cut sample geometry is shown in Figure 1. Data of samples were collected as shown in Table 4 and Table 5, such that different CH values for different blades were collected to present different wearing levels of blades.

In a summary, the dependent variables of the blanking process are defined as burr length BL, as the first independent variable is sheet thickness ST and the second one is counts of hits CH. With these 3 variables, experimental runs are performed. The experimental runs are given in Table 5 and summarized in Table 6. Different trades of grain-oriented electrical steels Type1 to Type5 were cut at 4 different dates with different counts of hits values of blades. 20 pieces produced from each type of grade at once. Both sides of the blades (A side and B side) were considered individually and CH values were recorded to represent the wearing level of the blades. Actual thickness values of samples were recorded as ST values by 3 points in each mitered edge along the width, W. Measurement of sheet thicknesses and BL of cut samples executed by a micrometer within 1 μm scale.

Table 4 Experimental setup; CH values of blades, dates, sample types and group numbers

| Type Nu. | Counts of Hits CH | | Fixing Date of Blades | | Group Nu. |
	A Side Blade CH_A	B Side Blade CH_B	A Side	B Side	
Type1	69520	586753	02.04.20	22.02.20	1
Type2	69542	586801	02.04.20	22.02.20	1
Type3	69563	586825	02.04.20	22.02.20	1
Type4	69586	586846	02.04.20	22.02.20	1
Type5	69607	686867	02.04.20	22.02.20	1
Type1	179132	668567	02.04.20	22.02.20	2
Type2	179154	668588	02.04.20	22.02.20	2
Type3	179176	668603	02.04.20	22.02.20	2
Type4	179198	668630	02.04.20	22.02.20	2
Type5	179220	668651	02.04.20	22.02.20	2
Type1	203727	642597	19.01.21	28.10.20	3
Type2	203751	641979	19.01.21	28.10.20	3
Type3	203775	642001	19.01.21	28.10.20	3
Type4	203779	642023	19.01.21	28.10.20	3
Type5	203823	642045	19.01.21	28.10.20	3
Type1	429935	90466	19.01.21	15.02.21	4
Type2	429958	90487	19.01.21	15.02.21	4
Type3	429980	90508	19.01.21	15.02.21	4
Type4	430002	90529	19.01.21	15.02.21	4
Type5	430024	90550	19.01.21	15.02.21	4

Nihat ÇELİK, Alaaddin TOKTAŞ

Mathematical Modelling of Shear Cutting Process of Grain Oriented Electrical Steels Using Regression ...

Table 5 *BL* and *ST* Measuring from GEORG TBA 400

| | | A Side of blades | | | | | | | | B Side of blades | | | | | | | |
| | | N_1 | | | | N_{20} | | | | N_1 | | | | N_{20} | | | |
Group	Type	ST values	$ST_{avg.}$	BL values	$BL_{max.}$	ST values	$ST_{avg.}$	BL values	$BL_{max.}$	ST values	$ST_{avg.}$	BL values	$BL_{max.}$	ST values	$ST_{avg.}$	BL values	$BL_{max.}$
Group 1	Type1	284		0		282		0		285		6		284		8	
		285	284	2	2	284	283	2	2	285	285	8	8	283	283	8	8
		282		1		282		1		284		1		282		1	
	Type2	224		1		225		3		224		7		224		12	
		225	223	1	1	224	224	3	3	224	224	11	11	223	224	11	12
		220		1		224		2		224		1		224		0	
	Type3	260		1		258		1		259		2		255		13	
		261	260	2	2	256	257	2	2	260	259	2	2	258	257	10	13
		259		1		257		1		257		1		258		1	
	Type4	265		5		263		2		266		7		264		8	
		265	266	2	5	264	264	1	2	267	267	5	7	264	264	6	8
		267		0		264		1		267		2		265		1	
	Type5	288		1		285		4		288		10		285		8	
		287	287	2	2	285	284	1	4	288	288	0	10	285	284	2	8
		286		2		283		2		287		2		283		1	
Group 2	Type1	288		6		289		0		288		10		289		11	
		287	286	0	6	288	288	1	1	287	287	10	10	288	288	8	11
		284		0		286		1		285		2		288		2	
	Type2	224		1		223		1		222		11		222		12	
		224	224	0	1	222	222	0	1	223	222	18	18	223	222	14	14
		223		1		222		0		222		2		222		2	
	Type3	256		3		260		1		257		13		257		11	
		256	256	1	3	257	258	1	1	259	258	3	13	256	256	11	11
		256		0		258		0		257		3		256		3	
	Type4	267		3		265		1		266		7		266		5	
		268	267	1	3	266	266	1	1	266	266	6	7	267	266	5	5
		267		1		266		0		265		1		266		2	
	Type5	287		1		284		2		287		13		288		12	
		287	287	1	1	286	285	1	2	286	286	9	13	287	287	6	12
		287		0		285		1		286		4		286		1	
Group 3	Type1	297		7		295		4		297		10		294		10	
		298	298	1	7	294	295	1	4	299	299	5	10	297	295	3	10
		300		2		297		3		301		1		295		5	
	Type2	227		6		227		7		224		11		226		6	
		224	225	4	6	228	227	4	7	224	224	14	14	227	227	10	10
		223		3		225		3		224		5		228		8	
	Type3	258		9		260		12		260		13		260		15	
		259	258	2	9	282	268	4	12	257	259	2	13	260	260	9	15
		258		1		262		1		260		7		261		2	
	Type4	259		10		261		9		261		16		260		10	
		258	259	2	10	261	260	7	9	258	259	1	16	260	260	3	10
		259		1		258		2		258		11		260		1	
	Type5	287		5		290		6		286		7		288		10	
		285	286	3	5	289	289	3	6	286	286	7	7	287	287	1	10
		285		2		289		2		287		2		287		1	
Group 4	Type1	290		1		293		2		287		1		291		1	
		288	287	1	4	290	290	3	3	286	286	1	1	287	287	1	1
		282		4		288		1		286		1		283		1	
	Type2	228		3		226		1		228		2		225		2	
		229	228	6	6	227	226	4	4	227	227	2	2	225	225	1	2
		227		1		226		2		226		1		224		1	
	Type3	259		3		259		3		254		4		260		2	
		256	257	3	3	260	260	5	5	253	254	1	4	260	260	2	3
		255		3		262		1		255		3		259		3	
	Type4	265		1		259		1		261		1		260		2	
		259	262	6	6	257	258	1	4	261	261	2	2	260	259	2	2
		261		3		257		4		261		2		258		2	
	Type5	289		1		288		4		289		2		292		1	
		287	287	1	2	289	288	1	4	289	289	1	2	290	290	2	2
		286		2		288		2		288		2		289		2	

As mentioned before, the maximum value of measuring is recorded to represent *BL* values in regression analysis. So, 240 different *BL* and 240 different *ST* measurements are

Nihat ÇELİK, Alaaddin TOKTAŞ

Mathematical Modelling of Shear Cutting Process of Grain Oriented Electrical Steels Using Regression ...

recorded in Table 5. On the other hand, an average of 8 different *CH* values is recorded in Table 4.

This research was executed for exploring a regression model for defined process variances. For this purpose, the General Full Quadratic Regression model is applied as given in Equation (1) below. The β vector which is composed of the parameters of the regression mode is given in Equation (2). Finally, the calculation of the β vector and the definitions of Y and X matrices are given in Equations (3) and (4), respectively:

$$Y_u = \beta_0 + \sum_{i=1}^{n1} \beta_i X_{iu} + \sum_{i=1}^{n} \beta_{ii} X_{iu}^2 + \sum_{i<j}^{n} \beta_{ij} X_{iu} X_{ju} + e_u \tag{1}$$

$$\beta^T = [\beta_0, \beta_1, \beta_2, \dots, \beta_n] \tag{2}$$

$$\beta = (X^T X)^{-1} (X^T Y) \tag{3}$$

$$Y = \begin{bmatrix} y_1 \\ y_2 \\ y_3 \\ \dots \\ y_N \end{bmatrix} \quad X = \begin{bmatrix} 1 & x_{11} & x_{21} & x_{11}^2 & x_{21}^2 & x_{11} x_{21} \\ 1 & x_{12} & x_{22} & x_{12}^2 & x_{22}^2 & x_{12} x_{22} \\ 1 & x_{13} & x_{23} & x_{13}^2 & x_{23}^2 & x_{13} x_{23} \\ & & & \dots & & \\ 1 & x_{1N} & x_{2N} & x_{1N}^2 & x_{2N}^2 & x_{1N} x_{2N} \end{bmatrix} \tag{4}$$

As described above, the variance of the shear-cutting process is defined as Sheet Thickness (*ST*) and Counts of Hits of blades (*CH_A* and *CH_B*.). Accepting with initial conditions of the blade are identic, and all other cutting parameters of blades are stationary, intact, and the only parameter that can be observed is the Count of Hits, values of *CH_A* and *CH_B* integrated as *CH*. Also, in the same manner, the researcher integrated *BL_A* and *BL_B* as if one variance *BL*.

For *ST* spot checks, an average of 3 points along mitered edge *W* is accepted to represent actual *ST* values as shown in Figure 1. All *BL* and *ST* checks were recorded from the first sample of N_1 and the last sample of N_{20} of the sample groups. Table 6 shows the combined measuring of variances produced by merging and simplifying of Tables 4 and 5. Some of the rows which have responded values very close to each other are extracted from main

Table 6. So the modeled number of rows decreased to 17.

Table 6 Summarize of measurements

CH	ST	BL
179164	223.0	7
179208	266.5	3
203761	225.7	7
429945	288.5	4
429990	258.5	5
430012	259.7	6
430024	287.8	4
586763	283.8	8
586811	223.8	12
586856	265.5	8
668577	287.5	11
669613	257.0	13
642607	297.2	10
641989	225.5	14
642055	286.8	10
90518	256.8	4
90560	289.5	2

3. RESULTS AND DISCUSSIONS

By running the Equations (1-4) through the data presented in Table 6, the regression equation for *BL* is calculated. For this, the Minitab statistical package is used. The calculated model is presented in Equation (5):

$$BL = 72{,}0602852442791 - (0{,}000029801809832 x CH) - (0{,}42722756659429 x ST) + (0{,}00000000004238 \ x CH^2) + (0{,}00065412941627 x ST^2) + (0{,}00000004535513 x ST x \ CH) \tag{5}$$

Equation (6) is used to calculate the R^2 value (which is used to determine if the factors are adequate to represent the change in the response):

$$R^2 = \frac{\beta^T X^T Y - n\overline{Y}^2}{Y^T Y - n\overline{Y}^2} \tag{6}$$

From the equation, R^2 is calculated as 0.9896 (which is very close to 1) and this means *CH* and *ST* is seems too sufficient to explain the

Nihat ÇELİK, Alaaddin TOKTAŞ

Mathematical Modelling of Shear Cutting Process of Grain Oriented Electrical Steels Using Regression ...

variation at *BL* and cannot need to use additional blanking process parameters.
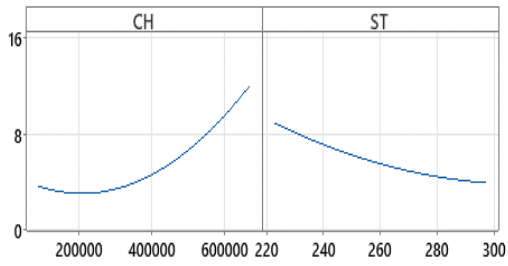
Figure 4 How *BL* changes one of *CH* and *ST*

Figure 4 shows that no multicollinearity effect on the model. Each variance varies response with different affection ratios.
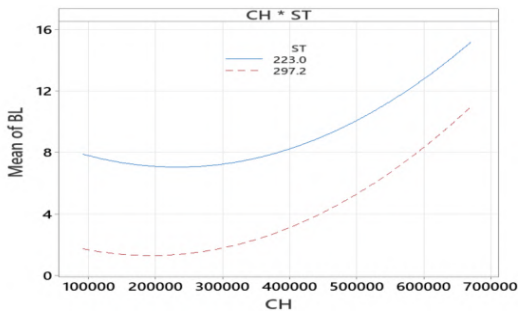
Figure 5 How *BL* changes with *CH*ST* and *ST*

Figure 5 shows how *BL* changes with the setting of *CH* separately and the interactions of *CH*ST*.

Figure 6, Residuals vs Fitted values scattering plots shows no clustering and heteroscedasticity on change of variance. No constant variance scattering plot was observed from residuals vs fitted values. Only one observation (Row 10) shows us a large residual. Scattering around zero seems random.
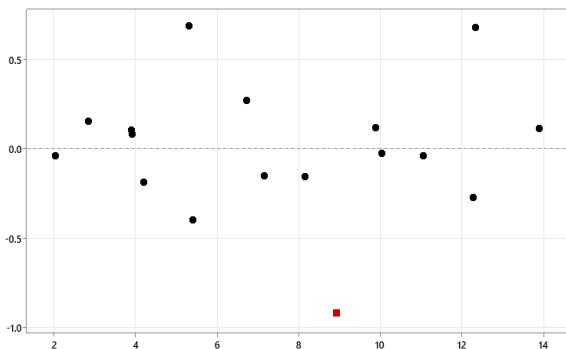
Figure 6 Residuals vs Fitted values
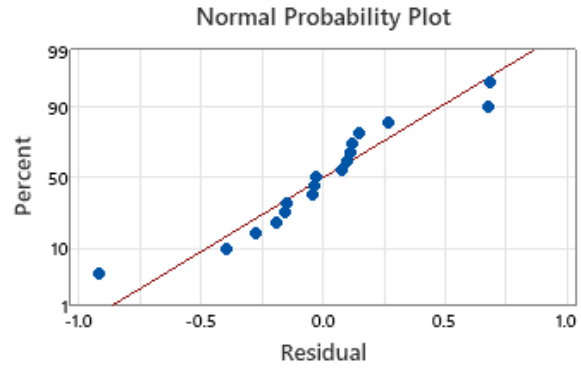
Figure 7 Normal probability plot
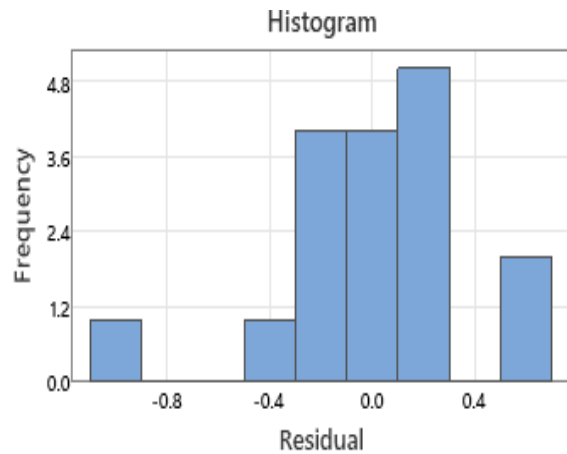
Figure 8 Histogram of residuals about normal

Figure 7 shows normal probability plot of residuals and Figure 8 shows the normal distribution of residuals. Finally, Analysis of Variance (ANOVA) is performed using Minitab. The ANOVA results are summarized in Table 7.

P value is found very smaller than (0.000<0.05) which means the model is significant at a 95% confidence level. Verification of calculated results with experimentally measured values is given in Table 7.

As is seen from Table 8, the maximum residual value is -0.91729937, and the maximum absolute deviation ratio is 12.9%. and the average percentage of residuals can be calculated as 3.35%.

Nihat ÇELİK, Alaaddin TOKTAŞ

Mathematical Modelling of Shear Cutting Process of Grain Oriented Electrical Steels Using Regression ...

Table 7 Analysis of Variance

Source	DF	Adj SS	Adj MS	F-Value	P-Value
Model	5	212.006	42.401	209.25	0.000
Linear	2	159.066	79.533	392.50	0.000
CH	1	138.386	138.386	682.94	0.000
ST	1	42.287	42.287	208.69	0.000
Square	2	30.325	15.163	74.83	0.000
CH*CH	1	26.164	26.164	129.12	0.000
ST*ST	1	1.763	1.763	8.70	0.013
2-Way Interaction	1	0.918	0.918	4.53	0.057
CH*ST	1	0.918	0.918	4.53	0.057
Error	11	2.229	0.203		
Total	16	214.235			

Table 8 Matching of experimental and calculated results of the model

CH	ST	BL	Fitted BL	Residuals	Residuals (%)
179164	223.0	7	7.15110295	-0.15110295	-2.11%
179208	266.5	3	2.84861529	0.15138471	5.31%
203761	225.7	7	6.73000941	0.26999059	4.01%
429945	288.5	4	3.89818487	0.10181513	2.61%
429990	258.5	5	5.39656857	-0.39656857	-7.35%
430012	259.7	6	5.31446752	0.68553248	12.90%
430024	287.8	4	3.92126833	0.07873167	2.01%
586763	283.8	8	8.15850585	-0.15850585	-1.94%
586811	223.8	12	12.27467597	-0.27467597	-2.24%
586856	265.5	8	8.91729937	-0.91729937	-10.29%
668577	287.5	11	11.04108672	-0.04108672	-0.37%
669613	257.0	13	12.32334083	0.67665917	5.49%
642607	297.2	10	9.88155331	0.11844669	1.20%
641989	225.5	14	13.88728650	0.11271350	0.81%
642055	286.8	10	10.02789691	-0.02789691	-0.28%
90518	256.8	4	4.18961699	-0.18961699	-4.53%
90560	289.5	2	2.03852059	-0.03852059	-1.89%

When the model applies to process control of wearing level of blades can be predicted without any other measure and the burr length of mitered coils will have kept under the desired level.

4. CONCLUSION

The shear-cutting process is very a critical stage of the transformer core production process. Observations on GEORG TBA 400 model cut-to-length blanking machinery in BEST Transformer have been made and data recorded for optimizing burr length. As variable of burr length represents the plastic deformation level of mitered laminations. Burr lengths should be under control and limited range regarding IEC 60604-02. When a regression model occurred for the blanking process, dependent and independent variables process chosen as mentioned above, a meaningful model derived with $R^2 = 0.9896$ and model proposed for practice process control beneficial. For the next step of the study, the selection type of predictor variances and observation method of independent variables can be improved; wearing level of blades values can be derived by optical inspections. Further, for a more precious model, hardness and type of laminations can also join the observations. Hopefully, producing more efficient power transformer cores and reducing no-load losses of transformers in the grid will complement additional value and motivation to the next generations.

A mathematical process control model based on regression analysis can be raised to get useful and confidential process control activities for the traditional process shear-cutting process. Predictors observed physically and known experientially might be in the model.

Authors' Contribution
The authors contributed equally to the study.

Nihat ÇELİK, Alaaddin TOKTAŞ

Mathematical Modelling of Shear Cutting Process of Grain Oriented Electrical Steels Using Regression ...

The Declaration of Ethics Committee Approval

This study does not require ethics committee permission or any special permission.

The Declaration of Research and Publication Ethics

The authors of the paper declare that they comply with the scientific, ethical, and quotation rules of SAUJS in all processes of the paper and that they do not make any falsification of the data collected. In addition, they declare that Sakarya University Journal of Science and its editorial board have no responsibility for any ethical violations that may be encountered and that this study has not been evaluated in any academic publication environment other than Sakarya University Journal of Science.

REFERENCES

[1] I. Wadi, R. Balendra, "Using neural networks to model the blanking process," Journal of Materials Processing Technology, vol. 91, no. 1, pp. 52–65, Jun. 1999.

[2] P. Baudouin, M. de Wulf, L. Kestens, Y. Houbaert, "The effect of the guillotine clearance on the magnetic properties of electrical steels," Journal of Magnetism and Magnetic Materials, vol. 256, no. 1–3, pp. 32–40, Jan. 2003.

[3] A. Peksoz, S. Erdem, N. Derebasi, "Mathematical model for cutting effect on magnetic flux distribution near the cut edge of non-oriented electrical steels," Computational Materials Science, vol. 43, no. 4, pp. 1066–1068, Oct. 2008.

[4] E. S. Al-Momani, A. T. Mayyas, I. Rawabdeh, R. Alqudah, "Modeling blanking process using multiple regression analysis and artificial neural networks," Journal of Materials Engineering and Performance, vol. 21, no. 8, 2012.

[5] N. A. K. Bashah, N. Muhamad, B. Md Deros, A. Zakaria, S. Ashari, A. Mobin, M. S. M. A. Lazat, "Multi-regression modelling for spring-back effect on automotive body in white stamped parts," Materials and Design, vol. 46, pp. 175–190, Apr. 2013.

[6] A. D. Karaoglan, N. Celik, "A new painting process for vessel radiators of transformer: wet-on-wet," Journal of Applied Statistics, vol. 43, no. 2, pp. 370–386, 2016.

[7] J. Park, M. Kil, J. Kim, B. Kang, "A Predictive Model of Flexibly-reconfigurable Roll Forming Process using Regression Analysis" Procedia Engineering, pp. 1266–1271, 2017.

[8] O. Cavusoglu, H. Gürün, "The relationship of burr height and blanking force with clearance in the blanking process of AA5754 aluminium alloy," Transactions of Famena, vol. 41, no. 1, pp. 55–62, 2017.

[9] T. Y. Badgujar, V. P. Wani, "Stamping Process Parameter Optimization with Multiple Regression Analysis Approach," in Materials Today: Proceedings, Elsevier Ltd, 2018, pp. 4498–4507.

[10] L. Bohdal, R. Patyk, K. Tandecka, S. Gontarz, D. Jackiewicz, "Influence of shear-slitting parameters on workpiece formation, cut edge quality and selected magnetic properties for grain-oriented silicon steel," Journal of Manufacturing Process, vol. 56, pp. 1007–1026, Aug. 2020.

[11] T. Zhou, L. He, Z. Zou, F. Du, J. Wu, P. Tian, "Three-dimensional turning force prediction based on hybrid finite element and predictive machining theory considering edge radius and nose radius," Journal of Manufacturing Process, vol. 58, pp. 1304–1317, 2020.

Nihat ÇELİK, Alaaddin TOKTAŞ

Mathematical Modelling of Shear Cutting Process of Grain Oriented Electrical Steels Using Regression ...

[12] S. Neseli, I. Asilturk, L. Celik, "Determining the optimum process parameter for grinding operations using robust process," Journal of Mechanical Science and Technology, vol. 26, no. 11, pp. 3587–3595, 2012.

[13] Z. Patonai, R. Kicsiny, G. Géczi, "Multiple linear regressionbased model for the indoor temperature of mobile containers," Heliyon, vol. 8, no. 12, Dec. 2022.

[14] M. Hanief, M. F. Wani, M. S. Charoo, "Modeling and prediction of cutting forces during the turning of red brass (C23000) using ANN and regression analysis," Engineering Science and Technology, an International Journal, vol. 20, no. 3, pp. 1220–1226, 2017.

[15] H. W. Lee, W. T. Kwon, "Determination of the minute range for RSM to select the optimum cutting conditions during turning on CNC lathe," Journal of Mechanical Science and Technology, vol. 24, no. 8, pp. 1637–1645, 2010.

[16] D. R. Patel, M. B. Kiran, V. Vakharia, "Modeling and prediction of surface roughness using multiple regressions: A noncontact approach," Engineering Reports, vol. 2, no. 2, Feb. 2020.

Title: Venom Peptides of Crotalus atrox Against SARS-Cov-2 Spike Protein and Human ACE2 Receptor by Molecular Docking Analysis

Authors: Suleyman ILHAN

Venom Peptides of *Crotalus atrox* Against SARS-Cov-2 Spike Protein and Human ACE2 Receptor by Molecular Docking Analysis

Suleyman ILHAN [*1] iD

Abstract

Venoms are composed of about 100 to 500 pharmacologically active compounds. Less than 0.01% of these compounds have been identified and a significant majority of them act on unknown receptors. Here, the potential Severe Acute Respiratory Syndrome Coronavirus 2 (SARS-CoV-2) activities of selected *Crotalus atrox* venom peptides (CVPs) including Atrolysin D (AD), vascular apoptosis-inducing protein-1 (VAIP-1), Catrocollastatin (CC), and Calcium-Free Phospholipase A2 (CFP) were investigated via molecular docking analysis. CVPs were docked against human angiotensin-converting enzyme-2 (ACE-2) and 3-chymotrypsin-like protease (3CLpro) viral spike protein. All CVPs had low binding energies to both 3CLpro and ACE2, suggesting that they interacted strongly with the active sites of enzymes, compared to the reference drugs lopinavir and ritonavir. The binding energy of 3CLpro was -139.517 kcal/mol, -96.239 kcal/mol, -121.590 kcal/mol, -259.424 kcal/mol with AD, VAIP-1, CC, and CFP, respectively. CFP showed a very strong binding activity with 3CLpro, suggesting that it could be a very effective compound in inhibiting the SARS-CoV-2 virus. The binding energy of ACE2 was -101.165 kcal/mol, -73.064 kcal/mol, -106.918 kcal/mol, -82.830 kcal/mol with AD, VAIP-1, CC, and CFP, respectively. AD made a much stronger bond with ACE2 than reference drugs, showing that it could be used as a virus-protective component in humans. The results suggest a potential drug candidate for the development of therapeutics against Coronavirus disease 2019 (COVID-19). *In vitro* and *in vivo* experiments are needed to confirm these compounds' potential preventive and therapeutic effects.

Keywords: Crotalus atrox venom, COVID-19, SARS-CoV-2, 3CLpro, ACE-2.

1. INTRODUCTION

Many people have died as a result of the breakout and quick spread of the coronavirus disease 2019 (COVID-19) epidemic brought on by the SARS-CoV-2 coronavirus. New mutations have emerged, extending to the disease's complexity. According to estimates from the World Health Organization, the SARS-CoV-2 epidemic killed more than 6 million people and infected more than 700 million individuals across many different nations. As a result, the fight to stop this epidemic has spread globally. The COVID-19 epidemic continues to represent a serious threat to humanity despite several

* Corresponding author: suleyman.ilhan@cbu.edu.tr (S. ILHAN)
[1] Manisa Celal Bayar University
ORCID: https://orcid.org/0000-0002-6584-3979

Suleyman ILHAN

Venom Peptides of Crotalus atrox Against SARS-Cov-2 Spike Protein and Human ACE2 Receptor by Molecula...

vaccinations and pharmacological treatment attempts because of the weakened immune system.

Angiotensin-converting enzyme, also known as ACE, produced on the surface of host cells is bound by spike protein (glycoprotein S) by the SARS-CoV-2 virus, which preferentially targets lung cells [1]. Angiotensin-converting enzyme I (ACE-I) and angiotensin-converting enzyme II (ACE-II) are both enzymes that are involved in the production of angiotensin. ACE-II found in the human body is involved in controlling blood pressure by converting angiotensin I to angiotensin II. It has been determined that SARS-CoV-2 in humans uses ACE2 as its cellular entrance receptor [2].

The viral particle that gets inside the cell is not encoded, and when the -coronavirus genome is transcribed, it often results in an 800 kDa polypeptide. Pp1a and pp1ab in ORF1a and ORF1b are prepared for polyprotein synthesis [3]. These polyproteins are proteolytically broken down into a variety of proteins by the enzymes papain-like protease (PLpro) and 3-chymotrypsin-like protease (3CLpro). 3CLpro can cleave the polypeptide at various sites into 16 different nonstructural polypeptides to produce various proteins involved in viral genome replication and transcription [4]. 3′ terminus of the gene, which exhibits extreme polymorphism, contains 3CLpro, which is crucial for the replication of viral particles. It is also thought to be a key target for halting the spread of the illness by obstructing the viral polyprotein's active cleavage sites. This information on SARS-CoV-2 has led to the acceptance of ACE2 and 3CLpro as prospective targets for the creation of antiviral medications [4].

There are many studies ongoing to search for new vaccines/drugs for COVID-19. Researchers from around the world are working together to accelerate the development of potential treatments and vaccines for the virus. Many organizations, including the WHO, and the National Institutes of Health are dedicated to researching new treatments and vaccines for the virus. Natural compounds (herbs, spices, and medicines made from animals) are the richest source of reference for the search for anti-viral molecules [5–8]. Plants are investigated because of their high antioxidant and immune-enhancing effects, and animal venoms are also investigated because they contain active compounds with different mechanisms of action. Among the natural compounds, snake venoms are a source of potentially helpful therapeutic chemicals because of their biological activities [9, 10]. They might contain substances useful in the design or development of pharmaceuticals, leading to the identification of novel proteins and protein families. *Crotalus* sp. belongs to the family of pit vipers. They are venomous and are typically found in parts of North, Central, and South America. They have a distinctive rattle at the end of their tail that they use as a warning signal when they feel threatened. *C. atrox*, also known as the western diamondback rattlesnake, is a venomous species of rattlesnake. The venom of *C. atrox* consists of several proteins including phospholipases A2, C-type lectins, metalloproteinases, hyaluronidase, and bradykinin-potentiating peptides. These proteins have various effects on prey such as paralysis, pain, and hemorrhagic activity. Since the venom proteins of *C. atrox* have a wide variety of protein cocktails, it is conceivable whether there is an interaction between the spike protein of COVID-19, which may be relevant in evaluating potential therapeutic treatments.

A computer method called molecular docking is used to estimate the interactions between two molecules, usually small molecules like pharmaceuticals. The two molecules must fit into a binding site, and the fit is then evaluated by evaluating the energies of their interactions [11]. It is a research method that fuses physical and chemical principles with complex computational algorithms to provide a useful tool for analyzing the source and mechanism of potential new compounds [12].

Suleyman ILHAN

Venom Peptides of Crotalus atrox Against SARS-Cov-2 Spike Protein and Human ACE2 Receptor by Molecula...

Therefore, to comprehend the underpinnings of COVID-19, computational research to shed light on snake venom protein interactions would be useful.

In this study, the interactions of *C. atrox* venom peptides (CVPs) Atrolysin D (AD), vascular apoptosis-inducing protein-1 (VAIP-1), Catrocollastatin (CC), and Calcium-Free Phospholipase A2 (CFP) with 3CLpro and ACE2 receptors were investigated, and potential anti-viral molecules targeting SARS-CoV-2 were explored.

2. MATERIALS AND METHODS

2.1. Receptor Preparation

The SARS-CoV-2 main protease 3CLpro (PDB ID: 6LU7) and ACE2 (PDB ID: 1R42) were chosen as receptors. The protein databank's PDB format was used to download the three-dimensional (3D) structures of the 3CLpro and ACE2 proteins (https://www.rcsb.org/). The load distribution, hydrogenation, and water removal processes all made use of the PyMOL software. Then, using MG Tools by AutoDock Vina program, hydrogen atoms were added to the acceptor molecule [13]. For future investigations, the structure was saved in PDB format.

2.2. Ligand Preparation

Identified snake venom proteins' three-dimensional structure were retrieved in PDB format from PubChem: Atrolysin D (PDB ID: 1ATL), vascular apoptosis-inducing protein-1 (PDB ID: 2ERO), Catrocollastatin (PDB ID: 2DW2), Calcium-Free Phospholipase A2 (PDB ID: 1PP2). Autodock Vina 4.2.5.1 software was used for water removal, hydrogenation, and adjusting the load distribution.

2.3. Molecular Docking

Computational Docking uses statistical and machine-learning methods to predict the interaction between molecules. It can be used to visualize and study protein-ligand interactions, design novel drugs, and predict drug effectiveness. By using Autodock Vina, high throughput molecular docking was performed. The grid center for 3CLpro was set as X= 21.41, Y=3.62 and Z=21.94 with dimensions of the grid box 60 A˚× 60 A˚× 60 A˚. The grid center for ACE2 was set as X=19.81, Y=-5.57 and Z=14.73 with the grid box 60 A˚× 60 A˚× 60 A˚. After calibration and optimization, the same grid box size and other parameters were applied to the docking experiments of all four proteins, and the entire setup was performed to generate different docked conformations. To see how molecules' secondary structures resembled, PyMOL was utilized.

3. RESULTS AND DISCUSSION

A computational technique called *in silico* docking is used to anticipate the binding affinity of a small molecule drug to a target protein. *In silico* docking can be used to find possible small molecule inhibitors for antiviral drug development that can attach to viral proteins and interfere with their function, reducing viral reproduction and infection. Snake venoms are produced in venom glands and contains several proteins, enzymes, and peptides with various biological activity. While the majority of a snake's venom is utilized for defense and predation, some of the venom's components have been discovered to have medicinal qualities and are used as medications for a variety of medical disorders. Some examples of drugs developed from snake venom can be listed as anti-venoms, blood pressure medications, pain medications, anti-cancer agents and neurological medications [9]. Overall, drugs obtained from snake venoms have great potential for treating a variety of medical conditions. Here, to explore a possible therapeutic target for COVID-19 disease, 3CLpro and human ACE-2 receptors were docked with CVPs using *in silico* methods. Since hydrogen bonds (H-bonds) and steric interactions (such as Van der Waals

Suleyman ILHAN

Venom Peptides of Crotalus atrox Against SARS-Cov-2 Spike Protein and Human ACE2 Receptor by Molecula...

interactions) are vital for ligand-target protein interactions and binding affinity, we investigated the binding affinity of the venom between the SARS-CoV-2 target protein 3CLpro and human ACE2. PubChem CID, molecular formula and 2D protein structures of the venom were obtained from the PubChem library database. The binding energies, H-bond interaction scores and amino acid interactions with 3CLpro and ACE2 ligands are presented in Table 1.

All CVPs had low binding energies to 3CLpro, suggesting that they interacted strongly with the enzyme's active sites. The binding energies of these CVPs ranged from -96.239 to -259.424 kcal/mol for 3CLpro which were comparable with the binding energies of reference drugs lopinavir (-126,713 kcal/mol) and ritonavir (-108,731 kcal/mol). The binding energy of 3CLpro was -139.517 kcal/mol, -96.239 kcal/mol, -121.590 kcal/mol, -259.424 kcal/mol with AD, VAIP-1, CC, and CFP, respectively (Table 1). The most prominent binding energy values were calculated as -139.517 kcal/mol for AD and -259.424 kcal/mol for CFP, which were lower than the reference drugs lopinavir and ritonavir, indicating a strong binding affinity. CFP is a human neutrophil-calcium modulating protein isolated from *C. atrox* venom [14]. Although its biological activities have not been studied much, it has many interesting properties such as heat stability, activity on non-aqueos and lipid molecules. CFP showed a very strong binding activity with 3CLpro, suggesting that it can also be very effective in virus. CFP also formed hydrogen interaction with Cys29, and steric interactions with Asp49 and Phe5 (Figure 1A-B). AD is a hemorrhagic metalloproteinase isolated from *C. atrox* venom. It is a reprolysin subfamily of zinc metalloproteinases and is an effective inhibitor of platelet aggregation [15]. AD had high binding affinity with 3CLpro and formed hydrogen interactions with Arg167, Gly169, Glu143 and Pro168. It also formed steric interactions with Val138, Leu170, His142, Leu108, Arg167 and Glu143 (Figure 1C-D). CC is another peptide isolated from *C. atrox* venom, is an inhibitor of collagen-induced platelet aggregation prothrombin activator [16]. It had a -121.590 kcal/mol binding energy which was lower than reference drug Ritonavir. It formed hydrogen interactions with Leu447, Ala479, Cys 481 and steric interactions with Glu480 (Figure 2A-B). VAIP-1 is an apoptosis-inducing peptide that target vascular endothelial cells and has the lowest binding energy with 3CLpro [17]. It formed hydrogen interactions with His18 and Arg13, and steric interactions with Gln16 and Arg13 (Figure 2C-D). All CVPs also displayed low values of binding energy to ACE2. These CVPs had binding energies that varied from -73.064 to -106.918 kcal/mol (Table 1). All tested CVPs had binding energies with ACE2 higher or similar to the reference drugs Lopinavir (-80.524 kcal/mol) and Ritonavir (-73.550 kcal/mol).

Suleyman ILHAN

Venom Peptides of Crotalus atrox Against SARS-Cov-2 Spike Protein and Human ACE2 Receptor by Molecula...

Table 1 Interaction of the SARS-CoV2 Main Protease 3CLpro with *C. atrox* venom proteins.

Protein name	Ligand	Docking Score (Binding Energy, Kcal/mol)	H Bond	Amino acid Residue	
Atrolysin D	3CLPro	-139.517	-8.573	Val138, Arg167, Gly169, Thr139, Leu108,	Leu170, Ile165, His142, Glu143, Pro168
	ACE2	-101.165	-9.278	Gly109, Thr139, Tyr176, Ile165, Gly169, Pro168	Glu143, Cys164, Val138, Arg167, Leu170,
Vascular Apoptosis-Inducing protein-1	3CLPro	-96.239	-6.138	Glu480, Ala479, Glu445	Cys481, Leu447,
	ACE2	-73.064	-9.247	Asp582, Met585	Leu587,
Catrocollastatin	3CLPro	-121.590	-8.440	Asp416, Gly442,	Glu407, Asn425
	ACE2	-106.918	-6.147	Gln424, Cys417, Asp416	Asn422, Glu407,
Calcium-Free Phospholipase A2	3CLPro	-259.424	-5.00	Cys29(R), Asp49(R), His48(R), Phe5(R)	
	ACE2	-82.830	-5.140	Leu19, Glu6, Cys29, His48	
Lopinavir	3CLPro	-126,713	-7.414	Cys95, Thr96	
	ACE2	-80.524	-11.160	Asn98, Thr96, Cys95, Gly94, Ile3, Pro1	
Ritonavir	3CLPro	-108,731	-3.045	Asn98, Ile3, Thr96, Gln2	
	ACE2	-73.550	-15.621	Asn98, Ile3, Thr96, Pro1	

Suleyman ILHAN

Venom Peptides of Crotalus atrox Against SARS-Cov-2 Spike Protein and Human ACE2 Receptor by Molecula...
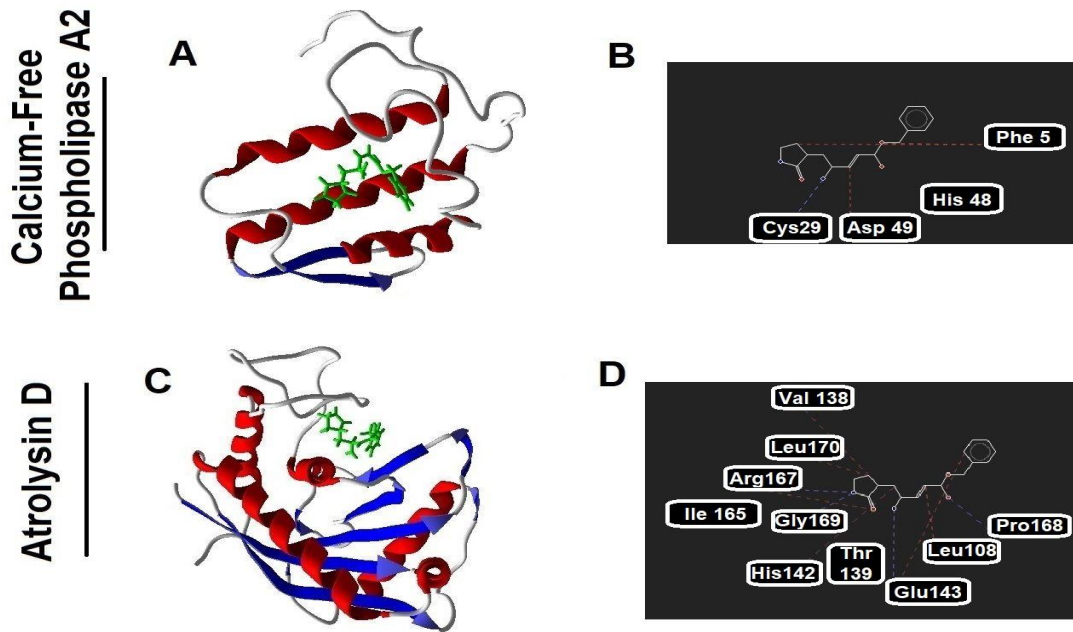
Figure 1 (A) Molecular docking of SARS CoV-2 main protease (3CLpro) and Calcium-free phospholipase A2 (B) interactions with key residues. (C) Molecular docking of SARS CoV-2 main protease (3CLpro) and Atrolysin D and (D) interactions with key residues (Red dashes show steric interactions and blue dashes show hydrogen bonds)
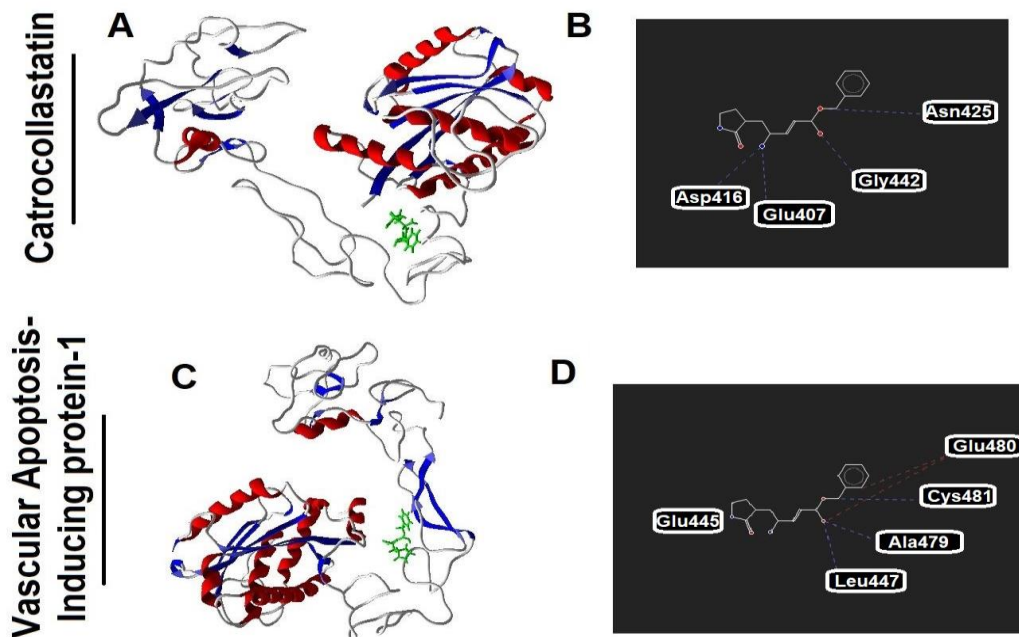
Figure 2 (A) Molecular docking of SARS CoV-2 main protease (3CLpro) and Catrocollastatin (B) interactions with key residues. (C) Molecular docking of SARS CoV-2 main protease (3CLpro) and Vascular apoptosis-inducing protein-1 (D) interactions with key residues (Red dashes show steric interactions and blue dashes show hydrogen bonds)

Suleyman ILHAN

Venom Peptides of Crotalus atrox Against SARS-Cov-2 Spike Protein and Human ACE2 Receptor by Molecula...

Figure 3 (A) Molecular docking of ACE2 and Calcium-free phospholipase A2 (B) interactions with key residues. (C) Molecular docking of ACE2 and Atrolysin D (D) interactions with key residues (Red dashes show steric interactions and blue dashes show hydrogen bonds)

Figure 4 (A) Molecular docking of ACE2 and Catrocollastatin and (B) interactions with key residues. (C) Molecular docking of ACE2 and Vascular apoptosis-inducing protein-1 (D) interactions with key residues (Red dashes show steric interactions and blue dashes show hydrogen bonds)

Suleyman ILHAN

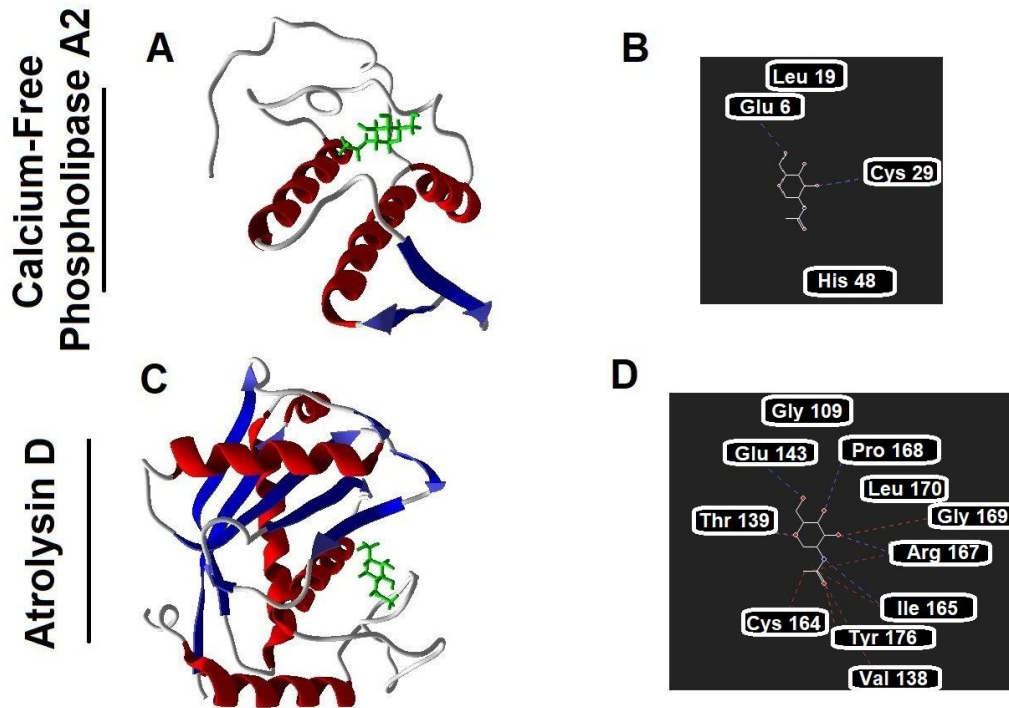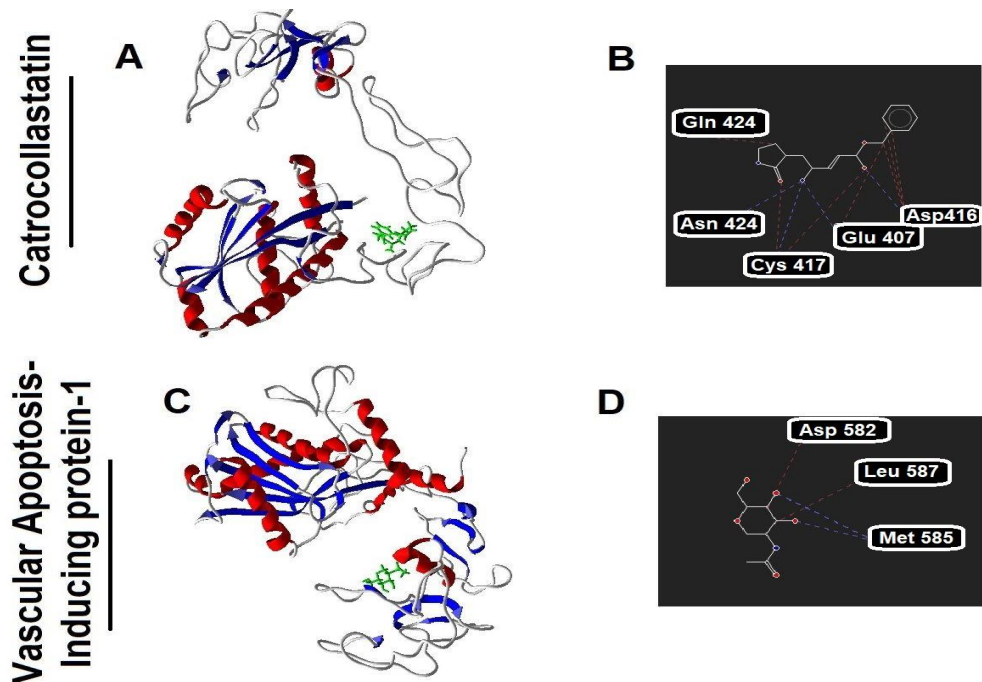Venom Peptides of Crotalus atrox Against SARS-Cov-2 Spike Protein and Human ACE2 Receptor by Molecula...

The binding energy of ACE2 was -101.165 kcal/mol, -73.064 kcal/mol, -106.918 kcal/mol, -82.830 kcal/mol with Atrolysin D (AD), VAIP-1, Catrocollastatin (CC), and Calcium-Free Phospholipase A2 (CFP), respectively (Table 1). VAIP-1 with the lowest binding score almost the same as Ritonavir. It formed hydrogen bonding with Met585 and steric interactions with Leu587 and Asp582 (Figure 3A-B). AD formed hydrogen interactions with Glu143, Thr139, Pro168, Arg167, and Ile165; formed steric bonds with Thr139, Cys164, Tyr176, Val138, Ile165, and Gly169 (Figure 3C-D). The peptide with the greatest binding affinity to human ACE2 was found as CC. Compared to Lopinavir and Ritonavir, CC had a higher affinity for binding hydrogen bonds with Asn422, Cys417, Glu407, and Asp416 and steric interactions with Gln424, Cys417, Glu407, and Asp416 (Figure 4A-B). CFP had the similar results to Lopinavir and it formed hydrogen bonds with Cys29 and Glu6 (Figure 4C-D).

These *in silico* analysis results highlight the CVPs tested as potential anti-SARS-CoV-2 components. However, it is important to validate the results of *in silico* docking using *in vitro* and *in vivo* studies to ensure that the compounds are effective and safe for use as antiviral drugs.

Funding

Authors' Contribution

The author confirms sole responsibility for the following: study conception and design, data collection, analysis and interpretation of results, and manuscript preparation.

The Declaration of Conflict of Interest/ Common Interest

No conflict of interest or common interest has been declared by the authors.

The Declaration of Ethics Committee Approval

This study does not require ethics committee permission or any special permission.

The Declaration of Research and Publication Ethics

The authors of the paper declare that they comply with the scientific, ethical and quotation rules of SAUJS in all processes of the paper and that they do not make any falsification on the data collected. In addition, they declare that Sakarya University Journal of Science and its editorial board have no responsibility for any ethical violations that may be encountered, and that this study has not been evaluated in any academic publication environment other than Sakarya University Journal of Science.

REFERENCES

[1] T. P. Sheahan, Sims, A. C., Zhou, S., Graham, R. L., Pruijssers, A. J., Agostini, M. L., Baric, R. S., "An orally bioavailable broad-spectrum antiviral inhibits SARS-CoV-2 in human airway epithelial cell cultures and multiple coronaviruses in mice," Science translational medicine, vol. 12, no. 541, 2020.

[2] I. Ahmad, R. Pawara, S. Surana, H. Patel, "The Repurposed ACE2 Inhibitors: SARS-CoV-2 Entry Blockers of Covid-19," Topics in Current Chemistry, vol. 379, no. 6. 2021.

[3] J. Shang Wan, Y., Luo, C., Ye, G., Geng, Q., Auerbach, A., Li, F., "Cell entry mechanisms of SARS-CoV-2," Proceedings of the National Academy of Sciences, vol. 117, no. 21, 2020.

[4] C. B. Jackson, M. Farzan, B. Chen, H. Choe, "Mechanisms of SARS-CoV-2 entry into cells," Nature Reviews Molecular Cell Biology, vol. 23, no. 1. 2022.

Suleyman ILHAN

Venom Peptides of Crotalus atrox Against SARS-Cov-2 Spike Protein and Human ACE2 Receptor by Molecula...

[5] A. A. Alqathama, Ahmad, R., Alsaedi, R. B., Alghamdi, R. A., Abkar, E. H., Alrehaly, R. H., Abdalla, A. N., "The vital role of animal, marine, and microbial natural products against COVID-19," Pharmaceutical Biology, vol. 60, no. 1. 2022.

[6] T. Joshi, Joshi, T., Sharma, P., Mathpal, S., Pundir, H., Bhatt, V., Chandra, S., "In silico screening of natural compounds against COVID-19 by targeting Mpro and ACE2 using molecular docking," European Review for Medical and Pharmacological Sciences, vol. 24, no. 8, 2020.

[7] A. D. Fuzimoto, C. Isidoro, "The antiviral and coronavirus-host protein pathways inhibiting properties of herbs and natural compounds - Additional weapons in the fight against the COVID-19 pandemic?," Journal of Traditional and Complementary Medicine, vol. 10, no. 4. 2020.

[8] A. E. Siniavin, Streltsova, M. A., Nikiforova, M. A., Kudryavtsev, D. S., Grinkina, S. D., Gushchin, V. A., Utkin, Y. N., "Snake venom phospholipase A2s exhibit strong virucidal activity against SARS-CoV-2 and inhibit the viral spike glycoprotein interaction with ACE2," Cellular and Molecular Life Sciences, vol. 78, no. 23, 2021.

[9] T. M. A. El-Aziz, A. G. Soares, J. D. Stockand, "Snake venoms in drug discovery: Valuable therapeutic tools for life saving," Toxins, vol. 11, no. 10. 2019.

[10] Y. Utkin, A. Siniavin, I. Kasheverov, V. Tsetlin, "Antiviral Effects of Animal Toxins: Is There a Way to Drugs?," International Journal of Molecular Sciences, vol. 23, no. 7. 2022.

[11] L. Pinzi, Rastelli G., "Molecular docking: Shifting paradigms in drug discovery," International Journal of Molecular Sciences, vol. 20, no. 18. 2019.

[12] V. Salmaso, Moro S., "Bridging molecular docking to molecular dynamics in exploring ligand-protein recognition process: An overview," Frontiers in Pharmacology, vol. 9, no. 8, 2018.

[13] O. Troot, A. J. Olson, "Software News and Update AutoDock Vina: Improving the Speed and Accuracy of Docking with a New Scoring Function, Efficient Optimization, and Multithreading," Journal of Computational Chemistry, vol. 31, no. 16, 2010.

[14] T. W. Wu, D. O. Tinker, "Phospholipase A2 from crotalus atrox venom. I. Purification and some properties," Biochemistry, vol. 8, no. 4, 1969.

[15] K. Shimokawa, L. G. Jia, J. D. Shannon, J. W. Fox, "Isolation, sequence analysis, and biological activity of atrolysin E/D, the non-RGD disintegrin domain from Crotalus atrox venom," Archives of biochemistry and biophysics, vol. 354, no. 2, 1998.

[16] R. M. Kini, C. Y. Koh, "Metalloproteases affecting blood coagulation, fibrinolysis and platelet aggregation from snake venoms: Definition and nomenclature of interaction sites," Toxins, vol. 8, no. 10. 2016.

[17] E. Kikushima, Nakamura, S., Oshima, Y., Shibuya, T., Miao, J. Y., Hayashi, H., Araki, S., "Hemorrhagic activity of the vascular apoptosis-inducing proteins VAP1 and VAP2 from Crotalus atrox," Toxicon, vol. 52, no. 4, 2008.

Title: Synthesis and Characterization of Novel Water-Soluble Tetra-Substituted Zn(II) Phthalocyanine Containing Triazole and Galactose Moieties

Authors: Yasemin BAYĞU

Synthesis and Characterization of Novel Water-Soluble Tetra-Substituted Zn(II) Phthalocyanine Containing Triazole and Galactose Moieties

Yasemin BAYĞU*[1]

Abstract

In this study, new water-soluble non-peripheral tetra-substituted zinc complex of phthalocyanine which is contain galactose moieties was synthesized. ZnPc-I was prepared from the galactose substituted dicyano compound by the cyclotetramerization reaction. This dicyano compound was synthesized by Click reaction between 3-(pent-4-yn-1-yloxy)phthalonitrile and 6-azido-6-deoxy1,2:3,4-di-O-isopropylidene-α-D-galactopyranose. ZnPc-II was obtained by hydrolysis of the protected isopropylidene groups in ZnPc-I in TFA and water mixture. The galactose linked Zn(II) phthalocyanine was achieved to dissolve in common polar solvents and water. All of the new compounds were characterized by elemental analysis, ^{1}H NMR, ^{13}C NMR, IR, UV–vis and MS spectral data.

Keywords: Zinc(II) phthalocyanine, galactose, click reaction, water soluble phthalocyanine

1. INTRODUCTION

Phthalocyanine (Pc) compound having 18 π-electron systems contains four nitrogen atoms in the central cavity and it is known as blue-green-coloured [1]. Phthalocyanines and their metal complexes are widely used a wide range of areas for a long time beacuse of their matchless electronic properties of the phthalocyanine core, high degree of aromaticity and the ability to be added different substituents. Their applications such as non-linear optical devices [2], sensors [3], liquid crystals [4], dye-sensitized solar cells (DSSCs) [5], Langmuir-Blodgett films [6], and photodynamic therapy [7] can be showed as example. Phthalocyanines are generally soluble in commonly used organic solvents due to substituents such as alkyl, alkoxy, crown ethers.

Photodynamic therapy (PDT) is a clinical treatment method that depended on the use of light to treat a number of cancers such as early gastrointesti, oesophageal, lung and skin cancer [8]. A non-toxic, photosensitizing drug known as a photosensitizer (PS) is used in this treatment method. The photosensitizer causes the formation of reactive oxygen species, which is known as singlet oxygen, from molecular oxygen by using light of the appropriate wavelength. Phthalocyanines are used as second generation photosensitizers [9] because they have photophysical and photochemical properties such as no dark toxicity, strong absorption at long wavelengths, high singlet oxygen production

---

* Corresponding author: ybaygu@pau.edu.tr (Y. BAYĞU)
[1] Pamukkale University
ORCID: https://orcid.org/0000-0003-3776-9633

Yasemin BAYĞU

Synthesis and Characterization of Novel Water-Soluble Tetra-Substituted Zn(II) Phthalocyanine Contain...

efficiency, chemical stability and penetration into deep tissues [10, 11]. Phthalocyanine compounds must be water-soluble for to be used as photodynamic therapy agents. For this reason, substituents such as carboxylate, sulfonate and quaternized amino groups can be added to their peripheral, non-peripheral or axial positions. However anionic sulfonated phthalocyanines tend to aggregate in water [12]. In conclucion their photosensitizing ability is lost for their use in PDT. Therefore galactosed or glucosed substitued phthalocyanines have prepared in literature [13, 14]. Morever, carbohydrate moieties such as galactose suggests the specific affinity for tumour tissues for application as photosensitizers in PDT, because the cancer cell gets its energy from carbohydrate. [15-17].

Click Chemistry which was called by Sharpless is used to connect various functional groups together [18]. Click reactions that are selective, cheap and easy are obtained by using copper(I) catalyst between azide and alkyne compounds with high yield [19]. Thanks to these characteristics, Click reactions are commonly used in the synthesis of carbohydrate-containing porphyrins derivatives [20, 21].

In this study, the synthesis and characterization of zinc(II) phthalocyanines, whose galactose derivatives are protected by acetyl units and galactose derivatives contain hydroxyl groups, were reported. A new water-soluble zinc(II) phthalocyanine containing alkyl-linked triazole units and tetra-substituted galactose groups was synthesized. This new compound exhibited the partially-aggregated behavior in aqueous media. The structures of all new compounds were confirmed by using elemental analysis, ^{1}H and ^{13}C NMR, FT-IR, UV-vis, and MS spectral techniques.

2. EXPERIMENTAL

2.1. General

All chemicals which were used for synthesis of reactions were purchased from commercial suppliers and n-pentanol was dried according to the procedure [22]. FT-IR spectra were recorded on Perkin-Elmer UATR Two spectrometer. ^{1}H and ^{13}C NMR spectra were measured by Agilent-vnmrs 400/54 and Varian Mercury plus 300 MHz spectrometers. Mass spectra were determined on a Micromass Quattro Ultima LC–MS/MS and on a Bruker Daltonics Microflex LT MALDI-TOF spectrometers. The UV-vis absorption spectra were measured on a Shimadzu UV-1601 spectrophotometer by using double-beamed in 1 mL quartz cuvette. Elemental analyses were determined on a Costech ECS 4010 instrument. Melting points were measured on an electro thermal melting point apparatus in a sealed tube.

2.2. Synthetic Procedures and Spectral Data

2.2.1. Preparation of 3-(3-(1-((((3aR,5R,5aS,8aS,8bR)-2,2,7,7-tetramethyltetrahydro-5H-bis([1,3]dioxolo)[4,5-b:4',5'-d]pyran-5-yl)methyl)-1H-1,2,3-triazol-4-l)propoxy)phthalonitrile (3):

A suspension of copper(II) acetate monohydrate (0.2 g, 0.98 mmol) and sodium-L-ascorbate (0.4 g, 2.01 mmol) in water (35 mL) was added to the mixture of compound 1 (1.05 g, 5 mmol) and compound 2 (2.15 g, 7.5 mmol) in *tert*-butanol (35 mL). Then, the mixture was stirred under argon atmosphere at room temperature for overnight. The end of this period, the reaction mixture was poured into water (70 mL) and stirred and then extracted with dichloromethane (3x25 mL). The collected organic extracts was washed brine solution (50 mL) and dried over anhydrous $MgSO_4$. The product was stirred with diethyl ether and filtered off. Then dried in vacuo to give cream coloured solid. Yield:

Yasemin BAYĞU

Synthesis and Characterization of Novel Water-Soluble Tetra-Substituted Zn(II) Phthalocyanine Contain...

1.93 g (77.82%), m.p: 150-152 °C. ^{1}H NMR (300 MHz, CDCl$_3$), (δ: ppm): 7.63 (s, 1H, HC=C), 7.53-7.30 (s, 3H, C-H)$_{arom}$, 5.45 (s, 1H, -OCH), 4.62-4.30 (m, 4H, -OCH), 4.17 (m, 2H, -OCH$_2$), 4.15 (d, 2H, -NCH$_2$), 2.93 (m, 2H, -CCH$_2$), 2.25 (m, 2H, -CH$_2$CH$_2$), 1.46-1.24 (s, 12H, CH$_3$). ^{13}C NMR (75 MHz, CDCl$_3$), (δ: ppm):161.51, 134.90, 134.83, 125.26, 125.20, 117.21, 115.6, 113.30, 110.08, 109.20, 105.02, 96.40, 71.42, 71.35, 70.89, 68.89, 67.48, 50.65, 28.40, 26.18, 26.11, 25.10, 24.61, 21.81. FT-IR (ATR, cm^{-1}): 3151 (triazole), 3087 (C-H)$_{arom.}$, 2995-2903 (C-H)$_{aliph}$, 2234 (C≡N), 1299, 1070, 1007. MS (m/z): 496.03 [M+H]$^+$, 518.01 [M+Na]$^+$, 597.05 [M+2K+Na]$^+$. Anal. cald. for C$_{25}$H$_{29}$N$_5$O$_6$: C, 60.60; H, 5.90; N, 14.13. Found: C, 60.76; H, 5.94; N, 14.20.

2.2.2. Preparation of ZnPc-I:

Non-peripheral substitue dinitrile compound (**3**) (0.25 g, 0.5 mmol), anhydrous zinc(II) acetate (33 mg, 0.18 mmol) and 5 drops of DBU in dry pentanol (3.5 mL) were heated and stirred at 155 °C under argon atmosphere for 24 h in a Schlenck system.. After cooling to room temperature, the reaction mixture was poured into hexane (20 mL) and then centrifuged. Purification of the crude product was carried out by column chromatography on silica gel using dichlorometane/ethanol (98:3) to give green solid. Yield: 66 mg (26.4%), m.p> 300 °C. ^{1}H NMR (400 MHz, CDCl$_3$), (δ: ppm): 9.20 (s, 4H, HC=C), 8.09-7.51 (s, 12H, C-H)arom, 5.44 (s, 4H, -OCH), 4.58-4.28 (m, 16H, -OCH), 4.21 (m, 8H, OCH$_2$), 4.14 (m, 8H, -NCH$_2$), 2.97 (s, 8H, -CCH$_2$), 2.57 (m, 8H, -CH$_2$CH$_2$), 1.45-1.16 (s, 48H, CH$_3$). ^{13}C NMR (100 MHz, CDCl$_3$), (δ: ppm): 156.17, 153.60, 141.62, 136.25, 134.55, 125.73, 122.46, 115.44, 109.76, 109.69, 108.89, 96.06, 71.04, 70.62, 70.19, 67.97, 67.11, 50.26, 29.12, 25.88-24.32, 21.93. UV-vis (CHCl$_3$): λmax (log ε): 705 (5.26), 637 (4.51), 322 (4.65). FT-IR (ATR, cm^{-1}): 3149 (triazole), 3048 (C-H)arom., 2933-2856 (C-H)aliph, 1627 (C=N), 1451, 1324, 1152. MS (m/z): 2045.68 [M]$^+$. Anal. cald. for C$_{100}$H$_{116}$N$_{20}$O$_{24}$Zn: C, 58.66; H,

5.71; N, 13.68; Zn, 3.19. Found: C, 58.78; H, 5.85; N, 13.76; Zn, 3.32.
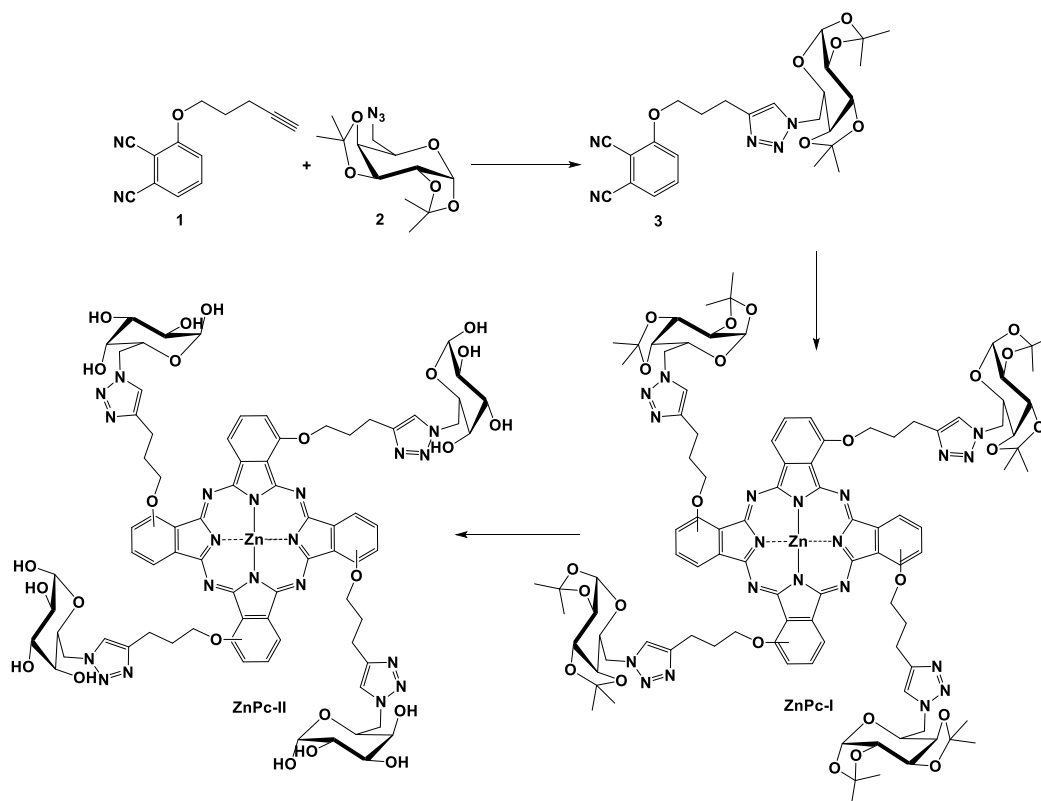
2.2.3. Preparation of ZnPc-II:

ZnPc-I (61.35 mg, 0.03 mmol) was stirred in trifluoro acetic acid water mixture [(9:1) (1.5 mL)] at room temperature for 35 minute. Diethyl ether (6 mL) was added to the solution at the end of this period and the product precipitated. The green solid was filtered off, washed with diethyl ether and then dried under vacuo. Yield: 46.09 mg, (89.06%), m.p> 300 °C. ^{1}H NMR (400 MHz, DMSO-d$_6$), (δ: ppm): 8.59 (s, 4H, HC=C), 8.07-7.57 (s, 12H, C-H)$_{arom}$, 4.96-353 (m, 52 Gal-H and -OH), 3.14 (s, 8H, -CCH$_2$), 2.57 (m, 8H, -CH$_2$CH$_2$). ^{13}C NMR (100 MHz, CDCl$_3$), (δ: ppm): 156.17, 146.98, 146.31, 140.03, 136.35, 123.24, 119.58, 115.19, 102.25, 97.91, 76.42, 72.07, 70.01, 69.26, 68.78, 51.31, 29.60, 21.92. UV-vis λmax (log ε): 708 (5.31), 638 (4.58), 327 (4.62) in DMSO, 682 (4.64), 319 (4.47) in H$_2$O. FT-IR (ATR, cm^{-1}): 3269 (OH), 3153 (triazole), 2924-2882 (C-H)$_{aliph}$, 1673 (C=N), 1268, 1198, 1058. MS (m/z): 1725.95 [M]$^+$. Anal. cald. for C$_{76}$H$_{84}$N$_{20}$O$_{24}$Zn: C, 52.86; H, 4.90; N, 16.22; Zn, 3.79. Found: C, 53.03; H, 5.02; N, 16.39; Zn, 3.93.

3. RESULTS AND DISCUSSION

The synthetic routes were described to prepare Zn(II) phthalocyanines in Scheme 1. The precursor compound 3 was synthesized via Husgein 1,3-dipolar cycloaddition reaction between 3-(pent-4-yn-1-yloxy)phthalonitrile [23] and 6-azido-6-deoxy1,2:3,4-di-O-isopropylidene-α-D-galactopyranose [24] in the presence of copper(II) acetate monohydrate and sodium-L-ascorbate in water/tert-butanol mixture (1:1) at room temperature in high yield (77.82%). FT-IR spectrum of this compound was showed characteristic vibrations at 3151 cm^{-1} for triazole and at 2234 cm^{-1} for C≡N moieties (Figure 1). In the ESI mass spectra of compound 3 at m/z = 496.03, 518.01, 597.05 signals should be concerned [M+H]$^+$,

Yasemin BAYĞU

Synthesis and Characterization of Novel Water-Soluble Tetra-Substituted Zn(II) Phthalocyanine Contain...

[M+Na]+ and [M+2K+Na+H]+ ion peaks respectively (Figure 2). These mass spectra were confirmed the structure. The characteristic triazole resonances at δ = 7.63 ppm in ¹H NMR spectra and δ = 134.9 and 125.20 ppm in ¹³C NMR spectra were confirmed the formation of compound 3 (Figure 3 and Figure 4).
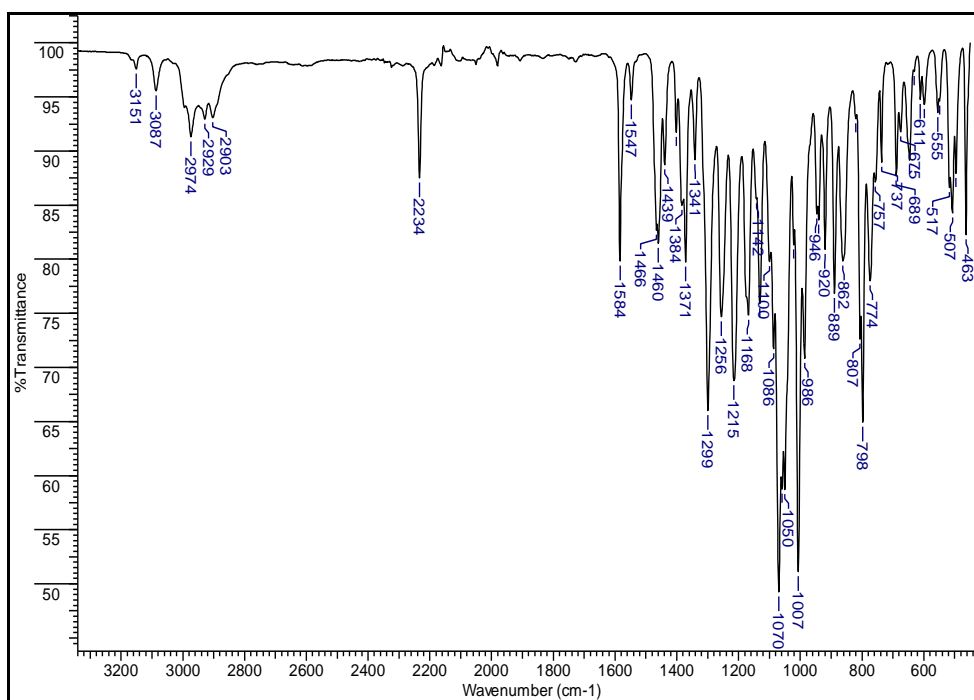

Scheme 1 The synthesis procedure of ZnPc-II
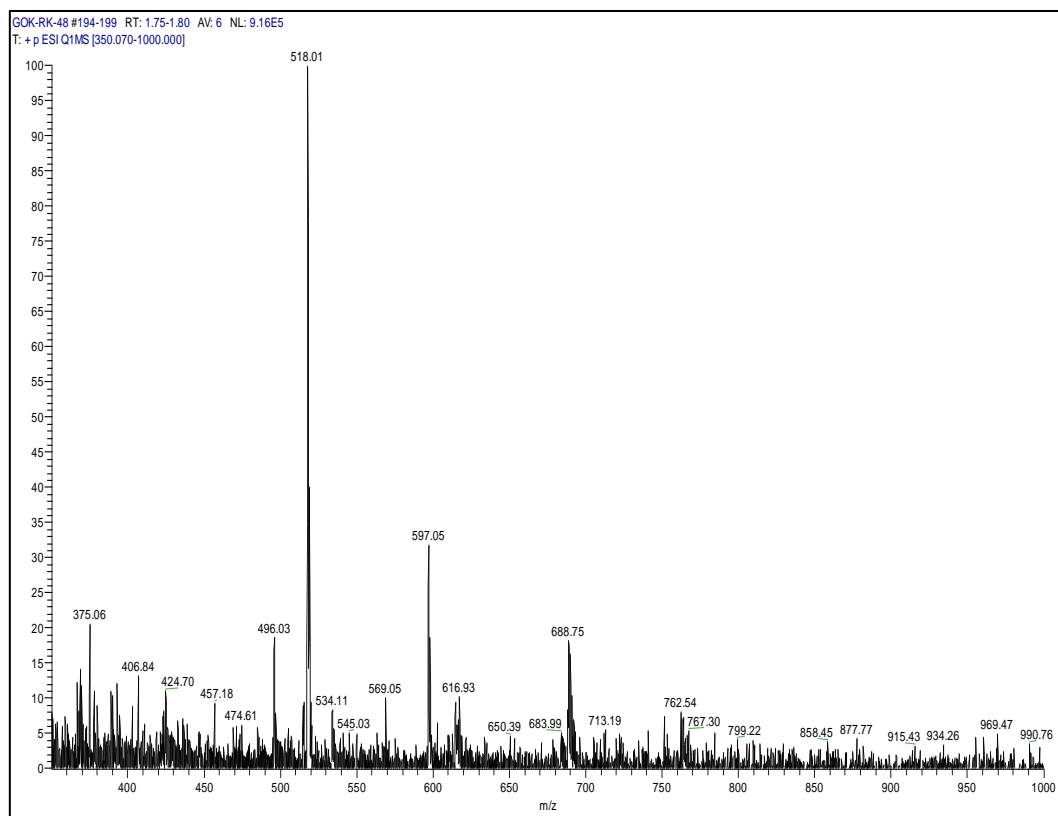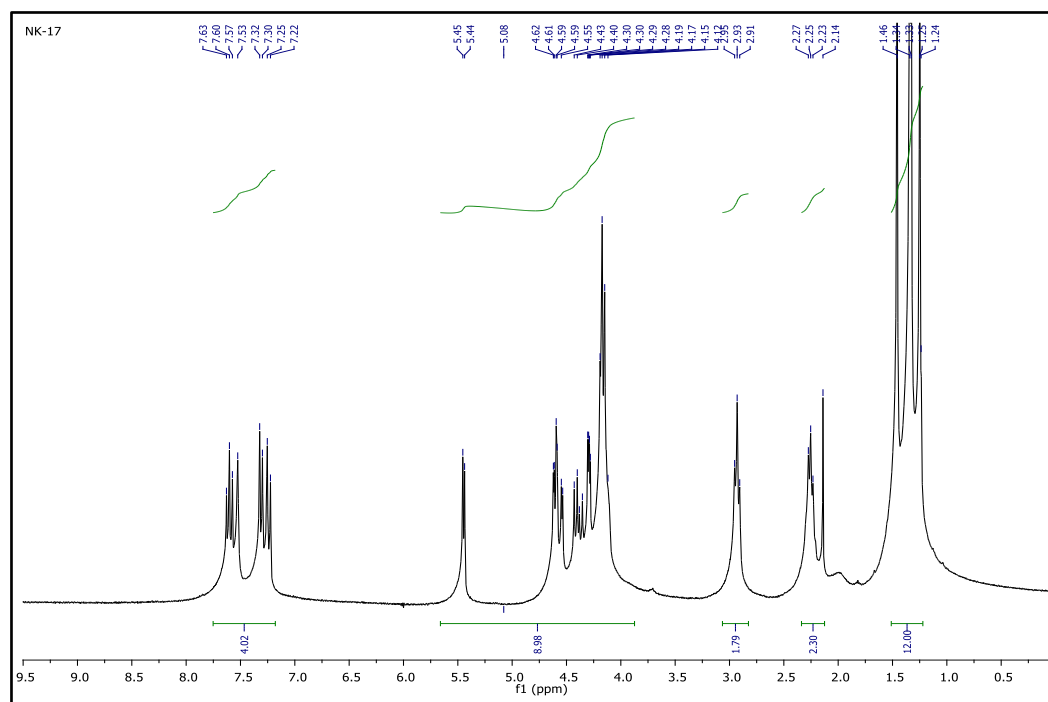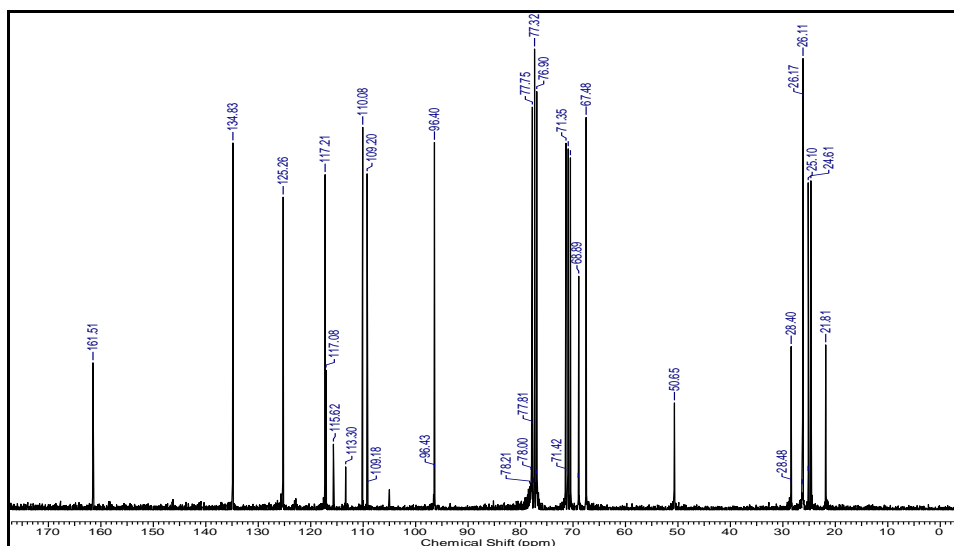

Figure 1 IR spectrum of compound 3

Yasemin BAYĞU

Synthesis and Characterization of Novel Water-Soluble Tetra-Substituted Zn(II) Phthalocyanine Contain...

Figure 2 Mass spectrum of compound 3

Figure 3 ^{1}H-NMR Spectrum of compund 3

Yasemin BAYĞU

Synthesis and Characterization of Novel Water-Soluble Tetra-Substituted Zn(II) Phthalocyanine Contain...

Figure 4 ^{13}C-NMR Spectrum of compund 3

Zn(II) phthalocyanine (ZnPc-I) was prepared from compund 3 by the template reaction with anhydrous Zn(II) acetate and a few drop of DBU in dry n-pentanol under reflux in inert atmosphere. Purification of the ZnPc-I by column chromatography on silica gel using dichlorometane/ethanol (98:3) gave a blue-green solid in yield 26.4%. The phthalocyanine formations was supported by disappearance of characteristic C≡N stretching vibration at 2234 cm^{-1} in the precursor compound 3 in the FT-IR spectra. In addition to that, the novel signal at 1627 cm^{-1} concerning C=N moieties also supported the phthalocyanine formation (Figure 5). The molecular ion peak at m/z = 2045.68 [M]$^+$ confirmed the proposed structure in the MALDI-TOF mass spectrum of ZnPc-I, (Figure 6). A proton belonging to triazole groups was observed at δ = 9.20 and the other aromatic ring protons were observed at δ = 8.09-7.51 ppm in the ^{1}H NMR spectrum of ZnPc-I (Figure 7). In the ^{13}C NMR spectrum of ZnPc-I, the disappearance of characteristic C≡N signal belonging to the precursor compound 3 at δ = 113.30 ppm and the appearance of the novel signals at δ = 141.62 ppm concerning C=N moieties was indicated the phthalocyanine formation (Figure 8).

Figure 5 IR spectrum of ZnPc-I
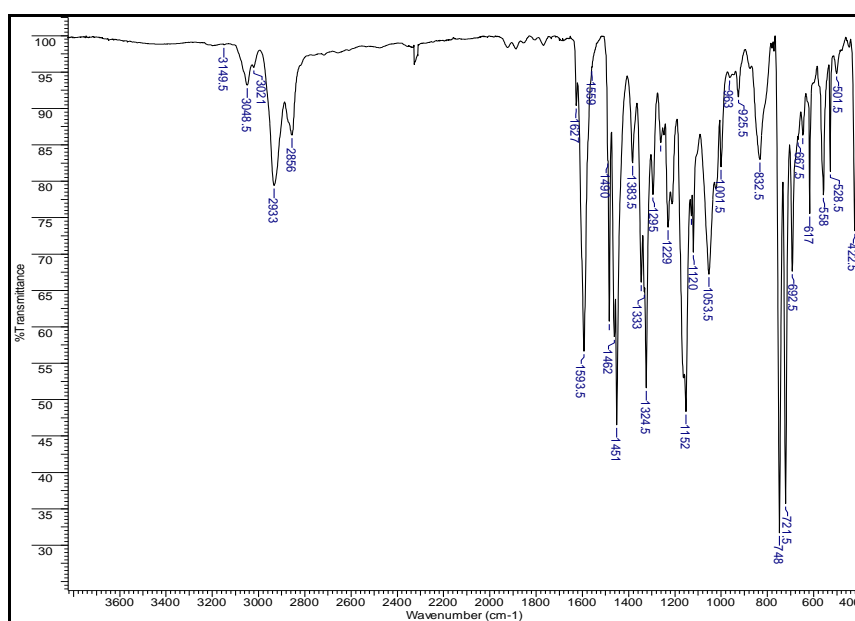
Yasemin BAYĞU

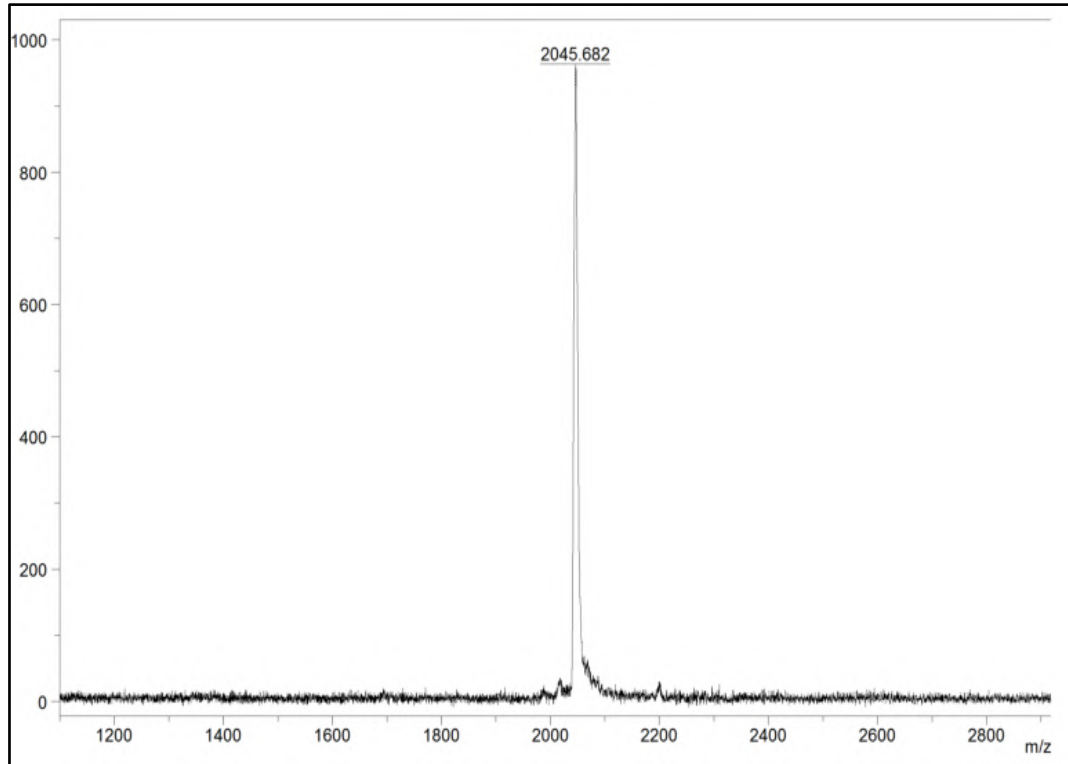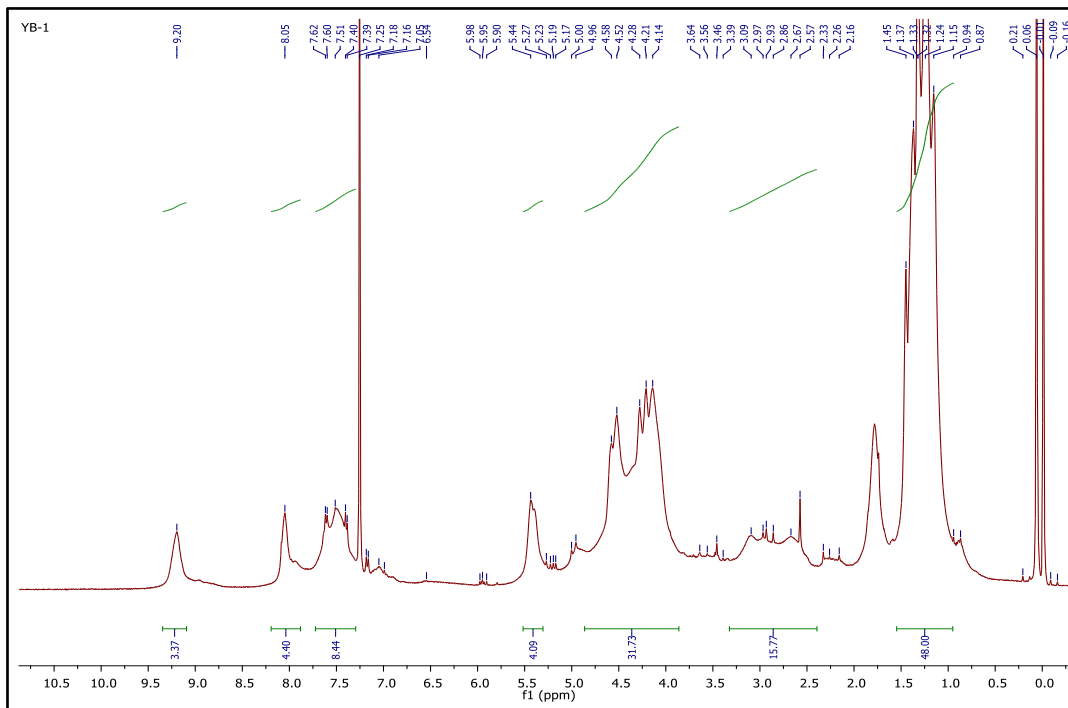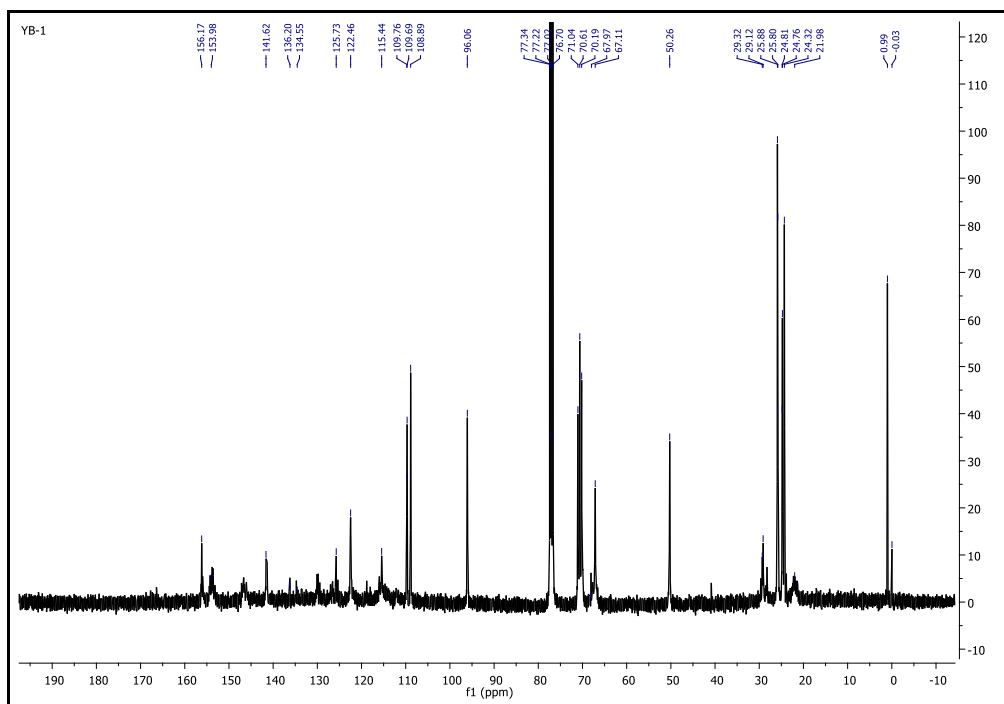Synthesis and Characterization of Novel Water-Soluble Tetra-Substituted Zn(II) Phthalocyanine Contain...

Figure 6 Mass spectrum of ZnPc-I

Figure 7 ^{1}H NMR spectrum of ZnPc-I

Yasemin BAYĞU

Synthesis and Characterization of Novel Water-Soluble Tetra-Substituted Zn(II) Phthalocyanine Contain...

Figure 8 ^{13}C NMR spectrum of ZnPc-I

ZnPc-I was stirred in a mixture of trifluoro acetic acid and water (9:1) at room temperature for 35 minute. As a result of this process, the isopropylidene groups of ZnPc-I were deprotected and ZnPc-II was obtained in very high yield (89.07%). This compund dissolved in water due to galactose units. The presence of O—H stretching vibrations at 3269 cm^{-1} in FT-IR spectrum of this compound supported the removal of the protecting groups (Figure 9). The molecular ion peak being at m/z =1725.95 [M]$^+$ was confirmed the structure in the MALDI-TOF mass spectrum of ZnPc-II (Figure 10). The chemical shifts at δ = 1.45–1.16 ppm should be indicated the disappearance of isopropylidene group of ZnPc-II (Figure 11). The observed novel moieties at δ = 25.88–24.32 ppm in the ^{13}C NMR spectrum of ZnPc-II also showed the formation of ZnPc-II (Figure 12).

Figure 9 IR spectrum of ZnPc-II

Yasemin BAYĞU

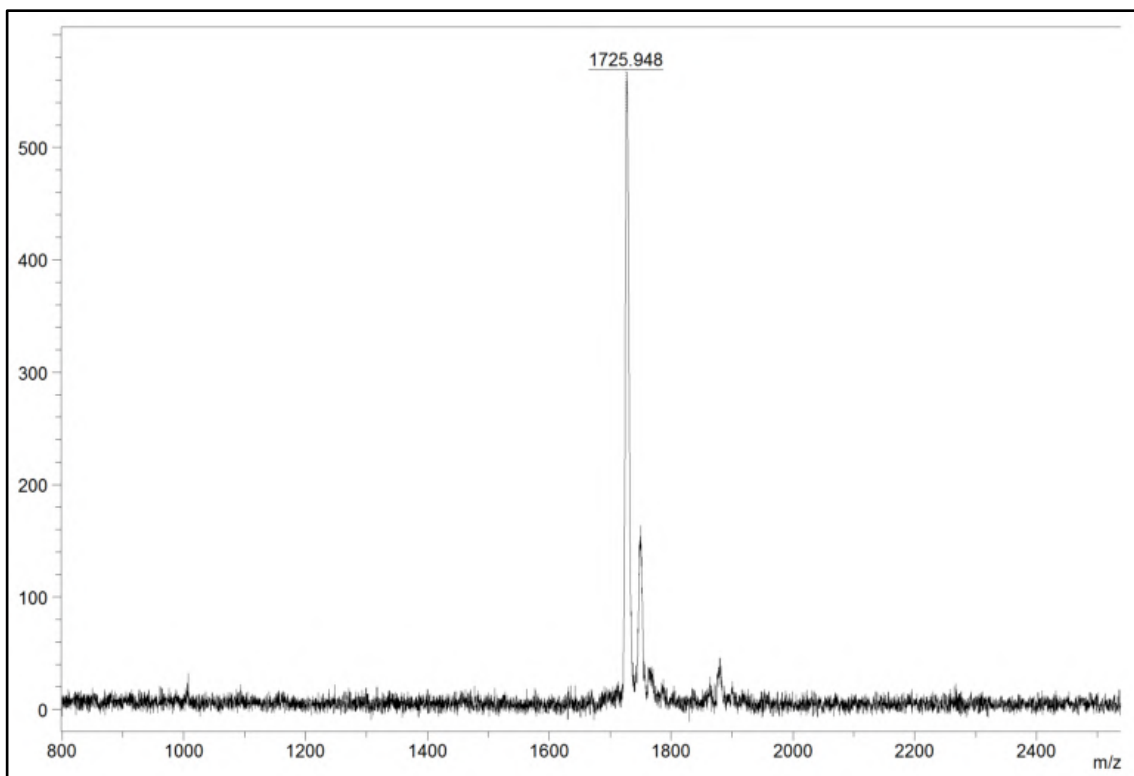Synthesis and Characterization of Novel Water-Soluble Tetra-Substituted Zn(II) Phthalocyanine Contain...

Figure 10 Mass spectrum of ZnPc-II

Figure 11 ^{1}H NMR spectrum of ZnPc-II

Yasemin BAYĞU

Synthesis and Characterization of Novel Water-Soluble Tetra-Substituted Zn(II) Phthalocyanine Contain...
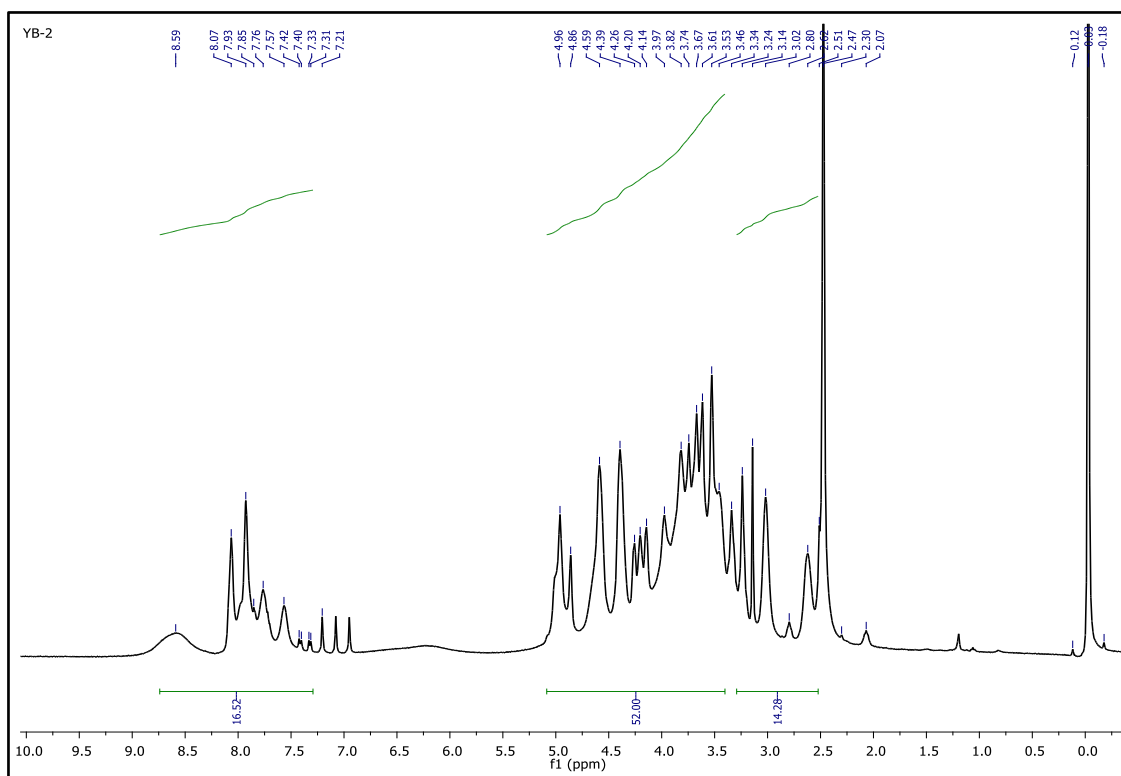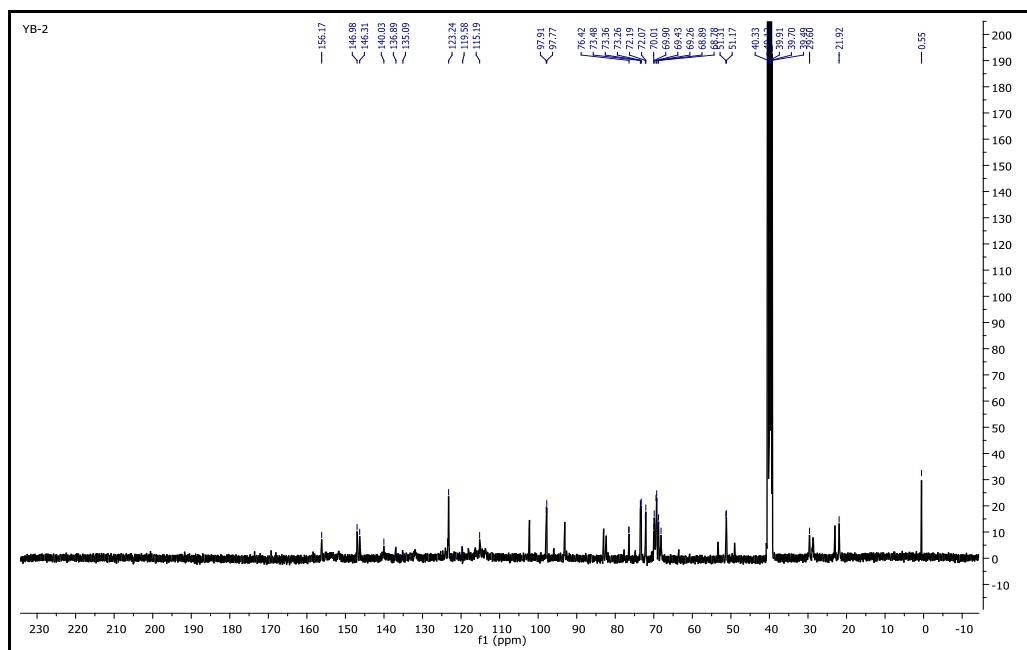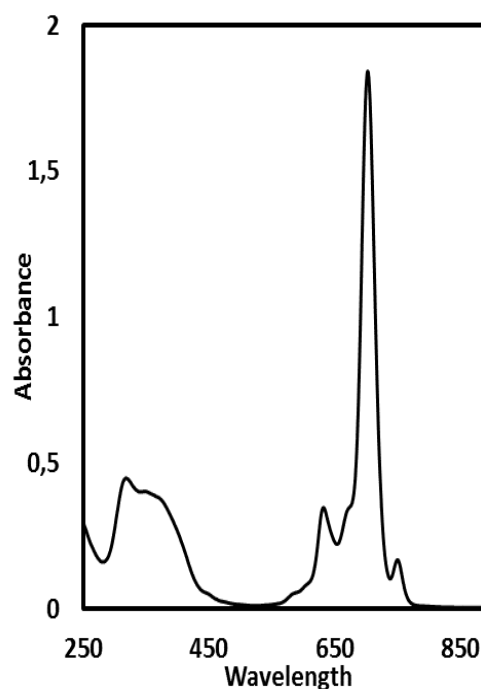

Figure 12 ^{13}C NMR spectrum of ZnPc-II

The synthesized novel zinc(II) phthalocyanines ZnPc-I and ZnPc-II exhibited in the ground state typical electronic absorption having with the characteristic π→π* transitions of the phthalocyanine core in Q band region. These absorbtions were observed at λ = 705 nm in chloroform for ZnPc-I and 708 nm in DMSO, 682 nm in water for ZnPc-II respectively. These single and narrow transitions in Q band region of UV-vis spectra where are shown in Figure 13 and Figure 14 indicated the monomeric and non-aggregated behaviors of ZnPc-I in chloroform and ZnPc-II in DMSO. The UV-vis spectra of ZnPc-II showed that the intensity of Q band is much lower in water than in DMSO. This situation can be comment as showing aggregated behaviors of ZnPc-II. However this aggregation is much lower than according to in a similar study [25]. Alkyl groups linked by triazole rings in ZnPc-I and ZnPc-II compunds may have prevented aggregation.

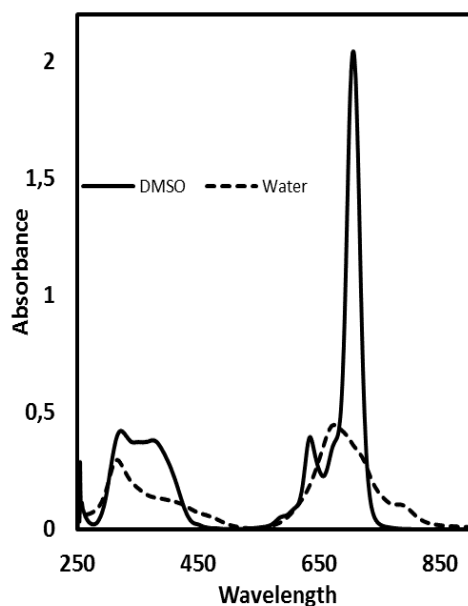Figure 13 UV-vis Spectrum of ZnPc-I (10^{-5} M in chloroform)

Yasemin BAYĞU

Synthesis and Characterization of Novel Water-Soluble Tetra-Substituted Zn(II) Phthalocyanine Contain...

Figure 14 UV-vis Spectrum of ZnPc-II (10^{-5} M in water and DMSO)

4. CONCLUSION

In summary, compund 3 was synthesized using Husgein 1,3-dipolar cycloaddition reaction between 3-(pent-4-yn-1-yloxy)phthalonitrile (1) and azido of galactose compound (2). ZnPc-I was obtained from tetramerization of compound 3. ZnPc-II was prepared with hydrolysis of ZnPc-I. All of novel compounds was characterized by various spectral data. Thus water soluble and partially aggregated phthalocyanine containing four D-galactose units was obtained. This new water soluble compound due to carbohydrate moieties can be used for the potential application as photosensitizers in PDT.

Authors' Contribution
The author designed this study, carried out all experiments and wrote the manuscript.

The Declaration of Ethics Committee Approval
This study does not require ethics committee permission or any special permission.

The Declaration of Research and Publication Ethics
The authors of the paper declare that they comply with the scientific, ethical and quotation rules of SAUJS in all processes of the paper and that they do not make any falsification on the data collected. In addition, they declare that Sakarya University Journal of Science and its editorial board have no responsibility for any ethical violations that may be encountered, and that this study has not been evaluated in any academic publication environment other than Sakarya University Journal of Science.

REFERENCES

[1] C. C. Leznoff, A. B. P. Lever (Eds.), "Phthalocyanines—Properties and Applications," Vols. 1–4, VCH, New York, 1989.

[2] N. Farajzadeh, G. Kösoğlu, M. Erdem, G. Eryürek, M. Burkut Koçak, "Nonlinear optical properties of peripheral symmetrically and non-symmetrically 4-(trifluoromethoxy)phenoxy substituted zinc phthalocyanines," Synthetic Metals, vol. 266, pp. 116440, 2020.

[3] Y. Baygu, R. Capan, M. Erdogan, C. Ozkaya, Acikbas, Kabay, Y. Gok, "Synthesis, characterization and chemical sensor properties of a novel Zn(II) phthalocyanine containing 15-membered dioxa-dithia macrocycle moiety," Synthetic Metals, vol. 280, pp. 116870, 2021.

[4] A. J. Duro, G. de la Torre, J. Barbera, J. L. Serrano, T. Torres, "Synthesis and Liquid-Crystal Behavior of Metal-Free and Metal-Containing Phthalocyanines Substituted with Long-Chain Amide Groups," Chemistry of Materials, vol. 8, no. 5, pp. 1061, 1996.

[5] B. Yıldız, B. S. Arslan, E. Güzel, M. Nebioglu, N. Menges, I. Sisman, M. K.

Yasemin BAYĞU

Synthesis and Characterization of Novel Water-Soluble Tetra-Substituted Zn(II) Phthalocyanine Contain...

Sener, "Non-aggregating zinc phthalocyanine sensitizer with bulky diphenylphenoxy donor groups and pyrazole-3-carboxylic acid anchoring group for coadsorbent-free dye-sensitized solar cells," Solar Energy, vol. 226, pp. 173–179, 2021.

[6] L. Valli, "Phthalocyanine-based Langmuir–Blodgett films as chemical sensors," Advances in Colloid and Interface Science, vol. 116, no. 1-3, pp. 13-44, 2005.

[7] T. Nyokong, V. Ahsen (Eds.), "Photosensitizers in Medicine, Environment and Security," Springer, Dordrecht Heidelberg London New York, 2012.

[8] C. Hopper, "Photodynamic therapy: a clinical reality in the treatment of cancer," The Lancet Oncology, vol. 1, pp. 212-219, 2000.

[9] Y. Uruma, L. Sivasamy, P. M. Y. Yoong, K. Onuma, Y. Omura, M. Doe, M. Osaki, F. Okada, "Synthesis and biological evaluation of glucose conjugated phthalocyanine as a second-generation photosensitizer," Bioorganic & Medicinal Chemistry, vol. 27, no. 15, pp. 3279-3284, 2019.

[10] H. T., Akçay, M. Piskin, Ü. Demirbas, R. Bayrak, M. Durmus, E. Menteşe, H. Kantekin, "Novel triazole bearing zinc(II) and magnesium(II) metallo-phthalocyanines: Synthesis, characterization, photophysical and photochemical properties," Journal of Organometallic Chemistry, vol. 745-746, pp. 379-386, 2013.

[11] G. Reddy, E. D. Enrico Della Gaspera, L. A. Jones, L. Giribabu, "Self-assembly of a symmetrical dimethoxyphenyl substituted Zn(II) phthalocyanine into nanoparticles with enhanced NIR absorbance for singlet oxygen generation," Journal of Photochemistry & Photobiology, A: Chemistry, vol. 408, pp. 113123, 2021.

[12] A. Ogunsipe, T. Nyokong, "Photophysical and photochemical studies of sulphonated non-transition metal phthalocyanines in aqueous and non-aqueous media," Journal of Photochemistry & Photobiology, A: Chemistry, vol. 173, no. 2, pp. 211, 2005.

[13] Z. Iqbal, M. Hanack, T. Ziegler, "Synthesis of an octasubstituted galactose zinc(II) phthalocyanine," Tetrahedron Letters, vol. 50, no. 8, pp. 873–875, 2009.

[14] A. O. Ribeiro, J. P. C. Tomé, M. G. P. M. S. Neves, A. C. Tomé, J. A. S. Cavaleiro, Y. Iamamoto, T. Torres, "[1,2,3,4-Tetrakis(α/β-d-galactopyranos-6-yl)phthalocyaninato]zinc(II): a water-soluble phthalocyanine," Tetrahedron Letters, vol. 47, no. 52, pp. 9177–9180, 2006.

[15] T. K. Horne, M. J. Cronjé, "Novel carbohydrate-substituted metallo-porphyrazine comparison for cancer tissue-type specificity during PDT," Journal of Photochemistry and Photobiology B: Biology, vol. 173, pp. 412-422, 2017.

[16] A. M. Otto, "Warburg effect(s)—a biographical sketch of Otto Warburg and his impacts on tumor metabolism," Cancer and Metabolism, vol. 4, no. 5, pp. 1-8, 2016.

[17] M. V. Liberti, J. W. Locasale, "The Warburg effect: how does it benefit cancer cells?," Trends in Biochemical Sciences, vol. 41, no. 3, pp. 211–218. 2016.

Yasemin BAYĞU

Synthesis and Characterization of Novel Water-Soluble Tetra-Substituted Zn(II) Phthalocyanine Contain...

[18] R. Huisgen, "1,3-Dipolar Cycloadditions Past and Future," Angewandte Chemie International Edition, vol. 2, pp. 565-598, 1963.

[19] H. C. Kolb, M. G. Finn, K. B. Shapless, "Click Chemistry: Diverse Chemical Function from a Few Good Reactions," Angewandte Chemie International Edition, vol. 40, pp. 2004-2021, 2001.

[20] Y. Baygu, B. Yıldız, N. Kabay, Y. Gök, "Novel magnesium and zinc porphyrazines containing galactose moieties: synthesis via click reaction and characterization," Inorganic Chemistry Communications, vol. 71, pp. 35-40, 2016.

[21] F. Bächle, N. Siemens, T. Ziegler, "Glycoconjugated Phthalocyanines as Photosensitizers for PDT – Overcoming Aggregation in Solution," European Journal of Organic Chemistry, vol. 2019, pp. 7089-7116, 2019.

[22] D. D. Perin, W. L. F. Armarego, D. R. Perin, "Purification of Laboratory Chemicals," 2nd ed., Pergamon Press, New York, 1985.

[23] Z. Kanat, H. Dinçer, "The synthesis and characterization of nonperipherally tetra terminal alkynyl substituted phthalocyanines and glycoconjugation via the click reaction," Dalton Transactions, vol. 43, pp. 8654–8663, 2014.

[24] J. A. F. Joosten, B. Evers, R. P. van Summeren, J. P. Kamerling, J. F. G Vliegenthart, "Synthesis of β-D-Galp-(1→4)-β-D-GlcpNAc-(1→2)-α-D-Manp-(1→O)(CH2)7CH3 Mimics to Explore the Substrate Specificity of Sialyltransferases and trans-Sialidases," European Journal of Organic Chemistry, vol. 18, no. 6, pp. 3569-3586, 2003.

[25] A. R. M. Soares, J. P. C., Tomé, M. G. P. M. S. Neves, A. C. Tomé, J. A. S. Cavaleiro, T. Torres, "Synthesis of water-soluble phthalocyanines bearing four or eight D-galactose units," Carbohydrate Research, vol. 344, no. 4, pp. 507–510, 2009.

Title: Two Significant Factors Affecting the Dimensions of the ZnO Nanorods During Chemical Bath Deposition: Precursor Solution Concentration and HMTA Content

Authors: Memnune KARDEŞ, Koray ÖZTÜRK

Two Significant Factors Affecting the Dimensions of the ZnO Nanorods During Chemical Bath Deposition: Precursor Solution Concentration and HMTA Content

Memnune KARDEŞ*[1] (iD), Koray ÖZTÜRK[1] (iD)

Abstract

The effects of zinc ion concentration and hexamethylene tetramine (HMTA) content of the aqueous precursor solution on the aspect ratios of the one-dimensional (1D) ZnO nanorods during chemical bath deposition (CBD) were investigated. The ZnO nanorods were grown on these seeded substrates by the low-temperature CBD method at 95 °C for 5 h. In the first part of this investigation the zinc nitrate hexahydrate (ZNH) to HMTA molar ratio was kept constant at a ratio of 1:1 for each of the CBD solutions prepared with different Zn^{+2} ion concentrations of 0.025, 0.035, 0.050, and 0.075 M. The number densities of the nanorods (i.e., number of nanorods per unit area) were increased with the increasing concentration. In the second part, the ZNH to HMTA molar ratio was varied to differ from the 1:1 value and, in turn, to obtain the precursor solutions relatively rich in Zn^{+2} or OH^- ions. Here, the concentration of the precursor solution was kept constant at 0.05 M. The lateral growth perpendicular to the c-axis of the ZnO nanorods was found to be suppressed with the increasing HMTA content (e.g., for the ZNH to HMTA molar ratio of 0.4: 1) due to its capping effect. However, the precursor solution containing an excessive amount of HMTA led to a decrease in the probability of crystal growth, which has been attributed to the OH^- ion enrichment.

Keywords: ZnO nanorods, CBD, HMTA, aspect ratio, crystal growth

1. INTRODUCTION

One-dimensional (1D) ZnO nanorods are promising candidates among nanomaterials, which have been the building blocks of many electronic, optoelectronic, photovoltaic, and photocatalytic applications in recent years [1, 2]. Especially in photocatalytic applications, it is important to increase the surface-to-volume ratio as the efficiency increases when the molecules are adsorbed on (relatively) larger catalyst surface area. The surface-to-volume ratio of ZnO nanorods is extremely high, and their structure (along the rod growth direction) is more conducive to charge carrier transfer and the effective separation of electron-hole pairs [3, 4]. ZnO nanostructures have been synthesized by a wide variety of methods, including spray pyrolysis, chemical vapor transport (CVT), chemical vapor deposition (CVD), pulsed laser deposition (PLD), sol-gel, chemical bath deposition

---

* Corresponding author: memnunedaglar@gtu.edu.tr (M. KARDEŞ)
[1] Gebze Technical University, Materials Science and Engineering Department
E-mail: k.ozturk@gtu.edu.tr
ORCID: https://orcid.org/0000-0002-5073-6564, https://orcid.org/0000-0003-1795-0777

(CBD), and hydrothermal synthesis [5–8] CBD is one of the most widely used methods because of its low cost and temperature requirement. The most important advantage of the CBD method is that almost any substrate can be used for the growth of vertical ZnO nanorods by forming a ZnO seed layer [9, 10]. The quality of the crystal growth depends on the growth time and temperature, and on the chemical bath conditions, such as the nature and concentrations of chemicals, the pH of the growth solution, and the control of additives to control the structural morphology of ZnO nanorods [11]. Previous studies have revealed that it is possible to control the aspect ratio of ZnO nanorods on the substrate by varying the bath temperature in the CBD process. Poornajar et al. [12] reported that the aspect ratio (length/diameter) of ZnO nanorods increased as the growth temperature (80-90°C) increased. Abdulrahman et al. investigated [13] the effects of different growth temperatures (65-115°C) on the crystal structure of ZnO nanorods and emphasized that the aspect ratio increased with growth temperature up to 95°C and it tended to decrease with increasing temperature to 115 °C. Zn^{2+} and O^{2-} ions tend to be adsorbed into polar planes such as (001) to minimize the surface energy during the ZnO nanorod growth process. Temperatures that provide sufficient thermal energy (e.g., 95 °C) lead to anisotropic growth of ZnO nanorods along the c-axis. However, at low temperatures, sufficient thermal energy may not be supplied for the ions to be adsorbed on polar surfaces. Therefore, the ions will adsorb randomly in different crystallographic planes such as (101) and (100) [14, 15]. Moreover, the reaction rate in the CBD process results in the formation of structures of different sizes and irregular morphology. Therefore, it is required to control the chemical reaction by using convenient additives such as organic ligands and surfactants. Amine molecules such as hexylamine, ethylenediamine, trimethylamine and butylamine are frequently used as additives in the CBD precursor solution [16]. Hexamethylenetetramine

(HMTA) is a nonionic, heterocyclic tertiary amine that is highly soluble in water and often preferred as a reducing agent and pH regulator among amine molecules. In recent studies, it has been revealed that HMTA acts as a capping agent that promotes anisotropic growth along the c-axis in addition to its OH^- ion provider (pH regulator) effect [17, 18]. Considering the importance of surface area in photocatalytic reactions, studies with different molar ratios will be carried out to determine the effect of HMTA concentration in the precursor solution on ZnO nanorods morphology.

In this study, the effects of precursor solution concentration and HMTA content on the growth of ZnO nanorods were investigated. To facilitate effective crystal growth, all nanorod arrays to be characterized were grown on the seeded chemically stable and optically transparent glass lamella. The five-step wet chemical dip-coating technique was used to provide complete coverage of the glass surfaces with the ZnO seed layer. ZnO nanorods were successfully grown on the seeded glass substrate by a low-temperature (~95 °C) CBD method. The molar ratio of Zn^{2+}/OH^- is crucial in the morphology control of ZnO nanostructures. The multiple roles of HMTA were revealed by examining in detail the structural properties of grown ZnO nanorods by non-equimolar zinc nitrate hexahydrate (ZNH) and hexamethylenetetramine (HMTA) concentrations over a wide range.

2. METHODS

The surface must be clean (free of impurities) and suitable for chemical bonding. For this purpose, glass lamellas (2.5 cm x 1cm x 7.5 cm) were placed vertically in the chalet. It was kept overnight at 70 °C (oven) in an aqueous solution of hydrochloric acid (HCl, Merck 36.7%) prepared at a ratio of 1:5 by volume. Then, the lamellas were washed with distilled water, and they were kept in 0.2 M NaOH (Merck) aqueous solution at 70 °C for 4 hours. The glass surface was activated after

washing with distilled water and drying at 80 °C for 1 hour. The presence of active nucleation sites lowers the thermodynamic barrier and supports the nucleation and crystal growth stages. Therefore, a two-step seed-mediated process was followed to grow ZnO nanorods. ZnO seed solution was prepared by stirring 0.1 M zinc acetate dihydrate ($Zn(C_2H_3O_2).2H_2O$, Merck) (ZAD) and 0.2 M NaOH in 100 mL of ethanol at 60 °C for 2 hours (pH~10.1). Activated glass surfaces were coated using dip-coating technique at a speed of 100 mm/min and dried at 130 °C for 5 minutes. It has been reported that optimum seed thickness is obtained by 4-6 dip-coating cycles to promote crystallization and alignment of ZnO nanorods [19, 20]. Therefore, this coating step was repeated 5 times. In our previous study [21], the effect of different annealing temperatures (250-400 °C) of the seed layer on the crystallinity and orientation of the ZnO nanorods was investigated. Good crystallinity and sufficient seed densities were obtained at 400 °C. Therefore, the seeded samples were annealed at 400 °C in the present study.

CBD precursor solutions were prepared by mixing zinc nitrate hexahydrate (ZNH) ($Zn(NO_3)_2 \cdot 6H_2O$, Sigma Aldrich) and hexamethylenetetramine (HMTA) ($C_6H_{12}N_4$, Merck) aqueous solutions at room temperature. The molar ratio of the solution was fixed at 1:1, whereas concentrations are set as 0.025, 0.035, 0.050, and 0.075 M. The effect of HMTA concentration in the precursor solution on the aspect ratios of ZnO nanorods was evaluated by changing the ZNH: HMTA molar ratios. For this, precursor solutions rich in Zn^{+2} ions (1:1/4 (Z4), 1:1/2.5 (Z2.5), 1:1/1.5 (Z1.5) and 1:1 (Z1) (ZNH: HMTA)) and vice versa OH^- ions (1/4:1 (Z0.25), 1/2.5:1 (Z0.4) and 1/1.5:1 (Z0.6) (HMTA: ZNH)) were prepared. The value corresponding to state 1 for each sample was fixed at 0.05 M. ZnO nanorods were synthesized by CBD method in 5 hours at 95 °C on the seeded glass substrates. At the end of the reaction, the samples were washed several times with acetone and distilled water,

respectively. Finally, samples were kept in an oven at 150 °C for 30 minutes to evaporate the excess water. The crystal structures of all samples were determined by X-ray diffraction analysis (XRD, Rigaku DMax 200) using Cu-Kα radiation with a scanning range of $2\theta = 20 - 70°$ and a wavelength of $\lambda = 1.5406$ nm. In addition, the morphologies of the ZnO nanorods were investigated using scanning electron microscopy (SEM, Philips XL30SFEG). Before and after the CBD process, the pH values of the precursor solutions were measured by the pH meter (Ohaus Starter 300).

3. CONCLUSIONS AND DISCUSSION

3.1. The Effect of Molar Concentration

The crystallographic structures of ZnO nanorods grown with 0.025, 0.035, 0.05, and 0.075 M concentrations are shown in Figure 1a. All observed diffraction peaks in the XRD patterns are consistent with the standard diffraction peaks of the hexagonal wurtzite phase of ZnO (JCPDS No. 36-1451). No other impurity diffraction peaks were represented. The strong diffraction peaks are located at $2\theta = 34.4°$, $2\theta = 31.7°$, and $2\theta = 36.2°$, and the corresponding planes of ZnO are (002), (100) and (101), respectively [22, 23]. The texture of ZnO nanorods for all samples were achieved along the polar c-axis corresponding to the (002) plane of ZnO. It was observed that the orientation along the c-axis increased with increasing molar concentration. The peak intensities of the sample of Z35 (0.035 M) were considerably higher than the other samples (Figure 1b). On the other hand, the orientation was partially impaired when the concentration increased from 0.050 to 0.075 M. The deformation of orientation was due to the impact of HMTA on the growth characteristics of ZnO nanorods.

Furthermore, the preferred orientation of ZnO nanorods was evaluated according to the texture coefficient (TC) expressed in Equation 1:

$$TC_{(002)} = \frac{I_{(002)}/I_{(002)}^{\circ}}{I_{(002)}/I_{(002)}^{\circ} + I_{(101)}/I_{(101)}^{\circ}} \qquad (1)$$

where $I_{(h\,k\,l)}$ is the obtained XRD peak intensity corresponding to (h k l) plane and $I_{(h\,k\,l)}^{\circ}$ is the intensity of the (h k l) plane related to the standard powder diffraction intensities of the (h k l) plane [12, 24]. The calculated $TC_{(002)}$ values of all samples are listed in Table 1. The degree of c-orientation of the Z35 sample is ~0.92 which validates a high preferential orientation of ZnO nanorods along the c-axis. However, the $TC_{(002)}$ value of ~0.72 of the Z25 sample confirmed its random orientation (Figure 1b).

Table 1 The texture coefficient of (002) plane ($TC_{(002)}$) of ZnO nanorods grown at different concentrations (i.e., 0.025, 0.035, 0.05, and 0.075 M)

Samples	$TC_{(002)}$
Z25	0.79
Z35	0.92
Z50	0.88
Z75	0.85

Top and cross-sectional SEM views of ZnO nanorods were grown by CBD with 0.025, 0.035, 0.05 and 0.075 M concentrations are shown in Figure 2. ZnO nanorods with the hexagonal cross-section were successfully grown in all samples, while lengths and diameters of nanorods were slightly varied.

Figure 1 a) XRD patterns of ZnO nanorods grown at different molar concentrations (i.e., 0.025, 0.035, 0.05, and 0.075 M) and b) Enlargement of the region between 30-40°
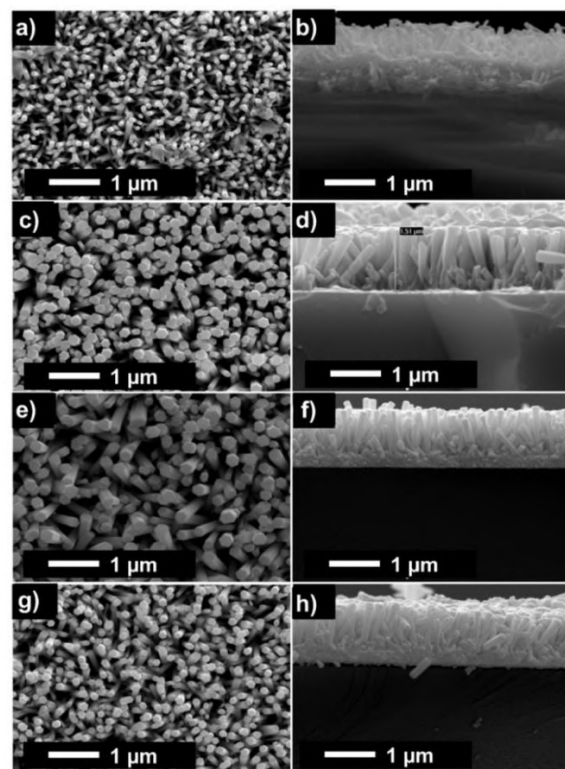
Figure 2 The top and cross-sectional SEM views of ZnO nanorods synthesized at a, b) 0.025, c, d) 0.035, e, f) 0.05, and g, h) 0.075 M

It has been seen that ZnO nanorods with low molar concentration (0.025 M) were randomly oriented and the number of nanorods per unit area is relatively less (Figure 2a, b). The vertical alignment of nanorods improved with increasing molar

Memnune KARDEŞ, Koray ÖZTÜRK

Two Significant Factors Affecting the Dimensions of the ZnO Nanorods During Chemical Bath Deposition:...

concentration (Figure 2c-h). During growth in a solution containing 0.025 M HMTA, the HMTA concentration in the solution at the bottom of the nanorods gradually decreases and this reduces the steric hindrance effect. The higher the HMTA concentration, the more controlled growth occurs. On the other hand, the number of nanorods for the sample of Z75 (Figure 2e, f) was quite high and this negatively affected the alignment.

The diameters, lengths, and aspect-ratios of ZnO nanorods synthesized at different concentrations measured via SEM images are listed in Table 2. All values were the arithmetic mean and standard deviation of 10 measurements. The average diameters of ZnO nanorods were 120, 250, 200, and 175 nm for the sample of Z25, Z35, Z50, and Z75, respectively. The average length of ZnO nanorods were 660, 1450, 1220, and 1040 nm for the sample of Z25, Z35, Z50, and Z75, respectively. The mean diameter and length values of the Z35 sample were quite high compared to the other samples, and these data confirm that the peak intensities are high in XRD patterns. However, the maximum aspect-ratio was achieved with the sample with 0.05 M concentration.

Table 2 The diameters, lengths, and aspect-ratios of ZnO nanorods grown at different concentrations (i.e., 0.025, 0.035, 0.05, and 0.075 M) calculated via SEM images

Samples	Diameter (nm)	Length (nm)	Aspect-Ratio
Z25	120 ± 20	660 ± 100	5.6
Z35	250 ± 18	1450 ± 90	5.8
Z50	200 ± 17	1220 ± 80	6.2
Z75	175 ± 19	1040 ± 80	5.9

3.2. The Effect of HMTA Content

The effect of hexamethylenetetramine (HMTA) concentration used as a reducing agent and pH regulator in CBD precursor solution on ZnO nanorods morphology was investigated. Top and cross-sectional SEM images of ZnO nanorods grown with different ZNH: HMTA molar ratios are shown in

Figure 3 and Figure 4. It has been seen that ZnO nanorods were successfully grown for all ZNH:HMTA ratios rich in Zn^{2+} ions (i. e., 1:1/4 (Z4), 1:1/2.5 (Z2.5), 1:1/1.5 (Z1.5), and 1:1 (Z1)) (Figure 3). It was clearly seen that the lengths of the nanorods increased, and their alignment improved with decreasing $[Zn^{2+}:OH^-]$ molar ratio.

Figure 3 Top (a-g) and cross-sectional (b-h) SEM views of ZnO nanorods grown using solution with ZNH: HMTA molar ratios of a, b) 4, c, d) 2.5, e, f) 1.5 and g, h) 1

On the other hand, SEM images for ZNH:HMTA ratios rich in OH^- ions (i.e., 1/4:1 (Z0.25), 1/2.5:1 (Z0.4), and 1/1.5:1 (Z0.6)) are shown in Figure 4. ZnO nanorods were able to be grown for the ZNH:HMTA ratio of 0.6. However, the molar ratios of 0.25 and 0.4 were insufficient for the nucleation of nanorods (Figure 4a-d). Moreover, ZnO nanorods were almost absent at the higher molar ratio of 0.4 (Figure 4c, d), while the crystal growth was partially present at the 0.25 molar ratio (Figure 4a, b).

The diameter, length, and aspect-ratios of ZnO nanorods were measured for all samples

using top SEM views and the values (the arithmetic mean and standard deviations of 10 measurements) were listed in Table 3. Also, the pH values before and at the end of the CBD reaction as a function of the ZNH: HMTA ratio are shown in Figure 5.
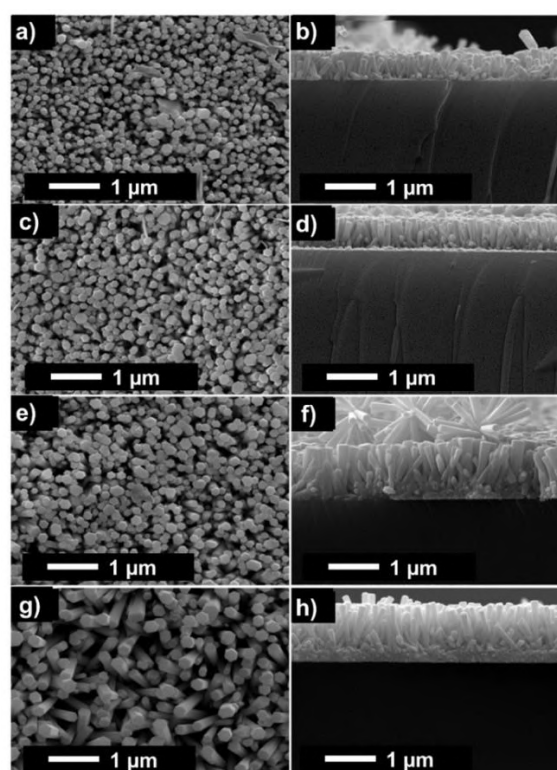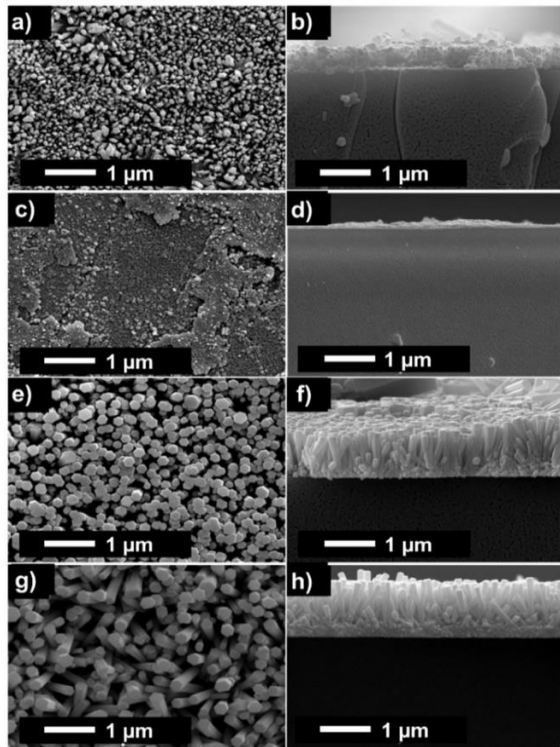

Figure 4 Top (a-g) and cross-sectional (b-h) SEM views of ZnO nanorods grown using solution with ZNH: HMTA molar ratios of a, b) 0.25, c, d) 0.4, e, f) 0.6 and g, h) 1

It has been observed that the lengths of ZnO nanorods increased rapidly when the ZNH: HMTA molar ratio decreased from 4 to 1. On the other hand, the pH values of the solutions rich in Zn^{2+} ions (i.e., ZNH:HMTA ratio between 1 and 4) almost remained constant at values of ~6.8 and ~6.4 before and after the CBD process, respectively. However, the lengths of nanorods were decreased when the molar ratio decreased below 1. The pH values of the solutions rich in OH^- ions (i.e., ZNH:HMTA ratio between 0.25 and 1) before and after the CBD process are strongly decreased from ~7.0 to ~7.8 and ~7.0 to ~7.5, respectively (Figure 5). The diameters of the ZnO nanorods reached the largest value in the sample with a molar ratio of 0.6 ZNH: HMTA (ZS0.6).

Table 3 The diameters, lengths, and aspect-ratios of ZnO nanorods grown at different concentrations (i.e., 0.025, 0.035, 0.05, and 0.075 M) calculated via SEM images

Samples	Diameter (nm)	Length (nm)	Aspect-Ratio
Z4	180 ± 21	500 ± 80	2.7
Z2.5	190 ± 18	600 ± 100	3.1
Z1.5	250 ± 17	920 ± 100	3.6
Z1	200 ± 17	1220 ± 80	6.1
Z0.6	180 ± 20	1010 ± 100	5.6
Z0.4	-	-	-
Z0.25	130 ± 22	230 ± 50	1.7

The aspect ratios of ZnO nanorods reached to a maximum value of 6.1 for the Z1 coded sample. When the HMTA concentration is increased further, the solution is enriched with OH^- ions and the Zn^{2+} ion concentration decreases. Thus, the probability of nucleation is reduced. Moreover, the decrease in the diameter of nanorods with increasing HMTA ratio is direct evidence that HMTA significantly suppresses radial growth and promotes axial growth. While HMTA acts as a pH regulator, it also plays multiple roles with a steric hindrance effect that inhibits lateral growth.
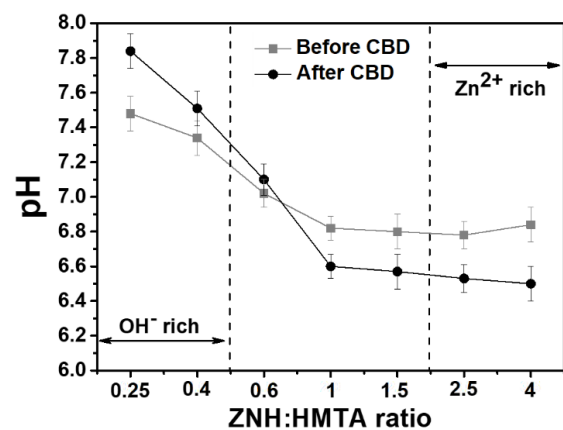

Figure 5 Evolution of the pH values before (gray dots) and after (black dots) CBD as a function of the [ZNH: HMTA] ratio
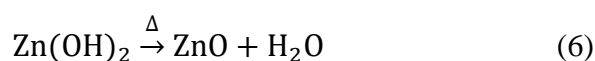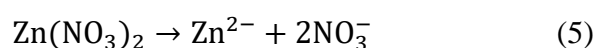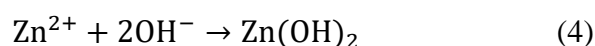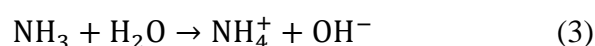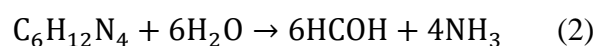
In the photocatalysis process, the organic pollutant molecules are adsorbed on the photocatalyst sample surfaces. The catalytic reactions take place on the surfaces of the catalyst. Therefore, the geometric factors

such as diameter, length, and surface area of ZnO nanorods are crucial in the photocatalytic degradation rates. In previous studies, it was revealed that a high aspect ratio supplied more adsorption sites for the efficient catalytic reaction [25, 26]. Reduced aspect ratios, however, lead to the adsorption of molecules mostly on the top surfaces. On the other hand, excessively lengthened nanorods may prevent UV light penetration on entire surfaces. Therefore, the aspect ratio of ZnO nanorods is expected to be at an optimum level for adequate interactions with UV light [21].

3.3. Growth Mechanism of ZnO nanorods

The preferential growth mechanism of ZnO nanorods by CBD is explained by thermodynamic considerations. The top and lateral faces of ZnO nanorods are composed by polar c-planes with lower surface energy and non-polar m-planes, respectively. Total free energy is minimized when the surface area of non-polar m-plane vertical lateral faces is improved by promoting axial growth at the expense of radial growth [27, 28]. The axial growth rate typically exceeds the radial growth rate due to kinetic factors. Therefore, ZnO nanorods is generally terminated with a polar c-plane due to the electrostatic interactions of Zn^{2+} and OH^- ions in the precursor solution. However, it should be noted that growth rates are limited by the mass transport of chemicals in the precursor solution [29]. The priority of binding to the polar surfaces of ZnO by chelating HMTA molecules is due to the capping agent effect. HMTA can bind to the crystal surfaces of ZnO in two ways. It occurs by hydrogen bonding between ammonium cations and O^{-2} crystal ions, or by a covalent bond between basic N atoms and the acidic Zn^{2+} region. HMTA prevents Zn^{2+} entry to the lateral surfaces and facilitates its anisotropic growth in the [001] direction by binding to the non-polar lateral surfaces of ZnO [30]. Commonly, it provides $-OH$ ions to regulate the pH of the acidic solution because of Zn^{2+} hydrolysis. HMTA can play an active role in

the morphology of ZnO nanorods, both as a capping agent and as a pH regulator depending on the molar ratio of ZNH:HMTA. The HMTA source decomposes to form formaldehyde and ammonia with sufficient thermal energy by reaction (2). Ammonia reacts with water to provide OH^- ions dissolved in water through reaction (3) and (4), and these ions can react with Zn^{2+} to form ZnO by reaction (5) and (6). Typical reactions are described below [10]:

$$C_6H_{12}N_4 + 6H_2O \rightarrow 6HCOH + 4NH_3 \qquad (2)$$

$$NH_3 + H_2O \rightarrow NH_4^+ + OH^- \qquad (3)$$

$$Zn^{2+} + 2OH^- \rightarrow Zn(OH)_2 \qquad (4)$$

$$Zn(NO_3)_2 \rightarrow Zn^{2-} + 2NO_3^- \qquad (5)$$

$$Zn(OH)_2 \xrightarrow{\Delta} ZnO + H_2O \qquad (6)$$

4. CONCLUSION

The multiple roles of HMTA content and the concentration of CBD solution on the dimension of ZnO nanorods were investigated in this study. ZnO nanorods were successfully grown on the glass substrate by seed-mediated approach using the low-temperature CBD method. The effects of zinc ion concentration and HMTA content of the CBD solution on the crystal orientation and aspect ratios of ZnO nanorods were investigated. The crystallinity and morphological analysis indicated that the orientation and number densities of the nanorods (i.e., the number of nanorods per unit area) were increased with the increasing molar concentration from 0.025 to 0.05. Moreover, ZNH: HMTA molar ratio of precursor solution is critical in the growth of ZnO in liquid phase by CBD. It was found that increasing HMTA content promoted the growth of ZnO nanorods along the c-axis, and the lateral growth was suppressed by the capping effect of HMTA. It is revealed that the largest axial growth rate of ZnO nanorods was reached for the [ZNH: HMTA] ratio of 1. HMTA induces vertical growth of ZnO

nanorods along the c-axis through a steric hindrance effect that inhibits lateral growth. However, excessive HMTA content led to a reduced probability of crystal growth attributed to OH^- ion enrichment.

Authors' Contribution

The authors who have made substantial contributions to the work reported in the manuscript are:

M.K.: Term, Conception and design of study, Visualization, Writing - Original Draft, Data Curation, Investigation, Formal analysis, Validation, Methodology.
K.Ö.: Supervision, Project administration, Term, Conceptualization, Writing- Original Draft, Data Curation, Investigation, Formal analysis, Validation, Methodology.

The Declaration of Conflict of Interest/ Common Interest

No conflict of interest or common interest has been declared by the authors.

The Declaration of Ethics Committee Approval

This study does not require ethics committee permission or any special permission.

The Declaration of Research and Publication Ethics

The authors of the paper declare that they comply with the scientific, ethical and quotation rules of SAUJS in all processes of the paper and that they do not make any falsification on the data collected. In addition, they declare that Sakarya University Journal of Science and its editorial board have no responsibility for any ethical violations that may be encountered, and that this study has not been evaluated in any academic publication environment other than Sakarya University Journal of Science.

REFERENCES

[1] I. Udom, M. K. Ram, E. K. Stefanakos, A. F. Hepp, D. Y. Goswami, "One dimensional-ZnO nanostructures: Synthesis, properties and environmental applications", Materials Science in Semiconductor Processing, vol. 16, no. 6, pp. 2070–2083, 2013.

[2] M. Samadi, M. Zirak, A. Naseri, M. Kheirabadi, M. Ebrahimi, A. Z. Moshfegh, "Design and tailoring of one-dimensional ZnO nanomaterials for photocatalytic degradation of organic dyes: a review", Research on Chemical Intermediates, vol. 45, pp. 2197–2254, (2019).

[3] C. J. Chang, M. H. Hsu, Y. C. Weng, C. Y. Tsay, C. K. Lin, "Hierarchical ZnO nanorod-array films with enhanced photocatalytic performance", Thin Solid Films, vol. 528, pp. 167–174, 2013.

[4] T. Cossuet, E. Appert, J. L. Thomassin, V. Consonni, "Polarity-Dependent Growth Rates of Selective Area Grown ZnO Nanorods by Chemical Bath Deposition", Langmuir, vol. 33, no. 25, pp. 6269–6279, 2017.

[5] B. Astinchap, R. Moradian, M. N. Tekyeh, "Investigating the optical properties of synthesized ZnO nanostructures by sol-gel: The role of zinc precursors and annealing time", Optik, vol. 127, no. 20, pp. 9871–9877, 2016.

Memnune KARDEŞ, Koray ÖZTÜRK

Two Significant Factors Affecting the Dimensions of the ZnO Nanorods During Chemical Bath Deposition:...

[6] A. A. Mohd Raub, J. Yunas, M. A. Mohamed, B. Bais, A. A. Hamzah, J. Ridwan, J. Kazmi, M. A. Hassan, "Synthesis and characterization of ZnO NRs with spray coated GO for enhanced photocatalytic activity", Ceramics International, vol. 48, no. 13, pp. 18238-18245, 2022.

[7] N. Lepot, M. K. Van Bael, H. Van den Rul, J. D'Haen, R. Peeters, D. Franco, J. Mullens, "Synthesis of ZnO nanorods from aqueous solution", Materials Letters, vol. 61, no. 13, pp. 2624–2627, 2007.

[8] L. Xu, Y. L. Hu, C. Pelligra, C. H. Chen, L. Jin, H. Huang, S. Sithambaram, M. Aindow, R. Joesten, S. L. Suib, "ZnO with different morphologies synthesized by solvothermal methods for enhanced photocatalytic activity", Chemistry of Materials, vol. 21, no. 13, pp. 2875–2885, 2009.

[9] N. T. Son, J. S. Noh, S. Park, "Role of ZnO thin film in the vertically aligned growth of ZnO nanorods by chemical bath deposition", Applied Surface Science, vol. 379, pp. 440-445, 2016.

[10] M. Kardeş, G. Başaran Dindaş, H. C. Yatmaz, N. Dizge, K. Öztürk, "CBD grown pure and Ce-doped ZnO nanorods: Comparison of their photocatalytic degrading efficiencies on AR88 azo dye under visible light irradiation", Colloids Surface A Physicochemical Engineering Aspects, vol. 607, pp. 125451, 2020.

[11] K. Mosalagae, D. M. Murape, L. M. Lepodise, "Effects of growth conditions on properties of CBD synthesized ZnO nanorods grown on ultrasonic spray pyrolysis deposited ZnO seed layers", Heliyon, vol. 6, no. 7, pp. e04458, 2020.

[12] M. Poornajar, P. Marashi, D. H. Fatmehsari, M. K. Esfahani, "Synthesis of ZnO nanorods via chemical bath deposition method: The effects of physicochemical factors", Ceramics International, vol. 42, no. 1, pp. 173–184, 2016.

[13] A. F. Abdulrahman, S. M. Ahmed, S. M. Hamad, A. A. Barzinjy, "Effect of Growth Temperature on Morphological, Structural, and Optical Properties of ZnO Nanorods Using Modified Chemical Bath Deposition Method", Journal of Electronic Materials, vol. 50, pp.1482–1495, 2021.

[14] Q. Liu, T. Yasui, K. Nagashima, T. Yanagida, M. Hara, M. Horiuchi, Z. Zhu, H. Takahashi, T. Shimada, A. Arima, Y. Baba, "Ammonia-Induced Seed Layer Transformations in a Hydrothermal Growth Process of Zinc Oxide Nanowires", The Journal of Physical Chemistry C, vol. 124, no. 37, pp. 20563-20568.

[15] S. Guillemin, L. Rapenne, H. Roussel, E. Sarigiannidou, G. Brémond, V. Consonni, "Formation mechanisms of ZnO nanowires: The crucial role of crystal orientation and polarity", The Journal of Physical Chemistry C, vol. 117, no. 40, pp. 20738–20745, 2013.

[16] A. S. Kamble, B. B. Sinha, K. Chung, M. G. Gil, V. Burungale, C. J. Park, J. H. Kim, P. S. Patil, "Effect of hydroxide anion generating agents on growth and properties of ZnO nanorod arrays", Electrochimica Acta, vol. 149, pp. 386–393, 2014.

[17] A. F. Abdulrahman, "Study the optical properties of the various deposition solutions of ZnO nanorods grown on glass substrate using chemical bath deposition technique", Journal of

Memnune KARDEŞ, Koray ÖZTÜRK

Two Significant Factors Affecting the Dimensions of the ZnO Nanorods During Chemical Bath Deposition:...

Ovonic Research, vol. 16, no. 3, pp. 181–188, 2020.

[18] V. Strano, R. Giovanni Urso, M. Scuderi, K. O. Iwu, F. Simone, E. Ciliberto, C. Spinella, S. Mirabella, "Double Role of HMTA in ZnO Nanorods Grown by Chemical Bath Deposition", The Journal of Physical Chemistry C, vol. 118, no. 48, pp. 28189–28195, 2014.

[19] B. Ikizler, S. M. Peker, "Effect of the seed layer thickness on the stability of ZnO nanorod arrays", Thin Solid Films, vol. 558, pp. 149–159, 2014.

[20] S. Guillemin, V. Consonni, E. Appert, E. Puyoo, L. Rapenne, H. Roussel, "Critical nucleation effects on the structural relationship between ZnO seed layer and nanowires", The Journal of Physical Chemistry C, vol. 116, no. 47, pp. 25106–25111, 2012.

[21] M. Kardeş, K. Öztürk, "Photocatalyst ZnO nanorod arrays on glass substrates: the critical role of seed layer in nanorod alignment and photocatalytic efficiencies", Chemical Engineering Communication, vol. 207, no. 11, pp. 1522-1535, 2020.

[22] J. Singh, S. S. Patil, M. A. More, D. S. Joag, R. S. Tiwari, O. N. Srivastava, "Formation of aligned ZnO nanorods on self-grown ZnO template and its enhanced field emission characteristics", Applied Surface Science, vol. 256, no. 21, pp. 6157–6163, 2010.

[23] P. Gu, X. Zhu, D. Yang, "Vertically aligned ZnO nanorods arrays grown by chemical bath deposition for ultraviolet photodetectors with high response performance", Journal of Alloys and Compounds, vol. 815, pp. 152346, 2020.

[24] Y. Kajikawa, S. Noda, H. Komiyama, "Preferred orientation of chemical vapor deposited polycrystalline silicon carbide films", Chemical Vapor Deposition, vol. 8, no. 3, pp. 99–104, 2002.

[25] A. Leelavathi, G. Madras, N. Ravishankar, "Origin of enhanced photocatalytic activity and photoconduction in high aspect ratio ZnO nanorods", Physical Chemistry Chemical Physics, vol. 15, no. 26, pp. 10795–10802, 2013.

[26] A. Das, R. G. Nair, "Effect of aspect ratio on photocatalytic performance of hexagonal ZnO nanorods", Journal of Alloys and Compounds, vol. 817, pp. 153277, 2020.

[27] K. M. McPeak, T. P. Le, N. G. Britton, Z. S. Nickolov, Y. A. Elabd, J. B. Baxter, "Chemical bath deposition of ZnO nanowires at near-neutral pH conditions without hexamethylenetetramine (HMTA): Understanding the role of HMTA in ZnO nanowire growth", Langmuir, vol. 27, no. 7, pp. 3672–3677, 2011.

[28] R. Parize, J. Garnier, O. Chaix-Pluchery, C. Verrier, E. Appert, V. Consonni, "Effects of Hexamethylenetetramine on the nucleation and radial growth of ZnO nanowires by chemical bath deposition", Journal of Physical Chemistry C., vol. 120, no. 9, pp. 5242–5250, 2016.

[29] W. Feng, B. Wang, P. Huang, X. Wang, J. Yu, C. Wang, "Wet chemistry synthesis of ZnO crystals with hexamethylenetetramine (HMTA): Understanding the role of HMTA in the formation of ZnO crystals", Materials Science in Semiconductor Processing, vol. 41, pp. 462–469, 2016.

Memnune KARDEŞ, Koray ÖZTÜRK

Two Significant Factors Affecting the Dimensions of the ZnO Nanorods During Chemical Bath Deposition:...

[30] H. Avireddy, H. Kannan, P. Shankar, G. K. Mani, A. J. Kulandaisamy, J. B. B. Rayappan, "Non-mutually exclusive dual role of hexamethylenetetramine on the growth of ZnO nanostructures and their sensing footprints", Materials Chemistry and Physics, vol. 212, pp. 394–402, 2018.

Title: Synthesis and Structural Investigations of 1,
2-bis(2-ethoxybenzylidene)hydrazine

Authors: Sevgi KANSIZ

New submission to SAUJS
http://dergipark.gov.tr/journal/1115/submission/start

Synthesis and Structural Investigations of 1, 2-bis(2-ethoxybenzylidene)hydrazine

Sevgi KANSIZ *[1] iD

Abstract

The titled compound, 1,2-bis(2-ethoxybenzylidene) hydrazine was developed using the reaction of 2-ethoxybenzaldehyde and hydrazine monohydrate in an ethanolic solution. In the Schiff-based hydrazine compound, $C_{18}H_{20}N_2O_2$, the mid-point of the nitrogen atoms of the central hydrazine moiety is located in inversion symmetry. In $C_{18}H_{20}N_2O_2$, C−H⋯N hydrogen bond linked the molecules, and the framework stabilized by weak C−H⋯π and π⋯π stacking interactions. MEP, HOMO and LUMO analysis were performed with the DFT/B3LYP method and the 6-311+G(d,p) basis set. The energies of frontier orbitals were calculated to understand specific molecular properties such as electronegativity, chemical reactivity, chemical hardness and softness. For investigating the contributions of various intermolecular contacts within the hydrazine compound, Hirshfeld surface analysis was performed. The largest contribution of the compound to the main interactions comes from the H⋯H (64%), C⋯H (16%) and N⋯H (9%) interactions.

Keywords: Schiff base, hydrazine, X-ray, DFT, Hirshfeld surface analysis

1. INTRODUCTION

Schiff base compounds are among the important inorganic materials due to their flexibility in coordination geometries, forming many metal complexes, easy synthesis and stability of their compounds [1-5]. Schiff base compounds are small molecules that are obtained as a result of the nucleophilic addition reaction of aldehydes or ketones with primary amines and contain carbon-nitrogen double bonds (-CH=N) [6]. Schiff base ligands can form highly stable 4, 5, or 6-ring aromatic compounds. For this, it is necessary having a second functional group close to the azomethine group and a

displaceable hydrogen atom. This group is preferably the hydroxyl group. Schiff base compounds, which are used extensively in the field of coordination chemistry due to their electron-donating ability, are used in many new areas [7] from the health field [8] to the dyeing industry [9] due to their properties such as electroluminescence effects [10], fluorescence [11], and nonlinear optics [12]. Hydrazine, which is a strong reducing agent, is frequently used in areas such as various industrial, pharmacological, and many other applications [13, 14]. Hydrazine derivatives having a wide range of uses as an intermediate in the synthesis of pharmaceutical drugs, as a polymerization catalyst and in plastic

* Corresponding author: sevgi.kansiz@samsun.edu.tr (S. KANSIZ)
[1] Samsun University, Faculty of Engineering, Department of Fundamental Sciences, Samsun, Türkiye
ORCID: https://orcid.org/0000-0002-8433-7975

processing, are also considerably used as a technological compound in the magnetic and biomedical fields [15].

In this study, a hydrazine-Schiff base compound, $C_{18}H_{20}N_2O_2$, 1,2-bis(2-ethoxybenzylidene) hydrazine was synthesized as a result of the condensation reaction of 2-ethoxybenzaldehyde and hydrazine monohydrate in an ethanolic solution. The theoretical calculations of the Schiff-based hydrazine compound, its structure was identified by the X-ray diffraction technique, were compared with the data obtained from the crystallographic analysis. In order to examine the theoretical structure of the 1,2-bis(2-ethoxybenzylidene) hydrazine molecule, the Gaussian package program was used and its three-dimensional approximate geometry was drawn in the GaussView program [16, 17]. In all theoretical calculations, the density functional method (DFT) and Becke type 3-parameter Lee-Yang-Par model (B3LYP) and 6-311+G(d,p) basis set were used [18]. After optimization, the frontier molecular orbitals energies, global hardness and softness parameters, electrophilic and nucleophilic regions on the molecular electrostatic potential map were determined, and the results were evaluated under these headings. In addition, visual representation of d_{norm}, shape index, and curvedness maps obtained by Hirshfeld surface analysis, percent contribution of atoms to interactions, and two-dimensional fingerprint determinations were obtained using the Crystal Explorer program [19].

1.1. Crystallographic Part

An appropriate single crystal was selected for the Schiff-based hydrazine derivative compound and data collection was obtained by STOE IPDS 2 image plate detector using MoKα radiation ($\lambda = 0.71073$Å). X-AREA as used for data collection and cell enhancement and X-RED was used for data reduction [20]. The structure of the Schiff-based hydrazine derivative compound was determined using the SHELXT structure solution program [21]. The direct methods were employed to solve the structure of the compound, followed by refinement using full-matrix least-squares techniques on F^2 using SHELXL [22]. The refinement was carried out against all reflections to ensure a thorough and accurate analysis of the structure. In the refinement process, the hydrogen atoms were constrained by difference maps, which allowed for a more precise determination of their positions. The hydrogen atoms were also refined isotropically, meaning that their thermal motion was assumed to be the same in all directions. In contrast, all non-hydrogen atoms were refined anisotropically, which means that their thermal motion was allowed to vary depending on the direction. This approach ensured that the most accurate positions and thermal parameters were determined for each atom in the compound. Detailed parameters of the crystal structure are given in Table 1.

Table 1 Experimental details of the title compound

CCDC number	2177378
Chemical formula	$C_{18}H_{20}N_2O_2$
Mr	296.36
Radiation type	Mo K\a
Wavelength	0.71073
Crystal System, Space Group	Monoclinic, P2$_1$/c
Data collection Diffractometer	STOE IPDS 2
Temperature	296
a, b, c (Å)	7.6871(11), 11.7638(11), 9.0832(12)
α, β, γ	90, 102.257(10), 90
Cell Volume, V	802.67(18)
μ (mm^{-1})	0.08
Absorption correction	integration
No. of measured, independent and observed [I > 2σ(I)] reflections	7323, 2592, 1505
No. of reflections	2592
No. of parameters	101
Crystal Size	0.75 x 0.67 x 0.58
F(000)	316
Theta range for data collection	1.7−31.6
Z	2
Limiting Indices	−9 ≤ h ≤ 11, −14 ≤ k ≤ 17, −13 ≤ l ≤ 13
R$_{int}$	0.052
Final R Indices [F^2 > 2σ (F^2)], wR(F^2), S	0.046, 0.128, 0.99
Δρ$_{max}$, Δρ$_{min}$ (e/Å^3)	0.18, −0.14

1.2. Methods

The utilization of DFT calculations with various parameters and analyses provides a comprehensive understanding of a molecule's electronic properties, reactivity, and stability. This knowledge can guide the design and synthesis of new compounds with desired properties. In this study, DFT was employed to optimize the molecular structure of the compound utilizing the B3LYP functional and the 6-311+G(d,p) basis set. The B3LYP functional is a hybrid functional that combines the Becke three-parameter exchange functional and the Lee-Yang-Parr correlation functional. The optimized structure was evaluated for stability using frontier orbitals (HOMO and LUMO) and susceptibility to chemical activity was also explored. Chemical activity parameters such as kinetic stability, chemical stability, and intramolecular charge transfer were also determined. Additionally, molecular electrostatic potential (MEP) analysis was used to identify electron-rich and poor regions. The optimized geometry of the compound, MEP map, and HOMO-LUMO energy gaps were visualized using the GuassView 5.0 software.

The analysis of Hirshfeld surfaces [23, 24], along with their corresponding two-dimensional (2D) fingerprint plots, is a powerful tool for investigating intermolecular interactions within a crystal structure [25-27]. The Hirshfeld surface is generated by mapping the electron density of a crystal structure onto a three-dimensional grid surrounding the molecule. Subsequent analysis of the surface provides information about intermolecular interactions within the crystal, such as the location and strength of hydrogen bonds and other non-covalent interactions. The d_{norm} property, which is used in this analysis, is a measure of the normalized contact distance between two atoms within a crystal structure. This property is defined in terms of the van der Waals (vdW) radii of the atoms, as well as the distances between their respective vdW surfaces. A 2D fingerprint plot is used to visualize the combination of the de and di properties of the Hirshfeld surface. This tool can be used to identify specific regions of the surface that correspond to particular types of intermolecular interactions and to compare the surface properties of different crystal structures. To perform these calculations and generate visualizations of the Hirshfeld surfaces and their associated 2D fingerprint plots, the Crystal Explorer 21 software package was employed.

1.3. Synthesis of 1,2-bis(2-ethoxybenzylidene) hydrazine

To synthesize 1,2-bis(2-ethoxybenzylidene) hydrazine, a solution of 2-ethoxybenzaldehyde (1.50 g, 10 mmol) in 10 mL of ethanol was added to a solution of hydrazine monohydrate (65%) (0.38 g, 5 mmol) in 5 mL of ethanol with constant stirring at 0°C. The resulting mixture was stirred at room temperature for 12 hours until a light-yellow solid precipitated. The mixture was then filtered and washed with cold ethanol before being left to dry at room temperature. The obtained solid was recrystallized from ethanol, resulting in a yield of 82% (1.45 g, 4.9 mmol) (Figure 1).
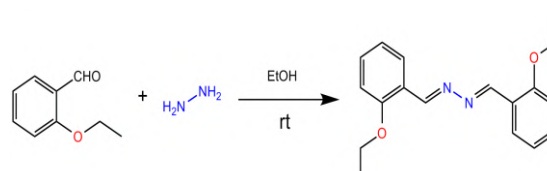
Figure 1 Synthesis of the title compound

2. CONCLUSIONS AND DISCUSSION

2.1. Crystal Structure of $C_{18}H_{20}N_2O_2$

The structure of the Schiff base hydrazine derivative mentioned in the title is presented in Figure 2. It is important to note that the asymmetric unit of this compound comprises one-half of the centrosymmetric molecule. X-ray analysis revealed that the Schiff-based hydrazine derivate compound, $C_{18}H_{20}N_2O_2$, crystallizes in the P2$_1$/c space group in the monoclinic system. Unit cell parameters; a = 7.6871(11), b = 11.7638(11), c = 9.0832(12)

Å, α=90°, β= 102.257(10)° and γ= 90°. The conformation of the Schiff base is nearly coplanar, which is evident from the C2—C1—N1—N1[i] torsion angle of 179.65 (12)°. This observation is further supported by the C3—C2—C1—N1 torsion angle of 6.29 (18)°, which confirms that the phenol ring and the Schiff base are coplanar. The bond lengths of C7–O1 and C8–O1 are 1.3612(14) Å and 1.4284(13) Å, respectively (Table 2). These values are in agreement with the standard values reported for single C—O bonds [28-30]. The bond lengths of C7–O1 and C8–O1 were calculated as 1.3613 Å and 1.4283 Å, respectively. These values are in close agreement with the experimental data obtained from the X-ray crystal structure, as illustrated in Figure 1, indicating that the DFT calculations accurately predicted the molecular geometry of the compound. The C1—N1 bond is notably short, measuring 1.2659 (13) Å, indicating the presence of a C=N double bond. In contrast, the hydrazine bond length of N1—N1[i] is relatively long, measuring 1.4059(17) Å, which suggests that a single bond exists. The N—N hydrazine bond length observed in this study appears to be consistent with previously reported values. While the value obtained in this study is 1.4059 (17) Å, which is slightly longer than the reported range of 1.360-1.376 Å [31-33] in other studies, this difference is not significant enough to suggest any discrepancies between the current results and previously reported values. Overall, these findings support the reliability and validity of the experimental measurements and provide useful information for further investigations of the electronic and chemical properties of the compound. Likewise, C7-O1-C8, C1-N1-N1[i] and C2-C1-N1 bond angles were obtained as 117.93(8)°, 112.75(12)° and 121.97(11)°. The bond angles of C7-O1-C8, C1-N1-N1[i] and C2-C1-N1 were calculated as 117.9372°, 112.7641° and 121.9653°, respectively. The good agreement between the calculated and experimental bond lengths and angles underscores the reliability and utility of DFT as a tool for predicting and understanding the properties and reactivity of molecules. In this way, the calculated bond lengths and angles provide valuable insights into the electronic structure and bonding patterns of the molecule, which are critical for understanding its chemical behavior. Therefore, the consistency between the optimized geometry given by the DFT calculations and the experimental crystal structure is a positive indication of the quality of the calculations and the confidence that can be placed in the results.

X-Ray

DFT
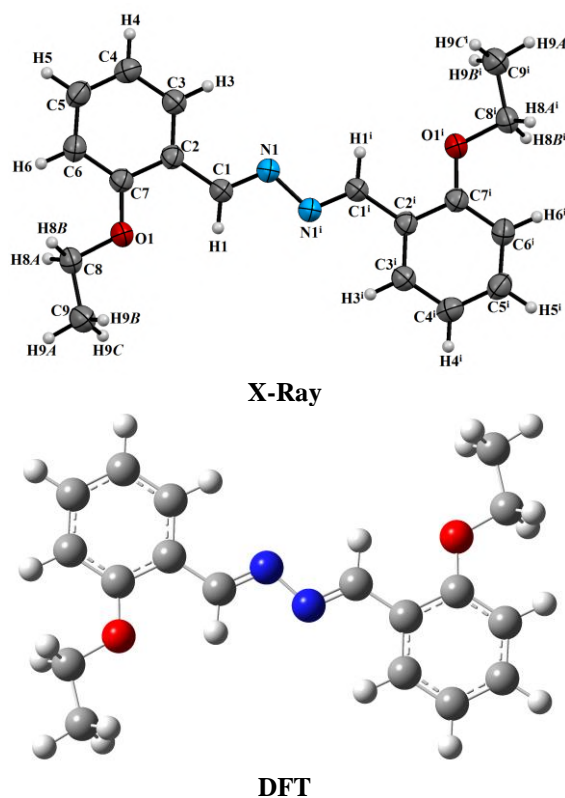
Figure 2 Molecular structure of the title compound

The molecules in $C_{18}H_{20}N_2O_2$ are linked by C4−H4···N1[i] hydrogen bond (Table 3). C4 atom (symmetry code: x, y, z) acts as a donor and forms C−H···N hydrogen bonds with the N1 atom (symmetry code: x, $-y-1/2$, $z-1/2$). In this interaction, the distances between the atoms of C4−H4 (D−H), H4···N1 (H···A) and C4···N1 (D···A) were obtained as 0.93, 2.62(3) and 3.5476(12) Å, respectively. Additionally, C8−H8B···Cg1 and π···π stacking interactions between the benzene rings stabilized the molecular structure, inhere Cg1 is the centered of the benzene ring and Cg1···Cg1 distance is 3.6442(12) Å with

a slippage of 0.659 Å. Some interactions are shown in Figure 3.
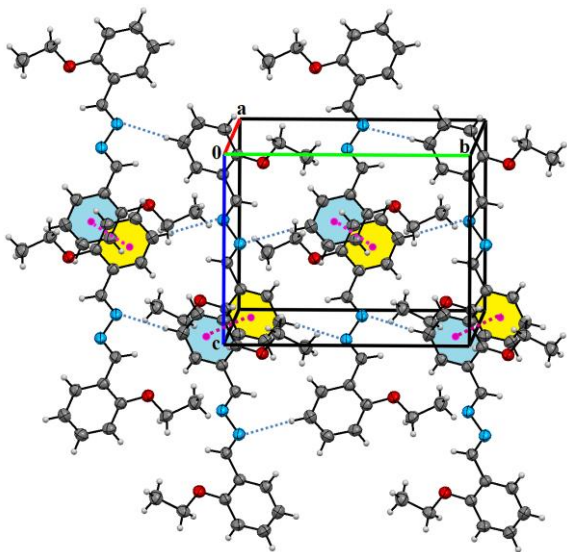
Figure 3 The crystal packing of the title compound

Table 2 Some selected geometric parameters for the title compound

Bond	(Å)	Angle	(deg)
N1−N1^i	1.4059(17)	C7−O1−C8	117.93(8)
C7−O1	1.3612(14)	C9−C8−O1	107.43(9)
C8−O1	1.4284(13)	C2−C7−O1	116.05(9)
C1−N1	1.2659(13)	C6−C7−O1	124.32(10)
C1−C2	1.4578(14)	C2−C1−N1	121.97(11)
C8−C9	1.4959(18)	C1−N1−N1^i	112.75(12)
C2−C3	1.3897(16)	C3−C2−C1	121.33(9)
C3−C4	1.3747(15)	C7−C2−C1	119.98(10)
C7−C2	1.4046(15)	C4−C3−C2	121.31(10)

Table 3 Interactions geometries in the title compound

D−H···A	D−H	H···A	D···A	D−H···A
C4−H4···N1^i	0.93	2.62	3.5476(12)	178(2)
C8−H8B···Cg1^{ii}	0.97	2.84	3.6689(12)	144(2)

Symmetry codes: (i) x, $−y−1/2$, $z−1/2$; (ii) $−x$, $−y$, $−z$.

2.2. Molecular Orbitals of C$_{18}$H$_{20}$N$_2$O$_2$

The ability of a molecule to donate electrons is defined as the HOMO energy (E$_{HOMO}$), while the ability to accept electrons is defined as the LUMO energy (E$_{LUMO}$). The electronic properties and reactivity of the Schiff-based hydrazine derivative compound were investigated by performing DFT calculations in the gas phase environment. To gain further

insight into the electronic structure of the molecule, the HOMO and LUMO surface views are given in Figure 4. Upon conducting this study, it was found that the energy gap for the compound was obtained as ΔE = 3.77 eV, and it was predicted that the optimized structure under investigation is stable. The parameters of hardness and softness for a molecule optimized in a gas phase environment are calculated based on the HOMO and LUMO orbital energies. The chemical hardness and softness parameters are important descriptors of the electronic properties and reactivity of a molecule [34-37]. The hardness parameter is defined as the resistance of a molecule to electron transfer and is calculated as the average of the energy difference between the HOMO and LUMO orbitals. A high hardness value indicates that the molecule has a strong resistance to electron transfer and is less reactive. On the other hand, the softness parameter is defined as the inverse of the hardness and represents the ease with which the molecule can undergo electron transfer. A low softness value indicates that the molecule is more reactive and has a higher tendency to undergo chemical reactions. These parameters can be used to predict the stability and reactivity of a molecule under different conditions and can provide valuable insights into the chemical properties of the compound. In this study, the hardness and softness parameters of the Schiff-based hydrazine derivative compound were calculated as 1.89 (eV)$^{-1}$ and 0.26 eV, respectively, indicating a high chemical hardness and low softness (Table 4). This high hardness value, combined with its low softness value, suggests that the molecule has high kinetic stability and low chemical activity, indicating its potential for use as a stable compound in various applications.

To further assess the stability of the molecule, chemical activity parameters, such as chemical potential, electronegativity, and hardness, were calculated. Chemical potential represents the energy required to add an electron to a system, and electronegativity indicates the tendency of an atom to attract

electrons. A high hardness value indicates a greater resistance of the molecule to electron transfer, whereas a low softness value indicates a greater tendency of the molecule to undergo chemical reactions. The studied molecule was found to have high chemical hardness, suggesting very little intramolecular charge transfer and a greater resistance to electron transfer. This suggests that the molecule has high kinetic stability and low chemical reactivity, making it a promising candidate for further studies in the field of organic synthesis and medicinal chemistry.
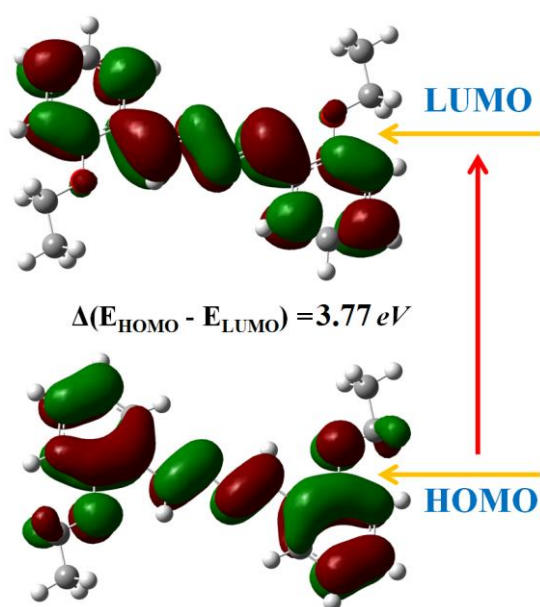
$\Delta(E_{HOMO} - E_{LUMO}) = 3.77\,eV$

Figure 4 The frontier molecular orbitals of the title compound

Table 4 The HOMO-LUMO and related descriptors of the title compound

Parameters	$C_{18}H_{20}N_2O_2$
E_{LUMO} (eV)	-1.98
E_{HOMO} (eV)	-5.75
Energy band gap $\|E_{HOMO} - E_{LUMO}\|$	3.77
Ionization potential ($I = -E_{HOMO}$)	5.75
Electron affinity ($A = -E_{LUMO}$)	1.98
Chemical hardness ($\eta = (I-A)/2$)	1.89
Chemical softness ($\zeta = 1/2\eta$)	0.26
Electronegativity ($\chi = (I+A)/2$)	3.86
Chemical potential ($\mu = -(I+A)/2$)	-3.86

2.3. Molecular Electrostatic Potential

Molecular electrostatic potential (MEP) is a valuable tool in understanding the reactivity and behavior of molecules [38-42]. It is a graphical representation of the electrostatic potential energy of a molecule at different points on its surface. MEP is calculated using quantum mechanical calculations, and the resulting MEP surface is often displayed using a color scale to highlight regions of positive or negative potential. In general, regions of high positive potential on an MEP surface correspond to electrophilic regions, while regions of high negative potential correspond to nucleophilic regions. The color scale you mentioned is often used to interpret the MEP surface, with red indicating the most positive potential and blue indicating the most negative potential. Intermediate colors such as orange, yellow, green are used to indicate potential values between these extremes. MEP can be used to predict how a molecule might react with other molecules or reagents, as electrophilic molecules will tend to react with nucleophilic molecules. Additionally, MEP can provide insights into the behavior of biological molecules, such as enzymes and receptors, by highlighting regions of the molecule that are most likely to interact with other molecules.

The MEP surface is given in Figure 5. The electron-poor region in the neutral molecule is coded in blue, while the electron-rich regions appear in red. The red spots positioned on nitrogen atoms are the most negative regions. These regions represent regions that are active in the formation of hydrogen bonds and have a high electrophilic affinity. Regions with the most positive nucleophilic nature are located in regions where hydrogen atoms are concentrated. The electronegativity of benzene rings showed a redshift. On the MEP top surface, there is a representation of the electron density in the form of two-dimensional surface curves. The fact that the structure is prone to chemical activity and the presence of intramolecular and intermolecular hydrogen bonds predict that the electrophilic nature of the structures is more dominant.
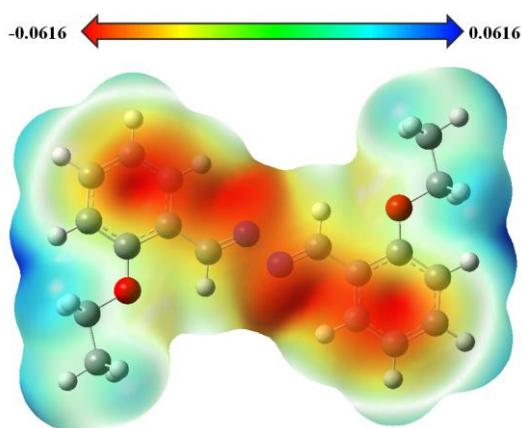
Figure 5 MEP map of the title compound

2.4. Hirshfeld Surface Analysis

The Hirshfeld surface analysis was employed as a tool to visualize the Van der Waals distances and identify intermolecular interaction points. Two-dimensional fingerprint determination was also carried out using Hirshfeld surface analysis to determine the percentage of interactions of atoms within the molecule. The equation for d_{norm} used in Hirshfeld surface analysis is defined as:

$$d_{norm} = (d_i - r_i^{vdw})/r_i^{vdw} + (d_e - r_e^{vdw})/r_e^{vdw}$$

Here, r_i^{vdw} represents the Van der Waals radius of the atom inside the surface, while r_e^{vdw} represents the Van der Waals radius of the atom outside the surface. The values of d_i and d_e represent the separations between the closest atoms inside and outside the surface, respectively. The d_{norm} value ranges between -1 and 1, where negative values represent contact regions shorter than the sum of the Van der Waals radii, while positive values represent regions with longer separations. The d_{norm} values close to zero indicate the absence of any interatomic interaction. Thus, the d_{norm} function is used to visualize the intermolecular contacts and non-covalent interactions between atoms in a molecule, providing information about the geometry and strength of these interactions. The Hirshfeld surface maps of d_{norm}, shape index, and curvedness (Figure 6) are used to analyze the intermolecular interactions and molecular packing in a crystal structure [43-47]. The shape index is a measure of the local

curvature of the surface and can be used to identify regions of the surface where there are $\pi\cdots\pi$ interactions between molecules. The curvedness, on the other hand, is a measure of the global curvature of the surface and can be used to identify regions where there are hydrogen bonds or other types of intermolecular interactions.

d_{norm}

Shape index
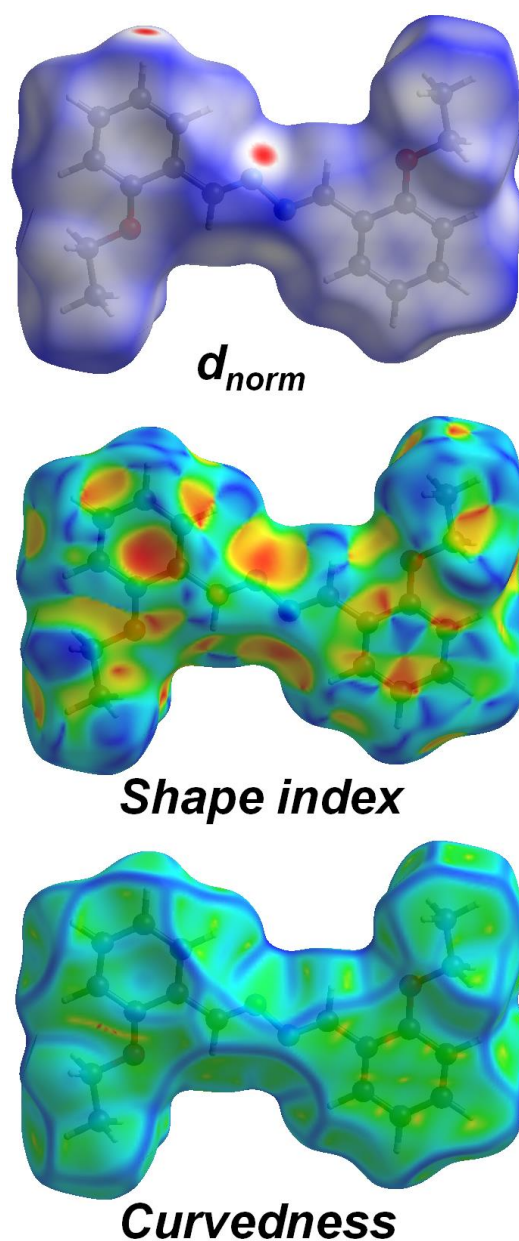
Curvedness

Figure 6 Hirshfeld surfaces of the title compound

Figure 6 presents the Hirshfeld surface maps that show the d_{norm}, shape index, and curvedness maps. The d_{norm} function is the most basic surface map that visualizes the contact areas shorter than the sum of the Van der Waals radius, and these regions are

colored in red. The blue-colored regions, on the other hand, represent intermolecular distances that are longer than the sum of the Van der Waals radii. The indices of the d_{norm} surface ranged between -0.1269 and 1.2504, while the shape index and curvedness were obtained between -1 and 1 and -4 and 4, respectively. The shape index provides a description of planar $\pi\cdots\pi$ interactions between molecules, which are represented by adjacent red and blue triangles in the shape index of the Hirshfeld surface.

Figure 8 Intermolecular interactions with percentages in the title compound

Figure 7 Two-dimensional fingerprint plots for the title compound

Additionally, hydrogen bonds on the Hirshfeld d_{norm} surface were shown in Figure 6, where the regions colored in red clearly demonstrated the presence of hydrogen bonds. Figure 7 shows the two-dimensional fingerprint maps, which indicate the contributions of different types of intermolecular interactions to the total Hirshfeld surface. H$\cdots$H interactions accounted for the largest contribution to the total Hirshfeld surface (64%), followed by C$\cdots$H (16%), N$\cdots$H (9%), C$\cdots$C (6.6%), O$\cdots$H (3.7%), and C$\cdots$O (1.7%), as shown in Figure 8. Overall, the Hirshfeld surface analysis provided valuable insights into the intermolecular interactions and the molecular properties of the compound.

3. CONCLUSION

In this study, the chemical activity and other calculations of the 1,2-bis(2-ethoxybenzylidene) hydrazine molecule, that structure was elucidated by X-ray diffraction analysis, was performed using Density Functional Theory (DFT). Theoretical computational methods allow us to have information about properties that cannot be obtained experimentally and to determine the chemical active site in advance. In this way, it helps us to make predictions about the molecular groups to be synthesized. In this context, the geometric parameters obtained from X-ray diffraction were compared with the geometric parameters obtained from the DFT method. Consequently, it revealed that the results are close to the experimental data. The hardness (1.89 eV) and softness (0.26 $(eV)^{-1}$) values of the optimized structure, whose energy range was calculated as 3.77 eV, predict that the molecule is quite stable with low chemical activity. In the MEP map, the most negative regions were illustrated in red on the nitrogen atoms, and these regions represent regions that are active in the formation of hydrogen bonds and have a high electrophilic affinity. The regions with the dominant nucleophilic nature are located in the regions where hydrogen atoms are concentrated. With Hirshfeld surface maps, the package structure and molecular interactions of the molecular structure were obtained and visualized. As a result of the Hirshfeld surface analysis, it was noticed that the H$\cdots\cdots$H (64%) and C$\cdots$H (16%) interactions made the greatest contribution to the Hirshfeld surface.

In summary, the Schiff-based hydrazine derivative compound was subjected to a comprehensive characterization using several analytical techniques, including single-crystal X-ray diffraction, DFT studies, and Hirshfeld surface analysis. The crystallographic data obtained from the X-ray diffraction experiment was in good agreement with the results of the DFT calculations and Hirshfeld surface analysis. The DFT studies provided a detailed understanding of the electronic properties, stability, and reactivity of the compound, while the Hirshfeld surface analysis allowed for the identification of specific intermolecular interactions in the crystal structure. Overall, the combined use of these techniques provided a thorough characterization of the compound and a deeper understanding of its properties and behavior.

Authors' Contribution
The authors contributed equally to the study.

The Declaration of Conflict of Interest/ Common Interest
No conflict of interest or common interest has been declared by the authors.

The Declaration of Ethics Committee Approval
This study does not require ethics committee permission or any special permission.

The Declaration of Research and Publication Ethics
The authors of the paper declare that they comply with the scientific, ethical and quotation rules of SAUJS in all processes of the paper and that they do not make any falsification on the data collected. In addition, they declare that Sakarya University Journal of Science and its editorial board have no responsibility for any ethical violations that may be encountered, and that this study has not been evaluated in any academic publication environment other than Sakarya University Journal of Science.

REFERENCES

[1] P. Noblia, M. Vieites, B. S. Parajon-Costa, E. J. Baran, H. Cerecetto, P. Draper, M. Gonzalez, O. E. Piro, E. E. Castellano, A. Azqueta, A. L. de Cerain A. Monge-Vega, D. Gambino, "Vanadium(V) complexes with salicylaldehyde semicarbazone derivatives bearing in vitro anti-tumor activity toward kidney tumor cells (TK-10): crystal structure of [(VO2)-O-V(5-bromosalicylaldehyde semicarbazone)]," Journal of Inorganic Biochemistry, vol. 99, no. 2, pp. 443–451, 2005.

[2] R. K. Mohapatra, A. K. Sarangi, M. Azam, M. M. El-ajaily, M. Kudrat-E-Zahan, S. B. Patjoshi, D. C. Dash, "Synthesis, structural investigations, DFT, molecular docking and antifungal studies of transition metal complexes with benzothiazole based Schiff base ligands," Journal of Molecular Structure, vol. 1179, pp. 65–75, 2019.

[3] T. Vijayan, J. Kim, M. Azam, S. L. Al-Resayes, A. Stalin, B. S. Kannan, M. Jayamani, A. Ayyakannu, S. Nallathambi, "Influence of co-ligand on the biological properties of Schiff base metal complexes: Synthesis, characterization, cytotoxicity, and antimicrobial studies," Applied Organometallic Chemistry, vol. e6542, 2021.

[4] N. Poulter, M. Donaldson, G. Mulley, L. Duque, N. Waterfield, A.G. Shard, S. Spencer, A. T. A. Jenkins, A. L.

Johnson, "Plasma deposited metal Schiff-base compounds as antimicrobials," New Journal of Chemistry, vol. 35, no. 7, pp. 1477–1484, 2011.

[5] M. Azam, S. M. Wabaidur, M. J. Alam, A. Trzesowska-Kruszynska, R. Kruszynski, M. Alam, S. I. Al-Resayes, S. Dwivedi, M. R. Khan, M. S. Islam, N. T. M. Ibaqami, "Synthesis, structural investigations and pharmacological properties of a new zinc complex with a N4-donor Schiff base incorporating 2-pyridyl ring," Inorganica Chimica Acta, vol. 487, pp. 97–106, 2019.

[6] P. G. Cozzi, "Metal-Salen Schiff base complexes in catalysis: practical aspects," Chemical Society Reviews, vol. 33, no. 7, pp. 410–421, 2004.

[7] P. R. Reddy, A. Shilpa, N. Raju, P. Raghavaiah, "Synthesis, structure, DNA binding and cleavage properties of ternary amino acid Schiff base-phen/bipy Cu(II) complexes," Journal of Inorganic Biochemistry, vol. 105, no. 12, pp. 1603–1612, 2011.

[8] D. W. Roberts, T. W. Schultz, A. M. Api, "Skin Sensitization QMM for HRIPT NOEL data: Aldehyde Schiff-Base domain," Chemical Research in Toxicology, vol. 30, no. 6, pp. 1309–1316, 2017.

[9] K. M. Abuamer, A. A. Maihub, M. M. El-Ajaily, A. M. Etorki, M. M. Abou-Krisha, "The role of aromatic Schiff bases in the dyes techniques," International Journal of Organic Chemistry, vol. 04, no. 01, pp. 7–15, 2014.

[10] V. G. Vlasenko, A. S. Burlov, T. A. Kuz'menko, A. T. Kozakov, A. V. Nikol'skii, A. L. Trigub, S. I. Levchenkov, "Synthesis, structure, and X-ray photoelectron spectra of cobalt

and copper complexes with 2-{(E)-[2-(4-hydroxybutylami-no)benzimidazol-1-yl]iminomethyl}phenol," Russian Journal of General Chemistry, vol. 88, no. 12, pp. 2550–2558, 2018.

[11] A. K. Satapathy, S. K. Behera, A. Yadav, L. N. Mahour, C. V. Yelamaggad, K. L. Sandhya, B. Sahoo, "Tuning the fluorescence behavior of liquid crystal molecules containing Schiff-base: Effect of solvent polarity," Journal of Luminescence, vol. 210, pp. 371–375, 2019.

[12] B. Mohan, A. Jana, N. Das, S. Bharti, M. Choudhary, S. Muhammad, S. Kumar, A. G. Al-Sehemi, H. Algarni, "A dual approach to study the key features of nickel (II) and copper (II) coordination complexes: Synthesis, crystal structure, optical and nonlinear properties," Inorganica Chimica Acta, vol. 484, pp. 148–159, 2019.

[13] E. W. Schmidt, "Hydrazine and Its Derivatives: Preparation, Properties, Applications," John Wiley & Sons, 2nd ed., 2001.

[14] M. Yuan, D. B. Mitzi, "Solvent properties of hydrazine in the preparation of metal chalcogenide bulk materials and films," Dalton Transactions, pp. 6078–6088, 2009.

[15] S. Basak, K. S. Rane, P. Biswas, "Hydrazine-assisted, low-temperature aerosol pyrolysis method to synthesize γ-Fe2O3," Chemistry Materials, vol. 20, no. 15, pp. 4906–4914, 2008.

[16] R. Dennington II, T. Keith, J. Millam, Gauss View, Version 4.1.2, Semichem Inc, Shawnee Mission, KS, 2007.

[17] M. J. Frisch, G. W. Trucks, H. B. Schlegel, G. E. Scuseria, M. A. Robb, J. R. Cheeseman Jr, J. A. Montgomery, T. Vreven, K. N. Kudin, J. C. Burant, J. M.

Millam, S. S. Iyen-gar, J. Tomasi, V. Barone, B. Mennucci, M. Cossi, G. Scalmani, N. Rega, G. A. Pe-tersson, H. Nakatsuji, M. Hada, M. Ehara, K. Toyota, R. Fukuda, J. Hasegawa, M. Ishida, T. Nakajima, Y. Honda, O. Kitao, H. Nakai, M. Klene, X. Li, J. E. Knox, H. P. Hratchian, J. B. Cross, V. Bakken, C. Adamo, J. Jaramillo, R. Gomperts, R. E. Stratmann, O. Yazyev, R. C. Austin, C. Pomelli, J. W. Ochterski, P. Y. Ay-ala, K. Morokuma, G. A. Voth, P. Salvador, J. J. Dannenberg, V. G. Zakrzewski, S. Dapprich, A. D. Daniels, M. C. Strain, O. Farkas, D. K. Malick, A. D. Rabuck, K. Raghavachari, J. B. Foresman, J. V. Ortiz, Q. Cui, A. G. Baboul, S. Cliford, J. Cioslowski, B. B. Stefanov, G. Liu, A. Liashenko, Piskorz P, I. Komaromi, R. L. Martin, D. J. Fox, T. Keith, M. A. Al-Laham, C. Y. Peng, A. Nanayakkara, M. Challacombe, P. M. W. Gill, B. Johnson, W. Chen, M. W. Wong, C. Gonzalez, J. A. Pople, Gaussian 03, Revision E.01, Gaussian, Inc., Wallingford, CT, 2004.

[18] C. Lee, W. Yang, R. G. Parr, "Development of the Colle-Salvetti correlation-energy formula into a functional of the electron density," Physical Review B, vol. 37, pp. 785–789, 1988.

[19] M. J. Turner, J. J. MacKinnon, S. K. Wolff, D. J. Grimwood, P. R. Spackman, D. Jayatilaka, M. A. Spackman. Crystal explorer Ver. 17.5. University of Western Australia, 2017. http://hirshfeldsurface.net.

[20] Stoe & Cie *X-AREA* and *X-RED32* , Stoe & Cie, Darmstadt, Germany, 2002.

[21] G. M. Sheldrick, "SHELXT - Integrated space-group and crystal-structure deter-mination," Acta Crystallographica Section A: Foundations and Advances, vol. 71, pp. 3–8, 2015.

[22] G. M. Sheldrick, "Crystal Structure Refinement with SHELXL," Acta Crystallographica Section C: Structural Chemistry, vol. 71, pp. 3–8, 2015.

[23] P. R. Spackman, M. J. Turner, J. J. McKinnon, S. K. Wolff, D. J. Grimwood, D. Jayatilaka, M. A. Spackman, "CrystalExplorer: A program for Hirshfeld surface analysis, visualization and quantitative analysis of molecular crystals," Journal of Applied Crystallography, vol. 54, no. 3, pp. 1006-1011, 2021.

[24] M. A. Spackman, D. Jayatilaka, "Hirshfeld surface analysis," Crystal Engineering Communication, vol. 11, pp. 19–32, 2009.

[25] O. Simsek, M. Dincer, N. Dege, E. Saif, I. Yilmaz, A. Cukurovali, "Crystal structure and Hirshfeld surface analysis of (Z)-4-{[4-(3-methyl-3-phenylcyclobutyl) thiazol-2-yl] amino}-4-oxobut-2-enoic acid," Acta Crystallographica Section E: Crystallographic Communications, vol. 78, no. 2, pp. 120–124, 2022.

[26] R. Yankova, I. Tankov, T. Tsaneva, "Crystal structure, intermolecular interactions and NLO properties for imidazolium hydrogen sulfate ionic liquid," Journal of Molecular Structure, vol. 1273, pp. 134307, 2023.

[27] S. Atalay, M. Macit, H. Bulbul, "Crystal structure and computational studies of N-((2-ethoxynaphthalen-1-yl) methylene)-4-fluoroaniline," European Journal of Chemistry, vol. 12, no. 4, pp. 454-458, 2021.

[28] M. N. Tahir, A. Ali, M. Khalid, M. Ashfaq, M. Naveed, S. Murtaza, I. Shafiq, M. A. Asghar, R. Orfali, S. Perveen, "Efficient synthesis of imine-carboxylic acid functionalized compounds: Single crystal, Hirshfeld

surface and quantum chemical exploration," Molecules, vol. 28, no. 7, pp. 2967, 2023.

[29] H. Gökce, F. Şen, Y. Sert, B. F. Abdel-Wahab, B. M. Kariuki, G. A. El-Hiti, "Quantum computational investigation of (E)-1-(4-methoxyphenyl)-5-methyl-N′-(3-phenoxybenzylidene)-1 H-1, 2, 3-triazole-4-carbohydrazide," Molecules, vol. 27, no. 7, pp. 2193, 2022.

[30] G. Kaştaş, Ç. A. Kaştaş, "Scrutinizing the two new o-hydroxy Schiff bases from the point of tautomeric behavior and non-covalent interactions (H-bond, Br⋯ Br, π⋯ π and CH⋯ π) in their supramolecular architectures," Journal of Molecular Structure, vol. 1184, pp. 427-434, 2019.

[31] M. R. Albayati, S. Kansız, H. Lgaz, S. Kaya, N. Dege, I. H. Ali, R. Salghi, I. M. Chung, "Synthesis, experimental and theoretical characterization of (E)-2-((2, 3-dimethylphenyl) amino)-N'-(furan-2-ylmethylene) benzohydrazide," Journal of Molecular Structure, vol. 1219, pp. 128518, 2020.

[32] A. A. B. OmarAli, A. J. M. Al-Karawi, N. Dege, S. Kansız, H. A. Ithawi, "Synthesis and X-ray crystal structures of two different zinc (II) complexes of N, N′-cyclohexane-1, 2-diylidene-bis (4-fluorobenzoylhydrazide) based on zinc salt effect," Journal of Molecular Structure, vol. 1217, pp. 128387, 2020.

[33] A. A. OmarAli, A. J. M. Al-Karawi, A. A. Awad, N. Dege, S. Kansız, E. Agar, Z. A. Hussein, I. R. Mohammed, "Two new zinc (II) and mercury (II) complexes based on N, N′-(cyclohexane-1, 2-diylidene) bis (4-fluorobenzohydrazide): synthesis, crystal structures and antibacterial activities," Acta Crystallographica Section C: Structural Chemistry, vol. 76, no. 5, pp. 476-482, 2020.

[34] R. Sathyanarayanan, M. Selvapandiyan, C. Senthilkumar, M. Srinivasan, P. Ramasamy, "Crystal growth, Hirshfeld surface, quantum chemical calculations, optical, photoluminescence and thermal analyses of sodium D-isoascorbate monohydrate single crystal," Journal of Molecular Structure, vol. 1275, pp. 134637, 2023.

[35] A. Gannouni, W. Tahri, T. Roisnel, S. I. Al-Resayes, M. Azam, R. Kefi, "Single crystal investigations, Hirshfeld surface analysis, DFT studies, molecular docking, physico-chemical characterization, and biological activity of a novel non-centrosymmetric compound with a copper transition metal precursor," ACS Omega, vol. 8, no. 8, pp. 7738-7748, 2023.

[36] J. Makhlouf, Y. El Bakri, A. Valkonen, K. Saravanan, S. Ahmad, W. Smirani, "Growth, single crystal investigations, hirshfeld surface analysis, DFT studies, molecular dynamics simulations, molecular docking, physico-chemical characterization and biological activity of novel thiocyanic complex with zinc transition metal precursor," Polyhedron, vol. 222, pp. 115937, 2022.

[37] R. Saddik, S. A. Brandán, S. Mortada, C. Baydere, O. Roby, N. Dege, S. Tighadouini, M. Tahiri, M. A. Faouzi, K. Karrouchi, "Synthesis, crystal structure, Hirshfeld surface analysis, DFT and antihyperglycemic activity of 9-allyl-2, 3, 9, 10a-tetrahydrobenzo [b] cyclopenta [e][1, 4] diazepin-10 (1H)-one," Journal of Molecular Structure, vol. 1283, pp. 135283, 2023.

[38] L. Guo, B. Tan, X. Zuo, W. Li, S. Leng, X. Zheng, "Eco-friendly food spice 2-Fur-furylthio-3-methylpyrazine as an

excellent inhibitor for copper corrosion in sulfuric acid medium," Journal of Molecular Liquids, vol. 317, 113915, 2020.

[39] Z. Demircioğlu, G. Kaştaş, Ç.A. Kaştaş, R. Frank, "Spectroscopic, XRD, Hirshfeld surface and DFT approach (chemical activity, ECT, NBO, FFA, NLO, MEP, NPA&MPA) of (E)-4-bromo-2-[(4- bromophenylimino) methyl]-6-ethoxyphenol," Journal of Molecular Structure, vol. 1191, pp. 129–137, 2019.

[40] H. Lgaz, R. Salghi, S. Masroor, S.H. Kim, C. Kwon, S.Y. Kim, Y.J. Yang, I.M. Chung, "Assessing corrosion inhibition characteristics of hydrazone derivatives on mild steel in HCl: insights from electronic-scale DFT and atomic-scale molecular dynamics," Journal of Molecular Liquids, vol. 308, 112998, 2020.

[41] M. Azam, P.K. Sahoo, R.K. Mohapatra, M. Kumar, A. Ansari, I.S. Moon, A. Chutia, S.I. Resays, S.K. Biswal, "Structural investigations, Hirsfeld surface analyses, and molecular docking studies of a phenoxo-bridged binuclear zinc(II) complex," Journal of Molecular Structure, vol. 1251, 132039, 2022.

[42] S. I. Al-Resayes, M. Azam, A. Trzesowska-Kruszynska, R. Kruszynski, S. M. Soliman, R. K. Mohapatra, Z. Khan, "Structural and theoretical investigations, Hirshfeld surface analyses, and cytotoxicity of a naphthalene-based chiral compound," ACS Omega, vol. 5, pp. 27227–27234, 2020.

[43] A. Saeed, S. Ashraf, U. Flörke, Z. Y. D. Espinoza, M. F. Erben, H. Pérez, "Supramolecular self-assembly of a coumarine-based acylthiourea synthon directed by π-stacking interactions:

Crystal structure and Hirshfeld surface analysis," Journal of Molecular Structure, vol. 1111, pp. 76-83, 2016.

[44] S. Adhikari, A. H. Sheikh, S. Kansız, N. Dege, N. Baildya, G. Mahmoudi, N. A. Choudhury, R. J. Butcher, W. Kaminsky, S. Talledo, E. M. Lopato, S. Bernhard, J. Kłak, "Supramolecular Co (II) complexes based on dithiolate and dicarboxylate ligands: Crystal structures, theoretical studies, magnetic properties, and catalytic activity studies in photocatalytic hydrogen evolution," Journal of Molecular Structure, pp. 135481, 2023.

[45] M. K. Gümüş, S. Kansiz, G. B. Tulemisova, N. Dege, E. Saif, "Crystal structure and Hirshfeld surface analysis of 3-(hydroxymethyl)-3-methyl-2, 6-diphenylpiperidin-4-one," Acta Crystallographica Section E: Crystallographic Communications, vol. 78, no. 1, pp. 29-32, 2022.

[46] D. M. Al-thamili, A. I. Almansour, N. Arumugam, S. Kansız, N. Dege, S. M. Soliman, M. Azam, R. S. Kumar, "Highly functionalized N-1-(2-pyridinylmethyl)-3, 5-bis [(E)-arylmethylidene] tetrahydro-4 (1H)-pyridinones: Synthesis, characterization, crystal structure and DFT studies," Journal of Molecular Structure, vol. 1222, pp. 128940, 2020.

[47] Z. Setifi, N. Cubillán, C. Glidewell, D. M. Gil, E. Torabi, M. Morales-Toyo, N. Dege, F. Setifi, M. Mirzaei, "A combined experimental, Hirshfeld surface analysis, and theoretical study on fac-[tri (azido)(tris (2-pyridyl) amine) iron (III)]," Polyhedron, vol. 233, pp. 116320, 2023.

Title: Conversion of Cellulose to 5-HMF in the Presence of Silica-Alumina Catalysts Synthesized by Dual Template at Low Temperature

Authors: Halit L. HOSGUN, Özlem TOPCU, E. Zafer HOSGUN, Berrin BOZAN

Conversion of Cellulose to 5-HMF in the Presence of Silica-Alumina Catalysts Synthesized by Dual Template at Low Temperature

Halit L. HOSGUN [*1] iD, Özlem TOPCU[1] iD E. Zafer HOSGUN[2] iD, Berrin BOZAN[2] iD

Abstract

In this study, which incorporates many principles of green chemistry (use of renewable feedstocks, catalysis, improvement of energy efficiency, and harmless solvents and auxiliaries), the single-phase catalytic conversion of cellulose to 5-HMF in over silica-alumina catalysts was investigated. A series of dual-template silica-alumina catalysts with CTAB as the main template and F127 or triethylamine (TEA) as the co-template were synthesized at a low temperature of 60 °C and characterized by XRD, N_2 adsorption-desorption technique, FT-IR and pyridine adsorption FT-IR. The surface area is increased by using the second template in silica-alumina catalyst. In addition, the acidity of the surface was changed by using the second template. The cellulose conversion and yield of 5-HMF increased from 36% to 52% and from 3.13% to 4.24%, respectively, due to the properties gained by using the second template. 52% cellulose conversion and 8.13% selectivity of 5-HMF were obtained in aqueous medium, 220 °C and 6 h reaction time with the catalyst using TEA as co-template. Eco-friendly silica catalysts synthesized at low temperatures with a dual template can be considered as a potential alternative for the conversion of cellulose into value-added biobased products.

Keywords: Cellulose, 5-HMF, heterogeneous catalysis, green chemistry

1. INTRODUCTION

Despite the increasing demand for energy and chemicals, the supply of fossil resources such as oil, coal, and natural gas is gradually decreasing. In addition to this supply-demand imbalance, considering supply chain security and environmental issues, it is necessary to use alternative sources to fossil fuels for energy and chemical production. As an abundant raw material, lignocellulosic biomass can be used as a substitute for fossil resources [1, 2].

Cellulose, together with hemicellulose and lignin, is the main component of biomass. Many value-added products are derived from glucose by the hydrolysis reaction of cellulose, a polymer composed of multiple D-glucose units linked by β-1,4-glycosidic

Corresponding author: hlevent.hosgun@btu.edu.tr (H. L. HOŞGÜN)
[1] Faculty of Engineering and Natural Sciences, Department of Chemical Engineering, Bursa Technical University, Bursa, Türkiye
[2] Faculty of Engineering, Department of Chemical Engineering, Eskişehir Technical University, Eskişehir, Türkiye
E-Mail: ozlemtopcu005@gmail.com, ezhosgun@eskisehir.edu.tr, bbozan@eskisehir.edu.tr.,
ORCID: https://orcid.org/0000-0002-6699-666X, https://orcid.org/0000-0002-9756-4624, https://orcid.org/0000-0002-3810-701X, https://orcid.org/0000-0002-3112-5784

HOSGUN et al.

Conversion of Cellulose to 5-HMF in the Presence of Silica-Alumina Catalysts Synthesized by Dual Temp...

bonds. 5-HMF, one of the high value-added chemicals, is an important building block because it can be converted into many compounds currently derived from petroleum through various reaction pathways [3, 4].

The reaction steps for 5-HMF synthesis from cellulose is carried out in 3 steps [5]:

Step 1: Hydrolysis reaction of cellulose to glucose,

Step 2: Isomerization reaction of glucose to fructose,

Step 3: Dehydration reaction of fructose to 5-HMF.

Lewis acid catalysts are used for the isomerization reaction, while the steps of hydrolysis of cellulose to glucose and dehydration of fructose to 5-HMF take place in the presence of Bronsted acid catalysts [6].

There are numerous studies in the literature on the catalytic conversion of cellulose to 5-HMF using homogeneous catalysts such as metal chlorides [7, 8], mineral acids [9], and ionic liquids [10], as well as solid acid heterogeneous catalysts such as $SnNb_2O_6$-ZrO_2 [11], H-ZSM-5 [12], and niobium/carbon composites [13]. Due to the drawbacks of homogeneous catalysts such as corrosion, difficulty in separation from the product mixture, and environmental pollution, many researchers have preferred the use of heterogeneous catalysts in the synthesis of 5-HMF from cellulose [14, 15].

Silica-alumina catalysts with moderate acidity have been used in many industrial applications, e.g., hydrocarbon cracking [16, 17], in deoxygenation/ hydrodeoxygenation reactions [18, 19], in the conversion of methanol to olefins [20], and in bio-oil refining[21, 22]. In their two studies, Pham et al. used Al-incorporated SBA-15 and Al-MCM-41 catalysts to convert cellulose to 5-HMF. Al-incorporated SBA-15 catalysts prepared by the atom implantation method and containing 10% Al, achieved the highest conversion, selectivity, and efficiency values (62.14%, 68.51%, and 42.57%, respectively), while the Si:Al molar ratio was 30. The maximum cellulose conversion (69%) and 5-HMF selectivity (59.04%) were obtained with the MCM-41 catalyst. The authors emphasized that the main factor affecting 5-HMF selectivity and cellulose conversion is the Bronsted/Lewis acid ratio of the catalysts [23, 24].

There are various methods for the preparation of ordered metal oxides and zeolites. The use of various templates is one of these methods. In some cases, the use of two templates is preferred. In the literature, there are studies on zeolites (ZSM-5 [25, 26], HZSM-5 [27], AlPO-18 [28], SAPO-CLO [29]), alumina [30] and silica [31–33] synthesized using dual templates. Emdadi et al. synthesized nanolayer coupled ZSM-5 zeolites using Gemini-type surfactants and TPAOH as binary templates. The hydrophobic alkyl chains of the Gemini-type surfactant used in this study effectively limited the growth of ZSM-5 nanolayers. On the other hand, TPAOH played a simple role in the formation of a self-column of zeolite precursors to strengthen the interlamellar structure [34]. In their study, synthesizing a hierarchically layered titanosilicate-1, Wang et al. used the bolaform surfactant as the primary template and the co-template TPAOH. It was reported that the bolaform surfactant enabled the formation of ultrathin nanolayers of TS-1 crystals, while TPAOH induced and regulated nucleation [35]. Shi et al. reported surface area of 96 m^2/g and 102 m^2/g, respectively, in their alumina synthesis using SDS and CTAB single template, while the surface area of alumina using SDS and CTAB dual template was 140 m^2/g [36].

In this study, silica-alumina catalysts were synthesized by dual templating with CTAB as the main template and F127 or triethylamine (TEA) as co-templates. A series of samples were prepared by changing the molar ratio of CTAB to F127 or TEA (1:4, 1:8, 1:16). The

HOSGUN et al.

Conversion of Cellulose to 5-HMF in the Presence of Silica-Alumina Catalysts Synthesized by Dual Temp...

textural properties and crystal structures of the prepared samples were characterized and their catalytic activities in the conversion of cellulose to 5-HMF were evaluated. Water is used as a solvent in the conversion of cellulose into value-added chemicals. This study also covers many principles of green chemistry such as the use of cellulose as a feedstock (use of renewable feedstock), the preference of heterogeneous catalysts instead of homogeneous catalysts (catalysis), low-temperature synthesis (increase of energy efficiency) and the use of water as a solvent (benign solvents and auxiliaries).

2. EXPERIMENTAL

2.1. Materials

Aluminum nitrate nonahydrate ($Al(NO_3)_3$ $9H_2O$) from Fluka was used as the Al source. Sodium silicate solution as Si source, ($(Na_2O(SiO_2)_x$ $xH_2O)$, d=1.39 g/cm^3), Pluronic F127, and cellulose (CAS Number:9004-34-6, product code C6288) were supplied by Sigma-Aldrich. Cetyltrimethylammonium bromide (CTAB), sulfuric acid (d=1.83 g/cm^3, in >95% purity), and triethylamine (TEA, d=0.728 g/cm^3, in 99% purity) were purchased from Aldrich, Fischer Scientific, and Acros Organics, respectively. All chemicals were used as received.

2.2. Synthesis Procedure of Catalyst

Solution A and solution B are obtained by dissolving surfactant (CTAB and varying amounts of TEA or F127) and aluminum nitrate nonahydrate in water. Solution A, solution B and 2.5 mL of H_2SO_4 were added to the sodium silicate solution and stored in an oven at 60 °C for 7 days. The samples were then washed until the pH = 10 and filtered. The samples were then dried overnight and calcined in an oven (12 h at 550 °C, under heating conditions of 1 °C/min). The CT was coded for the samples synthesized with CTAB/TEA, whereas the CF was coded for the samples synthesized with CTAB/F127. The numbers at the end of the codes represent the molar ratio of CTAB:TEA or CTAB:F127 used. C stands for the sample prepared with CTAB.

2.3. Characterization Studies

X-ray diffraction analysis was performed to determine the crystal structure. XRD of Rigaku Ultima III brand operated with a voltage of 40 kV and 15 mA, scanning speed of 4 °C/min. The surface and pore properties of the catalysts were determined with nitrogen adsorption-desorption isotherms using the Micromeritics TriStar 3020 model. Prior to measurement, all samples were degassed under these conditions: first at 90 °C for 1 hour and then at 300 °C for 24 hours under vacuum. Surface area, pore volume, and pore diameter were calculated using BET (Brunauer-Emmet-Teller) theory using these isotherms. FTIR analyzes were performed using Perkin Elmer Spectrum Two spectrophotometer systems to identify characteristic peaks and functional groups. Spectra were recorded over the spectral range of 4000-400 cm^{-1} with a resolution of 4 cm^{-1}. The DRIFT analyses with pyridine-adsorbed patterns were performed on the same FT-IR instrument in the 400- 4000 cm^{-1} range.

The DRIFT analyses were used to determine the content of Brønsted and Lewis acid sites on the catalyst by infrared spectra of pyridine (Py-IR) adsorbed on the catalysts as in the literature [37].

2.4. Study on the Catalytic Conversion of Cellulose to 5-HMF Performance of Catalysts

Temperature had the greatest effect on cellulose degradation, as the temperature increases up to 220 °C when the concentration of ionic products increases in the subcritical water range [38]. The reaction temperature and time were selected from previous work for comparison of results[14, 38]. The reactions were carried out in a Teflon-lined autoclave at 220 °C for 6 h. The ratio of cellulose to catalyst was 4:1 (w/w) and the

HOSGUN et al.

Conversion of Cellulose to 5-HMF in the Presence of Silica-Alumina Catalysts Synthesized by Dual Temp...

reaction was carried out in an aqueous medium. After filtration through a 0.45 μm filter, the collected clear liquids were analyzed by High Performance Liquid Chromatography (HPLC, Agilent 1100, USA). The HPLC system was equipped with a refractive index detector (Agilent) and a Bio-Rad column (300 mm × 7.8 mm, Aminex HPX-87H) at 60 °C. The mobile phase was 0.005 M H_2SO_4 at a flow rate of 0.6 mL min^{-1}. Cellulose conversion (X), 5-HMF yield (Y), and selectivity (S) were calculated using the following equations:

$$X_{\text{Cellulose}} (\%) = \frac{\text{Amount of cellulose reacted (g)}}{\text{Initial amount of cellulose (g)}} \times 100 \quad (1)$$

$$Y_{\text{5-HMF}} (\%) = \frac{\text{Produced 5-HMF (mole)}}{\text{Glucose content of cellulose (mole)}} \times 100 \quad (2)$$

$$S_{\text{5-HMF}} (\%) = \frac{\text{Produced 5-HMF (mole)}}{\text{Cellulose reacted (mole)}} \times 100 \quad (3)$$

The glucose content of cellulose was determined using moles of glucose units in cellulose.

3. RESULTS

3.1. Characterization of the Catalysts

The N_2 adsorption-desorption isotherms and the pore size distribution curves of catalysts prepared with CTAB/F127 and CTAB/TEA dual templates are shown in Figure 1 and Figure 2, respectively. As can be seen in Figure 1 and Figure 2, the catalysts prepared with dual templates exhibit a type IV isotherm with a pronounced H3 hysteresis loop according to the IUPAC classification. The BET, external and microporous surface areas, and pore volumes of all catalysts are listed in Table 1. The silica-alumina catalyst synthesized with CTAB has a relatively low surface area (41.8 m²/g). Using F127 or TEA with CTAB as a template significantly increases the surface area of the catalysts. Increasing the molar ratio of TEA and F127 increased the surface area and pore volume of the catalysts. However, further increasing the molar ratio of F127 from 8 to 16 decreased surface areas. The results also showed that the

catalysts with TEA had smaller micropore surface area. According to the BJH pore size distribution results, it was found that TEA resulted in smaller mesoporous silica particles, while F127 increased the particle diameter. This is compatible with the literature [39].
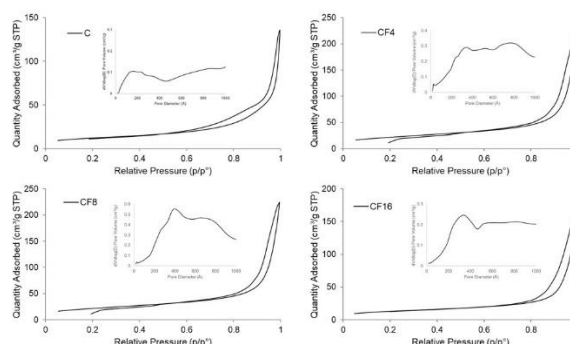
Figure 1 N_2 adsorption-desorption isotherms and BJH pore size distribution plots (insets) of the catalysts prepared with CTAB/F127
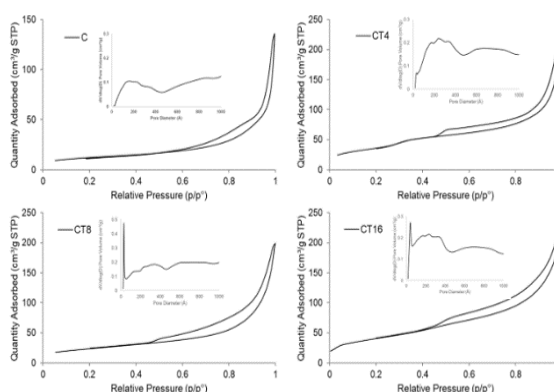
Figure 2 N_2 adsorption-desorption isotherms and BJH pore size distribution plots (insets) of catalysts prepared with CTAB/TEA

Table 1 Texture parameters of the catalysts.

Sample	S_{BET} (m²/g)	S_{ext} (m²/g)[a]	S_{micro} (m²/g)[b]	V_{pore} (cm³/g)
C	41.8	33.9	7.9	0.183
CT4	85.0	76.6	8.4	0.293
CT8	136.6	135.9	0.7	0.348
CT16	145.8	142.9	2.9	0.357
CF4	76.18	63.74	12.44	0.334
CF8	80.23	66.54	13.69	0.452
CF16	45.10	36.85	8.25	0.246

a: BJH adsorption branch
b t-Plot method

The XRD patterns of the synthesized catalysts are shown in Figure 3. A peak centered

HOSGUN et al.

Conversion of Cellulose to 5-HMF in the Presence of Silica-Alumina Catalysts Synthesized by Dual Temp...

approximately at $2\theta = 23°$ in the XRD pattern indicates that the catalysts are amorphous. This result is consistent with the literature [40, 41]. There are no alumina diffraction lines in the XRD patterns of the samples. This can be explained by the fact that almost all Al is contained in SiO_2 [42].

Figure 3 XRD patterns of catalysts

The FTIR spectra of the catalysts are shown in Figure. 4. Absorption bands around 1100 cm^{-1}, 820 cm^{-1} and at 470 cm^{-1} were identified. The band at 470 cm^{-1} can be attributed to the bending vibrations of Si-O-Si. The other two bands at 820 cm^{-1} and 1100 cm^{-1} are due to the Al-O-Al stretching and the asymmetric stress vibrations of Si-O (Si), respectively [43, 44].
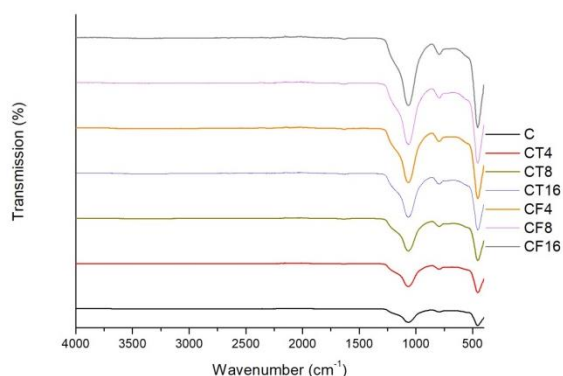
Figure 4 FTIR spectra of the samples

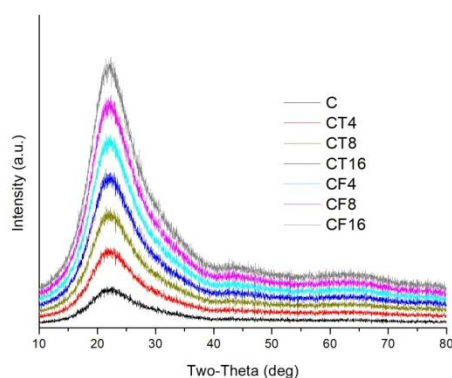Pyridine was adsorbed on the synthesized catalysts and the acidic properties were investigated using the FT-IR spectra (see in Figure 5). The peaks around 1540 cm^{-1} and 1450 cm^{-1} correspond to Brønsted acids and Lewis acids, respectively. The band at 1490 cm^{-1} is attributed to the presence of both

Brønsted and Lewis acid sites [45, 46]. While CTAB itself does not exhibit Brønsted or Lewis acid peaks, use of the co-template resulted in Brønsted and Lewis acids.
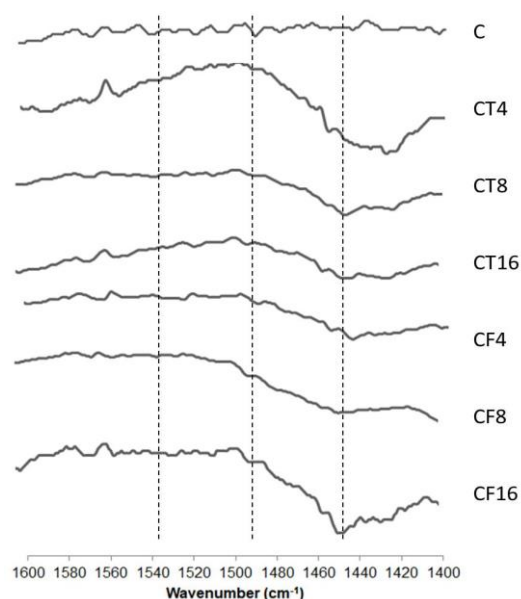
Figure 5 The infrared spectra of the catalysts adsorbed with pyridine

3.2. Results of the Catalytic Activity Studies

The results of the experiments on the synthesis of 5-HMF from cellulose in the presence of catalysts synthesized with the dual template using CTAB as the main template and F127 or triethylamine (TEA) as the co-template are shown in Table 2. The conversion of cellulose was 36%, and the yield and selectivity of 5-HMF were 3.13% and 9.64%, respectively, with the catalyst when only CTAB was used as the template, at 220 °C and 6h, respectively. This result could be due to the absence of Brønsted and Lewis acid sites of the catalyst. The combination of CTAB and TEA has a positive effect on the conversion of cellulose to 5-HMF. At a molar ratio of CTAB:TEA of 1:4, the conversion of cellulose was increased by 45%, while the yield of 5-HMF increased slightly. Further increasing the molar ratio of CTAB:TEA resulted in lower conversion of cellulose but higher yield of 5-HMF. Catalysts synthesized with CTAB and F127 as dual templates were not as effective as CTAB/TEA in the

conversion of cellulose. CTAB/F127 catalysts showed a slight increase in both the conversion of cellulose and the yield of 5-HMF at all molar ratios. Only a 1:8 CTAB/F127 has a high selectivity of 11.02%.

Table 2 Values for conversion, yield and selectivity values obtained from experiments carried out with different catalysts.

Sample	$X_{Cellulose}$ (%)	Y_{5-HMF} (%)	S_{5-HMF} (%)
C	36	3.13	9.64
CT4	52	3.84	8.13
CT8	39	4.04	11.63
CT16	42	4.24	11.09
CF4	38	3.67	10.6
CF8	39	3.86	11.02
CF16	41	3.35	8.96

The results obtained in this study were compared with studies from the literature on the conversion of cellulose to 5-HMF carried out in a single phase (Table 3). Although high cellulose conversion or 5-HMF efficiency was obtained in a short time with the homogeneous catalysts $FeCl_3$ and $CrCl_3$, there are difficulties in the separation of the product mixture. As for the reaction conditions, ionic liquids were often used, which are expensive and practically unsuitable for large-scale applications. Considering the surfaces of the catalysts and the water used as reaction medium in this study, we can assume that the obtained results are consistent with those reported in the literature. A catalytic conversion of cellulose using only water as a solvent, as in this study, was performed by Nandiwala et al. In the study by Nandiwala et al. in the presence of a bimodal-HZ-5 catalyst with a Si/Al ratio of 30 at a cellulose/catalyst ratio of 1:2 (the cellulose/catalyst ratio in this study was 4:1), 67% cellulose conversion and 46% 5-HMF yield were achieved [12].

Table 3 Some studies on the synthesis of 5-HMF from cellulose in a single phase in the literature.

Catalyst	Solvent	co-solvent / co-catalyst	Cellulose/Catalyst (g/g)	Reaction Time	Reaction Temperature (°C)	X_{Cell} (%)	Y_{5-HMF} (%)	Reference
$FeCl_3$	Water	1-ethyl-3-methylimidazolium chloride	0.1/0.06	10 min	140	72.4	23.6	Abou-Yousef et.al.[7]
$CrCl_3$	Water	1-ethyl-3-methylimidazolium chloride	0.1/0.06	10 min	140	35.6	84.9	Abou-Yousef et.al.[7]
Bimodal-HZ-5	Water	-	0.25/0.5	4 hr	190	67	46	Nandiwale et.al.[12]
Phosphotungstic acid (PHA)	THF	Water	0.5/0.5	6 hr	190	na	8.50	Fan et.al.[14]
Amberlyst-15	THF	-	0.5/0.2	6 hr	190	na	9.30	Fan et.al.[14]
Al-MCM-41	Water	1-butyl 3-imidazium chloride	2/0.2	2 hr	170	69	40.56	Pham et.al.[24]
Sulfuric acid modified Active Carbon	Water	1-Butyl-3-methylimidazolium chloride	0.1/0.05	1 hr	120	na	36.33	Tyagi et.al.[47]
Cr doped Sulfuric acid modified Active Carbon	Water	1-Butyl-3-methylimidazolium chloride	0.1/0.05	1	120	na	49.02	Tyagi et.al.[47]
$ChnH5-nCeW_{12}O_{40}$	Water	-	0.5/0.2	5 hr	160	74	13.6	Lai et.al.[48]
$Cr[(DS)H_2PW_{12}O_{40}]_3$	Water	-	0.2 g/0.06 mmol	2 hr	150	77.1	52.7	Zhao et.al.[49]
CT-4	Water	-	1/0.25	6 hr	220	52	3.84	This study

na: not available

4. CONCLUSION

This study was carried out considering many rules of green chemistry, namely synthesis at low-temperature, use of water as an environmentally friendly solvent, reaction in the presence of a heterogeneous catalyst and use of renewable raw materials. In summary, dual templated silica-alumina catalysts were synthesized at low temperature, and their catalytic activity was tested for the conversion of cellulose to 5-HMF in water as solvent. The

HOSGUN et al.

Conversion of Cellulose to 5-HMF in the Presence of Silica-Alumina Catalysts Synthesized by Dual Temp...

use of co-templates in the synthesis of the catalysts resulted in an increase in surface area from 41.8 m^2/g to 145.8 m^2/g. In addition to the increase in the surface area of the catalyst synthesized using single CTAB as a template, it was observed that the acidity of the surface area of the catalysts synthesized using the dual template also changed. Catalysts synthesized using TEA as co-template showed better cellulose conversion and 5-HMF yield after 6 h reaction time in water at 220 °C compared to catalysts synthesized using F127 as co-template. When cellulose was converted in the presence of CT16 catalyst, the highest 5-HMF yield of up to 4.24% was obtained at 42% cellulose conversion. This is the first report describing the synthesis of 5-HMF from cellulose using a silica-alumina catalyst synthesized at low temperature as a dual template. The results obtained in this study for cellulose conversion and 5-HMF yield, carried out according to green chemistry rules, are compatible with other studies on 5-HMF synthesis from cellulose in the literature.

Authors' Contribution

HLH: Supervision, Investigation, Analysis and interpretation of the data.
ÖT: performed the experiments and collected data, interpretation of the data.
EZH: Investigation, HPLC analysis, interpretation of the data.
BB: Supervision, interpretation of the data, revised and editing the manuscript.

The Declaration of Conflict of Interest/ Common Interest

No conflict of interest or common interest has been declared by the authors.

The Declaration of Ethics Committee Approval

This study does not require ethics committee permission or any special permission.

The Declaration of Research and Publication Ethics

The authors of the paper declare that they comply with the scientific, ethical and quotation rules of SAUJS in all processes of the paper and that they do not make any falsification on the data collected. In addition, they declare that Sakarya University Journal of Science and its editorial board have no responsibility for any ethical violations that may be encountered, and that this study has not been evaluated in any academic publication environment other than Sakarya University Journal of Science.

REFERENCES

[1] L. T. Mika, E. Cséfalvay, Á. Németh, "Catalytic Conversion of Carbohydrates to Initial Platform Chemicals: Chemistry and Sustainability", Chemical Reviews, vol. 118, no. 2, pp. 505-613, 2018.

[2] F. A. Kucherov, L. V. Romashov, G. M. Averochkin, V. P. Ananikov, "Biobased C$_6$ -Furans in Organic Synthesis and Industry: Cycloaddition Chemistry as a Key Approach to Aromatic Building Blocks", ACS Sustainable Chemistry & Engineering, vol. 9, no. 8, pp. 3011-3042, 2021.

[3] S. Van de Vyver, J. Geboers, P. A. Jacobs, B. F. Sels, "Recent Advances in the Catalytic Conversion of Cellulose", ChemCatChem, vol. 3, no. 1, pp. 82-94, 2011.

[4] A. Guleria, G. Kumari, S. Saravanamurugan, "Cellulose valorization to potential platform chemicals", In Biomass, Biofuels, Biochemicals, S. Saravanamurugan, A. Pandey, H. Li, A. Riisager Elsevier, 2020, pp. 433-457.

[5] F. Delbecq C. Len, "Recent Advances in the Microwave-Assisted Production of Hydroxymethylfurfural by Hydrolysis of Cellulose Derivatives—A Review", Molecules, vol. 23, no. 8, pp. 1973, 2018.

HOSGUN et al.

Conversion of Cellulose to 5-HMF in the Presence of Silica-Alumina Catalysts Synthesized by Dual Temp...

[6] Y. Zhao, S. Wang, H. Lin, J. Chen, H. Xu, "Influence of a Lewis acid and a Brønsted acid on the conversion of microcrystalline cellulose into 5-hydroxymethylfurfural in a single-phase reaction system of water and 1,2-dimethoxyethane", RSC Advances, vol. 8, no. 13, pp. 7235-7242, 2018.

[7] H. Abou-Yousef, E. B. Hassan, P. Steele, "Rapid conversion of cellulose to 5-hydroxymethylfurfural using single and combined metal chloride catalysts in ionic liquid", Journal of Fuel Chemistry and Technology, vol. 41, no. 2, pp. 214-222, 2013.

[8] L. Zhang, Y. Tian, Y. Wang, L. Dai, "Enhanced conversion of α-cellulose to 5-HMF in aqueous biphasic system catalyzed by $FeCl_3$-$CuCl_2$", Chinese Chemical Letters, vol. 32, no. 7, pp.2233-2238, 2021.

[9] J. Shen C. E. Wyman, "Hydrochloric acid-catalyzed levulinic acid formation from cellulose: data and kinetic model to maximize yields", AIChE Journal, vol. 58, no. 1, pp. 236-246, 2012.

[10] L. Zhou, R. Liang, Z. Ma, T. Wu, Y. Wu, "Conversion of cellulose to HMF in ionic liquid catalyzed by bifunctional ionic liquids", Bioresource Technology, vol. 129, pp. 450-455, 2013.

[11] M. Wu, M. Huang, L. Chen, Q. Ma, J. Zhou, "Direct conversion of cellulose to 5-hydroxymethylfurfural over $SnNb_2O_6$–ZrO_2 catalyst", Reaction Kinetics, Mechanisms and Catalysis, vol. 130, no. 2, pp. 903-918, 2020.

[12] K. Y. Nandiwale, N. D. Galande, P. Thakur, S. D. Sawant, V. P. Zambre, V. V. Bokade, "One-Pot Synthesis of 5-Hydroxymethylfurfural by Cellulose Hydrolysis over Highly Active Bimodal Micro/Mesoporous H-ZSM-5 Catalyst", ACS Sustainable Chemistry & Engineering, vol. 2, no. 7, pp. 1928-1932, 2014.

[13] X. Li, K. Peng, Q. Xia, X. Liu, Y. Wang, "Efficient conversion of cellulose into 5-hydroxymethylfurfural over niobia/carbon composites", Chemical Engineering Journal, vol. 332, pp. 528-536, 2018.

[14] G. Fan, Y. Wang, Z. Hu, J. Yan, J. Li, G. Song, "Synthesis of 5-hydroxymethyl furfural from cellulose via a two-step process in polar aprotic solvent", Carbohydrate Polymers, vol. 200, pp. 529-535, 2018.

[15] Y. Han, L. Ye, X. Gu, P. Zhu, X. Lu, "Lignin-based solid acid catalyst for the conversion of cellulose to levulinic acid using γ-valerolactone as solvent", Industrial Crops and Products, vol. 127, pp. 88-93, 2019.

[16] A. Ishihara, "Preparation of Amorphous Silica-Alumina Using the Sol–Gel Method and its Reactivity for a Matrix in Catalytic Cracking", Catalysis Survey Asia, vol. 16, no. 1, pp. 36-47, 2012.

[17] F. Nadolny, B. Hannebauer, F. Alscher, S. Peitz, W. Reschetilowski, R. Franke, "Experimental and theoretical investigation of heterogeneous catalyzed oligomerization of a mixed C4 stream over modified amorphous aluminosilicates", Journal of Catalysis, vol. 367, pp. 81-94, 2018.

[18] R. E. Nugraha, D. Prasetyoko, N. Asikin-Mijan, H. Bahruji, S. Suprapto, Y. H. Taufiq-Yap, A. Abdul Jalil, "The effect of structure directing agents on micro/mesopore structures of aluminosilicates from Indonesian kaolin as deoxygenation catalysts", Microporous and Mesoporous Materials, vol. 315, pp. 110917, 2021.

HOSGUN et al.

Conversion of Cellulose to 5-HMF in the Presence of Silica-Alumina Catalysts Synthesized by Dual Temp...

[19] H. Taghvaei, A. Moaddeli, A. Khalafi-Nezhad, A. Iulianelli, "Catalytic hydrodeoxygenation of lignin pyrolytic-oil over Ni catalysts supported on spherical Al-MCM-41 nanoparticles: Effect of Si/Al ratio and Ni loading", Fuel, vol. 293, p. 120493, 2021.

[20] P. Sadeghpour, M. Haghighi, A. Ebrahimi, "Ultrasound-assisted rapid hydrothermal design of efficient nanostructured MFI-Type aluminosilicate catalyst for methanol to propylene reaction", Ultrasonics Sonochemistry, vol. 72, pp. 105416, 2021.

[21] M. Zabeti, T. S. Nguyen, L. Lefferts, H. J. Heeres, K. Seshan, "In situ catalytic pyrolysis of lignocellulose using alkali-modified amorphous silica alumina", Bioresource Technology, vol. 118, pp. 374-381, 2012.

[22] Y. Zhai, P. Zhu, S. Li, C. Zhang, Z. Li, X. Xu, G. Chen, Z. Tan, R. Zhang, Y. Liu, "Hydrotreatment of bio-oil over Pd-based catalysts", Journal of Renewable and Sustainable Energy, vol. 6, no. 4, pp. 043129, 2014.

[23] S. T. Pham, M. B. Nguyen, G. H. Le, T. T. T. Pham, T. T. T. Quan, T. D. Nguyen, T. L. Son, T. A. Vu, "Cellulose Conversion to 5 Hydroxymethyl Furfural (5-HMF) Using Al-Incorporated SBA-15 as Highly Efficient Catalyst", Journal of Chemistry, vol. 2019, pp. 1-8, 2019.

[24] S. T. Pham, M. B. Nguyen, G. H. Le, T. D. Nguyen, C. D. Pham, T. S. Le, T. A. Vu, "Influence of Brønsted and Lewis acidity of the modified Al-MCM-41 solid acid on cellulose conversion and 5-hydroxylmethylfurfuran selectivity", Chemosphere, vol. 265, pp. 129062, 2021.

[25] X. Yan, B. Liu, J. Huang, Y. Wu, H. Chen, H. Xi, "Dual Template Preparation of MFI Zeolites with Tuning Catalytic Properties in Alkylation of Mesitylene with Benzyl Alcohol", Industrial & Engineering Chemistry Research, vol. 58, no. 8, pp. 2924-2932, 2019.

[26] S. Bosnar, V. Rac, D. Stošić, A. Travert, G.Postole, A. Auroux, S. Škapin, L. Damjanović-Vasilić, J. Bronić, X. Du, S. Marković, V. Pavlović, V. Rakić, "Overcoming phase separation in dual templating: A homogeneous hierarchical ZSM-5 zeolite with flower-like morphology, synthesis and in-depth acidity study", Microporous and Mesoporous Materials, vol. 329, pp. 111534, 2022.

[27] W. Wang, J. Xie, P. Wang, L. Chen, C. Au, S. Yin, "Dual-template synthesis of HZSM-5 zeolites with tailored activity in toluene methylation with CH_3Br", Chinese Journal of Chemical Engineering, vol. 27, no. 8, pp. 1846-1850, 2019.

[28] Y. Tu, T. Zhan, T. Wu, F. Zhang, I. Kumakiri, X. Chen, H. Kita, "Rapid synthesis of AlPO-18 molecular sieve for gas separation with dual-template agent", Microporous and Mesoporous Materials, vol. 327, pp. 111436, 2021.

[29] L. Sun, W. Zhang, Z. Li, M. Yang, Y. Wang, X. Zhang, P. Tian, Z. Liu, "Dual-template directed aminothermal syntheses and characterization of silicoaluminophosphates SAPO-CLO and ECR-40", Microporous and Mesoporous Materials, vol. 315, pp. 110915, 2021.

[30] Q. Miao, X. Huang, J. Li, Y. Duan, L. Yan, Y. Jiang, S. Lu, "Hierarchical macro-mesoporous Mo/Al_2O_3 catalysts prepared by dual-template method for oxidative desulfurization", Journal

HOSGUN et al.

Conversion of Cellulose to 5-HMF in the Presence of Silica-Alumina Catalysts Synthesized by Dual Temp...

Porous Materials, vol. 28, no. 6, pp. 1895-1906, 2021.

[31] T. Kaneko, F. Nagata, S. Kugimiya, K. Kato, "Morphological control of mesoporous silica particles by dual template method", Ceramics International, vol. 44, no. 16, pp. 20581-20585, 2018.

[32] Q. Wang, H. Wang, Y. Wu, L. Cheng, L. Zhu, J. Zhu, Z. Li, Y. Ke, "Pore size control of monodisperse silica particles by dual template sol–gel method", Journal of Sol-Gel Science and Technology, vol. 94, no. 1, pp. 186-194, 2020.

[33] L. Du, H. Song, S. Liao, "Tuning the morphology of mesoporous silica by using various template combinations", Applied Surface Science, vol. 255, no. 23, pp. 9365-9370, 2009.

[34] L. Emdadi, Y. Wu, G. Zhu, C.-C. Chang, W. Fan, T. Pham, R. F. Lobo, D. Liu, "Dual Template Synthesis of Meso- and Microporous MFI Zeolite Nanosheet Assemblies with Tailored Activity in Catalytic Reactions", Chemistry of Materials, vol. 26, no. 3, pp. 1345-1355, 2014.

[35] M. Wang, X. Wang, Q. You, Y. Wu, X. Yang, H. Chen, B. Liu, Q. Hao, J. Zhang, X. Ma, "Dual-template synthesis of hierarchically layered titanosilicate-1 zeolites for catalytic epoxidation of cyclooctene", Microporous and Mesoporous Materials, vol. 323, pp. 111207, 2021.

[36] J. Shi, Y. Chen, T. Liu, H. Liang, "Preparation of mesoporous γ-Al_2O_3 catalysts by dual template method", Journal of Dispersion Science and Technology, vol. 41, no. 10, pp. 1471-1479, 2020.

[37] V. Şimşek, "Investigation of Catalytic Sustainability of Silica-Based Mesoporous Acidic Catalysts and Ion-Exchange Resins in Methyl Acetate Synthesis and Characterizations of Synthesized Catalysts", Arabian Journal for Science and Engineering, vol. 44, no. 6, pp. 5301-5310, 2019.

[38] A. Yüksel, "Levulinik Asit Üretimi İçin Selülozun Sıcak-Basınçlı Suda Hidrotermal Muamelesi", Uludağ University Journal of The Faculty of Engineering, vol. 21, no. 2, pp. 415-415, 2016.

[39] D. M. Oliveira A. S. Andrada, "Synthesis of ordered mesoporous silica MCM-41 with controlled morphology for potential application in controlled drug delivery systems", Cerâmica, vol. 65, no. 374, pp. 170-179, 2019.

[40] S. Musić, N. Filipović-Vinceković, L. Sekovanić, "Precipitation of amorphous SiO_2 particles and their properties", Brazilian Journal of Chemical Engineering, vol. 28, no. 1, pp. 89-94, 2011.

[41] R. Maddalena, C. Hall, A. Hamilton, "Effect of silica particle size on the formation of calcium silicate hydrate [C-S-H] using thermal analysis", Thermochimica Acta, vol. 672, pp. 142-149, 2019.

[42] S. T. Pham, M. B. Nguyen, G. H. Le, T. T. T. Pham, T. T. T. Quan, T. D. Nguyen, T. L. Son, T. A. Vu, "Cellulose Conversion to 5 Hydroxymethyl Furfural (5-HMF) Using Al-Incorporated SBA-15 as Highly Efficient Catalyst", Journal of Chemistry, vol. 2019, pp. 1-8, 2019.

[43] B. K. Singh, R. Tomar, S. Kumar, A. Jain, B. S. Tomar, V. K. Manchanda, "Sorption of 137Cs, 133Ba and 154Eu by synthesized sodium aluminosilicate

HOSGUN et al.

Conversion of Cellulose to 5-HMF in the Presence of Silica-Alumina Catalysts Synthesized by Dual Temp...

(Na-AS)", Journal of Hazardous Materials, vol. 178, no. 1-3, pp. 771-776, 2010.

[44] Y. Liu, F. Zeng, B. Sun, P. Jia, I. T. Graham, "Structural Characterizations of Aluminosilicates in Two Types of Fly Ash Samples from Shanxi Province, North China", Minerals, vol. 9, no. 6, pp. 358, 2019.

[45] J. Zheng, J. Ma, Y. Wang, Y. Bai, X. Zhang, R. Li, "Synthesis and Catalytic Property of a Zeolite Composite for Preparation of Dimethyl Ether from Methanol Dehydration", Catalysis Letters, vol. 130, no. 3-4, pp. 672-678, 2009.

[46] E. Soghrati, T. K. C. Ong, C. K. Poh, S. Kawi, A. Borgna, "Zeolite–supported nickel phyllosilicate catalyst for C O hydrogenolysis of cyclic ethers and polyols", Applied Catalysis B: Environmental, vol. 235, pp. 130-142, 2018.

[47] U. Tyagi, N. Anand, D. Kumar, "Synergistic effect of modified activated carbon and ionic liquid in the conversion of microcrystalline cellulose to 5-Hydroxymethyl Furfural", Bioresource Technology, vol. 267, pp. 326-332, 2018.

[48] F. Lai, F. Yan, P. Wang, S. Wang, S. Li, Z. Zhang, "Highly efficient conversion of cellulose into 5-hydroxymethylfurfural using temperature-responsive $ChnH_{5-n}CeW_{12}O_{40}$ (n = 1–5) catalysts", Chemical Engineering Journal, vol. 396, pp. 125282, 2020.

[49] S. Zhao, M. Cheng, J. Li, J. Tian, X. Wang, "One pot production of 5-hydroxymethylfurfural with high yield from cellulose by a Brønsted–Lewis–surfactant-combined heteropolyacid catalyst", Chemical Communications, vol. 47, no. 7, pp. 2176, 2011.

Title: Encoder Hurwitz Integers: Hurwitz Integers that have the "Division with Small Remainder" Property

Authors: Ramazan DURAN

Encoder Hurwitz Integers: Hurwitz Integers that have the "Division with Small Remainder" Property

Ramazan DURAN*[1] iD

Abstract

Considering error-correcting codes over Hurwitz integers, prime Hurwitz integers are considered. On the other hand, considering transmission over Gaussian channel, Hurwitz integers, whose the norm is either a prime integer or not a prime integer, are considered. In this study, we consider Hurwitz integers, the greatest common divisor of components of which is one, i.e., primitive Hurwitz integers. We show, with the help of a proposition, that some primitive Hurwitz integers accompanied by a related modulo function are not suitable for constructing Hurwitz signal constellations. To solve this problem, we show, with the help of a proposition, the existence of primitive Hurwitz integers that have the "division with small remainder" property used to construct the Hurwitz constellations. We also call the set of these integers named as "Encoder Hurwitz Integers" set. Moreover, we examine some properties of the mentioned set. In addition, we investigate the performances of Hurwitz signal constellations, which are constructed accompanied by a related modulo function using Hurwitz integers, each component of which is in half-integers, for transmission over the additive white Gaussian noise (AWGN) channel by means of the constellation figure of merit (CFM), average energy, and signal-to-noise ratio (SNR).

Keywords: Quaternion integers, Hurwitz integers, residual class, signal constellations, code constructions

1. NTRODUCTION

A Gaussian integer is a complex number, each component of which is in integers. The set of Gaussian integers that is denoted by $\mathbb{Z}[i]$ is shown by $\mathbb{Z}[i] = \{\alpha = \alpha_1 + \alpha_2 i : \alpha_1, \alpha_2 \in \mathbb{Z}, i^2 = -1\}$. Let $\alpha = \alpha_1 + \alpha_2 i$ be a Gaussian integer. The conjugate of a Gaussian integer α is equal to $\bar{\alpha} = \alpha_1 - \alpha_2 i$. The norm of a Gaussian integer α is equal to $N(\alpha) = \alpha_1^2 + \alpha_2^2$. The inverse of a Gaussian integer α is equal to $\alpha^{-1} = \dfrac{\bar{\alpha}}{N(\alpha)}$, where $N(\alpha) \neq 0$. A Gaussian integer α is called a prime Gaussian integer if its norm is a prime integer. A Gaussian integer α is called a primitive Gaussian integer if the greatest common divisor (gcd) of its components is one, i.e. $\gcd(\alpha_1, \alpha_2) = 1$. In [1], codes over Gaussian integers were first presented by Huber. His original idea is to

---
* Corresponding author: rduran@aku.edu.tr (R. DURAN)
[1] Department of Mathematics, Faculty of Arts and Sciences, Afyon Kocatepe Univeristy, Afyonkarahisar, Turkey
ORCID: https://orcid.org/0000-0002-8076-0557

regard a finite field as a residue class of the Gaussian integer ring modulo a prime Gaussian integer. Moreover, the Euclidean division is used to get a unique element of the minimal norm in each residue class, which represents each element of a finite field. Therefore, each element of a finite field can be represented by a Gaussian integer with the minimal Galois norm in the residue class. The visualization of the residue classes of Gaussian integers, Eisenstein-Jacobi integers, quaternion integers, Lipschitz integers, or Hurwitz integers, respectively, is called a signal constellation, which is a communication term. In coding theory, each element of the signal constellation refers to a complex-value codeword. Huber is used prime Gaussian integers such that $1 \equiv p \mod 4$, where $p = \alpha\bar{\alpha}$ and $\alpha_1 > \alpha_2 > 0$. In this study, we consider primitive Gaussian integers, the norm of which is either a prime integer or not a prime integer, where $\alpha_1 > \alpha_2 > 0$. Codes over Gaussian integer rings were studied in papers [2-5].

Quaternions are a number system that extends complex numbers. Let $\pi = \pi_1 + \pi_2 i + \pi_3 j + \pi_4 k$ be a quaternion. Here π_1 is the real part, and $\pi_2 i + \pi_3 j + \pi_4 k$ is the imaginary part. Multiplication of two quaternions has no commutative property, in general. Multiplication of two quaternions has commutative property if their imaginary parts are parallel or conjugate to each other. A quaternion π is called a quaternion integer just if π_1, π_2, π_3 and π_4 are in integers. In [6], Özen and Güzeltepe studied codes over quaternion integers, which have the commutative property. Codes over quaternion integers were studied in papers [6-10]. A quaternion integer π is called a Lipschitz integer just if its components are in integers. A Lipschitz integer π is called a primitive Lipschitz integer if the greatest common divisor of its components is one. Codes over Lipschitz integers were studied in papers [11-14, 19, 27].

A quaternion integer π is called a Hurwitz integer just if its components are either in $\mathbb{Z}$ or in $\mathbb{Z} + \frac{1}{2}$. A Hurwitz integer π is called a primitive Hurwitz integer if the greatest common divisor of its components is one. In [15], Güzeltepe studied the classes of linear codes over Hurwitz integers equipped with a new metric that refer as the Hurwitz metric. In [16], Rohweder et al. presented a new algebraic construction technique to construct finite sets of Hurwitz integers by a respective modulo function. Moreover, they investigated the performances of Hurwitz signal constellations constructed by Lipschitz integers for transmission over the additive white Gaussian noise (AWGN) channel. Codes over Hurwitz integers were studied in papers [15-21].

This work is organized as follows: In the next section, we give some basic information used throughout this paper. In Section III, we define a new set named "encoder Hurwitz integers". This set comprises to the Hurwitz integers that have the "division with small remainder" property. In Section IV, we investigate the performances of Hurwitz signal constellations constructed by primitive Hurwitz integers, whose components are in $\mathbb{Z} + \frac{1}{2}$, for transmission over the AWGN channel by means of constellation figure of merit (CFM), average energy, and signal-noise-to ratio (SNR). Finally, we conclude the paper in Section V.

2. PRELIMINARIES

We begin with some basic definitions.

Definition 2.1 Let $\pi = \pi_1 + \pi_2 i + \pi_3 j + \pi_4 k$ be a quaternion. A quaternion integer π is called a Hurwitz integer just if either $\pi_1, \pi_2, \pi_3, \pi_4 \in \mathbb{Z}$ or $\pi_1, \pi_2, \pi_3, \pi_4 \in \mathbb{Z} + \frac{1}{2}$. The set of all Hurwitz integers that is denoted by $\mathcal{H}$ is shown by

$$\mathcal{H} = \begin{cases} \pi_1 + \pi_2 i + \pi_3 j + \pi_4 k : \pi_1, \pi_2, \pi_3, \pi_4 \in \mathbb{Z} \\ or\ \pi_1, \pi_2, \pi_3, \pi_4 \in \mathbb{Z} + \dfrac{1}{2} \end{cases}$$

$$= \mathcal{H}(\mathbb{Z}) \bigcup \mathcal{H}\left(\mathbb{Z} + \frac{1}{2}\right).$$

For instance, $\pm 1 \pm \frac{1}{2} i \pm \frac{1}{2} j \pm \frac{1}{2} k$ and $\pm \frac{1}{2} \pm \frac{1}{2} j$ are not Hurwitz integers, but $\pm \frac{3}{2} \pm \frac{5}{2} i \pm \frac{1}{2} j \pm \frac{7}{2} k$ is a Hurwitz integer and so on. The ring of Hurwitz integers forms a subring of the ring of all quaternions since it is closed under multiplication and addition. The conjugate of a Hurwitz integer π is $\bar{\pi} = \pi_1 - \pi_2 i - \pi_3 j - \pi_4 k$. The norm of a Hurwitz integer π is $N(\pi) = \pi \cdot \bar{\pi} = \pi_1^2 + \pi_2^2 + \pi_3^2 + \pi_4^2$. The inverse of a Hurwitz integer π is $\pi^{-1} = \dfrac{\bar{\pi}}{N(\pi)}$, where $N(\pi) \neq 0$.

Definition 2.2 Let π be a Hurwitz integer. The Hurwitz integer π is called a prime Hurwitz integer if its norm is a prime integer.

For instance, $\pi = 2 - 3i + j + 3k$ and $\beta = \dfrac{3}{2} + \dfrac{5}{2} i - \dfrac{3}{2} j + \dfrac{7}{2} k$ are the prime Hurwitz integers since $N(\pi) = 2^2 + (-3)^2 + 1^2 + 3^2 = 23$ and

$$N(\beta) = \left(\frac{3}{2}\right)^2 + \left(\frac{5}{2}\right)^2 + \left(-\frac{3}{2}\right)^2 + \left(\frac{7}{2}\right)^2 = 23.$$

Definition 2.3 Let $\pi = \pi_1 + \pi_2 i + \pi_3 j + \pi_4 k$ be a Hurwitz integer. If π is a Hurwitz integer, whose each component is in integers, then it is called a primitive Hurwitz integer just if the greatest common divisor of its components is one, i.e. $\gcd(\pi_1, \pi_2, \pi_3, \pi_4) = 1$. If π is a Hurwitz integer, whose each component is in half-integers, then it is called a primitive Hurwitz integer just if the greatest common divisor of its numerators is one.

Note that, in this study, unless otherwise stated, we consider primitive Hurwitz integers, the norm of which is either a prime integer or not a prime integer, where $\pi_1 \geq \pi_2 \geq \pi_3 \geq \pi_4 > 0$.

Definition 2.4 [15] Let α and π be Hurwitz integers. If there exists $\lambda \in \mathcal{H}$ such that $q_1 - q_2 = \lambda \alpha$, then $q_1, q_2 \in \mathcal{H}$ are said to be right congruent modulo π. This relation is denoted by $q_1 \equiv_r q_2$. Here, $\equiv_r$ is represented as the right congruent. This relation $q_1 \equiv_r q_2$ is an equivalence relation. The elements in the right ideal $\langle \pi \rangle = \{\lambda \pi : \lambda \in \mathcal{H}\}$ define a normal subgroup of the additive group of the ring $\mathcal{H}$. The set of cosets to $\langle \pi \rangle$ in $\mathcal{H}$ defines the Abelian group denoted by $\mathcal{H}_\pi = \mathcal{H}/\langle \pi \rangle$. Analogous results are valid for left congruent modulo π.

Note that we consider the left congruent modulo an element π in the Hurwitz integers rings. Therefore, we consider the elements in the left ideal $\langle \pi \rangle = \{\pi \lambda : \lambda \in \mathcal{H}\}$.

Definition 2.5 A notation for the nearest integer rounding is denoted by $[\![\cdot]\!]$. It is rounding a rational number to the integer closest to it. Each component is rounded to the integer closest to it for a quaternion, respectively.

Considering half-integers, the rounding is done by the following. We take an example $\dfrac{\pi_1}{2}$, where π_1 is an odd integer. If π_1 is an odd negative integer, then we round it as

- $\left[\!\!\left[\dfrac{\pi_1}{2} \right]\!\!\right] = \dfrac{\pi_1}{2} + \dfrac{1}{2},$ (1)

- $\left[\!\!\left[-\dfrac{\pi_1}{2} \right]\!\!\right] = -\left[\!\!\left[\dfrac{\pi_1}{2} \right]\!\!\right] = -\left(\dfrac{\pi_1}{2} + \dfrac{1}{2} \right).$ (2)

If π_1 is a positive integer, then we round it as

- $$\left\llbracket \frac{\pi_1}{2} \right\rrbracket = \frac{\pi_1}{2} - \frac{1}{2}, \qquad (3)$$

- $$\left\llbracket -\frac{\pi_1}{2} \right\rrbracket = -\left\llbracket \frac{\pi_1}{2} \right\rrbracket = -\left(\frac{\pi_1}{2} - \frac{1}{2} \right). \qquad (4)$$

For instance, let $\pi = \frac{5}{4} + \frac{1}{2}i - \frac{1}{2}j - \frac{5}{2}k$ be a Hurwitz quaternion. By eq. (1), eq. (2), eq. (3) and eq. (4), we get

$$\llbracket \pi \rrbracket = \left\llbracket \frac{5}{4} + \frac{1}{2}i - \frac{1}{2}j - \frac{5}{2}k \right\rrbracket$$

$$= \left\llbracket \frac{5}{4} \right\rrbracket + \left\llbracket \frac{1}{2} \right\rrbracket i - \left\llbracket \frac{1}{2} \right\rrbracket j - \left\llbracket \frac{5}{2} \right\rrbracket k$$

$$= 1 + 0 \cdot i - 0 \cdot j - 2 \cdot k = 1 - 2k .$$

In the rest of this study, we consider eq. (3) and eq. (4) since π is a primitive Hurwitz integer.

Definition 2.6 Let π be a primitive Hurwitz integer, and let $z \in \mathbb{Z}_{N(\pi)}$. The modulo function $\mu : \mathbb{Z}_{N(\pi)} \to \mathcal{H}_\pi$ is defined by

$$\mu_\pi(z) = z \bmod \pi = z - \pi \cdot \llbracket \pi^{-1} z \rrbracket = z - \pi \left\llbracket \frac{\bar{\pi} z}{N(\pi)} \right\rrbracket. \qquad (5)$$

Here, $\mathbb{Z}_{N(\pi)}$ is the well-known residual class set of ordinary integers ring with $N(\pi)$ elements, $\mathcal{H}_\pi$ is the left residual class set of z with respect to the modulo function in eq. (5), and $\mu_\pi(z)$ is given the remainder of z with respect to the modulo function in eq. (5). The quotient ring of the Hurwitz integers modulo this equivalence relation, which we denote as $\mathcal{H}_\pi = \{ z \bmod \pi \mid z \in \mathbb{Z}_{N(\pi)} \}$. This set contains $N(\pi)$ elements. If π is a prime Hurwitz integer, then the modulo function μ

defines a bijective mapping from $\mathbb{Z}_{N(\pi)}$ to $\mathcal{H}_\pi$. Therefore, the modulo function μ is a ring isomorphism. Because there exists an inverse map [22], and we have $\mu(z_1 + z_2) = \mu(z_1) + \mu(z_2)$ and $\mu(z_1 z_2) = \mu(z_1)\mu(z_2)$, for any $z_1, z_2 \in \mathbb{Z}_{N(\pi)}$. If π is a primitive Hurwitz integer, the modulo function μ is a group isomorphism with respect to addition between $\mathbb{Z}_{N(\pi)}$ and $\mathcal{H}_\pi$.

A signal constellation is a physical diagram describing all the possible symbols a signaling system uses to transmit data. It is an aid in designing better communications systems. [23]. These symbols represent the codewords. In other words, they represent the elements, defined as the complex-value codewords, in the set of the residual class of Hurwitz integers ring. Thus, in the rest of this study, we use the "signal constellation" term instead of "the set of residual class" term. We can take an example, "Hurwitz signal constellation" instead of the "residue classes of modulo an element π in the Hurwitz integers rings". You can find more details about signal constellation in [23].

You can find more details about the arithmetic properties of quaternions and Hurwitz integers in [24-25].

3. ENCODER HURWITZ INTEGERS

The Euclid division algorithm states that given positive integers a and b, there exist unique integers q and r such that $a = bq + r$ and $0 \le r < b$. Here, a is the dividend, b is the divisor, q is the quotient, and r is the remainder. Considering Hurwitz integers, the Euclid division algorithm states that given Hurwitz integers θ and π, there exist unique Hurwitz integers β and γ such that $\theta = \pi\beta + \gamma$ and $0 \le N(\gamma) \le N(\pi)$. In other words, Hurwitz integers, each component of which is in $\mathbb{Z} + \frac{1}{2}$, satisfy the Euclid division

algorithm but Hurwitz integers, each component of which is in integers, do not. We call that Hurwitz integers that satisfy the Euclid division have the "division with small remainder" property. The key point is that the Euclid division algorithm is not worked with some Hurwitz integers. Note that, in this study, we consider the primitive Hurwitz integers. Therefore, in this study, we investigate which primitive Hurwitz integers satisfy the Euclid division or not.

The following proposition shows that the remainder and dividend are equal to each other for the primitive Hurwitz integers, each component of which is an odd integer.

Proposition 3.1 Let π be a primitive Hurwitz integer, each component of which is an odd integer. Then,

$$N\left(\mu_\pi\left(\frac{N(\pi)}{2}\right)\right) = N(\pi) \tag{6}$$

with respect to the modulo function in eq. (5).

Proof Let $\pi = \pi_1 + \pi_2 i + \pi_3 j + \pi_4 k$ be a primitive Hurwitz integer, each component of which is an odd integer. By eq. (5),

$$\mu_\pi\left(\frac{N(\pi)}{2}\right) = \frac{N(\pi)}{2} - \pi \left\|\dfrac{\dfrac{\bar{\pi}N(\pi)}{2}}{N(\pi)}\right\|$$

$$= \frac{N(\pi)}{2} - \pi \left\|\frac{\bar{\pi}}{2}\right\|$$

$$= \frac{N(\pi)}{2} - (\pi_1 + \pi_2 i + \pi_3 j + \pi_4 k)\left\|\frac{\pi_1 - \pi_2 i - \pi_3 j - \pi_4 k}{2}\right\|.$$

By eq. (3) and eq. (4), $\left\|\dfrac{\pi_1}{2}\right\| = \dfrac{\pi_1}{2} - \dfrac{1}{2}$,

$\left\|-\dfrac{\pi_2}{2}\right\| = -\left(\dfrac{\pi_2}{2} - \dfrac{1}{2}\right)$, $\left\|-\dfrac{\pi_3}{2}\right\| = -\left(\dfrac{\pi_3}{2} - \dfrac{1}{2}\right)$,

and $\left\|-\dfrac{\pi_4}{2}\right\| = -\left(\dfrac{\pi_4}{2} - \dfrac{1}{2}\right)$. Then, we get

$$\mu_\pi\left(\frac{N(\pi)}{2}\right) = \frac{N(\pi)}{2} - (\pi_1 + \pi_2 i + \pi_3 j + \pi_4 k)\left[\left(\frac{\pi_1}{2} - \frac{1}{2}\right)\right.$$

$$\left. - \left(\frac{\pi_2}{2} - \frac{1}{2}\right)i - \left(\frac{\pi_3}{2} - \frac{1}{2}\right)j - \left(\frac{\pi_4}{2} - \frac{1}{2}\right)k\right]$$

$$= \frac{N(\pi)}{2} - \left[\frac{\pi_1^2 - \pi_1}{2} - \left(\frac{\pi_1\pi_2 - \pi_1}{2}\right)i - \left(\frac{\pi_1\pi_3 - \pi_1}{2}\right)j\right.$$

$$- \left(\frac{\pi_1\pi_4 - \pi_1}{2}\right)k + \left(\frac{\pi_2\pi_1 - \pi_2}{2}\right)i + \left(\frac{\pi_2^2 - \pi_2}{2}\right)$$

$$- \left(\frac{\pi_2\pi_3 - \pi_2}{2}\right)k + \left(\frac{\pi_2\pi_4 - \pi_2}{2}\right)j + \left(\frac{\pi_3\pi_1 - \pi_3}{2}\right)j$$

$$+ \left(\frac{\pi_3\pi_2 - \pi_3}{2}\right)k + \left(\frac{\pi_3^2 - \pi_3}{2}\right) - \left(\frac{\pi_3\pi_4 - \pi_3}{2}\right)i$$

$$+ \left(\frac{\pi_4\pi_1 - \pi_4}{2}\right)k - \left(\frac{\pi_4\pi_2 - \pi_4}{2}\right)j$$

$$\left. + \left(\frac{\pi_4\pi_3 - \pi_4}{2}\right)i + \left(\frac{\pi_4^2 - \pi_4}{2}\right)\right]$$

$$= \frac{N(\pi)}{2} - \left[\frac{\pi_1^2 + \pi_2^2 + \pi_3^2 + \pi_4^2 - \pi_1 - \pi_2 - \pi_3 - \pi_4}{2}\right.$$

$$+ \left(\frac{-\pi_1\pi_2 + \pi_1 + \pi_2\pi_1 - \pi_2 - \pi_3\pi_4 + \pi_3 + \pi_4\pi_3 - \pi_4}{2}\right)i$$

$$+ \left(\frac{-\pi_1\pi_3 + \pi_1 + \pi_2\pi_4 - \pi_2 + \pi_3\pi_1 - \pi_3 - \pi_4\pi_2 + \pi_4}{2}\right)j$$

$$\left. + \left(\frac{-\pi_1\pi_4 + \pi_1 - \pi_2\pi_3 + \pi_2 + \pi_3\pi_2 - \pi_3 + \pi_4\pi_1 - \pi_4}{2}\right)k\right]$$

$$= \frac{N(\pi)}{2} - \frac{N(\pi)}{2} + \frac{\pi_1 + \pi_2 + \pi_3 + \pi_4}{2}$$

$$+ \left(\frac{-\pi_1 + \pi_2 - \pi_3 + \pi_4}{2}\right)i + \left(\frac{-\pi_1 + \pi_2 + \pi_3 - \pi_4}{2}\right)j$$

$$+\left(\frac{-\pi_1-\pi_2+\pi_3+\pi_4}{2}\right)k$$

$$=\frac{\pi_1+\pi_2+\pi_3+\pi_4}{2}+\left(\frac{-\pi_1+\pi_2-\pi_3+\pi_4}{2}\right)i$$

$$+\left(\frac{-\pi_1+\pi_2+\pi_3-\pi_4}{2}\right)j+\left(\frac{-\pi_1-\pi_2+\pi_3+\pi_4}{2}\right)k\,.$$

Therefore, we get

$$N\left(\mu_\pi\left(\frac{N(\pi)}{2}\right)\right)=N\left(\frac{\pi_1+\pi_2+\pi_3+\pi_4}{2}\right.$$

$$+\left(\frac{-\pi_1+\pi_2-\pi_3+\pi_4}{2}\right)i+\left(\frac{-\pi_1+\pi_2+\pi_3-\pi_4}{2}\right)j$$

$$+\left.\left(\frac{-\pi_1-\pi_2+\pi_3+\pi_4}{2}\right)k\right)$$

$$=\frac{4\left(\pi_1^2+\pi_2^2+\pi_3^2+\pi_4^2\right)}{4}=\pi_1^2+\pi_2^2+\pi_3^2+\pi_4^2\,.$$

Consequently, $N(\mu_\pi(\frac{N(\pi)}{2}))=N(\pi)$. This completes the proof.

The following proposition implies that the primitive Hurwitz integers, each component of which is in integers, do not have the "division with small remainder" property.

Proposition 3.2 Let π be a primitive Hurwitz integer, each component of which is in integers, and let β be a Hurwitz integer, where $N(\beta)\neq 0$. Then, $N\left(\mu_\pi\left(\beta\right)\right)\leq N\left(\pi\right)$.

Proof Let π be a primitive Hurwitz integer, each component of which is in integers, and let $\beta=\beta_1+\beta_2i+\beta_3j+\beta_4k$ be a Hurwitz integer, where $N\left(\beta\right)\neq 0$. By eq. (5), we get

$$\mu_\pi\left(\beta\right)=\beta-\pi\left[\!\!\left[\frac{\pi\beta}{N\left(\beta\right)}\right]\!\!\right]\,.$$

Then, we get

$$\pi^{-1}\mu_\pi(\beta)=\pi^{-1}\beta-\pi^{-1}\pi\left[\!\!\left[\frac{\bar\pi\beta}{\bar\pi\pi}\right]\!\!\right]=\pi^{-1}\beta-\left[\!\!\left[\frac{\beta}{\pi}\right]\!\!\right]$$

$$=\pi^{-1}\left(\beta_1+\beta_2i+\beta_3j+\beta_4k\right)$$

$$-\left[\!\!\left[\frac{\beta_1+\beta_2i+\beta_3j+\beta_4k}{\pi}\right]\!\!\right]$$

$$=\pi^{-1}\beta_1+\pi^{-1}\beta_2i+\pi^{-1}\beta_3j+\pi^{-1}\beta_4k$$

$$-\left[\!\!\left[\pi^{-1}\beta_1+\pi^{-1}\beta_2i+\pi^{-1}\beta_3j+\pi^{-1}\beta_4k\right]\!\!\right]$$

$$=\pi^{-1}\beta_1+\pi^{-1}\beta_2i+\pi^{-1}\beta_3j+\pi^{-1}\beta_4k$$

$$-\left[\!\!\left[\pi^{-1}\beta_1\right]\!\!\right]-\left[\!\!\left[\pi^{-1}\beta_2\right]\!\!\right]i-\left[\!\!\left[\pi^{-1}\beta_3\right]\!\!\right]j-\left[\!\!\left[\pi^{-1}\beta_4\right]\!\!\right]k$$

$$=\pi^{-1}\beta_1-\left[\!\!\left[\pi^{-1}\beta_1\right]\!\!\right]+\left(\pi^{-1}\beta_2-\left[\!\!\left[\pi^{-1}\beta_2\right]\!\!\right]\right)i$$

$$+\left(\pi^{-1}\beta_3-\left[\!\!\left[\pi^{-1}\beta_3\right]\!\!\right]\right)j+\left(\pi^{-1}\beta_4-\left[\!\!\left[\pi^{-1}\beta_4\right]\!\!\right]\right)k\,.$$

Hereby, we get

$$\left|\pi^{-1}\beta_1-\left[\!\!\left[\pi^{-1}\beta_1\right]\!\!\right]\right|\leq\frac{1}{2}\,,$$

$$\left|\pi^{-1}\beta_2-\left[\!\!\left[\pi^{-1}\beta_2\right]\!\!\right]\right|\leq\frac{1}{2}\,,$$

$$\left|\pi^{-1}\beta_3-\left[\!\!\left[\pi^{-1}\beta_3\right]\!\!\right]\right|\leq\frac{1}{2}\,,$$

$$\left|\pi^{-1}\beta_4-\left[\!\!\left[\pi^{-1}\beta_4\right]\!\!\right]\right|\leq\frac{1}{2}\,.$$

Then, we get

$$\left(\pi^{-1}\beta_1-\left[\!\!\left[\pi^{-1}\beta_1\right]\!\!\right]\right)^2\leq\frac{1}{4}\,,$$

$$\left(\pi^{-1}\beta_2-\left[\!\!\left[\pi^{-1}\beta_2\right]\!\!\right]\right)^2\leq\frac{1}{4}\,,$$

$$\left(\pi^{-1}\beta_3 - \left[\!\left[\pi^{-1}\beta_3\right]\!\right]\right)^2 \le \frac{1}{4},$$

$$\left(\pi^{-1}\beta_4 - \left[\!\left[\pi^{-1}\beta_4\right]\!\right]\right)^2 \le \frac{1}{4}.$$

Therefore, we get

$$N\left(\pi^{-1}\mu_\pi(\beta)\right) = \left(\pi^{-1}\beta_1 - \left[\!\left[\pi^{-1}\beta_1\right]\!\right]\right)^2$$

$$+\left(\pi^{-1}\beta_2 - \left[\!\left[\pi^{-1}\beta_2\right]\!\right]\right)^2 + \left(\pi^{-1}\beta_3 - \left[\!\left[\pi^{-1}\beta_3\right]\!\right]\right)^2$$

$$+\left(\pi^{-1}\beta_4 - \left[\!\left[\pi^{-1}\beta_4\right]\!\right]\right)^2$$

$$\le \left(\frac{1}{2}\right)^2 + \left(\frac{1}{2}\right)^2 + \left(\frac{1}{2}\right)^2 + \left(\frac{1}{2}\right)^2 = 1.$$

Consequently, since $N\left(\mu_\pi(\beta)\right) \le N(\pi)$

$$N\left(\pi^{-1}\mu_\pi(\beta)\right) = \frac{1}{N(\pi)}N\left(\mu_\pi(\beta)\right) \le 1.$$ This

completes the proof.

Example 1   Let $\pi = 3 + i + j + 3k$ be a primitive Hurwitz integer. By eq. (5), the Hurwitz signal constellation is

$$\mathcal{H}_\pi = \begin{cases} \mu_\pi(0) = 0,\ \mu_\pi(1) = 1,\ \mu_\pi(2) = 2, \\ \mu_\pi(3) = 3, \mu_\pi(4) = -2 - 2j, \\ \mu_\pi(5) = -1 - 2j, \mu_\pi(6) = -2j, \\ \mu_\pi(7) = 1 - 2j, \mu_\pi(8) = 2 - 2j, \\ \mu_\pi(9) = 3 - 2j, \mu_\pi(10) = 4 - 2j, \\ \mu_\pi(11) = -3 + 2j, \mu_\pi(12) = -2 + 2j, \\ \mu_\pi(13) = -1 + 2j, \mu_\pi(14) = 2j, \\ \mu_\pi(15) = 1 + 2j, \mu_\pi(16) = 2 + 2j, \\ \mu_\pi(17) = -3,\ \mu_\pi(18) = -2, \mu_\pi(19) = -1 \end{cases}. \quad (7)$$

This set must contain twenty elements, but it contains nineteen elements since $\mu_\pi(10) \equiv \pi \equiv 0 \bmod \pi$, where $N\left(\mu_\pi(10)\right) = N(\pi) = 20$. Consequently, the Hurwitz integer $\pi = 3 + i + j + 3k$ does not have the "division with small remainder"

property (see Proposition 3.2). In other words, the Euclidean division algorithm does not work for the primitive Hurwitz integer $\pi = 3 + i + j + 3k$. In addition, to be a Euclidean metric, the inequality $d(\alpha,\beta) + d(\beta,\theta) \ge d(\alpha,\theta)$ should be verified, where $\alpha, \beta, \theta \in \mathcal{H}_\pi$. Because the conditions i) $d(\alpha,\beta) = 0$ if and only if $\alpha = \beta$, and ii) $d(\alpha,\beta) = d(\beta,\alpha)$ are supplied. We consider $\alpha = \mu_\pi(10) = 4 - 2j$, $\beta = \mu_\pi(19) = -1$ and $\theta = \mu_\pi(18) = -2$ in (7). $d(\alpha,\beta) = 29$ since $N(\beta - \alpha) = 29$, $d(\beta,\theta) = 1$ since $N(\theta - \beta) = 1$, and $d(\alpha,\theta) = 40$ since $N(\theta - \alpha) = 40$. Therefore, $29 + 1 = 30 \ge 40$ since $d(\alpha,\beta) + d(\beta,\theta) \ge d(\alpha,\theta)$. This is a contradiction. The Euclidean metric does not satisfy the Hurwitz signal constellation $\mathcal{H}_\pi$ constructed by the primitive Hurwitz integer $\pi = 3 + i + j + 3k$.

In the following definition, we define a new set named the encoder Hurwitz integer, which consists of the primitive Hurwitz integers that have the "division with small remainder" property.

Definition 3.1 Let $\pi = \pi_1 + \pi_2 i + \pi_3 j + \pi_4 k$ be a primitive Hurwitz integer. If a primitive Hurwitz integer π does not satisfy the condition $N\left(\mu_\pi\left(\frac{N(\pi)}{2}\right)\right) = N(\pi)$ (see proposition 3.2) with respect to the related modulo function, then it is called an encoder Hurwitz integer. Note that a primitive Hurwitz integer π, each component of which is in $\mathbb{Z} + \frac{1}{2}$, is an encoder Hurwitz integer.

The above definition is flexible. So, the set of encoder Hurwitz integers is expandable or collapsible depending on the related modulo technique. According to Definition 3.1, the set of encoder Hurwitz integers in this study

consists of the primitive Hurwitz integers, each component of which is not an odd integer (or each component of which is not the same parity). In other words, the set of encoder Hurwitz integers in this study consists of the primitive Hurwitz integers, each component of which is either in $\mathbb{Z} + \dfrac{1}{2}$ or not an odd integer (or components are not the same parity). In mathematics, parity is the property of an integer of whether it is even or odd [26].

Let us now show that the modulo function μ is a ring isomorphism when π is an encoder Hurwitz integer.

Theorem 3.1 Let π be an encoder Hurwitz integer, and let $z_1, z_2 \in \mathbb{Z}_{N(\pi)}$. The map $\mu : \mathbb{Z}_{N(\pi)} \to \mathcal{H}_\pi$ is a ring homomorphism.

Proof Let π be an encoder Hurwitz integer and, let $z_1, z_2 \in \mathbb{Z}_{N(\pi)}$. By eq. (5), we get

$$\mu_\pi(z_1) = z_1 \bmod \pi = z_1 - \pi \left\lfloor\!\!\left\lfloor \frac{\overline{\pi} z_1}{N(\pi)} \right\rceil\!\!\right\rceil$$

and

$$\mu_\pi(z_2) = z_2 \bmod \pi = z_2 - \pi \left\lfloor\!\!\left\lfloor \frac{\overline{\pi} z_2}{N(\pi)} \right\rceil\!\!\right\rceil.$$

We suppose that $\lambda_1 = \left\lfloor\!\!\left\lfloor \dfrac{\overline{\pi} z_1}{N(\pi)} \right\rceil\!\!\right\rceil$ and $\lambda_2 = \left\lfloor\!\!\left\lfloor \dfrac{\overline{\pi} z_1}{N(\pi)} \right\rceil\!\!\right\rceil$, where λ_1 and λ_2 are Hurwitz integers, each component of which is in integers. Therefore, we get

$$z_1 = \pi \lambda_1 + \mu_\pi(z_1) \tag{8}$$

and

$$z_2 = \pi \lambda_2 + \mu_\pi(z_2), \tag{9}$$

respectively. Since

$$\mu_\pi(z_1 + z_2) = = z_1 + z_2 - \pi \left\lfloor\!\!\left\lfloor \frac{\overline{\pi}(z_1 + z_2)}{N(\pi)} \right\rceil\!\!\right\rceil, \quad \text{eq.(8)}$$

and eq. (9), then we get

$$\mu_\pi(z_1 + z_2) = \pi \lambda_1 + \mu_\pi(z_1) + \pi \lambda_2 + \mu_\pi(z_2)$$

$$-\pi \left\lfloor\!\!\left\lfloor \frac{\overline{\pi}(\pi \lambda_1 + \mu_\pi(z_1) + \pi \lambda_2 + \mu_\pi(z_2))}{N(\pi)} \right\rceil\!\!\right\rceil$$

$$= \pi \lambda_1 + \mu_\pi(z_1) + \pi \lambda_2 + \mu_\pi(z_2)$$

$$-\pi \left\lfloor\!\!\left\lfloor \frac{\overline{\pi}\pi \lambda_1 + \overline{\pi}\mu_\pi(z_1) + \overline{\pi}\pi \lambda_2 + \overline{\pi}\mu_\pi(z_2)}{N(\pi)} \right\rceil\!\!\right\rceil$$

$$= \pi \lambda_1 + \mu_\pi(z_1) + \pi \lambda_2 + \mu_\pi(z_2)$$

$$-\pi \left(\lambda_1 + \lambda_2 \ - \pi \left\lfloor\!\!\left\lfloor \frac{\overline{\pi}\mu_\pi(z_1) + \overline{\pi}\mu_\pi(z_2)}{N(\pi)} \right\rceil\!\!\right\rceil\right).$$

Since λ_1 and λ_2 are the Hurwitz integers, each component of which is in integers, then $\lambda_1 + \lambda_2 \ = \lambda_1 + \lambda_2$. Hereby, we get

$$\mu_\pi(z_1 + z_2) = \pi \lambda_1 + \mu_\pi(z_1) + \pi \lambda_2$$

$$+ \mu_\pi(z_2) - \pi \lambda_1 - \pi \lambda_2 - \pi \left\lfloor\!\!\left\lfloor \frac{\overline{\pi}(\mu_\pi(z_1) + \mu_\pi(z_2))}{N(\pi)} \right\rceil\!\!\right\rceil$$

$$= \mu_\pi(z_1) + \mu_\pi(z_2) - \pi \left\lfloor\!\!\left\lfloor \frac{\overline{\pi}(\mu_\pi(z_1) + \mu_\pi(z_2))}{N(\pi)} \right\rceil\!\!\right\rceil.$$

By eq. (5), we get $\mu_\pi(z_1 + z_2) = (\mu_\pi(z_1) + \mu_\pi(z_2)) \bmod \pi$.

On the other hand, according to the modulo function in eq. (5), we get

$$\mu_\pi(z_1 z_2) = z_1 z_2 \bmod \pi = z_1 z_2 - \pi \left\lfloor\!\!\left\lfloor \frac{\overline{\pi}(z_1 z_2)}{N(\pi)} \right\rceil\!\!\right\rceil.$$

By eq. (8) and eq. (9), we get

$$\mu_\pi(z_1 z_2) = (\pi\lambda_1 + \mu_\pi(z_1))(\pi\lambda_2 + \mu_\pi(z_2))$$

$$-\pi\left[\!\left[\frac{\bar{\pi}(\pi\lambda_1 + \mu_\pi(z_1))(\pi\lambda_2 + \mu_\pi(z_2))}{N(\pi)}\right]\!\right]$$

$$= \pi\lambda_1\pi\lambda_2 + \pi\lambda_1\mu_\pi(z_2) + \mu_\pi(z_1)\pi\lambda_2$$

$$+\mu_\pi(z_1)\mu_\pi(z_2) - \pi\left[\!\left[\frac{\bar{\pi}\pi\lambda_1\pi\lambda_2 + \bar{\pi}\pi\lambda_1\mu_\pi(z_2)}{N(\pi)}\right.\right.$$

$$\left.\left.+\frac{\bar{\pi}\mu_\pi(z_1)\pi\lambda_2 + \bar{\pi}\mu_\pi(z_1)\mu_\pi(z_2)}{N(\pi)}\right]\!\right].$$

Since $N(\pi) = \pi\bar{\pi}$, then, we get

$$\mu_\pi(z_1 z_2) = \pi\lambda_1\pi\lambda_2 + \pi\lambda_1\mu_\pi(z_2) + \mu_\pi(z_1)\pi\lambda_2$$

$$+\mu_\pi(z_1)\mu_\pi(z_2) - \pi\ \lambda_1\pi\lambda_2\ -\pi\left[\!\left[\lambda_1\mu_\pi(z_2)\right]\!\right]$$

$$-\pi\left[\!\left[\frac{\bar{\pi}\mu_\pi(z_1)\pi\lambda_2}{N(\pi)}\right]\!\right] - \pi\left[\!\left[\frac{\bar{\pi}\mu_\pi(z_1)\mu_\pi(z_2)}{N(\pi)}\right]\!\right].$$

Since $\qquad \lambda_1\pi\lambda_2\ = \lambda_1\pi\lambda_2$,
$\left[\!\left[\lambda_1\mu_\pi(z_2)\right]\!\right] = \lambda_1\mu_\pi(z_2)\qquad$ and
$\left[\!\left[\dfrac{\bar{\pi}\mu_\pi(z_1)\pi\lambda_2}{N(\pi)}\right]\!\right] = \dfrac{\mu_\pi(z_1)\pi\lambda_2}{\pi}$, then we get

$$\mu_\pi(z_1 z_2) = \pi\lambda_1\pi\lambda_2 + \pi\lambda_1\mu_\pi(z_2) + \mu_\pi(z_1)\pi\lambda_2$$

$$+\mu_\pi(z_1)\mu_\pi(z_2) - \pi\lambda_1\pi\lambda_2 - \pi\lambda_1\mu_\pi(z_2)$$

$$-\mu_\pi(z_1)\pi\lambda_2 - \pi\left[\!\left[\frac{\bar{\pi}\mu_\pi(z_1)\mu_\pi(z_2)}{N(\pi)}\right]\!\right]$$

$$= \mu_\pi(z_1)\mu_\pi(z_2) - \pi\left[\!\left[\frac{\bar{\pi}\mu_\pi(z_1)\mu_\pi(z_2)}{N(\pi)}\right]\!\right].$$

By eq. (5), we get $\mu_\pi(z_1 z_2) = \mu_\pi(z_1)\mu_\pi(z_2)\bmod\pi$.

Consequently, μ function is a ring homomorphism. This completes this proof.

Theorem 3.2 Let π be an encoder Hurwitz integer. Then, $\mathbb{Z}_{N(\pi)} \cong \mathcal{H}_\pi$.

Proof Let π be an encoder Hurwitz integer and, let $z_1, z_2 \in \mathbb{Z}_{N(\pi)}$. According to Theorem 3.1, μ function is a ring homomorphism. The modulo function in Definition 2.6 is a surjective ring homomorphism since $\mathcal{H}_\pi = \{\mu_\pi(z) \mid z \in \mathbb{Z}_{N(\pi)}\} = \mathrm{Im}\mu$. If $z = 0$, then $\mu_\pi(0) = 0$. On the other hand, If $z \geq 1$, then $\mu_\pi(z) \geq 1$. Hereby, the modulo function μ is a bijective ring homomorphism since $Ker\mu = \{z \in \mathbb{Z}_{N(\pi)} \mid \mu_\pi(z) = 0\} = \{0\}$.

Consequently, the modulo function μ is a ring isomorphism since it is both a surjective ring homomorphism and a bijective ring homomorphism, i.e. $\mathbb{Z}_{N(\pi)} \cong \mathcal{H}_\pi$. This completes the proof.

The following proposition demonstrates that the encoder Hurwitz integers have the "division with small remainder" property.

Proposition 3.3 Let π be an encoder Hurwitz integer. Then, $N(\mu_\pi(z)) < N(\pi)$.

Proof Let $\pi = \pi_1 + \pi_2 i + \pi_3 j + \pi_4 k$ be an encoder Hurwitz integer. If encoder Hurwitz integer π, each component of which is in $\mathbb{Z} + \dfrac{1}{2}$, then $N(\mu_\pi(z)) < N(\pi)$ holds on. For encoder Hurwitz π, each component of which is in integers, let us analyze step by step.

Case 1 Let π be an encoder Hurwitz integer, each component of which is in integers. Suppose that let π_1 be an even integer, and let

π_2, π_3 and π_4 be odd integers. Therefore, $N(\pi)$ is an odd integer. By eq (5), we get

$$\mu_\pi(z) = z - \pi \left[\!\left[\pi^{-1} z \right]\!\right].$$

Therefore, we get

$$\pi^{-1}\mu_\pi(z) = \pi^{-1}z - \pi^{-1}\pi\left[\!\left[\pi^{-1}z\right]\!\right] = \pi^{-1}z - \left[\!\left[\pi^{-1}z\right]\!\right]$$

$$= \frac{\bar{\pi}z}{N(\pi)} - \left[\!\left[\frac{\bar{\pi}z}{N(\pi)}\right]\!\right].$$

Since $\bar{\pi} = \pi_1 - \pi_2 i - \pi_3 j - \pi_4 k$, then we get

$$\pi^{-1}\mu_\pi(z) = \frac{\pi_1 z}{N(\pi)} - \left(\frac{\pi_2 z}{N(\pi)}\right)i - \left(\frac{\pi_3 z}{N(\pi)}\right)j$$

$$- \left(\frac{\pi_4 z}{N(\pi)}\right)k - \left[\!\left[\frac{\pi_1 z}{N(\pi)}\right]\!\right] + \left[\!\left[\frac{\pi_2 z}{N(\pi)}\right]\!\right]i$$

$$+ \left[\!\left[\frac{\pi_3 z}{N(\pi)}\right]\!\right]j + \left[\!\left[\frac{\pi_4 z}{N(\pi)}\right]\!\right]k$$

$$= \frac{\pi_1 z}{N(\pi)} - \left[\!\left[\frac{\pi_1 z}{N(\pi)}\right]\!\right] - \left(\frac{\pi_2 z}{N(\pi)} - \left[\!\left[\frac{\pi_2 z}{N(\pi)}\right]\!\right]\right)i$$

$$- \left(\frac{\pi_3 z}{N(\pi)} - \left[\!\left[\frac{\pi_3 z}{N(\pi)}\right]\!\right]\right)j - \left(\frac{\pi_4 z}{N(\pi)} - \left[\!\left[\frac{\pi_4 z}{N(\pi)}\right]\!\right]\right)k.$$

Since π_1 is an even integer, π_2, π_3 and π_4 are odd integers, $N(\pi)$ is an odd integer, and $\frac{N(\pi)}{2}$ is not an integer, then we get

$$0 \le \left|\frac{\pi_1 z}{N(\pi)} - \left[\!\left[\frac{\pi_1 z}{N(\pi)}\right]\!\right]\right| < \frac{1}{2},$$

$$0 \le \left|\frac{\pi_2 z}{N(\pi)} - \left[\!\left[\frac{\pi_2 z}{N(\pi)}\right]\!\right]\right| < \frac{1}{2},$$

$$0 \le \left|\frac{\pi_3 z}{N(\pi)} - \left[\!\left[\frac{\pi_3 z}{N(\pi)}\right]\!\right]\right| < \frac{1}{2},$$

$$0 \le \left|\frac{\pi_4 z}{N(\pi)} - \left[\!\left[\frac{\pi_4 z}{N(\pi)}\right]\!\right]\right| < \frac{1}{2}.$$

Therefore, we get

$$N\left(\frac{\pi_1 z}{N(\pi)} - \left[\!\left[\frac{\pi_1 z}{N(\pi)}\right]\!\right]\right) + N\left(\frac{\pi_2 z}{N(\pi)} - \left[\!\left[\frac{\pi_2 z}{N(\pi)}\right]\!\right]\right)$$

$$+ N\left(\frac{\pi_3 z}{N(\pi)} - \left[\!\left[\frac{\pi_3 z}{N(\pi)}\right]\!\right]\right) + N\left(\frac{\pi_4 z}{N(\pi)} - \left[\!\left[\frac{\pi_4 z}{N(\pi)}\right]\!\right]\right)$$

$$< \left(\frac{1}{2}\right)^2 + \left(\frac{1}{2}\right)^2 + \left(\frac{1}{2}\right)^2 + \left(\frac{1}{2}\right)^2 = 1.$$

Hereby, we get

$$N\left(\pi^{-1}\mu_\pi(z)\right) = N\left(\pi^{-1}\right)N\left(\mu_\pi(z)\right)$$

$$= \frac{1}{N(\pi)}N\left(\mu_\pi(z)\right) < 1.$$

Consequently, $N(\mu_\pi(z)) < N(\pi)$.

Case 2 Let π be an encoder Hurwitz integer each component of which is in integers. Suppose that let π_1 and π_2 be even integers, and let π_3 and π_4 be odd integers. We should check whether to verify or not eq. (6) in Proposition 3.1 since $N(\pi)$ is an even integer. Let $z = \frac{N(\pi)}{2}$. Then, we get

$$\mu_\pi\left(\frac{N(\pi)}{2}\right) = \frac{N(\pi)}{2} - \pi\left[\!\left[\pi^{-1}\frac{N(\pi)}{2}\right]\!\right].$$

Therefore, we get

$$\pi^{-1}\mu_\pi(\frac{N(\pi)}{2}) = \pi^{-1}\frac{N(\pi)}{2} - \pi^{-1}\pi\left[\!\left[\pi^{-1}\frac{N(\pi)}{2}\right]\!\right]$$

$$= \frac{\bar{\pi}}{2} - \left[\!\left[\frac{\bar{\pi}}{2} \right]\!\right].$$

Since $\bar{\pi} = \pi_1 - \pi_2 i - \pi_3 j - \pi_4 k$, then we get

$$\pi^{-1} \mu_\pi \left(\frac{N(\pi)}{2} \right) = \frac{\pi_1}{2} - \left(\frac{\pi_2}{2} \right) i - \left(\frac{\pi_3}{2} \right) j - \left(\frac{\pi_4}{2} \right) k$$

$$- \left[\!\left[\frac{\pi_1}{2} \right]\!\right] + \left[\!\left[\frac{\pi_2}{2} \right]\!\right] i + \left[\!\left[\frac{\pi_3}{2} \right]\!\right] j + \left[\!\left[\frac{\pi_4}{2} \right]\!\right] k$$

$$= \frac{\pi_1}{2} - \left[\!\left[\frac{\pi_1}{2} \right]\!\right] - \left(\frac{\pi_2}{2} - \left[\!\left[\frac{\pi_2}{2} \right]\!\right] \right) i$$

$$- \left(\frac{\pi_3}{2} - \left[\!\left[\frac{\pi_3}{2} \right]\!\right] \right) j - \left(\frac{\pi_4}{2} - \left[\!\left[\frac{\pi_4}{2} \right]\!\right] \right) k .$$

$\left[\!\left[\frac{\pi_1}{2} \right]\!\right] = \frac{\pi_1}{2}$ and $\left[\!\left[\frac{\pi_2}{2} \right]\!\right] = \frac{\pi_2}{2}$ since π_1 and π_2 are even integers. By eq. (3), then $\left[\!\left[\frac{\pi_3}{2} \right]\!\right] = \frac{\pi_3 - 1}{2}$ and $\left[\!\left[\frac{\pi_4}{2} \right]\!\right] = \frac{\pi_4 - 1}{2}$ since π_3 and π_4 are odd integers. Therefore, we get

$$\pi^{-1} \mu_\pi \left(\frac{N(\pi)}{2} \right) = \frac{\pi_1}{2} - \frac{\pi_1}{2} - \left(\frac{\pi_2}{2} - \frac{\pi_2}{2} \right) i$$

$$- \left(\frac{\pi_3}{2} - \frac{\pi_3 - 1}{2} \right) j - \left(\frac{\pi_4}{2} - \frac{\pi_4 - 1}{2} \right) k = -\frac{1}{2} j - \frac{1}{2} k .$$

Hereby, we get

$$N \left(\pi^{-1} \mu_\pi \left(\frac{N(\pi)}{2} \right) \right) = N \left(-\frac{1}{2} j - \frac{1}{2} k \right)$$

$$N \left(\pi^{-1} \right) N \left(\mu_\pi \left(\frac{N(\pi)}{2} \right) \right) = \left(-\frac{1}{2} \right)^2 + \left(-\frac{1}{2} \right)^2$$

$$\frac{1}{N(\pi)} N \left(\mu_\pi \left(\frac{N(\pi)}{2} \right) \right) = \frac{1}{4} + \frac{1}{4} = \frac{1}{2}$$

$$N(\mu_\pi(\frac{N(\pi)}{2})) = \frac{N(\pi)}{2} .$$

Consequently, $N(\mu_\pi(\frac{N(\pi)}{2})) < N(\pi)$. On the other hand, let $z \neq \frac{N(\pi)}{2}$. Then we get

$$\mu_\pi(z) = z - \pi \left[\!\left[\pi^{-1} z \right]\!\right].$$

Hereby, we get

$$\pi^{-1} \mu_\pi(z) = \pi^{-1} z - \pi^{-1} \pi \left[\!\left[\pi^{-1} z \right]\!\right]$$

$$= \pi^{-1} z - \left[\!\left[\pi^{-1} z \right]\!\right] = \frac{\bar{\pi} z}{N(\pi)} - \left[\!\left[\frac{\bar{\pi} z}{N(\pi)} \right]\!\right].$$

Since $\bar{\pi} = \pi_1 - \pi_2 i - \pi_3 j - \pi_4 k$, then we get

$$\pi^{-1} \mu_\pi(z) = \frac{\pi_1 z}{N(\pi)} - \left(\frac{\pi_2 z}{N(\pi)} \right) i - \left(\frac{\pi_3 z}{N(\pi)} \right) j$$

$$- \left(\frac{\pi_4 z}{N(\pi)} \right) k - \left[\!\left[\frac{\pi_1 z}{N(\pi)} \right]\!\right] + \left[\!\left[\frac{\pi_2 z}{N(\pi)} \right]\!\right] i$$

$$+ \left[\!\left[\frac{\pi_3 z}{N(\pi)} \right]\!\right] j + \left[\!\left[\frac{\pi_4 z}{N(\pi)} \right]\!\right] k$$

$$= \frac{\pi_1 z}{N(\pi)} - \left[\!\left[\frac{\pi_1 z}{N(\pi)} \right]\!\right] - \left(\frac{\pi_2 z}{N(\pi)} - \left[\!\left[\frac{\pi_2 z}{N(\pi)} \right]\!\right] \right) i$$

$$- \left(\frac{\pi_3 z}{N(\pi)} - \left[\!\left[\frac{\pi_3 z}{N(\pi)} \right]\!\right] \right) j - \left(\frac{\pi_4 z}{N(\pi)} - \left[\!\left[\frac{\pi_4 z}{N(\pi)} \right]\!\right] \right) k .$$

Since $z \neq \frac{N(\pi)}{2}$, then we get

$$0 \leq \left| \frac{\pi_1 z}{N(\pi)} - \left[\!\left[\frac{\pi_1 z}{N(\pi)} \right]\!\right] \right| < \frac{1}{2},$$

$$0 \leq \left| \frac{\pi_2 z}{N(\pi)} - \left[\!\left[\frac{\pi_2 z}{N(\pi)} \right]\!\right] \right| < \frac{1}{2},$$

$$0 \leq \left| \frac{\pi_3 z}{N(\pi)} - \left[\!\left[\frac{\pi_3 z}{N(\pi)} \right]\!\right] \right| < \frac{1}{2},$$

$$0 \leq \left| \frac{\pi_4 z}{N(\pi)} - \left[\!\left[\frac{\pi_4 z}{N(\pi)} \right]\!\right] \right| < \frac{1}{2}.$$

Therefore, we get

$$N\left(\frac{\pi_1 z}{N(\pi)} - \left[\!\left[\frac{\pi_1 z}{N(\pi)} \right]\!\right] \right) + N\left(\frac{\pi_2 z}{N(\pi)} - \left[\!\left[\frac{\pi_2 z}{N(\pi)} \right]\!\right] \right)$$

$$+ N\left(\frac{\pi_3 z}{N(\pi)} - \left[\!\left[\frac{-\pi_3 z}{N(\pi)} \right]\!\right] \right) + N\left(\frac{\pi_4 z}{N(\pi)} - \left[\!\left[\frac{\pi_4 z}{N(\pi)} \right]\!\right] \right)$$

$$< \left(\frac{1}{2} \right)^2 + \left(\frac{1}{2} \right)^2 + \left(\frac{1}{2} \right)^2 + \left(\frac{1}{2} \right)^2 = 1.$$

Therefore, we get

$$N\left(\pi^{-1} \mu_\pi(z) \right) = N\left(\pi^{-1} \right) N\left(\mu_\pi(z) \right)$$

$$= \frac{1}{N(\pi)} N\left(\mu_\pi(z) \right) < 1.$$

Consequently, $N\left(\mu_\pi(z) \right) < N(\pi)$.

Case 3 Let π be an encoder Hurwitz integer, each component of which is in integers. Suppose that π_1, π_2 and π_3 are even integers, and π_4 is an odd integer. Therefore, $N(\pi)$ is an odd integer. Then we get

$$\mu_\pi(z) = z - \pi \left[\!\left[\pi^{-1} z \right]\!\right].$$

Hereby, we get

$$\pi^{-1} \mu_\pi(z) = \pi^{-1} z - \pi^{-1} \pi \left[\!\left[\pi^{-1} z \right]\!\right]$$

$$= \pi^{-1} z - \left[\!\left[\pi^{-1} z \right]\!\right] = \frac{\bar{\pi} z}{N(\pi)} - \left[\!\left[\frac{\bar{\pi} z}{N(\pi)} \right]\!\right].$$

Since $\bar{\pi} = \pi_1 - \pi_2 i - \pi_3 j - \pi_4 k$, then we get

$$\pi^{-1} \mu_\pi(z) = \frac{\pi_1 z}{N(\pi)} - \left(\frac{\pi_2 z}{N(\pi)} \right) i - \left(\frac{\pi_3 z}{N(\pi)} \right) j$$

$$- \left(\frac{\pi_4 z}{N(\pi)} \right) k - \left[\!\left[\frac{\pi_1 z}{N(\pi)} \right]\!\right] + \left[\!\left[\frac{\pi_2 z}{N(\pi)} \right]\!\right] i$$

$$+ \left[\!\left[\frac{\pi_3 z}{N(\pi)} \right]\!\right] j + \left[\!\left[\frac{\pi_4 z}{N(\pi)} \right]\!\right] k$$

$$= \frac{\pi_1 z}{N(\pi)} - \left[\!\left[\frac{\pi_1 z}{N(\pi)} \right]\!\right] - \left(\frac{\pi_2 z}{N(\pi)} - \left[\!\left[\frac{\pi_2 z}{N(\pi)} \right]\!\right] \right) i$$

$$- \left(\frac{\pi_3 z}{N(\pi)} - \left[\!\left[\frac{\pi_3 z}{N(\pi)} \right]\!\right] \right) j - \left(\frac{\pi_4 z}{N(\pi)} - \left[\!\left[\frac{\pi_4 z}{N(\pi)} \right]\!\right] \right) k.$$

Since π_4 is an odd integer, π_1, π_2 and π_3 are even integers, and $N(\pi)$ is an odd integer, then we get

$$0 \leq \left| \frac{\pi_1 z}{N(\pi)} - \left[\!\left[\frac{\pi_1 z}{N(\pi)} \right]\!\right] \right| < \frac{1}{2},$$

$$0 \leq \left| \frac{\pi_2 z}{N(\pi)} - \left[\!\left[\frac{\pi_2 z}{N(\pi)} \right]\!\right] \right| < \frac{1}{2},$$

$$0 \leq \left| \frac{\pi_3 z}{N(\pi)} - \left[\!\left[\frac{\pi_3 z}{N(\pi)} \right]\!\right] \right| < \frac{1}{2},$$

$$0 \leq \left| \frac{\pi_4 z}{N(\pi)} - \left[\!\left[\frac{\pi_4 z}{N(\pi)} \right]\!\right] \right| < \frac{1}{2}.$$

Hereby, we get

$$N\left(\frac{\pi_1 z}{N(\pi)} - \left[\!\left[\frac{\pi_1 z}{N(\pi)}\right]\!\right]\right) + N\left(\frac{\pi_2 z}{N(\pi)} - \left[\!\left[\frac{\pi_2 z}{N(\pi)}\right]\!\right]\right)$$

$$+ N\left(\frac{\pi_3 z}{N(\pi)} - \left[\!\left[\frac{\pi_3 z}{N(\pi)}\right]\!\right]\right) + N\left(\frac{\pi_4 z}{N(\pi)} - \left[\!\left[\frac{\pi_4 z}{N(\pi)}\right]\!\right]\right)$$

$$< \left(\frac{1}{2}\right)^2 + \left(\frac{1}{2}\right)^2 + \left(\frac{1}{2}\right)^2 + \left(\frac{1}{2}\right)^2 = 1.$$

Therefore, we get

$$N\left(\pi^{-1}\mu_\pi(z)\right) = N\left(\pi^{-1}\right) N\left(\mu_\pi(z)\right)$$

$$= \frac{1}{N(\pi)} N\left(\mu_\pi(z)\right) < 1.$$

Then, we get $N\left(\mu_\pi(z)\right) < N(\pi)$. Consequently, $N\left(\mu_\pi(z)\right) < N(\pi)$. This completes the proof.

The following examples give an example for each case in the proof of Proposition 3.3.

Example 2 (*Case 1*) $\pi = 1 + 3i + 2j + k$ is an encoder Hurwitz integer. By eq. (5), the Hurwitz signal constellation $\mathcal{H}_\pi$ is

$$\mathcal{H}_\pi = \begin{cases} \mu_\pi(0) = 0, \ \mu_\pi(1) = 1, \ \mu_\pi(2) = 2, \\ \mu_\pi(3) = i + j - 2k, \ \mu_\pi(4) = -1 + 2j + k, \\ \mu_\pi(5) = 2j + k, \ \mu_\pi(6) = 1 + 2j + k, \\ \mu_\pi(7) = 2 + 2j + k, \ \mu_\pi(8) = -2 - 2j - k, \\ \mu_\pi(9) = -1 - 2j - k, \ \mu_\pi(10) = -2j - k, \\ \mu_\pi(11) = 1 - 2j - k, \ \mu_\pi(12) = -i - j + 2k, \\ \mu_\pi(13) = -2, \ \mu_\pi(14) = -1, \end{cases}.$$

The set contains fifteen elements since $N(\pi) = 15$. The norm of each element in the set is less than the norm of the primitive Hurwitz integer (encoder Hurwitz integer) π.

Example 3 (*Case 2*) $\pi = 2 + 3i + j + 2k$ is an encoder Hurwitz integer. By eq. (5), the Hurwitz signal constellation $\mathcal{H}_\pi$ is

$$\mathcal{H}_\pi = \begin{cases} \mu_\pi(0) = 0, \ \mu_\pi(1) = 1, \ \mu_\pi(2) = 2, \mu_\pi(3) = 3, \\ \mu_\pi(4) = 1 + 2i + 2j - k, \mu_\pi(5) = -2 - 2j - k, \\ \mu_\pi(6) = -1 - 2j - k, \mu_\pi(7) = -2j - k, \\ \mu_\pi(8) = 1 - 2j - k, \mu_\pi(9) = 2 - 2j - k, \\ \mu_\pi(10) = -1 + 2j + k, \mu_\pi(11) = 2j + k, \\ \mu_\pi(12) = 1 + 2j + k, \mu_\pi(13) = 2 + 2j + k, \\ \mu_\pi(14) = -1 - 2i - 2j + k, \mu_\pi(15) = -2i - 2j + k, \\ \mu_\pi(16) = -2, \mu_\pi(17) = -1 \end{cases}.$$

The set contains eighteen elements since $N(\pi) = 18$. The norm of each element in the set is less than the norm of a primitive Hurwitz integer (encoder Hurwitz integer) π.

Example 4 (*Case 3*) $\pi = 2 + 3i + 2j + 2k$ is an encoder Hurwitz integer. By eq. (5), the Hurwitz signal constellation $\mathcal{H}_\pi$ is

$$\mathcal{H}_\pi = \begin{cases} \mu_\pi(0) = 0, \ \mu_\pi(1) = 1, \ \mu_\pi(2) = 2, \mu_\pi(3) = 3, \\ \mu_\pi(4) = 1 + 2i + 2j - 2k, \mu_\pi(5) = 2 + 2i + 2j - 2k, \\ \mu_\pi(6) = 3 - i - j + k, \mu_\pi(7) = -2 - i - j + k, \\ \mu_\pi(8) = -1 - i - j + k, \mu_\pi(9) = -i - j + k, \\ \mu_\pi(10) = 1 - i - j + k, \mu_\pi(11) = -1 + i + j - k, \\ \mu_\pi(12) = i + j - k, \mu_\pi(13) = 1 + i + j - k, \\ \mu_\pi(14) = 2 + i + j - k, \mu_\pi(15) = 3 + i + j - k, \\ \mu_\pi(16) = -2 - 2i - 2j + 2k, \\ \mu_\pi(17) = -1 - 2i - 2j + 2k, \ \mu_\pi(18) = -3, \\ \mu_\pi(19) = -2, \ \mu_\pi(17) = -1 \end{cases}.$$

The set contains twenty-one elements since $N(\pi) = 21$. The norm of each element in the set is less than the norm of a primitive Hurwitz integer (encoder Hurwitz integer) π.

Example 2 (case 1), example 3 (case 2), and example 4 (case 3) verify all the conditions to be a Euclidean metric. Also, the Euclidean division algorithm works for these primitive Hurwitz integers (encoder Hurwitz integers).

In the following example, according to the presented algebraic construction technique in [16] by Rohweder et al., we show that a Hurwitz integer π, each component of which

is in integers, does not have the "division with small remainder" property.

Example 5 In [16], Rohweder et al. presented the new construction method for Hurwitz integers by

$$\mu_\pi(z) = z - \left[\!\left[\frac{z\bar{\pi}}{N(\pi)}\right]\!\right]\pi,\tag{10}$$

where π is a primitive Hurwitz integer and $z \in \mathbb{Z}_{N(\pi)}$. They proposed four-dimensional Hurwitz signal constellations are obtained from the following mapping

$$\mathcal{H}_\pi = \mathcal{L}_\pi \bigcup \mathcal{O}_\pi,\tag{11}$$

where $\mathcal{L}_\pi$ is the subset of Lipschitz integers. It can be evaluated by

$$\mathcal{L}_\pi = \left\{\mu_\pi(a+bj) \mid a,b \in \mathbb{Z}_{N(\pi)}\right\},$$

where $\mathbb{Z}_{N(\pi)}$ denotes the ring of integers modulo $N(\pi)$. Also, $\mathcal{O}_\pi$ in eq. (11) is the corresponding coset of half-integers. It can be calculated by

$$\mathcal{O}_\pi = \left\{\mu_\pi(h+w) \mid h \in \mathcal{L}_\pi\right\},$$

where $w = \frac{1}{2} + \frac{1}{2}i + \frac{1}{2}j + \frac{1}{2}k$. With respect to the related modulo technique in [16], the size of the set in eq. (11) is $2N^2(\pi)$. We take an example $3+i$ in [16, Table I]. We have $\mu_\pi(5+5j)$ since $a = \frac{N(3+i)}{2} = 5$ and $b = \frac{N(3+i)}{2} = 5$. By eq. (10), we get

$$\mu_\pi(5+5j) = 5+5j - \left[\!\left[\frac{(5+5j)(3-i)}{10}\right]\!\right](3+i)$$

$$= 5+5j - \left[\!\left[\frac{15-5i+15j+5k}{10}\right]\!\right](3+i)$$

$$= 5+5j - (1+j)(3+i) = 5+5j-3-i-3j+k$$

$$= 2-i+2j+k.$$

Since $N(\mu_\pi(5+5j)) = N(3+i)$, then we get $5+5j = 0 \bmod(3+i)$. Also, $\mu_\pi(0) = 0$ since $a=0$ and $b=0$. So, we conclude that the set in eq. (11) has elements less than two hundred elements since $\mu_\pi(0) = \mu_\pi(5+5j) \equiv 0 \bmod(3+i)$. This contradicts the size of the Hurwitz signal constellation with two hundred elements. By Proposition 3.1, we say that the Hurwitz (Lipschitz) integer $3+i$ is not a suitable Hurwitz (Lipschitz) integer for constructing the Hurwitz signal constellation. Similarly, we can show that the primitive Hurwitz (Lipschitz) integer $2+2i+j+k$ is not a suitable Hurwitz (Lipschitz) integer for constructing the Hurwitz signal constellation with respect to the algebraic construction technique in [16].

4. PERFORMANCES OF HURWITZ SIGNAL CONSTELLATIONS FOR TRANSMISSION OVER AWGN CHANNEL

In this section, we present some distance and performance measures. In addition, we investigate the performances of Hurwitz signal constellations constructed by primitive Hurwitz integers (encoder Hurwitz integers), each component of which is in halves-integers, for transmission over the additive white Gaussian noise (AWGN) channel by the agency of the constellation figure of merit (CFM), average energy, and signal-to-noise ratio (SNR) gain.

We follow the procedures in [27] for distance, performance measures, and set partitioning property. The average energy of a signal constellation denoted by $\mathcal{E}_\pi$ is computed by

$$\mathcal{E}_\pi = \frac{1}{N(\pi)} \sum_{z=0}^{N(\pi)-1} N\left(\mu_\pi(z)\right).$$

The squared Euclidean distance of two Hurwitz integers in the Hurwitz signal constellation is defined as

$$d_E(\theta,\varphi) = N(\varphi-\theta),$$

and the minimum squared Euclidean distance of the signal constellation is

$$\delta_\pi^2 = \min_{\alpha \neq \beta} d_E(\theta,\varphi),$$

where $\theta, \varphi \in \mathcal{H}_\pi$. In [28], Forney and Wei proposed the constellation figure of merit (CFM) to compare signal constellations of different dimensions. The CFM is the ratio of the minimum squared Euclidean distance and the average energy per two-dimension. The CFM of a $M-$dimensional signal constellation is computed by

$$CFM = \frac{M\delta_\pi^2}{2\mathcal{E}_\pi}.$$

A higher CFM leads to better performance for transmission over an AWGN channel [27]. Signal-to-noise ratio (SNR or S/N) is a measure used in science and engineering that compares the level of a desired signal to the level of background noise [29]. SNR is defined by the ratio of signal power to the noise power, often expressed in decibels. A ratio higher than 1:1 (greater than 0 dB) indicates more signal than noise [29]. Asymptotic coding gain means a higher signal-to-noise ratio (SNR) [1]. The SNR of signal and noise power is computed by

$$SNR_{signal} = 10 \cdot \log_{10}\left(CFM \ of \ signal\right) \quad (12)$$

and

$$SNR_{noise} = 10 \cdot \log_{10}\left(CFM \ of \ noise\right), \quad (13)$$

respectively. As the noise, we consider the Gaussian signal constellation $\mathcal{G}_\alpha$, where α is a primitive Gaussian integer. Therefore, the SNR code gain of a Hurwitz signal constellation over the AWGN channel is

$$SNR_{dB} = SNR_{\mathcal{H}_\pi} - SNR_{\mathcal{G}_\alpha},$$

where Hurwitz signal constellation $\mathcal{H}_\pi$, and Gaussian signal constellation $\mathcal{G}_\alpha$. By eq. (12) and eq. (13),

$$SNR_{dB} = 10 \cdot \log_{10}\left(CFM \ of \ \mathcal{H}_\pi\right)$$

$$-10 \cdot \log_{10}\left(CFM \ of \ \mathcal{G}_\alpha\right)$$

$$= 10 \cdot \log_{10}\left(\frac{CFM \ of \ \mathcal{H}_\pi}{CFM \ of \ \mathcal{G}_\alpha}\right).$$

Note that the number of elements in the Hurwitz signal constellation and the Gaussian signal constellation should be the same to compare performances over the AWGN channel. According to the modulo function in Definition 2.6, the Hurwitz signal constellations that have the same size as Gaussian signal constellations almost show the same performances for transmission over the AWGN channel. Moreover, the squared Euclidean distance of the Hurwitz signal constellations and the Gaussian signal constellations, the size of which is the same, is one. The set partitioning aims to find a subset with a large squared Euclidean distance. Therefore, we obtain the Hurwitz signal constellations, which have the larger CFM, showing better performance for transmission over the AWGN channel.

A residue class ring of Hurwitz integers $\mathcal{H}_\lambda$ arises from the residue class ring of integers $\mathbb{Z}_{N(\lambda)} = \left\{0,1,\ldots,N(\lambda)-1\right\}$ for an integer $N(\lambda)$, where λ is a proposed primitive Hurwitz integer. If $N(\lambda)$ is not a prime integer, then we can partition the set $\mathcal{H}_\lambda$ into

subsets of equal size. Let $N(\lambda) = c \cdot d$. In other words, we can partition the set $\mathcal{H}_\lambda$ into c subsets $\mathcal{H}_\lambda^{(0)}, \ldots, \mathcal{H}_\lambda^{(c-1)}$ each with d elements. The subsets correspond to the Hurwitz signal constellations $\mathcal{H}_\lambda^{(0)}, \ldots, \mathcal{H}_\lambda^{(c-1)}$, where

$$\mathcal{H}_\lambda^{(0)} = \left\{ \mu_\lambda(0), \mu_\lambda(c), \mu_\lambda(2c), \ldots, \mu_\lambda((d-1)c) \right\},$$

and $\mathcal{H}_\lambda^{(1)}, \ldots, \mathcal{H}_\lambda^{(c-1)}$ are the cosets of $\mathcal{H}_\lambda^{(0)}$, i.e.

$$\mathcal{H}_\lambda^{(l)} = \left\{ \mu_\lambda(z) : \mu_\lambda(z-l) \in \mathcal{H}_\lambda^{(0)} \right\}, \quad \text{where}$$

$$\mathcal{H}_\lambda^{(l)} = \left\{ \begin{array}{l} \mu_\lambda(l), \mu_\lambda(l+2c), \mu_\lambda(l+3c) \\ , \ldots, \mu_\lambda(l+(d-1)c) \end{array} \right\}.$$

The subset $\mathcal{H}_\lambda^{(0)}$ is an additive subgroup of $\mathcal{H}_\lambda$ since the modulo function μ is an isomorphism with respect to addition.

The SNR gain of the subset of a proposed Hurwitz signal constellation over the AWGN channel is computed by

$$SNR_{dB} = 10 \cdot \log_{10} \left(\frac{CFM_{\mathcal{H}_\pi^{(0)}}}{CFM_{\mathcal{G}_\alpha}} \right),$$

where the subset of a proposed Hurwitz signal constellation $\mathcal{H}_\pi^{(0)}$, and Gaussian signal constellation $\mathcal{G}_\alpha$.

In the rest of this paper, we consider primitive Hurwitz integers (encoder Hurwitz integers) such that $\pi_1 \geq \pi_2 \geq \pi_3 \geq \pi_4 > 0$. We investigate the performance of Hurwitz signal constellations constructed by primitive Hurwitz integers (encoder Hurwitz integers), each component of which is in $\mathbb{Z} + \frac{1}{2}$, over the AWGN channel.

In Table 1, we present the performance of Hurwitz signal constellations constructed by primitive Hurwitz integers (encoder Hurwitz integers), each component of which is in $\mathbb{Z} + \frac{1}{2}$, over the AWGN channel by means of average energy, CFM, and SNR coding gain. In Table 1, the Hurwitz signal constellations obtained by the modulo function in Definition 2.6 have almost similar properties as Lipschitz signal constellations in the paper of Freudenberger et al. [27]. The performance of Hurwitz signal constellations in Table 1 is not so good but better than nothing according to the performance of the Lipschitz signal constellations in [27, Table I] over the AWGN channel. Moreover, the performances of proposed Hurwitz signal constellations constructed by primitive Hurwitz integers (encoder Hurwitz integers), each component of which is in integers, are the same as the performances of proposed Lipschitz signal constellations in [27, Table I].

In Table 2, we present the performance of the proposed Hurwitz signal constellation constructed by proposed primitive Hurwitz integers (encoder Hurwitz integers), each component of which is in $\mathbb{Z} + \frac{1}{2}$, over the AWGN channel by means of average energy, CFM, and SNR coding gain. The proposed Hurwitz signal constellations in Table 2 have advantage performances for transmission over the AWGN channel by set partitioning property. There also exist different proposed primitive Hurwitz integers (encoder Hurwitz integers) used to construct proposed Hurwitz signal constellations that have higher CFM and lower average energy in equal size. You can see the following examples. Moreover, the below examples are given clues about the construction of tables.

Example 6 We consider the proposed Hurwitz signal constellation with $N = 3 \cdot 13 = 39$ elements. There exist four different proposed primitive Hurwitz integers (encoder Hurwitz integers) used to construct the proposed Hurwitz signal constellation with $N = 39$. These proposed primitive Hurwitz integers (encoder Hurwitz integer)

are $\quad \dfrac{7}{2}+\dfrac{7}{2}i+\dfrac{7}{2}j+\dfrac{3}{2}k,\quad \dfrac{9}{2}+\dfrac{5}{2}i+\dfrac{5}{2}j+\dfrac{5}{2}k,$

$\dfrac{9}{2}+\dfrac{7}{2}i+\dfrac{5}{2}j+\dfrac{1}{2}k,$ and $\dfrac{11}{2}+\dfrac{5}{2}i+\dfrac{3}{2}j+\dfrac{1}{2}k.$

There is no Gaussian signal constellation with $N=39$ elements. Note that proposed primitive Hurwitz integers (encoder Hurwitz integers) are not to be the same size as primitive Gaussian integers. Therefore, we could use set partitioning property on proposed primitive Hurwitz integers (encoder Hurwitz integers). Firstly, we consider proposed primitive Hurwitz integers (encoder Hurwitz integer) $\dfrac{9}{2}+\dfrac{7}{2}i+\dfrac{5}{2}j+\dfrac{1}{2}k$ and $\dfrac{11}{2}+\dfrac{5}{2}i+\dfrac{3}{2}j+\dfrac{1}{2}k$. For the proposed Hurwitz signal constellation $\mathcal{H}_{9\,\frac{7}{2}+\frac{7}{2}i+\frac{5}{2}j+\frac{1}{2}k}$, the minimum squared Euclidean distance, average energy and CFM are 1, 12.5128 and 0.1598, respectively. The proposed Hurwitz signal constellation $\mathcal{H}_{\frac{9}{2}+\frac{7}{2}i+\frac{5}{2}j+\frac{1}{2}k}$ is partition the $c=3$ different subsets with each set $d=13$ elements. The minimum squared Euclidean distance, average energy, and CFM of Hurwitz signal constellation $\mathcal{H}^{(0)}_{\frac{9}{2}+\frac{7}{2}i+\frac{5}{2}j+\frac{1}{2}k}$ are 9, 11.5385, and 1.5600, respectively. The minimum squared Euclidean distance, average energy, and CFM of the Gaussian signal constellation $\mathcal{G}_{3+2i}$ with 13 elements are 1, 2.1539, and 0.4643, respectively. Therefore, the SNR coding gain of the proposed Hurwitz signal constellation $\mathcal{H}^{(0)}_{\frac{9}{2}+\frac{7}{2}i+\frac{5}{2}j+\frac{1}{2}k}$ is

$$SNR_{\frac{9}{2}+\frac{7}{2}i+\frac{5}{2}j+\frac{1}{2}k}=10\log\left(\dfrac{CFM \ of \ \mathcal{H}^{(0)}_{\frac{9}{2}+\frac{7}{2}i+\frac{5}{2}j+\frac{1}{2}k}}{CFM \ of \ \mathcal{G}_{3+2i}}\right)$$

$$=10\log\left(\dfrac{1.5600}{0.4643}\right)=5.26 \ dB.$$

The minimum squared Euclidean distance, average energy, and CFM of the proposed Hurwitz signal constellation $\mathcal{H}_{\frac{11}{2}+\frac{5}{2}i+\frac{3}{2}j+\frac{1}{2}k}$ are 1, 12.5128, and 0.1598, respectively. The proposed Hurwitz signal constellation $\mathcal{H}_{\frac{11}{2}+\frac{5}{2}i+\frac{3}{2}j+\frac{1}{2}k}$ is partition the $c=3$ different subsets with each set of $d=13$ elements. The minimum squared Euclidean distance, average energy, and CFM of Hurwitz signal constellation $\mathcal{H}^{(0)}_{\frac{11}{2}+\frac{5}{2}i+\frac{3}{2}j+\frac{1}{2}k}$ are 9, 11.5385, and 1.5600, respectively. The average energy, minimum squared Euclidean distance and CFM of Hurwitz signal constellations $\mathcal{H}^{(0)}_{\frac{9}{2}+\frac{7}{2}i+\frac{5}{2}j+\frac{1}{2}k}$ and $\mathcal{H}^{(0)}_{\frac{11}{2}+\frac{5}{2}i+\frac{3}{2}j+\frac{1}{2}k}$ are the same. So, Hurwitz signal constellations $\mathcal{H}^{(0)}_{\frac{9}{2}+\frac{7}{2}i+\frac{5}{2}j+\frac{1}{2}k}$ and $\mathcal{H}^{(0)}_{\frac{11}{2}+\frac{5}{2}i+\frac{3}{2}j+\frac{1}{2}k}$ have the same performances for transmission over the AWGN channel. Lastly, we consider proposed primitive Hurwitz integers (encoder Hurwitz integers) $\dfrac{7}{2}+\dfrac{7}{2}i+\dfrac{7}{2}j+\dfrac{3}{2}k,$ and $\dfrac{9}{2}+\dfrac{5}{2}i+\dfrac{5}{2}j+\dfrac{5}{2}k$. For both proposed Hurwitz signal constellations, the minimum squared Euclidean distance, average energy, and CFM are 1, 12.5128, and 0.1598, respectively. The average energy, minimum squared Euclidean distance and CFM of $\mathcal{H}^{(0)}_{\frac{7}{2}+\frac{7}{2}i+\frac{7}{2}j+\frac{3}{2}k,}$ and $\mathcal{H}^{(0)}_{\frac{9}{2}+\frac{5}{2}i+\frac{5}{2}j+\frac{5}{2}k}$ are 3, 11.5385 and 0.5200, respectively. Therefore, the SNR coding gain of these proposed Hurwitz signal constellations is

$$SNR_{dB}=10\log\left(\dfrac{0.5200}{0.4643}\right)=0.49 \ dB.$$

Consequently, the proposed Hurwitz signal constellations $\mathcal{H}_{9\,\frac{7}{2}+\frac{7}{2}i+\frac{5}{2}j+\frac{1}{2}k}$ and $\mathcal{H}_{\frac{11}{2}+\frac{5}{2}i+\frac{3}{2}j+\frac{1}{2}k}$ have higher CFM, better SNR coding gain, and larger minimum square Euclidean distance. We choose the proposed primitive

Hurwitz integer (encoder Hurwitz integer) $\frac{11}{2}+\frac{5}{2}i+\frac{3}{2}j+\frac{1}{2}k$ to represent in Table 2.

Example 7 We consider the proposed Hurwitz signal constellation with $N=3\cdot 29=87$ elements. There exist eight different proposed primitive Hurwitz integers (encoder Hurwitz integers) used to construct proposed Hurwitz signal constellations with $N=87$. These proposed primitive Hurwitz integers (encoder Hurwitz integers) are

$$\frac{11}{2}+\frac{11}{2}i+\frac{9}{2}j+\frac{5}{2}k, \qquad \frac{13}{2}+\frac{9}{2}i+\frac{7}{2}j+\frac{7}{2}k,$$

$$\frac{13}{2}+\frac{11}{2}i+\frac{7}{2}j+\frac{3}{2}k, \qquad \frac{13}{2}+\frac{13}{2}i+\frac{3}{2}j+\frac{1}{2}k,$$

$$\frac{15}{2}+\frac{7}{2}i+\frac{7}{2}j+\frac{5}{2}k, \qquad \frac{15}{2}+\frac{11}{2}i+\frac{1}{2}j+\frac{1}{2}k,$$

$$\frac{17}{2}+\frac{5}{2}i+\frac{5}{2}j+\frac{3}{2}k, \text{ and } \frac{17}{2}+\frac{7}{2}i+\frac{3}{2}j+\frac{1}{2}k.$$

There is no Gaussian signal constellation with $N=87$ elements. The minimum squared Euclidean distance, average energy, and CFM of proposed Hurwitz signal constellations constructed by these proposed primitive Hurwitz integers (encoder Hurwitz integers) are 1, 28.5057, and 0.0702, respectively. These proposed Hurwitz signal constellations are partition the $c=3$ different subsets with each set $d=29$ elements. We consider the Hurwitz signal constellations $\mathcal{H}^{(0)}_{\frac{13}{2}+\frac{11}{2}i+\frac{7}{2}j+\frac{3}{2}k}$, and $\mathcal{H}^{(0)}_{\frac{17}{2}+\frac{7}{2}i+\frac{3}{2}j+\frac{1}{2}k}$ with 29 elements. The minimum square Euclidean distance of these signal constellations is larger than others. The minimum square Euclidean distance of these signal constellations is 9, but the others are 6. Also, the average energy and CFM of these signal constellations are 27.5172 and 0.6541, respectively, but the others are 27.5172 and 0.4361, respectively. The minimum squared Euclidean distance, average energy, and CFM of the Gaussian signal constellation $\mathcal{G}_{5+2i}$ with 29 elements are 1, 4.8276, and 0.2071, respectively. Therefore, the SNR coding gain of Hurwitz signal constellations $\mathcal{H}^{(0)}_{\frac{13}{2}+\frac{11}{2}i+\frac{7}{2}j+\frac{3}{2}k}$ and $\mathcal{H}^{(0)}_{\frac{17}{2}+\frac{7}{2}i+\frac{3}{2}j+\frac{1}{2}k}$ is

$$SNR_{dB}=10\log\left(\frac{0.6541}{0.2071}\right)=4.99\ dB.$$

Table 1 Table of CFM, energy and SNR coding gain of Hurwitz signal constellations constructed by primitive Hurwitz integers (encoder Hurwitz integer), each component of which is in $\mathbb{Z}+\frac{1}{2}$, (d : The number of elements in the Hurwitz signal constellation, $\mathcal{G}_\alpha$: Gaussian signal constellation, $\mathcal{H}_\pi$: Hurwitz signal constellation)

d	Primitive Hurwitz Integers (π)	Signal Constellations		SNR [dB]
		CFM		
		ENERGY		
		$\mathcal{G}_\alpha$	$\mathcal{H}_\pi$	
5	$\frac{3}{2}+\frac{3}{2}i+\frac{1}{2}j+\frac{1}{2}k$	1.2500	1.6667	1.25
		0.8000	1.2000	
13	$\frac{5}{2}+\frac{3}{2}i+\frac{3}{2}j+\frac{3}{2}k$	0.4643	0.5200	0.49
		2.1538	3.8462	
17	$\frac{5}{2}+\frac{5}{2}i+\frac{3}{2}j+\frac{3}{2}k$	0.3542	0.3864	0.38
		2.8235	5.1765	
23	$\frac{9}{2}+\frac{3}{2}i+\frac{3}{2}j+\frac{1}{2}k$	0.2404	0.2551	0.26
		4.1600	7.8400	
29	$\frac{9}{2}+\frac{5}{2}i+\frac{3}{2}j+\frac{1}{2}k$	0.2071	0.2180	0.22
		4.8276	9.1724	
37	$\frac{11}{2}+\frac{5}{2}i+\frac{1}{2}j+\frac{1}{2}k$	0.1623	0.1690	0.18
		6.1622	11.8378	
41	$\frac{11}{2}+\frac{5}{2}i+\frac{3}{2}j+\frac{3}{2}k$	0.1464	0.1519	0.16
		6.8293	13.1707	
53	$\frac{13}{2}+\frac{5}{2}i+\frac{3}{2}j+\frac{3}{2}k$	0.1132	0.1165	0.12
		8.8302	17.1698	
61	$\frac{15}{2}+\frac{3}{2}i+\frac{3}{2}j+\frac{1}{2}k$	0.0984	0.1008	0.10
		10.1639	19.8361	
65	$\frac{11}{2}+\frac{11}{2}i+\frac{3}{2}j+\frac{3}{2}k$	0.0923	0.0945	0.10
		10.8308	21.1692	
73	$\frac{17}{2}+\frac{1}{2}i+\frac{1}{2}j+\frac{1}{2}k$	0.0822	0.0839	0.09
		12.1644	23.8356	
85	$\frac{13}{2}+\frac{13}{2}i+\frac{1}{2}j+\frac{1}{2}k$	0.0706	0.0719	0.08
		14.1467	27.8353	
89	$\frac{17}{2}+\frac{7}{2}i+\frac{3}{2}j+\frac{3}{2}k$	0.0674	0.0686	0.08
		14.8315	29.1685	
97	$\frac{19}{2}+\frac{5}{2}i+\frac{1}{2}j+\frac{1}{2}k$	0.0619	0.0628	0.06
		16.1649	31.8351	

Consequently, the Hurwitz signal constellations that have higher CFM and larger minimum square Euclidean distance

are $\mathcal{H}^{(0)}_{\frac{13}{2}+\frac{11}{2}i+\frac{7}{2}j+\frac{3}{2}k}$ and $\mathcal{H}^{(0)}_{\frac{17}{2}+\frac{7}{2}i+\frac{3}{2}j+\frac{1}{2}k}$. We choose the proposed primitive Hurwitz integer $\frac{13}{2}+\frac{11}{2}i+\frac{7}{2}j+\frac{3}{2}k$ to represent in Table 2.

Table 2 Table of CFM, energy and SNR coding gain of Hurwitz signal constellations constructed by proposed primitive Hurwitz integers (encoder Hurwitz integers), each component of which is in $\mathbb{Z}+\frac{1}{2}$, (N : The size of Hurwitz signal constellation, c : the number of subsets of the proposed Hurwitz signal constellation, d : the size of subsets of the proposed Hurwitz signal constellation, $\mathcal{G}_\alpha$: Gauss signal constellation, $\mathcal{H}^{(0)}_\lambda$: the subset of $\mathcal{H}_\lambda$, where $\mathcal{H}_\lambda$ is the proposed Hurwitz constellation)

$N = c \cdot d$	Proposed Primitive Hurwitz Integers (λ)	CFM		ENERGY		SNR $[dB]$
		$\mathcal{G}_\alpha$	$\mathcal{H}^{(0)}_\lambda$	$\mathcal{G}_\alpha$	$\mathcal{H}^{(0)}_\lambda$	
$15 = 3 \cdot 5$	$\frac{7}{2}+\frac{3}{2}i+\frac{1}{2}j+\frac{1}{2}k$	1.2500	1.6667	0.8000	3.600	1.25
$39 = 3 \cdot 13$	$\frac{11}{2}+\frac{5}{2}i+\frac{3}{2}j+\frac{1}{2}k$	0.4643	1.5600	2.1538	11.5385	5.26
$51 = 3 \cdot 17$	$\frac{11}{2}+\frac{7}{2}i+\frac{5}{2}j+\frac{3}{2}k$	0.3542	1.1591	2.8235	15.5294	5.15
$75 = 3 \cdot 25$	$\frac{13}{2}+\frac{9}{2}i+\frac{7}{2}j+\frac{1}{2}k$	0.2404	0.7653	4.1600	23.5200	5.03
$87 = 3 \cdot 29$	$\frac{13}{2}+\frac{11}{2}i+\frac{7}{2}j+\frac{3}{2}k$	0.2071	0.6541	4.8276	27.5170	4.99
$185 = 5 \cdot 37$	$\frac{21}{2}+\frac{13}{2}i+\frac{9}{2}j+\frac{7}{2}k$	0.1623	0.8447	6.1622	59.1892	7.16
$205 = 5 \cdot 41$	$\frac{27}{2}+\frac{9}{2}i+\frac{3}{2}j+\frac{1}{2}k$	0.1464	0.7593	6.8293	65.8537	7.15
$265 = 5 \cdot 53$	$\frac{27}{2}+\frac{15}{2}i+\frac{9}{2}j+\frac{5}{2}k$	0.1132	0.5824	8.8302	85.8491	7.11
$427 = 7 \cdot 61$	$\frac{33}{2}+\frac{21}{2}i+\frac{13}{2}j+\frac{3}{2}k$	0.0984	0.7058	10.1639	138.8520	8.56
$455 = 7 \cdot 65$	$\frac{33}{2}+\frac{11}{2}i+\frac{9}{2}j+\frac{3}{2}k$	0.0923	0.4724	10.8308	105.8460	7.09
$511 = 7 \cdot 73$	$\frac{33}{2}+\frac{21}{2}i+\frac{17}{2}j+\frac{15}{2}k$	0.0822	0.5874	12.1644	166.8490	8.54
$595 = 7 \cdot 85$	$\frac{33}{2}+\frac{29}{2}i+\frac{21}{2}j+\frac{3}{2}k$	0.0706	0.5030	14.1467	194.847	8.53
$623 = 7 \cdot 89$	$\frac{35}{2}+\frac{33}{2}i+\frac{13}{2}j+\frac{3}{2}k$	0.0674	0.4800	14.8315	204.1800	8.53
$873 = 9 \cdot 97$	$\frac{41}{2}+\frac{31}{2}i+\frac{29}{2}j+\frac{3}{2}k$	0.0619	0.5654	16.1649	286.5150	9.61

5. CONCLUSION

We showed, with the help of a proposition (Proposition 3.1), some Hurwitz integers are inappropriate for constructing Hurwitz signal constellations with $N(\alpha)$ elements, where α is a primitive Hurwitz integer. To solve this problem, we presented a proposition to help find out the primitive Hurwitz integers that have the division with small remainder (see Proposition 3.1). We also called the set of these integers the "Encoder Hurwitz Integers" set. We showed, with the help of a proposition (see Proposition 3.3), the Euclid division is satisfied by encoder Hurwitz integers. Moreover, we presented new Hurwitz signal constellations constructed by Hurwitz integers, each component of which is in half-integers. We investigated the performances of these signal constellations for transmission over the AWGN channel.

The Declaration of Conflict of Interest/ Common Interest
No conflict of interest or common interest has been declared by the author.

The Declaration of Ethics Committee Approval
This study does not require ethics committee permission or any special permission.

The Declaration of Research and Publication Ethics
The author of the paper declare that I comply with the scientific, ethical and quotation rules of SAUJS in all processes of the paper and that I do not make any falsification on the data collected. In addition, I declare that Sakarya University Journal of Science and its editorial board have no responsibility for any ethical violations that may be encountered, and that this study has not been evaluated in any academic publication environment other than Sakarya University Journal of Science.

REFERENCES

[1] K. Huber, "Codes over Gaussian integers," IEEE Transactions on Information Theory, vol. 40, no. 1, pp. 207–216, 1994.

[2] S. Bouyuklieva, "Applications of the Gaussian integers in coding theory," Proceedings of the 3rd International 39 Colloquium on Differential Geometry and its Related Fields, Veliko Tarnovo, Bulgaria, 2012, pp. 39–49.

[3] J. Freudenberger, F. Ghaboussi, S. Shavgulidze, "New coding techniques for codes over Gaussian integers," IEEE Transactions on Communications, vol. 61, no. 8, pp. 3114–3124, 2013.

[4] J. Freudenberger, F. Ghaboussi, S. Shavgulidze, "Set Partitioning and Multilevel Coding for Codes Over Gaussian Integer Rings," SCC 2013; 9th International ITG Conference on Systems, Communication, and Coding, Munich, Germany, pp. 1–5, 2013.

[5] M. Özen, M. Güzeltepe, "Quantum codes from codes over Gaussian integers with respect to the Mannheim metric," Quantum Information & Computation, vol. 12, pp. 813–819, 2012.

[6] M. Özen, M. Güzeltepe, "Codes over quaternion integers," European Journal of Pure and Applied Mathematics, vol. 3, no. 4, pp. 670–677, 2010.

[7] M. Özen, M. Güzeltepe, "Cyclic codes over some finite rings," Selcuk Journal of Applied Mathematics, vol. 11, no. 2, pp. 71–76, 2010.

[8] Y. J. Choie, S. T. Dougherty, "Codes over $\mathbb{Z}_{2m}$ and Jacobi forms over the quaternions," Applicable Algebra in Engineering, Communication and Computing, vol. 15, no. 2, pp. 129–147, 2004.

[9] M. Özen, M. Güzeltepe, "Cyclic codes over some finite quaternion integer rings," Journal of the Franklin Institute, vol. 348, no. 7, pp. 1312–1317, 2011.

[10] T. Shah, S. S. Rasool, "On codes over quaternion integers," Applicable Algebra in Engineering, Communication and Computing, vol. 24, no. 6, pp. 477–496, 2013.

[11] M. Güzeltepe, G. Çetinel, N. Sazak, "Constacyclic codes over Lipschitz integers," 2023. (Early access)

[12] O. Heden, M. Güzeltepe, "Perfect 1–error–correcting Lipschitz weight codes," Mathematical Communication, vol. 21, no. 1, pp. 23–30, 2016.

[13] M. Güzeltepe, "The MacWilliams identity for Lipschitz weight enumerators," Gazi University Journal of Science, vol. 29, no. 4, pp. 869–877, 2016.

[14] M. Özen, M. Güzeltepe, "Quantum codes from codes over Lipschitz integers," Global Journal of Pure and Applied Mathematics, vol. 7, pp. 201–206, 2011.

[15] M. Güzeltepe, "Codes over Hurwitz integers," Discrete Mathematics, vol. 313, no. 5, pp. 704–714, 2013.

[16] D. Rohweder, S. Stern, R. F. H. Fischer, S. Shavgulidze, J. Freudenberger, "Four-Dimensional Hurwitz Signal Constellations, Set Partitioning, Detection, and Multilevel Coding," in IEEE Transactions on Communications, vol. 69, no. 8, pp. 5079–5090, 2021.

[17] M. Güzeltepe, "On some perfect codes over Hurwitz integers," Mathematical Advances in Pure and Applied Sciences, vol. 1, no. 1, pp. 39–45, 2018.

[18] M. Güzeltepe, A. Altınel, "Perfect 1–error–correcting Hurwitz weight codes," Mathematical Communications, vol. 22, no. 2, pp. 265–272, 2017.

[19] M. Güzeltepe, O. Heden, "Perfect Mannheim, Lipschitz and Hurwitz weight codes," Mathematical Communications, vol. 19, no. 2, pp. 253–276, 2014.

[20] O. Heden, M. Güzeltepe, "On perfect $1-\varepsilon$–error-correcting codes," Mathematical Communications, vol. 20, no. 1, pp. 23–25, 2015.

[21] M. Güzeltepe, G. Güner, "Perfect codes over Hurwitz integers induced by circulant graphs," Journal of Universal Mathematics, vol. 5, no. 1, pp. 24–35, Mar. 2022.

[22] K. Abdelmoumen, H. Ben Azza, M. Najmeddine, "About Euclidean codes in rings," British Journal of Mathematics and Computer Science, vol. 4, no. 10, pp. 1356–1364, 2014.

[23] InetDaemon Enterprises. (2023). Signal constellation [Online]. Available: https://www.inetdaemon.com/tutorials/basic_concepts/communication/signals/constellation.shtml

[24] G. Davidoff, P. Sarnak, A. Valette, Elementary Number Theory, Group Theory, and Ramanujan Graphs, Cambridge University Press, 2003.

[25] J. H. Conway, D. A. Smith, On Quaternions and Octonions, A.K. Peters, 2003.

[26] Wikipedia. (2023). Parity (mathematics) [Online]. Available: https://en.wikipedia.org/wiki/Parity_(mathematics)

[27] J. Freudenberger, S. Shavgulidze, "New four-dimensional signal constellations from Lipschitz integers for transmission over the Gaussian channel," IEEE Transactions on Communications, vol. 63, no. 7, pp. 2420–2427, 2015.

[28] G. Forney, L. F. Wei, "Multidimensional constellations. I. Introduction, figures of merit, and generalized cross constellations," IEEE Journal on Selected Areas in Communications, vol. 7, no. 6, pp. 877–892, 1989.

[29] Wikipedia. (2023). Signal-to-noise ratio [Online]. Available: https://en.wikipedia.org/wiki/Signal-to-noise_ratio

Title: A Research on the Anatomical and Ecological Characteristic of Onosma mollis DC. (Boraginaceae)

Authors: Sibel ULCAY

A Research on the Anatomical and Ecological Characteristic of *Onosma mollis* DC. (Boraginaceae)

Sibel ULCAY *1 iD

Abstract

In this study, endemic *Onosma mollis* DC. it is aimed to examine the anatomical and ecological features of (Boraginaceae) plant in detail and to be compared with the other studies. According to the cross-sections, the root is secondary. Primary pith rays that 2-3 layered are observed. Epidermis is single-layered in stem transverse section. Eglandular hairs in the epidermis are simple, with one and two cells. Glandular hairs are capitate, digitate and with two cells. Just under the epidermis, 2-3 rows of collenchyma cells are formed. Both the upper and the lower surface of leaf is covered with numerous eglandular hairs. Eglandular hairs are 2-3 branched. Glandular hairs are of capitate, digitate and peltate type. The habitat of the *O. mollis* plant is mountain slopes, meadows, and prairies. The soil in which the species grows is clay and loamy. It is also classified as slightly alkaline, salty, calcareous, low phosphorus and high in potassium. According to its organic matter content, it is in the group of good humus soils.

Keywords: *Onosma*, *Onosma mollis*, Boraginaceae, anatomy, ecology

1. INTRODUCTION

Boraginaceae family is a big family containing approximately 154 genera and 2500 species, which is spread in the temperate and subtropical areas of the world and mainly in the Mediterranean region [1]. *Onosma* L. is a genus belonging to the Boraginaceae family and distributing 101 species of this genus in Türkiye. Among these species 50 of these are endemic [2 revised according to Firat and Binzet 2021 and add to references list]. The roots of the species belonging to the *Onosma* genus are used for purposes of treatment and as dye substance [3, 4]. It is used for cuts, swelling, wounds and ulcers in the continent of Asia and especially in India. Again, it is

mentioned that the dye obtained from the plant is used in religious ceremonies in the same region [5]. Some species belonging to the genus are used in Şanlıurfa and the surrounding region as chewing gum. It has been stated by Kahyaoğlu and Türkoğlu that *Onosma mollis* DC. species collected from Elazığ and its surrounding region had antimicromial effect against bacteria and yeast [6]. The *O. mollis* around the region of Gürün (Sivas) -Tohma stream is valuable with respect to medical and aromatic aspects and it has been stated by Bozkurt that it has characteristics that can be used in planting studies [7].

* Corresponding author: sibelulcay@gmail.com (S. ULCAY))
1 Kırşehir Ahi Evran University, Faculty of Agriculture, Department of Field Crops, Kırşehir
ORCID: https://orcid.org/0000-0002-2878-1721

Y-linoleic acid is present in most members of the Boraginaceae family. Stearidonic acid is the other chemical component which has been determined in members of stearidonic acid family. These compounds bear nutritional value and medical importance [8]. Velasco and Goffman state that these chemical compounds bear importance for the Boraginaceae family taxonomically [8]. Metcalfe and Chalk and Watson and Dallwitz have defined the characteristic features of Boraginaceae family [9, 10]. Akçin, Binzet and Orcan, Kodal, Binzet and Akçin, Güven et al., Akçin et al., Akçin and Binzet, Selvi et al., have conducted various studies relating with species belonging to *Onosma* and distributing in Turkey [11-18]. In these studies, the morphological, anatomical, micromorphological, palynological characteristics of some species belonging to the *Onosma* genus have been determined.

Anatomical features of organs such as root, stem and leaf of species having similar morphological features may reveal significant differences. In accordance, anatomical characteristics are used in taxonomy in recent years [19]. *Onosma* is a genus that has systematic and taxonomic problems. Anatomical and micromorphological studies also constitute an important criterion in the differentiation of species [20]. In this study, it has been aimed to determine the anatomical features of *O. mollis*. and to eliminate some deficiencies it has got and to reveal the ecological characteristics that have not been investigated before. The results obtained will contribute to other studies on the *Onosma* genus.

2. MATERIALS AND METHODS

O. mollis constituting research subject has been collected In May 2019 in Yıldızeli (Sivas) at a height of 1600 m, at 26 km northwest of the district. The identification of plant samples was made according to the Flora of Turkey [21]. Some of the materials that were collected were turned into herbarium specimens (Voucher and herbarium number: Sulcay60, 356), while some of them were made into stock samples having 70% alcohol (Stock number A94). Manual sections were taken to determine the anatomical features. Glycerin-gelatin was used as the examination medium in the sections. Preparations were made permanent by using the glycerin gelatin method [22]. Preparations have been examined with Nikon Eclipsse Ni microscope and Nikon DS-F1 screening system and photographs have been taken. 25 measurements on average were made from tissues such as epiderma and parenchyma collenchyma that were seen in the sections being examined. As a result of these measurements, minimum, maximum, average values and standard error values of the anatomical characters have been calculated.

For ecological studies soil samples have been taken from the area where plant samples were collected. During the field work, after removing the upper surface of the soil, a section of approximately 1 kg was taken with depth and diameter in the range of 0-20 cm. After these samples were dried in air and passed through a 2 mm sieve, they were made ready for analysis [23]. Soil analyzes have been conducted in 2 replications. Saturation percentage was obtained by saturating the colloid surface areas with water [24]. The pH and total salinity determinations were made in the saturation sludge [25, 26]. Organic material has been classified by using modified Walkey-Black wet burning method [27]. Total lime was made with Scheibler calcimeter [28] and it was classified according to Ülgen and Yurtsever [29]. Useful phosphorus determination was made by extracting soils with sodium bicarbonate (pH: 8.5, 0.5 N NaHCO$_3$) [30]. Changeable potassium was determined [31] by extracting it with ammonium acetate (pH: 7, 1 N NH$_4$OAc). Among the elements passing into the solution phase, concentration of phosphorus was determined by using the UV-VIS Spectrometer device, while the concentration of potassium was determined by using the Flame Spectrometer device.

3. RESULTS

3.1. Anatomical Results

In cross-sections taken from the root of the taxon, periderms cells are in 2-3 rows. Cortex parenchyma cells which are right at the bottom are polygonal in shape and have 10-15 rows. Phloem is circular in shape and form a large region. Cambium is in a crushed condition and it is not fully apparent. Endodermis is seen in the secondary root cross-section (Table 1). 2-3 layered primary pith arms are formed (Figure 1, A).

Epidermis cells are circular in shape and have a single row in the stem cross-section. Eglandular hairs on the epidermis are simple, having one and two cells (Figure 1, C). Short-stemmed capitate (Figure 1, D), digitate (Figure 1, D), peltate (Figure 1, E) are observed on the stem. Cuticle is observed on the epidermis cells of the stem. 2-3 rows of collenchyma cells surrounding the stem cross-section are observed right below the epidermis.
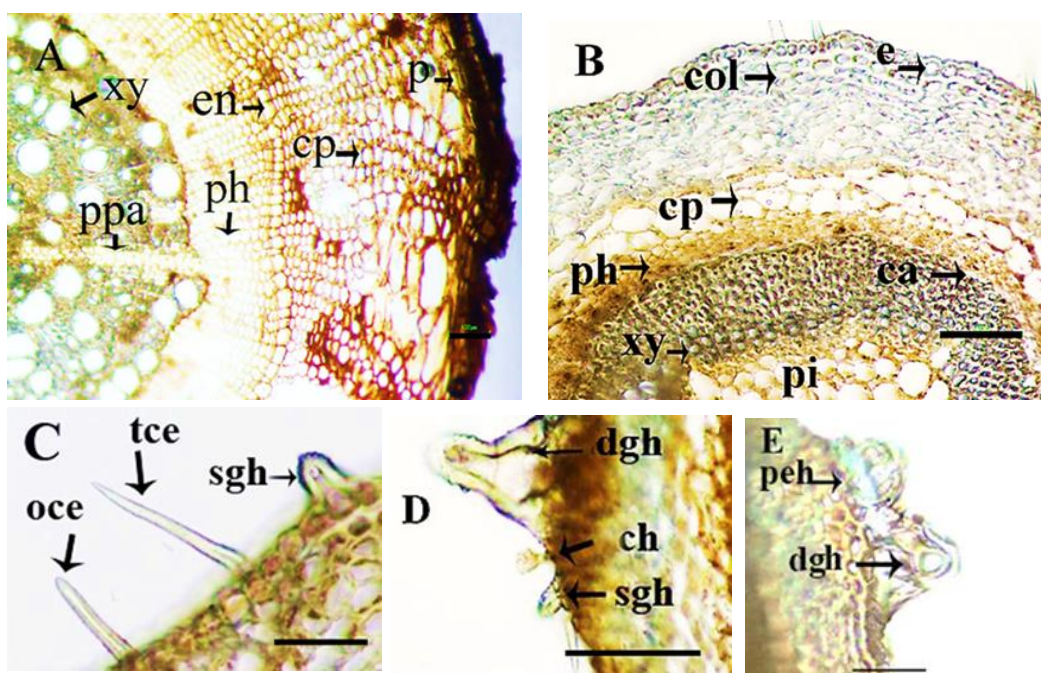

Figure 1 Cross-section of *O. molllis*. A root, B, C, D, E stem, ca; cambium, ch; capitate hair, col; collenchyma, cp; cortex parenchyma cell, dgh; digitate glandular hair, e; epidermis, en; endodermis, oce; one celled eglandular hair, tce; two celled eglandular hair, p; peridermis, peh; peltate hair, ph; phloem, ppa; primary pith arms, pi; pith, sch; short stalked capitate glandular hair, sgh; sesil glandular hair, tce; two celled hair, xy; xylem (Scale 100 μm)

Cortex parenchyma cells at the parts which are close to the collenchyma cells have been crushed. Cortex is constituted of 8-10 rows of parenchyma cells. Phloem is crushed under the cortex and it consists of cells in 3-4 rows. Cambium is not apparent. Pith consists of parenchyma cells (Table 1). Cuticle is present on the leaf lower epidermis and the cells are polygonal in shape and they have a dense sequence, and they are quite different with respect to size. At the lower epidermis, numerous simple eglandular hairs are observed (Figure 2, C, E) while digitate glandulars are also seen (Figure 2, C, F). On this surface, stomata cells with 3-5 neighboring cells are observed and stomata is anisocytic and anomocytic. Number of stomata is higher with respect to lower surface. On the upper surface stomata are anisocytic and anomocytic (Figure 2, D).

Table 1 Anatomical measurements of *O. mollis*

		Width (µm) Mean ± Se	Length (µm)-Mean± Se
Root	Periderm cells	19.57±3.02	33.95±4.80
	Trachea	48.97±11.42	
	Cortex cells	23.054±5.57	63.98±8.56
	Phloem	15.62±2.28	
	Endodermis	20.17±3.42	28.37±8.02
Stem	Epidermis cells	11.29±2.53	24.54±5.66
	Cortex cells	24.96±6.18	36.88±6.78
	Cuticle	4.88±1.54	
	Trachea	21.95±5.62	
	Pith parenchyma cells	35.16±7.5	
Leaf	Cuticle	7.71±1.58	
	Palisade parenchyma	20.46±3.30	50.20±7.27
	Spongy parenchyma	16.39±4.05	39.57
	Lower epidermis	14.21±3.96	23.18±4.60
	Upper epidermis	20.54±1.30	44.61±1.94
	Phloem	3.90±1.92	

Upper epidermis surface is having numerous, eglandular hairs, again. Eglandular hairs on the upper surface have 3-4 branched (Figure 2, H). Together with sessile capitate (Figure 2, I) and digitate glandular (Figure 2, G) hairs are also observed. In the leaf cross-section of the *O. mollis*, 2-3 rows of palisade parenchyma are observed at the bottom and top sections, while 2 rows of spongy parenchyma are seen in the middle, and the mesophyll is equifacial (Figure 2, B). 2-3 rows of collenchyma cells are present right below the lower epidermis cells. Phloem consists crushed cells in 3-4 rows (Figure 2, A).

3.2. Ecological Results

The habitat of the *O. mollis* plant is mountain slopes, meadows, and prairies. Saturation percentage of soil where the species grow is 62.7% and the soil is clayey and loam. It has a pH value of 8.01 and it is slightly alkaline. Total amount of water soluble salt of the soil is 26.4% and it is classified among saline soils. It is 1.46% in terms of lime and it is considered as calcareous soils. With respect to chemical features, available phosphorus amount of the soil is 4.47 kg/da and it is classified among Low Phosphorus soils. Amount of potassium that can be obtained is 733.85 kg/ha and it is classified as high. Amount of organic matter is 3.52% and it is classified in the group of Good Humus soils (Table 2).

4. DISCUSSIONS

In this study, the anatomical and ecological features of *O. mollis* species have been examined in detail. The root of the species has secondary features. Periderm is multilayered. In the species of *Onosma auriculata* Aucher ex DC, multilayered peridermis and secondary root structure have been determined by Akçin and Binzet [17]. Endodermis can be clearly seen. While endodermis is clearly seen in the species of *Onosma nana* DC. endodermis can not be distinguished in *Onosma discedens* Hausskn. ex. Bornm. [32]. No information has been found in the literature regarding the 2-3 layered primary pith arms in the *O. mollis* species.
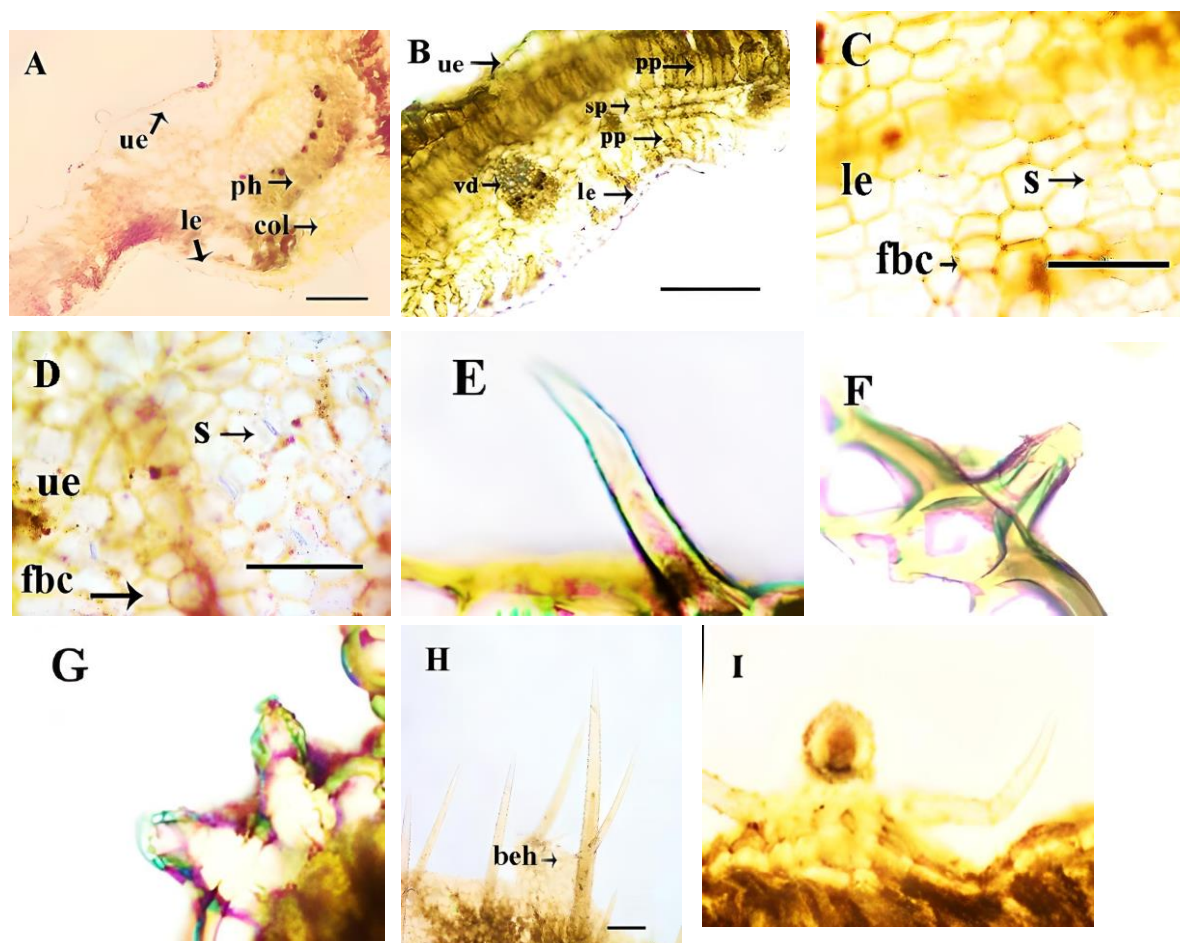
Figure 2 Cross section (A, B) and superficial section of leaf (C, D) *O. mollis*. F, G; digitate glandular hair, H: branched eglandular hair, I; capitate glandular hair. beh; branched eglandular hair, ph; phloem, ue; upper epidermis, le; lower epidermis, pp; palisade parenchyma, sp; spongy parenchyma, col; collenchyma, vb; vascular bundles, s; stomata, ue; upper epidermis, le: lower epidermis, fbc; feather base cell, (Scale 100 μm)

Table 2 Ecological characteristics of *O. mollis*

Physical properties					
Saturation (%)			Texture		
62.7			Clayey and loam		
Chemical properties					
Total Salt Soluble in Water (%)	pH	Lime (%)	Organic Matter (%)	Phosphorus (kg/da)	Potasyum (kg/da)
26.4	8.01	1.46	3.52	4.47	733.85

Stem epidermis cells of the *O. mollis* plant have single-row and they are hairy. In the species of *Onosma caucasica* Levin. ex M.Pop, stem epidermis cells have single-row and they are covered with characteristic hairs. These hairs are branched from the base and they have various types as being simple, unicellular, capitate and glandular [33]. Hairs of the *O. mollis* species are observed as being simple, unicellular, double-branched and capitate glandular hairs. A thin cuticle layer covers the stem as in the case with *O. caucasica* species [33]. Binzet and Akçin state that there is a thick cuticle in the species of *Onosma frutescens* Lam as well and 2-3 rows of collenchyma cells surround the stem

right below the epidermis [34]. It has been stated by Güven et al (2013) that in the species of *Onosma aucheriana* DC. and *Onosma roussaei* DC., there is collenchyma present in 1-6 rows at the sections close to the epidermis [16]. The cortex parenchyma cells in the section under the collenchyma cells are crushed in the species of *O. mollis* and parenchyma cells in parts close to the phloem are apparent. Teke and Binzet have stated that some of the cortex parenchyma cells are crushed in the plant of *Onosma nana* DC. as well [32]. In the stem cross-section of the plant that constitutes this study, 3-4 rows of prominent phloem cells and 1-2 rows of cambium are observed. In *O. angustissimum*, xylem, phloem and cambium are in distinguishable situation [35].

In the leaf cross section of the taxon, the palisade parenchyma consists of 2-3 rows of cells at the bottom and top, while the spongy parenchyma in the middle part consists of 2 rows of cells. In *O. papillosa* Riedl species, palisade parenchyma has 2-3 layers, while spongy parenchyma has 3-4 layers [17]. It was reported by Selvi et al. that the leaves are equifacial in *O. argentata* Hub. -Mor., *O. sericea* Willd. and *O. rechingeri* in Riedl taxa [18]. It was reported by Binzet and Teke that the leaves of *O. mollis* DC. and *O. halophylum* Boiss. & Heldr plants were also equifacial [36]. According to Daironas et al. only the upper epidermis side of *O. caucasica* plant has palisade parenchyma in the form of two layers [33]. In the plant of *O. rutila* Hub. -Mor. anomocytic and starocytic stomata is observed on the lower and upper leaf surface [17]. In the *O. mollis* plant, anomocytic and anisocytic stomata have been determined. Metcalfe and Chalk have stated that Boraginacaeae family had anomocytic and anisocytic stomata on both of the leaf surfaces [9].

O. bracteosum Hausskn. & Bornm is sandy-loamy, sandy-clayey, loamy and slightly alkaline, and its salt concentration is low [37]. The soil of the *O. mollis* plant is clayey and loamy and slightly alkaline. The soil of the plant that constitutes the subject of our research is classified in the group of salty, calcareous, low phosphorus and good humus soils.

5. CONCLUSION

As a conclusion, in this study anatomical and ecological characteristics of *O. mollis* have been examined in detail. The existence of primary pith arms in the root, the types of hair present on the stem and leaf, the presence of collenchyma and the ecological characteristics of the species have been revealed by us for the first time. The findings will contribute to a better understanding of the species and to clear the deficiencies.

Authors' Contribution
The authors contributed equally to the study.

The Declaration of Conflict of Interest/ Common Interest
No conflict of interest or common interest has been declared by the authors.

The Declaration of Ethics Committee Approval
This study does not require ethics committee permission or any special permission.

The Declaration of Research and Publication Ethics
The authors of the paper declare that they comply with the scientific, ethical and quotation rules of SAUJS in all processes of the paper and that they do not make any falsification on the data collected. In addition, they declare that Sakarya University Journal of Science and its editorial board have no

responsibility for any ethical violations that may be encountered, and that this study has not been evaluated in any academic publication environment other than Sakarya University Journal of Science.

REFERENCES

[1]   D. J. Mabberley, "The plant-book: a portable dictionary of the vascular plants" Cambridge university press", 1997.

[2]   A. Güner, S. Aslan, T. Ekim, M. Vural, M. Babaç, "Turkey Plant List (Vascular Plants)," Istanbul: Nezahat Gökyiğit Flora Botanic Garden and Research Association Publications, 2012.

[3]   J. Tsering, B. J. Gogoi, P. K. Hui, N. Tam, H. Tag, "Ethnobotanical appraisal on wild edible plants used by the Monpa community of Arunachal Pradesh," Indian Journal of Traditional Knowledge, vol.16, no. 4, pp. 626-637, 2017.

[4]   W. Younis, H. Asif, A. Sharif, H. Riaz, I. A. Bukhari, A. M. Assiri, "Traditional medicinal plants used for respiratory disorders in Pakistan: a review of the ethno-medicinal and pharmacological evidence," Chinese Medicine, vol.13(, no. 1, pp. 1-29, 2018.

[5]   P. K. Rana, P. Kumar, V. K. Singhal, J. C. Rana, "Uses of local plant biodiversity among the tribal communities of Pangi Valley of district Chamba in cold desert Himalaya, India," The Scientific World Journal, vol. 2014, pp. 1-15, 2014.

[6]   M. Kahyaoğlu, İ. Türkoğlu, "Antimicrobial activies of some plants collected ın Elazığ region," Journal of Science and Technology of Dumlupınar University, vol. 015, 1-8, 2008.J. O. Williams, "Narrow-band analyzer," Ph.D. dissertation, Dept. Elect. Eng.,

Harvard Univ., Cambridge, MA, USA, 1993.

[7]   S. G. Bozkurt, "Determining the possibilities of use in landscape architecture of some medicinal and aromatic plants grown in the valley of Gürün (Sivas)-Tohma Stream," Bartın Faculty of Forestry Journal, vol. 21, no. 1, pp. 66-80, 2019.

[8]   L. Velasco, F. D. Goffman, "Chemotaxonomic significance of fatty acids and tocopherols in Boraginaceae," Phytochemistry, vol. 52, no. 3, pp. 423-426, 1999.

[9]   C. R. Metcalfe, L. Chalk, 1979. Anatomy of Dicotyledons I. Oxford University Press, London, England. 279 p.

[10]   L. Watson, M. J Dallwitz, "Australian The families of angiosperms: Automated descriptions, with interactive identification and information retrieval," Systematic Botany vol. 4, no. 4 pp. 681 – 695, 1991.

[11]   Ö. E. Akçin, "The morphological and anatomical properties of endemic *Onosma armenum* DC.(Boraginaceae) species," International Journal of Natural and Engineering Sciences, vol. 1, no. 2, pp. 37-43, 2007.

[12]   Ö. E. Akçin, G. Şenel, Y. Akçin, "Leaf epidermis morphology of some *Onosma* (Boraginaceae) species from Turkey," Turkish Journal of Botany, vol. 37, no. 1, pp. 55-64, 2013.

[13]   G. Kodal, "Bazı *Onosma* L.(Boraginaceae) Türlerinin Anatomik Yönden İncelenmesi'', Yüksek Lisans Tezi, Karadeniz Teknik Üniversitesi,Fen Bilimleri Enstitüsü, Trabzon, Türkiye, 2007.

[14] R. Binzet, Ö. E. Akçin, "The morphological and anatomical properties of two endemic *Onosma* species (O. intertextum and O. sieheanum)," Acta Botanica Hungarica, vol. 51, no. 1-2, pp. 1-9, 2009.

[15] R. Binzet, N. Orcan, "A new species of *Onosma* (Boraginaceae) from southern Turkey," Novon: A Journal for Botanical Nomenclature, vol. 17, no. 1, pp. 8-10, 2007.

[16] S. Guven, O. Beyazoglu, S. Makbul, Z. Turkmen, A. Kandemir, "Anatomical features of six *Onosma* L.(Boraginaceae) species from Turkey," The Iranian Journal of Botany, vol. 19, no. 1, pp. 95-103, 2013.

[17] O. E. Akcin, R. Binzet, "Anatomy of three Onosma species from Turkey," Bangladesh Journal of Botany, vol. 48, no. 2, pp. 329-337, 2019.

[18] S. Selvi, R. Polat, E. Y. Babacan, M. O. Rahman, U. Çakilcioğlu, "Micromorphological and anatomical investigation on six species of *Onosma* L. (Boraginaceae) from Turkey," Bangladesh Journal of Plant Taxonomy, vol. 26, no. 1, pp. 69-81, 2019.

[19] N. Kharazian, "The taxonomy and variation of leaf anatomical characters in the genus Aegilops L.(Poaceae) in Iran," Turkish Journal of Botany, vol. 31, no. 1, pp. 1-9, 2007.

[20] R. Binzet, O. E. Akcin, "Pollen morphology of some *Onosma* species (Boraginaceae) from Turkey," Pakistan Journal of Botany, vol. 43, no. 2, pp. 731-741, 2011.

[21] P. H. Davis, "Flora of Turkey and the East Aegean Islands," Edinburgh University Press. vol 6, no. 15, pp. 326-336-24, 1978.

[22] Y. Vardar, "Preparation in Botany Techniques," Ege University Faculty of Science Printing Works, Izmir, no 1, 1987.

[23] M. C. Jackson, "Soil Chemical Analysis," Prentice Hall of India Private'Limited, New Delhi. pp. 183, 1962.

[24] I. Demiralay, "Soil physical analysis," Atatürk University, Faculty of Agriculture Publications, Erzurum, no. 143, pp. 131, 1993.

[25] C. A. Black, "Methods of soil analysis, Agronomy," The University of Wisconsin-Madison College of Agricultural and Life Sciences, no. 9, Part: 1 and 2. pp. 1572, 1965.

[26] A. Tüzüner, "Soil and water analysis laboratories handbook," T.C. Ministry of Agriculture, Forestry and Rural Affairs General Directorate of Rural Services, pp. 21-27, 1990.

[27] D. W. Nelson, L. E. Sommers, "Total carbon, organic carbon, and organic matter," P: 9611011. In D.L. Sparks (ed) Method of Soil Analysis: Chemical Methods. Part 3. SSSA, Madison, WI., 1996.

[28] F. Gülçur, "Physical and chemical analysis methods of soil," Istanbul University Faculty of Forestry Publications, İ. Ü.

[29] N. Ülgen, N. Yurtsever, "Turkey Fertilizer and Manure Guide," Soil and Fertilizer Research Institute publications. General Publication no. 209, Technical Publications no. T.66. Ankara, 1995.

[30] S. R. Olsen, V. Cole, F. S. Watanabe, and L. A. Dean, "Estimation of available phosphorus in soils by extraction with sodium bicarbonate,"

Washington, DC: US Department of Agriculture, vol. 939, p. 19, 1954.

[31] P. A. Helmke, D. L. Sparks, "Lithium, sodium, potassium, rubidium, and calcium, in Sparks, D.L., (Ed) Methods of Soil Analysis," Part 3, Chemical Methods, SSSA Book Series Number 5, SSSA., Madison, WI, s. 551-574, 1996.

[32] H. I. Teke, R. Binzet, "Anatomical, morphological and palynological studies of some *Onosma* L. (Boraginaceae) taxa endemic to Anatolia," Pakistan Journal of Botany, vol. 49, no. 2, pp. 579-588, 2017.

[33] J. V. Daironas, F. K. Serebryanaya and I. N. Zilfikarov, "Comparative Morphological and Anatomical Study of *Onosma caucasica* Levin. ex M. Pop. and *Onosma sericea* Willd.(Boraginaceae Juss.)," Pharmacognosy Journal, vol. 6, no. 5. 2014.

[34] R. Binzet, Ö. E. Akçin, "The anatomical properties of two *Onosma* L. (Boraginaceae) species from Turkey," Journal of Medicinal Plants Research, vol. 6, no. 17, pp. 3288-3294, 2012.

[35] Ö. E. Akçin, R. Binzet, "The micromorphological and anatomical properties of *Onosma* angustissimum Hausskn. & Bornm. and *O. cassium* Boiss.(Boraginaceae)," Bangladesh Journal of Plant Taxonomy, vol. 17, no. 1, pp. 1-8, 2010.

[36] R. Binzet, H. I. Teke, "The anatomical properties of *Onosma mollis* DC. and Onosma halophila Boiss. & Heldr.(Boraginaceae) from Turkey," Pakistan Journal of Botany, vol. 46, no. 5, pp. 1663-1668, 2014.

[37] Ö. E. Akçin, A. Engin, "The morphological, anatomical and ecological properties of endemic *Onosma bracteosum* Hausskn. & Bornm.(Boraginaceae) species," Turkish Journal of Botany, vol. 29, no. 4, pp. 317-325, 2005.

Title: The Effects of Route Optimization Software to the Customer Satisfaction

Authors: Ali DURDU, Muhammed Faik KAYA

The Effects of Route Optimization Software to the Customer Satisfaction

Ali DURDU[*1] ⓘD, Muhammed Faik KAYA[1] ⓘD

Abstract

Route optimization, which is a result of the advancement of technology today, makes companies profitable within months. The aim of this study is to explain the relation between route optimization software and the customer satisfaction. Route optimization softwares become widely used by the companies and this study touches briefly on the subject of the relation between route optimization software and customer satisfaction level. While explain this relation, the study described route optimization software, how it works and its execution areas. Hereafter, the article start to explain customer satisfaction and route optimization software's effects on customer satisfaction and conclude the study. In the drafting and writing process of this article, the topic is detaily searched and analyzed.

Keywords: Route optimization, customer satisfaction, software

1. INTRODUCTION

As of today, the usage of technological advancements by the companies are significantly increase because they are pretty simple and make the job easier than it seems. In addition to that, after the applying process of technology, companies become profitable within months. Altought the transition seems scary and risky process by the business owners and managers, the results are worth to take that decission because the technological advencements are generally increase the competetive advantage of companies in the presence of their rivals. Earlier to take transition decision, better the market pozition in an industry.

Recently, as the technology improve, companies start to benefit from it. One of these technologies is the route optimization. Route optimization simply sequencing the adresses that need to be visit and bring visibility to your deliveries. It counts all the constratints like fleet size/capacity, number of addresses to deliver, number of addresses to pick-up. In addition to these constraints it is also count the road blockages, park restrictions and even weather warnings. After the dispatcher import addresses into the system and then algorithmis start to find the best route and sequnce the addresses, withinn seconds it gives you the optimal route for your deliveries. According the features that provided by the route optimization company that the company choose, the dispatcher of a company can add and drop addresses and

* Corresponding author: ali.durdu@asbu.edu.tr (A. DURDU)
[1] Social Sciences University of Ankara
E-mail: muhammedfaik.kaya@student.asbu.edu.tr
ORCID: https://orcid.org/0000-0002-5347-4491, https://orcid.org/0000-0002-7161-2675

send the optimized route to the drivers' phone. This facility provides same-day delivery and/or same-day pick-up options. Route optimization has also green side which is trend concept for any business in these days [1]. The reason of green delivery is that with the optimized routes, drivers spend less time in traffic and they make less kilometer so that trucks consume less fuel which also decreases the carbon emmision. So that less fuel usage is just not cutting your cost but also decrease the carbon emmision and keep our environment green for the generations to come. This situation is kind of win-win for both the company and the environment. In addition to that, route optimization saves your time. Instead of manually dispatching all the routes whics takes to many times to organize, you can simply click one botton and it dispatch all the adresses perfectly and gives you more accurate results. Thus, as a delivery business you can give more time on other important functions of your company [2].

Customer satisfaction has important signafigance of any kind of companies because consumers are the main sources of your profit and no one wants to loose their satisfaction or trust. One of the way of customer satisfaction is making fast and safe deliveries. Even if its possible making same day deliveries would led to high level of customer satisfaction. This is where route optimization came into place. Route optimization facilitates same-day delivery option by doing so the companies can increase their customers' level of satisfaction. Moreover, the visibility of the deliveries has also positive impact on customer satisfaction because customers can know in which time period their cargos going to be delivered and plan rest of their day accordingly. The delivery time window also allows customer to determnine his/her own delivery time period. For instance a customer can choose as a delivery time period between 5 p.m. to 6 p.m. and the delivery company can optimize the route accordingly [3].

Chu et al. discussed how an online meal delivery platform can improve the performance of last mile delivery services using multi-source data. Delivery time is a critical but uncertain factor for online platforms, which are also considered to be the main challenges in order assignment and forwarding service. To overcome this challenge, they propose a data-driven optimization approach that combines machine learning techniques with capable vehicle routing optimization. Machine learning methods can provide more accurate predictions and are gaining more and more attention in the field of operations research. However, unlike the traditional predict and then optimize paradigm, they used a new intelligent predict then optimize framework generated by the decision error instead of the prediction target prediction error when applying machine learning [4].

Bányai proposed a real-time scheduling optimization model focusing on the energy efficiency of the operation. After the study is a systematic literature review, this article introduces a mathematical model of last mile delivery problems including scheduling and assignment problems. The aim of the proposed model is to determine the optimal assignment and scheduling for each order so as to minimize energy consumption allowing to increase energy efficiency. Next, a heuristic based on black hole optimization, whose performance is validated by different benchmark functions, is described. The scenario analysis in the proposed model validates the model and evaluates its performance to improve energy efficiency in last mile logistics [5].

Eskandaripour and Boldsaikhan reviewed numerous research findings on drone last-mile delivery in recent years, selecting a collection of mostly articles from 2011 to 2022. They analyzed their data in terms of key technical challenges such as routing, cargo distribution optimization, battery management, data communication and environmental protection. These challenges

have been seen to be interrelated in terms of enabling eco-friendly, efficient, lean, last-mile drone delivery [6].

Liu's study aimed to solve the last mile deployment of rural e-commerce logistics (RECL) for the survival of the third-party logistics enterprise. Taking into account the characteristics of RECL (long transport chain and low consumption density), a route optimization model for last mile distribution of RECL was established to maximize the profit of the state-subsidized logistics enterprise. The analysis results also show how the number of vehicles affects the maximum profit of the logistics enterprise and the scope of the RECL logistics network [7].

Ferrer et al. proposed a compromise programming model for multi-criteria optimization for humanitarian organizations to carry large amounts of aid for distribution after disasters. At this point, the proposed model includes multiple and often conflicting performance criteria for the last mile distribution, such as handling, time (deprivation), cost, scope, equity and safety. The proposed model is the first multi-criteria model capable of generating a tool program in humanitarian aid delivery. The proposed multi-criteria optimization is tested with a realistic test case based on the 2010 Pakistani floods [8].

2. ROUTE OPTIMIZATION AND USAGES AREAS

Recent technological advencements led to new opportunities for companies in every sector. It is important to keep track those opportunities and take the risk of applying process for your company. The businesses who took that risk and apply new technologies have gained competetive advantage over their rivals.

One of those technological advencements is route optimization. Route optimization tries to reduce the total distance that each truck made and increase the efficiency of deliveries. What mean by efficiency of deliveries is that it cuts cost via spending less hour in the traffic and decreases fuel consumption. It takes less time to dispatch all the addreses that need to be visit and increase the accurateness of the addresses because the human factor is not involved in dispatching process, if the dispatcher import all the addreses without making any mistakes then the algorithim sequence those addreses in a perfect manner [9].

The algorithims that help to optimize routes are playing crucial role here. Route optimization is a combinatorial optimization problem that aims to get around a given number of points with the least cost. For its solution, many heuristic algorithms that are used in many areas have been developed. The reason for the development of heuristic algorithms is that the route optimization problem is a problem that cannot be achieved with any algorithm. It is difficult to optimize Route optimization in polynomial time and close to optimum results can be found with the help of heuristic algorithms [1].

In addition, it brings flexibility to your deliveries. Every delivery includes different constraints for example their size, delivery time window, the tempurature range etc., and route optimization software counts all these constraints, algorithims work accordingly as a result it brings the optimal option for your deliveries [10].

Moreover in flexibility part urgent situation can happen in any company. There could be managerial crisis, liquidity crisis or environmental crisis. These can happen at any time and companies should be ready to all of these issues. In delivery companies the risk of crisis is much more because they are dealing with customers and they have fleet that anytime could led to a problem. For instance, one of driver can get sick or one of the truck could breakdown in that situatuion the dispatcher can easily assign the duties of the sick driver to other drivers, share the duties

and it does not let any delays and inconvenience in delivery process [11].

Also in dispatching process one of the trucks could breakdown in such situation it is important to have back-up plans, in such situation route optimization comes with life-saving feaute the re-optimization tool. Re-optimization allows the dispatcher to assign duties to any driver in the mission. However, this feature is not facilitated by all of the route optimization software companies. The companies who offer this quality generally charge higher prices compare to the others. That is why it is important to choose the right route optimization software company for your business [12].

Applying new technologies to your company is important but it also important that choosing the right company to use technology. There are several route optimization software companies and they are becoming more and more. The important decision that companies decide is which route optimization software company to work with. There are several factors that you need to consider before make an agreement with route optimization software company.

First thing that you need to consider is whether the optimization company's facilities is matching with your delivery portfolio and comes with a solution to your problems. If the route optimization software company supply all of your requirements you can move forward and consider other important factors. The next thing that you should care about is the useness of the software. It should not requires high level of training and examining because they are all cost for the company. That is why it should be easy to learn and use like a dailiy used applications WhatsApp, Twitter, Youtube. In addition to reason of easy to use is that the users of this software (dispatcher(s) and drivers) are avarage people, they do not have any technical knowledge about route optimization software that is why the software itself should be easy

to use and the users can get what they want easily and quickly.

Other important factor when we try to find best fit route optimization software to our company is that it should has accurate estimated time of arrival information. This is an important indicator because consumers like to see their deliveries' situation and they want to arrange their job according the arrival time of their delivery. More accurate estimation time of arrival information more you have satisfied customers which laterly mention in this article.

If all other requirements supplied, you should look for other important indicator which is efficiency of route optimization software. The map view of the software should be clear for the dispatcher and drivers so that there would not be any mistake made by them. Also the addresses must be clearly registered in order to prevent any wrong cargo delivery.

Last and may be the most important thing that you should consider before get route optmization software is application programing interface (API) integration. API integration is crucial because the dispatcher optimize the route on computer however in order to send this information to the drivers phone the route optimization software company needs to have mobile application that is available on ios and android application markets. The availability of the application is not enough by itself, it has to be working without any misinformation and error because only one single mistake can effect the whole delivery chain.

Route optimization software has been using by different industires with different purposess. However, surely these industires have one common goal which is to reduce cost and increase the efficiency of transportation. This is the main reason of having route optimization software by various of industryies and hundered of businesses.

Route Optimization has basic usage areas such as logistics and fleet management, food delivery services, health services, waste collection, and marketing. One of the sectors where route optimization is used the most is logistics. It is vitally important for the company to calculate the most ideal route, especially for long-distance cargo delivery [13].

By using route optimization, logistics companies can reduce the number of vehicles and drivers they have, thus reducing fuel budgets. Route optimization automates and distributes workloads across your fleet. GPS tracking devices connected to vehicles in the fleet track the location of these vehicles and collect historical data. Route optimization enables efficient weekly long-distance planning, including overnight stops and planned breaks. This routing also complies with regulations in various countries and regions.

Demand for ordering food from outside has surged, especially since the pandemic. Therefore, route optimization is a necessary path for both service quality and carrier safety in ordering food industry. Route optimization is also used in the food distribution sector, where delivery is made by motor courier, by determining the most efficient routes with routes calculated based on real road distances [13].

In a dynamic and competitive industry like the food industry, efficiently serving consumers is critical. Many food delivery companies face many challenges, including find the fastest routes and fulfill orders in a timely and appropriate manner.

One of the best use cases for route optimization is the healthcare industry. Route optimization isn't just for time-consuming emergencies. It also increases the efficiency of medical facilities in regular home visits to provide preventive health services. For example, routing injection teams to operate during the Covid-19 period can greatly improve the efficiency of healthcare also it helped to slow down the inflected people rate with the increasing rate of vaccination.

Moreover, route optimization allows healthcare workers to spend more time with their patients, thus improving the quality of testing and service and reducing costs as in other areas because healthcare workers get paid for the servie that they make not for travelling. In addition to that, it helps to make appointments more predictable. All these factors increase customer satisfaction and improve the quality of healthcare services.

Route optimization, which was started to be implemented in the city of Homestead in Florida, gave very positive results. The most appropriate point in the city and when to collect waste can be determined with a geographic information system (GIS) based route optimization modeling software. For this, parameters such as the amount of waste produced, the number of houses and workplaces served, and the distance from the collection point to the storage facility are used. In this way, the waste collection time from each region can be shortened [14].

Thanks to route optimization, municipalities can increase the number of waste collection points without increasing staff or building new facilities. Additionally, route optimization has benefits such as maximizing staff efficiency, reducing service costs, and significantly reducing fuel consumption [15].

Route optimization has also great impact on improving your marketing strategy. Marketing departments that have to work in the field can achieve great success with the right route optimization technology. Route optimization allows businesses to easily monitor changing market dynamics and customer status. This allows us to better understand our geographical distribution areas and specialize in the specific conditions of each region. Marketers are good at dealing with unexpected changes. Last-minute booking requests, varying weather conditions,

or transportation delays. In short, fast and effective route automation is critical for businesses that rely on field-based workforces, especially in times of change and uncertainty [16].

3. THE RELATIONSHIP BETWEEN ROUTE OPTIMIZATION AND CUSTOMER SATISFACTION

The term customer satisfaction is become an important parameter for almost every company because customers are the one who is the biggest source of profit to companies. In the absence of even one customer, companies need to find someone else to maintain its profit. In such situation the effect of one customer is also getting bigger and bigger with the help of again technology. The reason of that impact is social media and the online-shopping applications.

One single customers dissatisfaction has an impact on almost hundereds of potential buyers and it led you to lost those potential customers. In such situation, potential buyers are searching for buyers feedbacks, photos of the product and comparision videos. If they see any disturbunce about product, service or difficulities in delivery process, they would give up on that product. In addition to effect of social media and online shopping applications, a bad experince of a customer can effect the inner circle, familiy and friends and it again led to decrease in the sales of company. The researchs shows that customers are willing to pay more on the product just for having better customer service. They can even give up on the product that they used to buy just for better traited. This situation shows that having satisfied customers has great impact on companiy's succes. Therefore, resolving customer complaints and ensuring customer satisfaction required overcoming pretending. Companies that develop various strategies to ensure customer satisfaction in the sector can achieve their goals. Increasing this satisfaction level is possible by meeting the customer's needs and meeting their wishes [17].

Today, meeting customer demands in the shortest time and at the least cost is the most challenging task of maintaining any supply chain. The most challenging process in the sustainability of the supply chain is to meet customer demands in the shortest time and at the least cost. To solve this challenge, the vehicle routing problem (VRP) plays an important role in logistics. While a single warehouse is designed for customers in a modeled VRP, in real life a single warehouse will not be sufficient to meet customer demand or customer satisfaction. In this context, Rajak et al. proposed a model that solves the customer satisfaction-based multi-depot vehicle routing problem (MDVRPCS). Since MDVRPCS is an NP-hard problem, ant colony optimization (ACO) has been proposed to solve MDVRPCS. The proposed algorithm has been tested for well-known problem examples in the literature. The results show that the algorithm can obtain good optimal solutions [18].

Dynamic vehicle routing and scheduling problem is a well-known complex combinatorial optimization problem that has received great attention in recent years. Barkaoui presents an algorithm in his work that clearly aims to improve customer satisfaction, presenting a new strategy for integrating anticipated future visit requests during plan creation. An evaluation of the proposed algorithm was performed using a pre-designed hybrid genetic algorithm for the dynamic vehicle problem with time windows, which we modified to achieve customer satisfaction across multiple visits. The simulations and the value of the revisited algorithm utilizing the new strategy are compared and its effect on the level of customer satisfaction is clearly shown [19].

In their study, Zhang et al. proposed a route optimization model based on customer time satisfaction of the instant distribution system, since the actual factors in the instant distribution service scenario are not sufficient in the current distribution route optimization. The model proposed in the study includes real

factors in instant delivery such as flexible time window, pay-to-order mechanism, time required for seller to prepare goods before delivery, and delivery consolidation. In the developed model, a multi-objective optimization framework based on the customer's total cost function and time satisfaction was created. Double layer chromosome coding based on supplier-to-node mapping and access order was performed and non-dominant sequencing genetic algorithm version II (NSGA-II) was used to solve the problem. According to the numerical results, when the customer's time satisfaction is taken into account in the instant delivery routing problem, customer satisfaction has increased effectively and the balance between customer satisfaction and delivery cost has been achieved by Pareto optimization [20].
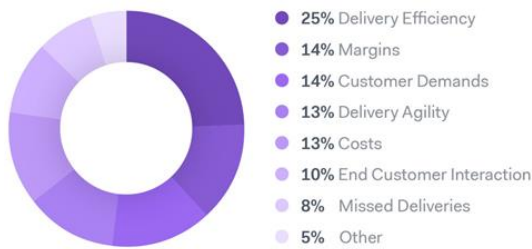

Figure 1 Bigges Last Mile Challenge [21]

A survey was conducted with 194 managers from leading global logistics providers in the industry and 129 supply chain managers from retailers, manufacturers and brands [12]. Participants in this study were asked questions about changing consumer behavior and increasing shipping costs. In the table formed by the answers, it is seen that the growth of e-commerce has led to a 33% increase in B2B (Business to Business) last mile delivery demand and a 67% increase for B2C (Business to Customer) businesses in the same period. Accordingly, with the increase in the volume of last mile deliveries, which is one of the biggest challenges, it becomes difficult to maintain efficiency and manage costs.

According to the graph that emerged as a result of the research in Figure 1, 25% of

companies today cite "Delivery Efficiency" as the biggest challenge in the final stage [16]. This is followed by "margins" with 14%, "Customer Demands" with 14%, "Delivery Agility" with 13%, "Costs" with 13%, "End Customer Interaction" with 10%, "Missed Deliveries" with 8% and "Others" with 5%. With the conclusion drawn from here, it is seen that the biggest difficulty is delivery efficiency.
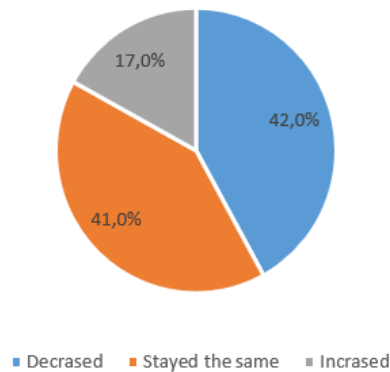
Figure 2 Margins of companies in last mile [21]

In the survey, the increase, decrease and stay of the margins of the companies that used last mile route optimization in the last 18 months were examined. As a result of the research, some surprises were found in the data obtained for the last mile challenges. For example, margin protection of companies and increased costs are ranked significantly lower than delivery efficiency. This can be caused by final rate increases among some of the major last mile providers causing last mile rates to vary. As can be seen in Figure 2, which was created in the light of the data obtained, the providers stated that the companies saw fixed or increasing margins the most, and only 42% had their margins decreased, 41% remained the same, and increased 17% [21].

The relationship between route optimization software and customer satisfaction is quite interesting topic to search about because it is kind of win win situation for both parties - customer and company-. It is a "win" for companies because with the help of the route optimization software, they can decrease cost

which include fuel, total distance, work shifts and increase the efficiency of deliveries. It is also a "win" for customers because it promotes on-time deliveries, visibility of the delivery, same-day delivery or pick-up options, accurate estimated time of arrival (ETA), customer update facility and preference of way to update [22].

The first effect of route optimization software to the customer satisfaction is on-time deliveries. On-time deliveries has significant effects on customer satisfaction because almost every customer would be happy if their cargo delivered at time. No one wants delays and cancels in their deliveries. Route optimization software offers this facility via powerfull algorithims that sequance the addreses and reduce the total distance. With the help of route optimization software delays that caused by delivery company almost become impossible because it has accurate estimated time of arrival data which is another effect that I detaily explain in the coming effects. On-time deliveries become almost impossible espacially in the Covid-19 era because the amount of online orders has increased significantly and delivery companies had hard times to supply that demand.

At that time, the importance of route optimization solution become apparent for delivery companies and for the satisfaction of the customers. In addition to pandemic era, in some important days in the year, cargo companies become too busy like valentines day, mothers day, chrismist era etc. and cargo companies cannot succesfuly deal with all the deliveries without the help of route optimization software. Moreover, the black friday madness become popular all over the world and online shopping plartforms are vanguards of this period that is why people show overfondness to discounted products and there is congestion in delivery process and lot of delays and cancels happen in the delivery process. As a result customers became aggrivied and there is absoulitly no satisfaction. Therefore route optimization

software effects the whole delivery process in a good way and increase the number of on time deliveries even in the peak times resulted with satisfied customers.

The second effect of rotue optmization software to the customer satisfaction is visibility of the delivery. This feature of the route optimization software increases the customer satisfaction because the customers can know exactly where their cargo is and want to get updated by the delivery company. If delivery company leave the customer in the dark and does not give any information about his/her cargo then customer would be disturb in that situation. This problem led to decrease in customer satisfaction. In order to prevent this, route optimization software comes with the feature of real-time tracking with the help of this feature customers can exactly now where their cargo is and if any urgent situation happen they can see that situation in the tracking page. In addition to that, the customers can see their drivers name, the vehicle type and the status of their cargo. Even this tracking page has not crithical importance, it gives customer confidence and make away with their concuesness while improving customer satisfaction [23, 24].

Another effect of route optimization software to the customer satisfaction is same-day delivery or pick-up options. This effect may be the most important tool for customer satisfaction because the avaibility of same-day delivery or pick-up shows that your system is working fluently there is not any problem and in particularly you are fast at your deliveries. Ten years ago, if you say same-day deliveres are possible then no one ever going to believe you but now it becomes even normal to our ears. Thanks to route optimization software, the delivery points can re-arrange with the option of "re-optimizing". If there is any same-day delivery option, the dispatcher can re-optimize the route and make the same-day delivery or pick-up possible. However, this feature is not available all the route optimization software companies. If same-day deliveries are important tool for the

companies then they should choose the company with offers re-optimization feature in its software product [25, 26].

The accurateness of estimate time of arrival has crucial effect on the customer satisfaction. Better estimation means more satisfied consumers in that equation. Every late delivery is not different than the failed delivery for all the delivery businesses that is why delivery businesses needs to deliver customers' cargos on time. Estimation of arrival could be very important in that sense because consumers can arrange their daily plans accordingly and they want their cargos in the estimated time of arrivals. Therefore, early deliveries even could be a problem because as the consumer make their plan according the estimated time of arrival, he/she could not be at home for recieving the package. Late deliveries is already problem for the consumer and it means failed delivery for business owner. So that route optimization software helps the delivery businesses to have better guess on estimated time of arrival and it increases the consumer satisfaction. In addition, some customers may want to recieve his/her delivery before/after certain hour or between certain hours, in that sense route optimization software allows the dispatcher the plan the route accordingly. The dispatcher needs to enter these parameters and just need to click optimize botton. The algorithims itselfs handle the rest and plan the route according the needs of the customers [27].

The last feature of route optimization software that effect customer satisfaction is the customer updating. Customer updating is an intregrated system tool with the route optimization. Sometimes despite the fact that all of your effort and plan, things can go bad and unlucky which resulted with late deliveries. At that time the communication with customer is essantial because the customer generally wonder what happened to his/her delivery. If as a delivery company, exceed the estimated time of arrival then it needs to update to its customer. Route optimization software offers this facility in its system. Generally this system is which means customer can also leave message to the courier like "leave it to door" and couirier will act accordingly. Moreover, there are bunch of ways to update the customer. The company can update the customer via e-mail, phone or sms according to preference of the customer. Generally most preffered way to update is SMS because it is quick and fast way to comunicate and the clients can get notification within seconds. It does not disturb you in your daily life like phone call and you can have it wherever you are you do not need internet connection for receiving SMS. As a result, communication and informing the customer increase the satisfaction level and promotes the usage of route optimization software among delivery companies.

4. CONCLUSION

In conclusion, the effects of technology to the businesses are seal their fate. The businesses which has applied this technological advencements to the their business became sector leaders and keep the competetive advantage against their rivals. On the other hand, companies which unable to apply those developments into their system cannot hold in competetive area of the sector and either bankrupted or lost their market position.

In order to keep track latest technological advencements, companies always looking for additional value activity actions. What can they bring to the company that maximizes its profit or minimizes cost. They should also looking for increasing efficiency in their work. Route optimization comes at that stage. It brings reliable, efficient and appliable solutions to delivery companies. Roiute optimization software minimizes cost via reducing fuel consumption and travel time which also led to decrease in carbon emmisons to the environment. Moreover, it increases the efficiency of deliveries which means that it requires less time to dispatch the addresses and less time to reach that addresses

with accurately. Additionally it is easy to apply to the companies. The only think that you business is to buy the software as a service product and let them do the rest. When compare its cost with the money that the business spend without the help of route optimization, the company company even become more profitable with the help of this software product.

Customer satisfaction side of the route optimization software is the topic that mainly covered in this article. Route optimization software has huge contribution to customer satisfaction in that respect. Nowadays it is hard to achiave customer satisfaction because customers can lot of alternatives and even in a single mistake the companies can loose a customer. To prevent such kind of situations, companies need to serve their customers as they deserved. Route optimization software is such a good opportunity for the companies that want to achiave customer satisfaction. It render benefits of on-time deliveries, visibility of the delivery, same-day delivery or pick-up options, accurate estimated time of arrival (ETA), customer update facility and preference of way to update. All these factors which explained detailly in the article contributes the customer satisfaction while decreasing the overall cost. Thanks to route optimization software the firm and the customer side are both satisfied.

Overall, route optimization software is a quite good option for delivery companies that is provided with the help of the technological advencements. Companies who use this route optimization software can get the benefits like reducing delivery cost, increasinf efficiency of deliveries and increasing number of profit. Thus, route optimization software has huge contribution on customer satisfaction. It makes happy faces for you and creates plased and loyal customers for the businesses. Route optimization sofware can bring the companies to the next level without taking any risk.

The Declaration of Conflict of Interest/ Common Interest
No conflict of interest or common interest has been declared by the author.

Authors' Contribution
The first author contributed 50%, the second author 50%.

The Declaration of Ethics Committee Approval
The author declares that this document does not require an ethics committee approval or any special permission.

The Declaration of Research and Publication Ethics
The author of the paper declares that he complies with the scientific, ethical, and quotation rules of SAUJS in all processes of the paper and that he does not make any falsification on the data collected. In addition, he declares that Sakarya University Journal of Science and its editorial board have no responsibility for any ethical violations that may be encountered and that this study has not been evaluated in any academic publication environment other than Sakarya University Journal of Science.

REFERENCES

[1]   S. Bozkurt Keser, A. Yazıcı, S. Günal, "A Multi-Criteria Heuristic Algorithm For Personalized Route Planning", Anadolu University Journal of Science and Technology A - Applied Sciences and Engineering, vol. 17, no. 2, pp. 299-313, 2016.

[2] Rotamopt, "Field Service Operations", https://www.rotamopt.com/field-service-operations (accessed Jan. 10, 2023).

[3] İ. Küçükoğlu, N. Öztürk, "Route Optimization of the Electric Vehicles with Heterogeneous Fleet / Heterojen Filoya Sahip Elektrikli Araçların Rota Optimizasyonu", Celal Bayar University Journal of Science, vol. 12, no. 3, pp. 525-533, 2016.

[4] H. Chu, W. Zhang, P. Bai, Y. Chen, "Data-driven optimization for last-mile delivery", Complex & Intelligent Systems, 2021.

[5] T. Bányai, "Real-time decision making in first mile and last mile logistics: How smart scheduling affects energy efficiency of hyperconnected supply chain solutions", Energies, vol. 11, no. 7, 2018.

[6] H. Eskandaripour, E. Boldsaikhan, "Last-Mile Drone Delivery: Past, Present, and Future", Drones, vol. 7, no. 2, 2023.

[7] W. Liu, "Route Optimization for Last-Mile Distribution of Rural E-Commerce Logistics Based on Ant Colony Optimization," in IEEE Access, vol. 8, pp. 12179-12187, 2020.

[8] J. M. Ferrer, F. J. Martín-Campo, M. T. Ortuño, A. J. Pedraza-Martínez, G. Tirado, B. Vitoriano, "Multi-criteria optimization for last mile distribution of disaster relief aid: Test cases and applications", European Journal of Operational Research, vol. 269, no. 2, pp. 501–515, 2018.

[9] Rotamopt, "Last Mile Operations", https://www.rotamopt.com/last-mile-operation (accessed Jan. 01, 2023).

[10] Optiyol, "Son Kilometre Operasyonları", https://www.optiyol.com/tr/son-kilometre-operasyonlari (accessed Jan. 8, 2023).

[11] Ç. Koç, O. Jabali, G. Laporte, "Long-haul vehicle routing and scheduling with idling options", Journal of the Operational Research Society, vol. 69, no. 2, pp. 235-246, 2018.

[12] Optimoroute, "Delivery Efficiency", https://optimoroute.com/delivery-efficiency/ (accessed Jan. 9, 2023)

[13] Maptriks, "Rota Optimizasyonunun 5 Temel Kullanım Alanı", (accessed Apr. 30, 2023)

[14] M. Gümüş, E. H. Özder, E. Hatınoğlu, A. Uçar, "Geri Dönüşüm Atıklarının Toplanmasında Rota Optimizasyonu: Alanya İlçesinde Bir Uygulama" , Journal of Turkish Operations Management , vol. 6, no. 1, pp. 1102-1112, 2022.

[15] Onfleet,"Features",https://onfleet.com/features (accessed Jan. 01, 2023).

[16] Onfleet, "6 Ways to Reduce Last-Mile Delivery Costs", https://onfleet.com/blog/6-ways-to-reduce-last-mile-delivery-costs/ (accessed Jan. 12, 2023).

[17] M. Kurnuç, S. Korucuk, O. Küçük, "Kalite İyileştirme Çalışmalarının Müşteri Memnuniyeti ve Müşteri Sadakatine Etkisi", The International New Issues in Social Sciences, vol. 1, no. 1, pp. 21-44, 2015.

[18] S. Rajak, P. Parthiban, R. Dhanalakshmi, "Multi-depot vehicle routing problem based on customer satisfaction", International Journal of Services, Technology and

Management, vol. 26, no. 2–3, pp. 252–265, 2020.

[19] M. Barkaoui, J. Berger, A. Boukhtouta, "Customer satisfaction in dynamic vehicle routing problem with time windows", Applied Soft Computing, vol. 35, pp. 423–432, 2015.

[20] Y. Zhang, C. Yuan, J. Wu, "Vehicle Routing Optimization of Instant Distribution Routing Based on Customer Satisfaction", Information, vol. 11, no. 1, 36, 2020.

[21] EFT, "The Last Mile Logistics Whitepaper,2018", https://blog.localz.com/hubfs/Whitepapers/Last%20Mile%20Logistics/TheLastMileLogisticsWhitePaper.pdf, (accessed Mar. 3, 2023).

[22] A. Babacan, M. R. Şimşek, "E-Ticaret Sektöründe Müşteri Memnuniyeti ve Sadakati Arasındaki İlişki: Bir Yapısal Eşitlik Modeli Uygulaması", Cumhuriyet Üniversitesi İktisadi ve İdari Bilimler Dergisi, vol. 19 no. 2, pp. 67-87, 2018.

[23] A.Munoz-Villamizar, EL. Solano-Charris, L. Reyes-Rubiano, J. Faulin, "Measuring Disruptions in Last-Mile Delivery Operations", Logistics, vol. 5, no. 1, 17, 2021.

[24] O.T. Laseinde, K. Mpofu, "Providing solution to last mile challenges in postal operations", International Journal of Logistics Research and Applications, vol. 20, no. 5, pp. 475-490, 2017.

[25] Y. Huang, K.M. Kockelman, V. Garikapati, "Shared automated vehicle fleet operations for first-mile last-mile transit connections with dynamic pooling", Computers, Environment and Urban Systems, vol. 92, 2022.

[26] E. Nathanail, M. Gogas, G. Adamos, "Assessing the Contribution of Urban Freight Terminals in Last Mile Operations" Transport and Telecommunication Journal, vol. 17, no.3, pp.231-241, 2016.

[27] J. Oršič, B. Jereb, M. Obrecht, "Sustainable Operations of Last Mile Logistics Based on Machine Learning Processes", Processes, vol. 10, no. 12, 2524, 2022.

Title: An Ethnobotanical Study on Plants Used in the Treatment of Gynecological Diseases in Some Provinces of the Eastern Anatolia Region

Authors: Songül KARAKAYA, Zehra KIMIŞOĞLU, Ümit İNCEKARA, Özkan AKSAKAL, Yusuf Ziya SÜMBÜLLÜ, Ahmet POLAT

An Ethnobotanical Study on Plants Used in the Treatment of Gynecological Diseases in Some Provinces of the Eastern Anatolia Region

Songül KARAKAYA[1]* iD, Zehra KIMIŞOĞLU[2] iD, Ümit İNCEKARA[3] iD, Özkan AKSAKAL[3] iD, Yusuf Ziya SÜMBÜLLÜ[4] iD, Ahmet POLAT[3] iD

Abstract

This work was supported by "The Republic of Turkey Ministry of Agriculture and Forestry General Directorate of Nature Conservation and National Parks." It was carried out to document the plants used by people living in and around Ardahan, Iğdır and Kars provinces between 2020-2021 for gynecological diseases. For this purpose, medicinal plants used by the public for therapeutic purposes were collected and determined, their use, and parts used were reported, and herbarium samples were prepared. Regular visits were arranged to the regions where the research was carried out, and surveys were conducted by interviewing and speaking with the area's people. It was determined that 34 medicinal plant taxa belonging to 18 plant families were used in gynecological diseases among the people of Ardahan, Iğdır and Kars provinces and their surroundings. These plants include 26 wild species and 7 cultivated species. It has been observed that the most commonly used medicina plant families in gynecological diseases are Asteraceae (6), Malvaceae (5) and Lamiaceae (3). Although traditional medicine is widely practiced in the regions where it is studied, it is rapidly being replaced by modern medicine and pharmacy.

Keywords: Eastern Anatolia, gynecological diseases, Ardahan, Iğdır, Kars

1. INTRODUCTION

The term ethnobotany was first introduced by the American botanist Dr. John William Hershberger during a conference in Philadelphia in 1895. He utilized this term to describe his research on "plants produced by primitive and indigenous peoples. Ethnobotany is defined as the study of the direct relationship and interaction between human populations and plants in different cultures. Ethnobotany investigates interactions and relationships between plants and humans. It has been reported that out of

* Corresponding author: songul.karakaya@atauni.edu.tr (S. KARAKAYA)
[1] Atatürk Üniversitesi, Eczacılık Fakültesi, Farmasötik Botanik AD, Erzurum, Türkiye
[2] Kafkas Üniversitesi, Fen-Edebiyat Fakültesi, Türk Dili ve Edebiyatı Bölümü, Kars, Türkiye
[3] Atatürk Üniversitesi, Fen Fakültesi, Biyoloji Bölümü, Erzurum, Türkiye
[4] Erzurum Teknik Üniversitesi, Fen-Edebiyat Fakültesi, Türk Dili ve Edebiyatı Bölümü, Erzurum, Türkiye
E-mail: zehra_kimisoglu@hotmail.com, umit.incekara@erzurum.edu.tr, ozkanaksakal@atauni.edu.tr, yzsumbullu@erzurum.edu.tr, ahmetpolat@atauni.edu.tr
ORCID: https://orcid.org/0000-0002-3268-721X, https://orcid.org/0000-0003-2029-9321, https://orcid.org/0000-0002-3283-5841, https://orcid.org/0000-0003-0760-7502, https://orcid.org/0000-0001-9841-4970, https://orcid.org/0000-0002-5172-9753

approximately 4.22 million flowering plants in the world, more than 50,000 are utilized for medicinal purposes. The World Health Organization (WHO) has shown that 80% of the world's population depends on traditional medicines, and the majority of these treatments involve plant extracts. In fact, three-quarters of the world's population cannot afford modern medicines and rely on traditional herbal drugs. Until the mid-19th century, herbs were the primary therapeutic agents utilized by people, and their role in medicine remains significant today. In the late 19th century, ethnobotany began to improve as a science offering novel tools for pharmaceutical search. Public institutions such as the WHO and private pharmaceutical companies have started investing in ethnobotanical discoveries [1].

Medicinal herbs are a significant component of local medicinal systems around the world. Ethnobotanical accumulation is accepted as part of a cultures "traditional" knowledge. For many years, Europe benefited from the ancient accumulation of local cultures, especially in newly discovered regions. Most of the modern drug molecules and some phytotherapeutic preparations utilized today are derived from herbs found in the traditional knowledge of indigenous cultures. In the 18th century, explorers such as British Richard Spruce and German Alexander von Humboldt studied the use of plants by indigenous communities in detail, including the preparation of curare, which was used as an arrow poison in South America and later became famous as an important muscle relaxant. The role of ethnobotany in the search for new drugs remained important until the second half of the 20th century, when other approaches became more popular [2].

The Eastern Anatolia Region is a mountainous and high region that is rich in terms of physical geography due to the mountains extending in the east-west direction and the basins between these mountains. While fertile agricultural areas are found in intermountain basins and tectonic depressions, high

mountains are important grazing areas. In this context, the region can be considered an important agriculture and animal husbandry area of our country. The region has difficult conditions, especially with its climatic and geographical structure. The reflection of environmental conditions on the cultural process and the traceability of this reflection through the data obtained through the studies carried out are of great importance [3, 4].

An estimated one million women in the world are exposed to urogenital infections such as non-sexually transmitted urinary tract infections and bacterial vaginosis every year. At least 75% of women have a history of genital infections. In various studies carried out in Turkey, genital tract infection was found to be a common problem. In a study, genital infections were found in 65.6% of women. Vaginal infections are diseases that can be treated and prevented or complications can be reduced with early diagnosis and treatment. Although it may not be commonly discussed, vaginal infections are a significant health issue due to their high prevalence and potential complications. These infections can lead to various problems, such as negative impacts on body image, an increase in vaginal symptoms or unpleasant odors, fear of contracting sexually transmitted diseases or cancer, avoidance of sexual activity due to pain or discomfort, physical fatigue and weakness, psychological issues, and anxiety about infertility. Additionally, they can result in economic losses, loss of time, and decreased workforce productivity. [5]. Numerical data on the use of medicinal plants in Ilıca (Erzurum) were evaluated and it reported that the rate of plants used in gynecological diseases and diabetes was 4.2% [6]. Numerical data on the use of medicinal plants in Iğdır were evaluated and it was reported that the ratio of plants used in gynecological diseases was 5.35% [7]. This research examined traditional plants used in gynecological diseases among the people in Ardahan, Iğdır and Kars provinces and their surroundings between 2020-2021.

KARAKAYA et al.

An Ethnobotanical Study on Plants Used in the Treatment of Gynecological Diseases in Some Provinces o...

2. MATERIALS AND METHODS

2.1. Study Areas

Study area
The Eastern Anatolia region, where the provinces selected as the study area are located, are neighbors of Central Anatolia Region in the west, Azerbaijan and Georgia in the northeast, Southeastern Anatolia Region and Iraq in the south, and Iran and Armenia in the east. Due to its geographical location, it has become an important crossroads for ancient communities/civilizations. The region is the highest region of our country and due to this feature, the winters are very harsh and rainy, and the summer season is short and dry. It is a region that is not very suitable for life with its rugged lands. For this reason, since ancient times, settlements have been established in suitable habitats, that is, on flat plains. Despite these difficult geographical conditions, the region has been the residence of many communities throughout the ages. The most important factor in this is rich natural resources and pasture areas of great importance for animal husbandry. The region is geographically divided into four sub-sections: "Upper Euphrates Section", "Erzurum-Kars Section", "Upper Murat Van Section" and "Hakkari Section" [8]. (Figure 1).

Figure 1 The location of the study areas in the region.

2.2. Data collection

Within the scope of the study, information was compiled by face-to-face interview method in field studies carried out in 120 villages (Ardahan-40, Iğdır-30 and Kars-50). In order to identify people with traditional knowledge, general information about the project was given by contacting the mukhtar beforehand and information was obtained about people with traditional knowledge. People with traditional knowledge were informed about the content of the project through the headmen and they were made available during the fieldwork. In addition, interview-based interviews were conducted with people in village coffeehouses, mosques, village/district solidarity/association unions, public education centers, agricultural chambers and cooperatives through questions and answers. Of the informants, 121 were women and 48 were men.

2.3. Plant Samples

Plants were collected from selected villages of Ardahan, Iğdır and Kars provinces between 2020-2021. Herbarium materials are kept in Atatürk University Biodiversity Application and Research Center and Iğdır University Biodiversity Application and Research Center herbariums. The collected plants were identified using "The Flora of Turkey and East Aegean Islands." [9,10]. Scientific names of plant species have been updated using the relevant databases (www.worldfloraonline.org.). [11].

3. RESULTS

Demographic characteristics of the participants were recorded through face-to-face interviews. Demographic characteristics of the participants are presented in Table 1.

It was determined that a total of 34 plant taxa belonging to 18 plant families were used in gynecological diseases among the people of Ardahan, Iğdır and Kars provinces and their surroundings. Of these, 27 are natural and 7 are cultivated plants. Detailed information about the family, Latin/scientific-local names, usage patterns and the relevant region of the plants used are given in Table 2.

KARAKAYA et al.

An Ethnobotanical Study on Plants Used in the Treatment of Gynecological Diseases in Some Provinces o...

Table 1 Demographic characteristics of the participants.

Demographic characteristics	Number
Age	*Total=169*
31-40	9
41-50	37
51-60	50
61-70	42
70 above	30
Gender	*Total=169*
Female	121
Male	48
Educational level	*Total=169*
Illiterate	82
Primary school	73
Secondary school	11
High school	3
Employment status	*Total=169*
Housewife	121
Farmer	32
Pensioned	12
Shepherd	2
Other jobs	2

Table 2 Plants used in gynecological diseases in ardahan, iğdır and kars provinces and surroundings.

Family Name	Species Name	Local Name	Usage methods	Province	Herbarium No.
Amaryllidaceae	*Allium cepa* L.*	Soğan	Lightly cooked onion is used externally for the fall of the umbilical cord.	Iğdır	-
			Onion peels are boiled with water and this mixture is placed in a jar. Drink a glass every morning on an empty stomach. So you have a child.	Kars	
Asparagaceae	*Asparagus officinalis* L.	Merajo	The fruits of the plant are eaten in the morning on an empty stomach for infertility.	Iğdır	ATA/G-27
Asteraceae	*Achillea millefolium* L.	Sarıçiçek, Kılıç otu	The decoction prepared with flowers is drunk 3 times a day on an empty stomach for menstrual cramps.	Kars	ATA/G-3
			The decoction prepared with the aerial parts of the plant is consumed in gynecological diseases.	Kars	
Asteraceae	*Arctium platylepis* (Boiss. & Bal.) Sosn. ex Grossh.	Gabalak	Leaves of *Arctium platylepis, Malva neglecta* and *Plantago major* are mixed and beaten. It is then boiled with milk. This mixture is wrapped around the belly of the woman who wants to get pregnant and left for 1-2 hours.		INWM000035
Asteraceae	*Helichrysum plicatum* DC.	Nego	The decoction prepared with the flowers of the plant is drunk against infertility.	Ardahan	INWM000030
Asteraceae	*Helichrysum arenarium* (L.) Moench	Altın otu	If the decoction prepared with the flowers of the plant is drunk on an empty stomach in the morning for 1 week, those who do not have children will have children.	Kars	ATA/G-238
Asteraceae	*Cirsium macrobotrys* (C. Koch) Boiss.	Meryemana	Decoction prepared with the flowers of the plant is drunk 1 tea glass on an empty stomach during menstruation against menstrual pain.	Kars	ATA/G-239

KARAKAYA et al.

An Ethnobotanical Study on Plants Used in the Treatment of Gynecological Diseases in Some Provinces o...

Table 2 Plants used in gynecological diseases in ardahan, iğdır and kars provinces and surroundings.
(continue)

Asteraceae	*Tanacetum coccineum* (Willd.) Grierson	Sender	The aerial parts of the plant are collected and boiled in water. It is added to the bath water and the genital area is washed with this water for the treatment of infertility.	Ardahan	ATA/G-209
Asteraceae	*Tanacetum vulgare* L.	Sendel	The decoction prepared with the aerial parts of the plant is drunk by women who do not have children.	Kars	ATA/G-240
Boraginaceae	*Alkanna tinctoria* (L.) Tausch	Havaciva, Havajo, Havaciva, Sormuk	The roots of the plant are collected, roasted in butter, wax is put on it and roasted a little more, the prepared mixture is kept at room temperature and applied to wounds and cracks after birth.	Ardahan	INWM000051
			The whole plant is dried and ground into powder, then baked with flour and oil. This mixture is used externally in gynecological diseases by applying it to the genital area.	Iğdır	
			Decoction prepared with plant roots is drunk in menstrual pain (1 glass of water in the mornings for 3 days).	Kars	
			A childless woman sits on hot water after boiling the aerial parts of *Alkanna orientalis, Malva neglecta* and *Plantago major.*	Iğdır	
Boraginaceae	*Alkanna orientalis* (L.) Boiss.	Havaciva, Havajo, Havaciva	The aerial parts of *Alkanna tinctoria, Malva neglecta* and *Plantago major* are boiled and a childless woman sits in hot water.	Iğdır	ATA/G-8
Capparaceae	*Capparis spinosa* L.	Gundrabeji, Kapari	The decoction prepared with the fruits of the plant is drunk in uterine inflammations.	Iğdır	
Caprifoliaceae	*Cephalaria procera* Fisch. & Avé-Lall.	Polya	The decoction prepared with the seeds of the plant is drunk in the morning on an empty stomach for menstrual pain.	Ardahan	ATA/G-53
Cucurbitaceae	*Cucurbita pepo* L.*	Gundribeji	Fruit seeds are removed and crushed with stones. Add garlic and green lentils and cook. The prepared mixture is fed to the woman who wants to have a child 3 days in a row.	Kars	-
Fabaceae	*Glycyrrhiza glabra* L.	Şirinbiyan	The woman who wants to have a child is seated on the water obtained by boiling the roots of this plant.	Iğdır	ATA/G-241
Gentianaceae	*Gentiana lutea* L.	Camışkıran	Drink 1 glass of the decoction prepared with the whole plant on an empty stomach for infertility.	Kars	INWM000043
Lamiaceae	*Lavandula stoechas* L.*	Karabaş otu	The decoction prepared with the aerial parts is drunk as an anti-inflammatory.	Kars	-
Lamiaceae	*Mentha longifolia* (L.) L.	Yarpuz	The flowering aerial part is added to the bath water. It relieves inflammation in gynecological diseases.	Ardahan	INWM000032
Lamiaceae	*Teucrium polium* L.	Sancı otu, Mervend, Mervende	The decoction prepared with the aerial parts of the plant is drunk for menstrual pain.	Iğdır	ATA/G-211
Malvaceae	*Alcea hohenackeri* Boiss.	Hatmi çiçeği, Hiro	The genital area of women without children is exposed to the steam of the boiled marshmallow flower. Drink 1 glass of the decoction prepared with flowers on an empty stomach in the morning for 1 week.	Kars	ATA/G-7
			The decoction prepared with the flowering aerial parts of the plant is drunk for infertility.	Kars	

KARAKAYA et al.

An Ethnobotanical Study on Plants Used in the Treatment of Gynecological Diseases in Some Provinces o...

Table 2 Plants used in gynecological diseases in ardahan, iğdır and kars provinces and surroundings.
(continue)

Malvaceae	*Alcea striata* Alef.	Hiro	The flowers of the plant are boiled and used as an anti-inflammatory in gynecological diseases.	Iğdır	ATA/G-242
			The decoction prepared with the plants above-ground parts is drunk in uterine inflammations.	Iğdır	
			It is used as a decoction prepared with the flowers of the plant and as an anti-inflammatory in gynecological diseases.	Iğdır	
Malvaceae	*Alcea calvertii* (Boiss.) Boiss	Gülhatı	An infusion prepared with flowers is given to the childless woman.	Ardahan	ATA/G-6
Malvaceae	*Alcea apterocarpa* Boiss.	Hiro	The decoction prepared with the flowers of the plant is used as an anti-inflammatory in gynecological diseases.	Iğdır	ATA/G-243
Malvaceae	*Malva neglecta* Wallr.	Gorgut Dolik, Ebemgümeci Ebem Kömeci,	The leaves of the plant are boiled. It is inserted into the vagina to relieve inflammation.	Ardahan	INWM000039
			The decoction prepared with the aerial parts of the plant is drunk as an anti-inflammatory in gynecological diseases.	Ardahan	
		Ebemgümeci	The aerial parts are boiled in milk. The woman who wants to have a child sits on it.	Iğdır	
		Ebe Kömeci Ebemkömeci	The decoction prepared with the aerial parts of the plant is drunk as an anti-inflammatory in gynecological diseases.	Ardahan	
		Doldolig, Dolig,	The decoction prepared with the aerial parts of the plant is drunk as an anti-inflammatory in gynecological diseases.	Iğdır	
		Ebegümeci	The aerial parts of *Alkanna tinctoria, Alkanna orientalis* and *Plantago major* are boiled and the childless woman sits in hot water.	Iğdır	
			Childless woman sits on hot water after *Malva neglecta* leaves and *Plantago lanceolata* leaves are boiled.	Iğdır	
			Leaves of *Arctium platylepis, Malva neglecta* and *Plantago major* are mixed and beaten. It is then boiled with milk. This mixture is wrapped around the belly of the woman who wants to get pregnant and left for 1-2 hours.	Iğdır	
			Women who do not have children are fed a meal prepared from the above-ground parts.	Iğdır	
			The childless woman sits in the decoction prepared with the above-ground parts of the plant.	Iğdır	
			The decoction prepared with the leaves of the plant is drunk twice a day for menstrual pain during menstruation.	Kars	
			The decoction prepared with buds is drunk 2 times a day for uterine inflammation.	Kars	
Pinaceae	*Pinus sylvestris* L.	Çam, Kara katran	Prepared with young, green pine cones, the decoction is drunk in the morning on an empty stomach as a menstrual cramp.	Ardahan	INWM000026
			The decoction prepared with pine cones from the plant is given to women with labor pains 2-3 times.	Kars	
Plantaginaceae	*Plantago lanceolata* L.	Pelheves	After the leaves of the plant are crushed, it is used externally for uterine inflammation.	Iğdır	ATA/G-164
			Childless woman sits on hot water after *Malva neglecta* leaves and *Plantago lanceolata* leaves are boiled.	Iğdır	

KARAKAYA et al.

An Ethnobotanical Study on Plants Used in the Treatment of Gynecological Diseases in Some Provinces o...

Table 2 Plants used in gynecological diseases in ardahan, iğdır and kars provinces and surroundings. (continue)

Plantaginaceae	*Plantago major* L.	Bağa Yaprağı, Pelheves	Leaves of *Arctium platylepis, Malva neglecta* and *Plantago major* are mixed and beaten. It is then boiled with milk. This mixture is wrapped around the belly of the woman who wants to get pregnant and left for 1-2 hours.	Iğdır	INWM000028
			The childless woman sits on the decoction prepared with the aerial parts of the plant.	Kars	
			The aerial parts of *Alkanna tinctoria, Malva neglecta* and *Alkanna orientalis* are boiled and a childless woman sits on hot water.	Iğdır	
Poaceae	*Hordeum vulgare* L.*	Arpa	The fruit stem of the plant is cooked and the honeycomb is added to it. This mixture is applied to the woman's vagina for infertility..	Ardahan	-
Poaceae	*Triticum aestivum* L.*	Buğday	After giving birth, women are fed a food called "hedik" made with wheat so that they have plenty of milk. Hedik is a food prepared by boiling wheat with water and salting it.	Iğdır	-
Polygonaceae	*Rumex crispus* L.	Evelik	If a glass of the infusion prepared with the leaves is drunk every morning until the disease ends, the uterus is cleaned.	Iğdır	INWM000029
Rosaceae	*Alchemilla pseudocarta linica* Juz.	Aslanpençesi (Göğebakan)	Tea, which is prepared as a decoction from the aerial parts of the plant, is consumed in uterine inflammation.	Kars	ATA/G-244
Rosaceae	*Rosa canina* L.	Şilan	The fruits of the plant are drunk after boiling in uterine inflammation.	Kars	INWM000038
Solanaceae	*Hyoscyamus niger* L.	Patpata, Patpat	The leaves of the plant are boiled with milk. In order to prevent infection in gynecological diseases, this mixture is applied externally to the genital area.	Ardahan	INWM000042
			The aerial parts of the plant are boiled and women without children sit on the steam.	Iğdır	
Solanaceae	*Solanum tuberosum* L.*	Patates	Lightly cooked potatoes are used externally in the fall of the umbilical cord.	Iğdır	-

* Cultivated plants

The most commonly used families in gynaecological diseases are Asteraceae (5- *Achillea millefolium* L., *Helichrysum arenarium* (L.) Moench, *H. plicatum* DC., *Tanacetum punctatum* (Desr.) Grierson, *T. vulgare* L.,), Malvaceae (5- *Alcea calvertii* (Boiss.) Boiss, *A. apterocarpa* Boiss., *A. striata* Alef., *A. hohenackeri* Boiss., *Malva neglecta* Wallr.) ve Lamiaceae (3- *Lavandula stoechas* L., *Mentha longifolia* (L.) L., *Teucrium polium* L.). The most commonly used herbs are *Alkanna tinctoria* (L.) Tausch, *Plantago major* L., *M. neglecta* and *Alcea striata* Alef.

4. DISCUSSION

As a result of the literature review, it was determined that most of the previous ethnobotanical studies in Ardahan, Iğdır and Kars regions covered the Eastern Anatolia. *Glycyrrhiza glabra* L., *T. polium*, *M. neglecta*, *Plantago lanceolata* L., *P. major* L., *Rumex crispus* L., *H. niger*, *M. longifolia*, which were determined to be used in Ardahan, Iğdır and Kars, were also included in our study. It has been determined that these plants are used for similar purposes [12-14]. In other ethnobotanical studies conducted in the Eastern Anatolia Region, *Amaranthus retroflex* L. [14, 15], *Mentha longifolia* (L.) Hudson subsp. *longifolia*, *Rumex patientia* L. [16], *Achillea biebersteinii* Afan., *A.*

KARAKAYA et al.

An Ethnobotanical Study on Plants Used in the Treatment of Gynecological Diseases in Some Provinces o...

coarctata Poir., *A. millefolium* L. subsp. *millefolium*, *A. wilhelmsii* C.Koch, *A. setacea* Waldst. & Kit., *Ajuga chamaepitys* (L.) Schreber subsp. *chia* (Schreber) Arcangeli var. *chia*, *Anchusa azurea* Miller, *Betula litwinowii* Doluch, *Cardamine uliginosa* Bieb., *Chenopodium album* L. subsp. *album* var. *album*, *C. murale* L., *Ferula caspica* Bieb., *Galium humifusum* Bieb., *G. tricornutum* Dandy, *Heracleum trachyloma* Fisch. & Mey., *Hypericum lydium* Boiss., *H. scabrum* L., *Juglans regia* L., *Plantago major* L. subsp. *intermedia* (Gilib.) Lange, *Rumex crispus* L., *Salvia hydrangea* DC. ex Bentham, *Scorzonera cana* (C. A. Meyer) var. *jacquiniana* (W. Koch) Chamberlain, *S. laciniata* L. subsp. *laciniata*, *S. suberosa* C.Koch subsp. *suberosa*, *S. tomentosa* L., *Tanacetum punctatum* (Desr.) Grierson, *Urtica dioica* L., *Verbascum cheiranthifolium* Boiss [14], *Cephalaria gigantea* (Ledeb.) Bobrov, *Marrubium catariifolium* Desr, *Tanecetum balsamita* L., *T. coccineum* (Willd.) Grierson subsp. *chamaemelifolium* (Somm. et Lev.) Grierson. [17] plants have been found to be used in gynecological diseases.

The medical folklore of the Eastern Anatolia Region is especially important because some settlements in this region are scattered and preserved. Many plants are known for their therapeutic properties in and around the provinces of Ardahan, Iğdır and Kars, and some of them are used in gynaecological diseases. Due to the limited industry and transportation facilities, most of the traditions that have been maintained in this region for many years have survived to the present day, and the plants that are among these traditions and have a therapeutic effect have taken their place in urban life as well as in the countryside. General information about these plants and their uses are presented in Table 2.

5. CONCLUSION

The fact that people increasingly prefer natural medicine is among the main reasons why plants gain even greater importance today. The study of folk medicine, which is a part of folk culture, contributes to a better analysis of the society in many ways and to the treatment methods developed by modern medicine. From the past to the present, the use of plants in gynecological diseases has been found in many sources. Although traditional medicine is widely practiced in the regions where it is studied, it is rapidly being replaced by modern medicine and pharmacy. In addition, traditional knowledge is rapidly disappearing due to the migration of people living in rural areas from villages to big cities, especially to Istanbul in recent years. This is particularly evident in the provinces of Ardahan and Kars. For this reason, despite the deep-rooted history in such provinces, the transfer and use of traditional knowledge has remained limited.

The Declaration of Conflict of Interest/ Common Interest
The authors have declared no conflict of interest.

Authors' Contribution
Concept: S.K., Z.K., Ö.A., Y.Z.S., Ü.İ., A.P., Design: S.K., Z.K., Ö.A., Ü.İ., Data Collection or Processing: S.K., Z.K., Ö.A., Y.Z.S., Ü.İ., A.P., Analysis or Interpretation S.K., Z.K., Ö.A., Y.Z.S., Ü.İ., A.P., Literature

KARAKAYA et al.

An Ethnobotanical Study on Plants Used in the Treatment of Gynecological Diseases in Some Provinces o...

Search: S.K., Z.K., Ü.İ., Writing: S.K., Z.K., Ü.İ.

The Declaration of Ethics Committee Approval

This study was carried out within the scope of the project named "Biyolojik Çeşitliliğe Dayalı Geleneksel Bilginin Kayıt Altına Alınması". Field studies in the related project were carried out under the coordination of the relevant village headmen, with the assignment of the Ministry of Agriculture and Forestry and the knowledge of the governorships.

The Declaration of Research and Publication Ethics

The authors of the paper declare that they comply with the scientific, ethical and quotation rules of SAUJS in all processes of the paper and that they do not make any falsification on the data collected. In addition, they declare that Sakarya University Journal of Science and its editorial board have no responsibility for any ethical violations that may be encountered, and that this study has not been evaluated in any academic publication environment other than Sakarya University Journal of Science.

REFERENCES

[1] U. R. Inayat, A. Aftab, I. Zafar, I. Farhana, A. Niaz, S. Muzammil, U. Sana, W. B. Rainer, "Historical perspectives of ethnobotany.,". Clinics in Dermatology, vol. 37, no. 4, pp. 382-388, 2019.

[2] M. Heinrich, "Ethnobotany and its Role in Drug Development.," Phytotherapy Research, vol. 14, no. 7, pp. 479–488, 2000.

[3] A, Baysal, "Nomadism and Transhumance Culture of the Eastern Anatolian Archeology: New Ideas in Light of Data.," U.Ü. Fen-Edebiyat Fakültesi Sosyal Bilimler Dergisi, vol. 13, no. 23, pp. 255-268, 2012.

[4] M. Çelik, İ. Kopar, H. Bayram, "Seasonal Drought Analysis of Eastern Anatolia Region.," Atatürk Üniversitesi Sosyal Bilimler Enstitüsü Dergisi Eylül, vol. 22, no. 3, pp. 1741-1761. 2018.

[5] S., Dalbudak, N., Bilgili, "GATA kadın hastalıkları ve doğum polikliniğine başvuran kadınların genital hijyen davranışları ve bu davranışların vajinal enfeksiyona etkisi.," Gülhane Tıp Derg., vol. 55, pp. 281-287, 2013.

[6] R. Polat, U. Çakılcıoğlu, F. Ertuğ, F. Satıl, "An evaluation of ethnobotanical studies in Eastern Anatolia.," Biological Diversity and Conservation, vol. 5, no.2, pp. 23-40, 2012.

[7] M. Ozturk, E. Altundağ, S. J. Ibadullayeva, V. Altay, B. Aslanipour, "A comparative analysis of medicinal and aromatic plants used in the traditional medicine of Iğdır (Turkey), Nakhchivan (Azerbaijan), and Tabriz (Iran).," Pakistan Journal of Botany, vol, 50, no. 1, pp. 337-343, 2018.

[8] S., Aydın, "Eastern Anatolia region in 4th and 3rd bc.," Master Thesis, Aydın: Aydın Adnan Menderes University. 2018.

[9] P. H. Davis, Flora of Turkey and the East Aegean Islands, Edinburgh University Press, Edinburhg, Scotland, 1965–1985.

[10] P. H. Davis, Flora of Turkey and the East Aegean Islands, Edinburgh University Press Edinburgh, Scotland, 1988.

[11] www.worldfloraonline.org. (Accessed 18.08.2022).

[12] E. Sezik, E. Yeşilada, M. Tabata, G. Honda, T. Yoshihisa, F. Tetsuro, T. Toshihiro, T. Yoshio, "Traditional

Medicine in Turkey Vııı. Folk Medicine in East Anatolia; Erzurum, Erzincan, Ağrı, Kars, Iğdır Provinces.," Economic Botany, vol. 51, no. 3, pp. 195-211, 1997.

[13] E. Altundağ, "Iğdır İlinin (Doğu Anadolu Bölgesi) Doğal Bitkilerinin Halk Tarafından Kullanımı.," PhD, İstanbul: İstanbul Üniversitesi. 2009.

[14] E., Altundağ, M., Özturk, "Ethnomedicinal studies on the plant resources of east Anatolia, Turkey.," Procedia-Social and Behavioral Sciences, vol, 19, pp. 756-777, 2011.

[15] F. Özgokçe, H. Ozelik, "Ethnobotanical Aspects of Some Taxa in East Anatolia.," Economic Botany, vol. 58, no. 4, pp. 697-704, 2004.

[16] L., Behçet, M., Arık, "An ethnobotanical investigation in east Anatolia (Turkey).," Turkish Journal of Nature and Science vol, 2, no. 1, pp. 1-14, 2013.

[17] N. Özhatay, F. Güneş, "An Ethnobotanical Study From Kars (Eastern) Turkey.," Biological Diversity and Conservation, vol. 4, no.1, pp. 30-41, 2011.

Title: Development of Cordierite Based Carrier Refractory Sagar Bodies for Bone Porcelain Firing Process

Authors: Murat ISPALARLI, Zuhal KARAAĞAÇ

Development of Cordierite Based Carrier Refractory Sagar Bodies for Bone Porcelain Firing Process

Murat ISPALARLI [*1] , Zuhal KARAAĞAÇ[1]

Abstract

During the firing process of porcelain tableware; Biscuit firing takes place at low temperatures (980-1000°C), while glazed firing takes place at high temperatures (1250-1280°C for soft porcelain, 1350-1380°C for hard porcelain). Biscuit firing in bone porcelain products, which is in the soft porcelain class, is done at higher temperatures than glazed firings. Due to the presence of bone ash in the Bone China recipe formulation, it causes the bodies to undergo vitrification in a narrow range and thus the final product to deform during sintering. Bone porcelain products are fired on carrier refractories called sagar so that they do not deform during sintering. Sagars are designed to support that model for each product model and do not shrink or deform during firing thanks to its low thermal expansion coefficient. In this study, a refractory body with a porous structure with the code of "PS1-Std" was developed by performing the characterization analyzes of refractory products with different technical properties supplied from different companies. In order to improve the mechanical properties by changing the ratios of talc, alumina, quartz and zircon in the recipe composition; A refractory product containing 8.47% zircon in its recipe composition and containing indialite, corundum, mullite, quartz and zircon phases after sintering has been developed. The microstructure images of the developed refractory product were examined with the support of SEM analysis. It has been observed that refractory products obtained as a result of recipe development studies offer a 10% longer service life than equivalent refractory products.

Keywords: Biscuit, bone porcelain, cordierite, sagar, vitrification

1. INTRODUCTION

As a ceramic material, bone porcelain (Bone China) emerges as an extremely superior product in terms of its technical and aesthetic properties. In terms of aesthetic properties, they constitute the most attractive and expensive tableware in the world, mainly in terms of translucency, whiteness, glossy glazed surface and high mechanical properties (high strength). According to the definition of the American Society for Testing and Material (ASTM), bone china is a soft porcelain with high translucency, containing 25% bone ash. Bone ash is used as an ingredient in the bone china body, and this addition gives this product its unique properties. The traditional composition of the bone china body includes

50% bone ash, 25% plastic clay (as plasticizer) and 25% cornish stone. The microstructures of bone porcelain are known as β-tricalcium phosphate (β-$Ca_3(PO_4)_2$) (β-TCP), anorthite ($CaAl_2SiO_8$), α-quartz (SiO_2) and calcium aluminosilicate glass. According to the BS EN 8654:2015 standard, it is defined as follows; Products that consist of a ceramic body containing at least 35% bone ash and defined as tricalcium phosphate are called bone china (Bone China) [1, 2].

The cornice stone mentioned in the bone porcelain body composition is basically a type of pegmatite. Mineralogically, it contains feldspar, quartz and mica and is used as a flux in the body. For this reason, feldspathic raw materials are preferred instead of this raw material. In general, potassium and sodium feldspars are used as a flux in porcelain. Anorthite is another mineral for white fired porcelain bodies [3, 4-7].

In bodies containing calcite, the anorthite phase is interesting because of the low temperature required for its formation and the properties it imparts to the final product. Anorthite; although lower temperatures are also mentioned in the literature, it generally begins to form as a result of the reaction of kaolin and wollastonite at temperatures of 1100°C and above. Two different crystallization structures are encountered in the formation of anorthite. If the primary crystallization structure of anorthite is encountered, anorthite also creates a high rate of vitrified phase and excessive shrinkage occurs. The use of anorthite is not appropriate, since a high rate of vitrified phase will occur in bodies with porous structure [8].

In Köseçavuş's thesis titled "Anorthite synthesis and characterization from volcanic tuff", anorthite was produced by powder metallurgy method using volcanic tuff and different proportions (2%, 4%, 6%) boron (boric acid). The samples obtained were sintered at different temperatures and it was observed that there was a stable change in temperature with the increase of boron ratio at

1100°C. Deformation was observed at 1200°C and 1300°C [9].

Bone porcelain production has always been a very difficult process; It requires strict control over a number of process parameters such as particle size distribution, temperature of the dryer, density of the mixture and biscuit baking temperature. One of the most important problems of bone porcelain production is the narrow firing range. Open pores that can be found in the structure are the most obvious parameters that restrict full permeability.

Permanent holes and damages may occur in the body due to its bad shape in firing applied below the optimum firing temperature. This is because bone ash contains carbonate, which acts as a powerful melter that can make the body quite malleable. When the pore relationship between a standard bone china and hard porcelain is examined; Parallel to the temperature increase, vitrification for hard porcelain takes place around 1200°C, which is well below the maximum firing temperature. In addition, bone porcelain has an apparent porosity of around 20% at this temperature. It is expected that the sintering of bone porcelain and the sintering of this product will be handled in two different stages.

Accordingly, in accordance with the remarkable changes in porosity and reduction in surface area, the existence of solid state sintering in the range of 700-800°C is mentioned, while the existence of liquid phase sintering, which is explained by the shrinkage and open pores that move away in parallel with the increase in bulk density, in the range of 1000-1150°C is mentioned. It is formed by the transformation of meta kaolin in clays into acicular-shaped mullite crystals and silica glass in the range of 950-1000ºC. As feldspars start to melt between 1010-1100ºC, the first interactions take place between the materials that make up the groups. Potassium feldspar melts at 1150ºC, sodium feldspar at 1050ºC. Potassium feldspar appears in the liquid phase below 1000 ºC in contact with the silicate and

if there is the effect of water vapor. The melting effects of feldspars with kaolin above 1050ºC cause the formation of a glassy phase and the formation of feldspar examination acicular (primary) mullite and row (secondary) mullite at the edges of the kaolin. Shrinkage occurs as a result of sintering of liquid phase components [1, 10, 11].

The first firing, called "Biscuit Firing", unlike the conventional porcelain production of bone china, is in the oxidizing atmosphere in the biscuit oven; Depending on the particle size distribution and final composition of the prepared bodies, they are fired at a temperature of approximately 1200-1300°C for an average of 15 hours. At this stage, a shrinkage of about 20% in the raw products tends to cause deformation and cracking. The product shrinks during firing and is very sensitive to overfiring. In order to prevent deformation during sintering, bone porcelain products are fired on a carrier refractory called sagar, which has a low thermal expansion coefficient and therefore does not cause shrinkage or deformation problems during firing. If the temperature rises slightly above the ripening point, it will cause the product to form bubbles and voids that cause a spongy body [12].

Playing a major role in the firing stage in the porcelain industry, refractories are defined as materials that are resistant to high temperatures and resistant to the effects of solid, liquid and gaseous substances at these temperatures. Of refractories; There are varieties based on magnesite or chrome magnesite, spinel, zircon, alumina and silica. Cordierite ceramics; It is used in the production of industrial ceramics due to its low coefficient of thermal expansion and excellent thermal shock resistance, high thermal and chemical stability. The stoichiometric formula of cordierite is $2MgO.2Al_2O_3.5SiO_2$ and its chemical composition is 13.7% MgO, 34.9% Al_2O_3 and 51.4% SiO_2. In a cordierite mixture consisting of clay, talc and alumina, at temperatures higher than 1250°C, clay and talc transform into mullite and protoenstatite ($MgO.SiO_2$). Then, cordierite phase is formed between 1250-1430°C from the alumina composition of mullite and protoenstatite. In the formation of cordierite phase, SiO_2 in the structure is released from both mullite and protoenstatite. However, while Al_2O_3 and MgO are only released from mullite and protoenstatite, here mullite plays the main role in the formation of cordierite. Because Al_2O_3 is the main component in cordierite formation compared to MgO. The coefficient of thermal expansion is more sensitive to MgO change than other ingredients [13, 14].

One of the negative features of cordierite ceramic is that it has low toughness properties. Different studies have been carried out by adding ZrO_2 to the formulation in order to improve its low toughness properties. It is a widely known phenomenon that the strength and toughness of ceramic materials increase with the transformation of zirconia from tetragonal to monoclinic. Although the toughening of zirconia has been applied to many ceramics, the most studied system is zirconia toughened alumina [15].

In this study, the development of an alternative formulation to carrier saggars for the imported bone porcelain process in bone porcelain production and the characterization analyses of the developed body were investigated by supporting it with (XRF, XRD, XRD, SEM, EDX).

2. MATERIALS AND METHOD

2.1. Analysis of Equivalent Products

Physical tests of equivalent products called cordierite, mullite-cordierite and sagar in the market were carried out in the Porland Porcelain R&D Center Laboratory. CIEL*a*b* color measurements of the products were made with the "Konica - CMA145" brand device and the results are given in Table 1.

Table 1 Color chromatic coordination measurements of alternative commercial products (CP)

Firm	Product	L*	a*	b*
CP1	Sagar	93.94	-0.41	4.33
CP2	Cordierite	95.98	-0.31	3.86
CP3	Cordierite	83.07	3.03	18.36
CP4	Mullite Cordierite	93.44	-1.14	3.82

Table 2 Alternative commercial products; Water absorption, apparent porosity, apparent relative density, bulk mass measurements

Analysis	CP1	CP2	CP3	CP4
Water Absorption (%)	16.53	14.36	10.82	11.23
Apparent porosity (%)	30.34	28.16	22.05	26.73
Apperent Relative Density (gr/cm^3)	02.63	02.73	02.61	03.25
Bulk Mass (gr/cm^3)	01.84	01.96	02.04	02.38

Table 3 Chemical analysis of commercial products

Oxide %	CP1	CP2	CP3	CP4
SiO_2	48.56	44.27	50.03	16.82
Al_2O_3	41.24	51.52	40.41	81.45
Fe_2O_3	01.12	00.45	01.19	00.43
TiO_2	00.24	00.49	00.54	00.25
CaO	00.18	00.15	00.24	00.11
MgO	07.28	02.49	06.73	00.10
Na_2O	00.00	00,00	00.00	00.29
K_2O	01.00	00.63	00.86	00.30
K.K.	00.38	00.00	00.00	00.25

Water absorption measurements and bulk densities of the products under vacuum were measured with the "Ceramic" device. Device - VSVD/60" brand device and results are given in Table 2. Characterization analysis of equivalent products were also made by the Ceramics Research Center (SAM). chemical compositions (XRF) are given in Table 3 and phase analysis results (XRD) are given in Table 4.

Table 4 Phase analysis of selected commercial products

(%)	CP1	CP2	CP3	CP4
İndialite	54.47 ±0	26.13 ±0	55.17 ±0	-
Corundum	-	8.26 ±0.4	-	-
Mullite	26.77 ±0.9	40.18 ±0.9	24.78 ±0.9	67.23 ±0.9
Amorf	18.76 ±1.6	20.39 ±1.6	15.61 ±1.9	32.77 ±1.9
Cristobalite	-	0.05 ±0.2	4.45 ±0.2	-

2.2. Experimental Studies

According to the results of the literature review and the analysis of equivalent products, considering the availability and costs of raw materials; The raw materials to be used in the study were determined by evaluating their chemical properties, physical properties, availability and cost.

In the study, the raw materials used to create the refractory body recipe and the raw materials whose chemical analyses were determined according to Table 5 were mixed in the ratios determined according to Table 6. "PS1-Std." PS2, PS3, PS4, PS5, PS6, PS7 and PS8 trial recipes were prepared in order to increase the thermal-mechanical activity of this standard recipe.

Table 5 Chemical analysis of raw materials (XRF) used in recipe preparation

%	Kaolin1	Kaolin2	Clay	Calcined Alumina	Talc	Zircon	Quartz	K-Feldspar
SiO_2	45.13	44.72	53.14	00.56	64.41	31.96	99.13	67.46
Al_2O_3	38.85	39.34	29.68	98.24	00.69	09.47	00.41	17.73
Fe_2O_3	00.78	00.49	02.40	00.02	00.34	00.15	00.03	00.09
TiO_2	00.09	00.08	01.33	00.03	00.08	00.35	00.04	00.03
CaO	00.12	00.09	00.66	00.06	01.26	01.45	00.02	00.10
MgO	00.60	00.38	00.67	00.26	24.84	07.99	00.00	00.00
Na_2O	00.56	00.55	00.53	00.68	00.49	04.52	00.04	02.72
K_2O	01.79	00.66	02.16	00.04	00.23	01.58	00.06	11.32
ZrO_2	00.00	00.00	00.00	00.00	00.00	41.85	00.00	00.00
K.K.	12.08	12.69	09.43	00.10	07.66	00.68	00.27	00.55

Table 6 The percentage (%) components of the raw materials that make up the cordierite-based bodies recipes

Raw Material (%)	PS1-Std.	PS2	PS3	PS4	PS5	PS6	PS7	PS8
Clay	07.92	09.75	09.66	09.30	08.88	08.85	08.47	08.47
Kaolin 1	19.80	23.90	23.67	22.79	21.77	21.68	20.76	20.76
Calcined Alumina	25.74	25.36	25.12	24.18	23.11	23.00	22.03	22.03
Kaolin 2	09.90	09.75	16.42	15.81	15.11	15.04	14.40	14.40
Talc	20.79	20.48	20.28	23.25	22.25	22.15	25.42	21.18
Quartz	10.89	10.73	04.85	04.65	04.44	04.42	04.23	04.23
K-Feldspar	04.96	00.00	00.00	00.00	00.00	00.00	00.00	00.00
Zircon	00.00	00.00	00.00	00.00	04.44	04.44	04.23	08.47
Bentonite	00.00	00.00	00.00	00.00	00.00	00.42	00.42	00.42

Raw materials were weighed according to the ratios determined in the recipe in Table 6 and loaded into the ball mill. In order to increase the thixotropy property of the mud, 0.42% bentonite was added to the recipe and the mud rheology was brought to the desired values. Standard production steps are as follows; By adding water to the raw material mixture, the liter weight of which will be adjusted in the range of 1350-1420 gr/lt in the mill and the desired TDA; D (90): ground to 15-20 µm range. After obtaining the particle size distribution approval according to Table 7 for the sludge suspension, it is filtered through a 100 DIN sieve and turned into KEK with a Filter Press. Then, the sludge (KEK) coming out of the Filter Press is opened with a mixer and filtered through a 60 DIN sieve with the help of electrolyte by adjusting its liter weight in the range of 1730-1800 gr/lt. The reason why sludge is grinded in a low liter mill first is to turn it into a KEK after the Filter Press and open it again, making the mud more plastic and increasing the shaping performance in the pressure casting method in mass production. However, since the trial stages of the study were carried out in the laboratory, the sludge was not made into cake with a filter press. However, in order to increase the plasticity of the mud and to analyze its rheological properties, the mud that was ground in the mill and reached the desired particle size distribution range was turned into sausage with the help of plaster molds. After turning the mud into sausage, it was opened again in the mixer. In order to determine the rheological values of the recipe suspensions, casting mud 1710-1720 gr/lt liter weigh was prepared.

Raw materials were weighed according to the ratios determined in the recipe in Table 6 and loaded into the ball mill. In order to increase the thixotropy property of the mud, 0.42% bentonite was added to the recipe and the mud rheology was brought to the desired values.

Standard production steps are as follows; By adding water to the raw material mixture, the liter weight of which will be adjusted in the range of 1350-1420 gr/lt in the mill and the desired TDA; D (90): ground to 15-20 µm range. After obtaining the particle size distribution approval according to Table 7 for the sludge suspension, it is filtered through a 100 DIN sieve and turned into KEK with a Filter Press. Then, the sludge (KEK) coming out of the Filter Press is opened with a mixer and filtered through a 60 DIN sieve with the help of electrolyte by adjusting its liter weight in the range of 1730-1800 gr/lt. The reason why sludge is grinded in a low liter mill first is to turn it into a KEK after the Filter Press and open it again, making the mud more plastic and increasing the shaping performance in the pressure casting method in mass production.

However, since the trial stages of the study were carried out in the laboratory, the sludge was not made into cake with a filter press. However, in order to increase the plasticity of the mud and to analyze its rheological properties, the mud that was ground in the mill and reached the desired particle size distribution range was turned into sausage with the help of plaster molds. After turning the mud into sausage, it was opened again in the mixer. In order to determine the rheological values of the recipe suspensions, casting mud 1710-1720 gr/lt liter weigh was prepared.

The firing of the prepared carrier refractory bodies was carried out in FORNO CERAMICA brand furnaces in the R&D Center laboratory of Porland Porcelain. Furnace regimes PS1-Std. determined on the basis of the coded prescription. The initial firing temperature for the sintering of the developed carrier refractory bodies was carried out for 18-20 hours at the same temperature (980°C-1000°C) with the biscuit firing applied in standard porcelain production. If the firing range of cordierite is too narrow and the sintering range is exceeded, the formation of a high amount of

liquid phase makes it difficult to bake these products. For the sintering of the recipes prepared within the scope of the study for the second firing; The oven regime with a peak temperature of 1300°C and a peak residence time of 60 minutes was chosen.

Table 7 Grain sizes after grinding of prescription suspensions

Grain size (µm)	D(10)	D(50)	D(90)
PS1-Std.	0.891	6.207	17.628
PS2	0.568	6.103	17.021
PS3	0.680	6.190	17.498
PS4	0.498	5.921	16.213
PS5	1.037	5.879	16.186
PS6	0.464	5.715	15.247
PS7	1.622	5.962	17.863
PS8	0.166	5.671	18.702

In order to determine the physical properties of the prepared bodies, Porland Porselen A.Ş. In the R&D Center laboratory; The drying and firing shrinkage of the samples were measured from the shrinkage rods after sintering and calculations were made according to the formulas in ASTM C-236 standard.

$$Sd = \frac{Lp-Ld}{Lp} x\ 100 \qquad (1)$$

It's here; Sd represents the dry shrinkage percentage (%), Lp represents the length of the wet test product (mm), and Ld represents the length of the test specimen after drying (mm).

$$St = \frac{Lp-Lf}{Lp} x\ 100 \qquad (2)$$

It's here; St firing shrinkage percentage (%) and Lf firing test sample length (mm). Strength measurements of sintered samples were calculated by three-point bending test. Rectangular bending strength formula in ASTM C 974 standard was used to calculate the strength values [16].

$$M = \frac{3PL}{2bd^2} \qquad (3)$$

It's here; M represents the bending strength (MPa), P is the applied load (N), L is the

distance between supports (mm), b is the sample width (mm), and d is the sample thickness (m). Deformation is the bending of the bar during sintering depending on temperature and time. After sintering, deformation bars are placed on millimetric paper and the amount of deformation is calculated. Water absorption test was performed according to BS EN 1217 standard method A and calculations were made. Here; The m^2 shows the weight of the sample after the water absorption test (gr) and the m1 shows the weight of the sample before the water absorption test [2, 17, 18].

$$Water\ Abs.(\%) = \left(\frac{(m_2 - m_1)}{m_1}\right) * 100 \qquad (4)$$

"PS1-Std. and PS8" coded samples; XRF (Rigaku brand, ZSX Primus Model X-Ray Fluorescent device with semi-quantitative chemical analysis) and XRD (Minifleks-600 model, Rigaku brand, X-Ray Diffraction device (2Θ=5°-70°)) analysis were performed. Electron microscope (SEM) analysis was performed on samples coded as

"PS1-Std. and PS8" by the Ceramics Research Center (SAM). For analysis, the surface of the samples was coated with gold (Au) and palladium (Pd), ensuring conductivity, and BSE images were taken and analyzed with elemental distribution (EDX).

3. FINDINGS AND DISCUSSION

Within the scope of the study, a total of 8 carrier refractory bodies recipes with the codes PS1-Std., PS2, PS3, PS4, PS5, PS6, PS7 and PS8 were prepared. The data on the rheological results of the suspensions are given in Table 8. The plasticity water, kneading water, water absorption percentages under vacuum and mechanical properties of dry, biscuit (after the 1st firing) and firing (after the second firing) of the prepared bodies are given in Table 9. Refractory bodies; The thermal expansion coefficients were measured at $\alpha300 \times 10^{-7}$ °C, $\alpha400 \times 10^{-7}$ °C and $\alpha500 \times 10^{-7}$ °C values after sintering in the furnace regime with a peak temperature of 1300 °C and a peak residence time of 60 minutes and are given in Table 10.

Table 8 Rheological values and molding processes of prescription suspensions

Values	PS1-Std.	PS2	PS3	PS4	PS5	PS6	PS7	PS8
Electrolyte amount (%)	0.1	0.1	0.12	0.12	0.12	0.15	0.15	0.15
Liter weight (gr/lt)	1720	1729	1710	1711	1711	1721	1724	1718
Viscosity (sn)	18	17	18	19	19	24	26	26
Thixotropy (sn)	1	1	1	1	1	2	2	2
5 min. flesh thickness (mm)	1.5	1.91	1.93	1.97	1.83	2.09	2.17	2.14

Table 9 Mechanical properties of the developed support refractory bodies

Test Methods	PS1-	PS2	PS3	PS4	PS5	PS6	PS7	PS8
Dry shrinkage (%)	3.1	1.95	2.1	2.5	2.65	2.13	2.4	2.31
Biscuit shrinkage (%)	3.78	2.92	3.2	3.27	3.13	3.64	3.42	3.65
Firing Shrinkage (%)	7.8	3.4	5.6	4.5	6.53	6.7	7.25	6.05
Dry Strength (kg/cm^2)	11.2	12.6	12.5	13.4	12.1	14.75	14.85	15.74
Biscuit Strength (kg/cm^2)	35.7	43.8	47.36	50.7	55.7	66.2	65.87	68.89
Firing Strength (kg/cm^2)	205	227	245	265	365	395	370	415
Deformation (mm)	4	1	1	2	2.5	2	3	2
Plasticity water (%)	25	26	28	27	29	38	37	38
Kneading water (%)	28	30	31	29	32	40	39	39
Water Absorption Vacuum	13	20	18	12	14	15	13	17

Table 10 Thermal expansion coefficients of refractory body samples

Samples	$\alpha\ 300x10^{-7}\ (^oC)$	$\alpha\ 400x10^{-7}\ (^oC)$	$\alpha\ 500x10^{-7}\ (^oC)$
PS1-Std.	34.2	37.6	37.7
PS2	30.5	31.2	33.6
PS3	27.5	28.2	29.3
PS4	27.8	29.2	30.2
PS5	27.5	28.2	29.2
PS6	26.6	27.3	28.2
PS7	26.4	27.3	28.0
PS8	26.7	27.7	28.8

In a cordierite mixture consisting of clay, talc and alumina, at temperatures higher than 1250 °C, clay and talc transform into mullite and protoenstatite (MgO.SiO2). Later, cordierite phase is formed between 1250-1430°C from the combination of mullite and protoenstatite with alumina. In the formation of cordierite phase, both mullite and protoenstatite are exposed as SiO2 in the structure. However, alumina and MgO are only released from mullite and protoenstatite, where mullite plays the main role in cordierite formation. Because Al2O3 is the main component in cordierite formation compared to MgO. The coefficient of thermal expansion is more sensitive to MgO change than other ingredients [14].

Thermal expansion coefficient measurements of refractory samples are given in Table 10.

According to Table 6; "PS1-Std." Talc raw material, which is used at the rate of 20.79% in the recipe composition, has been increased to 21.18% in the PS8 recipe. According to Table 5; It is seen that talc raw material contains 24.84% MgO according to its chemical composition. According to Mayer and Havas, it is known that the average coefficient of thermal expansion of MgO is 0.1x10-7°C-1. The percent increase in the MgO ratio in the PS8 coded recipe composition explains the decrease in the thermal expansion coefficient indicated in Table 10 [19]. PS1-Std. coded refractory body and PS8 coded refractory bodies are given comparatively in XRF (X-Ray Fluorescence) Table 11., XRD (X-Ray Diffraction) patterns are given comparatively in Graph 1.

Table 11 After sintering PS1-Std. and chemical analyses of PS8 coded refractory bodies (XRF)

(%)	SiO₂	Al₂O₃	Na₂O	MgO	CaO	TiO₂	Fe₂O₃	ZrO₂	ZnO	K₂O	P₂O₅	HfO₂	A.Z.
PS1Std	47.15	43.25	0.59	6.81	0.27	0.10	0.48	0.00	0.00	1.03	0.07	0.00	0.25
PS8	43.06	40.56	0.00	7.07	0.36	0.11	0.56	6.02	1.24	0.59	0.07	0.16	0.20

After the sintering process, indialite, corundum, quartz and mullite common phases were determined according to the XRD analysis results of the "PS1-Std. and PS8" coded refractory samples. Due to the addition of 8.47% zircon in the PS8 coded refractory body recipe, a different zircon phase was detected in the XRD analysis. For this reason, zircon phase was observed in the phase analysis of the PS8 coded body, different from

the standard body. In the literature, studies on the observation of corundum and quartz phase are mentioned as follows; "The cordierite phase starts to form around 1200 °C, but rather than forming alone, corundum, enstatite, fosterite, spinel, anorthite and quartz phases are encountered with this phase depending on the operating conditions, and therefore, thermal expansion coefficients are obtained at high values" [20-23].
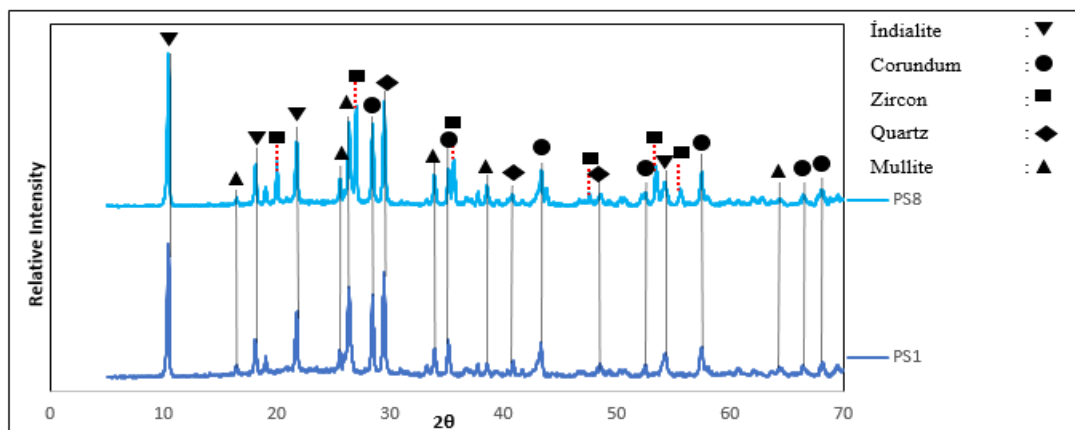
Graph 1 XRD diffraction patterns of refractory samples coded "PS1-Std" and "PS8" after sintering

In Graph 1, the microstructure images taken from the cross-sectional area of the PS1-Std coded and PS8 coded refractory samples, which were sintered in the furnace regime with a peak of 1300°C and a dwell time of 60 minutes, are given. While mullite crystals are clearly observed in the microstructure images of the PS1-Std coded refractory sample, with the addition of zircon in the PS8 coded refractory structure; Zircon appears as dispersed phases in a mullite matrix.

SEM (Scanning Electron Microscope) images of PS1 and PS8 coded samples; BSE (Reflected Electron) cross-sectional surface images are given in Figure 1. EDX analysis was applied to determine the elemental compositions in selected areas of the samples whose surface and cross-section images were given. Images of the regions selected for EDX analysis are given in Figure 2 and Figure 3. Elemental distributions are given in Table 12 and Table 13.
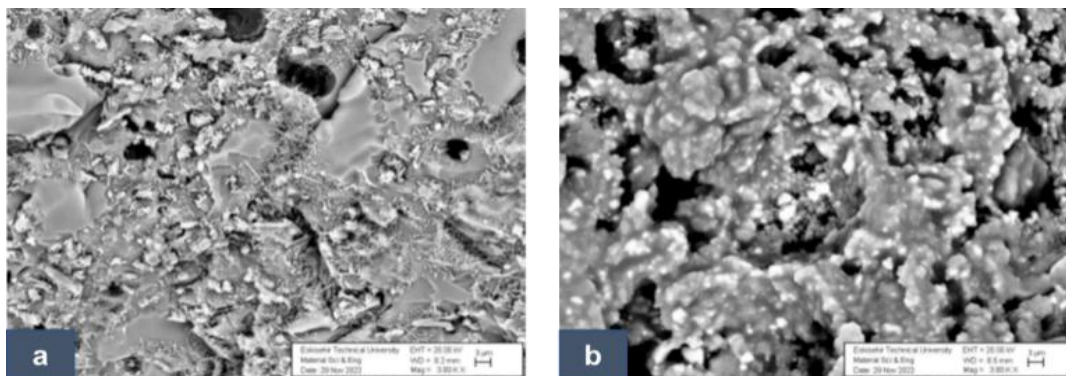
Figure 1 PS1-Std. and SEM analysis images of PS8 coded refractory samples; a) 3.00KX BSE image taken from the fracture surface of the PS1-Std coded sample, b) 3.00KX BSE image taken from the fracture surface of the PS8 coded sample

Kumar et al. in their study named "Processing and characterization of pure cordierite and zirconia-doped cordierite ceramic composite by precipitation technique"; There are two types of cordierite ceramics, porous and dense. Porous cordierite ceramic has much better thermal shock properties than dense one, but has poor mechanical resistance. In the study of Kumar et al., with the addition of pure cordierite (MgO: 13.8% wt., Al_2O_3: 34.8%

wt., SiO_2: 51.4% wt.) and zirconia at the rate of 5-20% by weight it is understood that the mechanical and thermal properties of the samples are improved in direct proportion. When the PS1-Std and PS8 coded refractory samples are examined, it is seen that both bodies have a porous structure. In the microstructure images of the PS8 coded refractory sample, dark grains represent

alumina and white grains represent zircon grains.

In the SEM images of both samples, three points were selected from the surface and EDX analysis was applied to determine their elemental distribution. PS1-Std the EDX analysis of the coded refractory sample is given in Figure 2 and the ele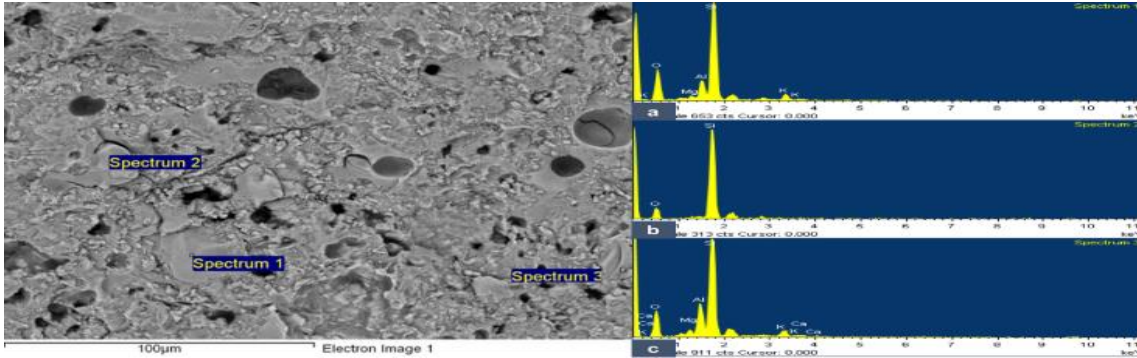mental analyses of the selected points are given in Table 12 the EDX analysis of the PS8 coded refractory sample is given in Figure 3 and the elemental analyses of the selected points are given in Table 13 [24].
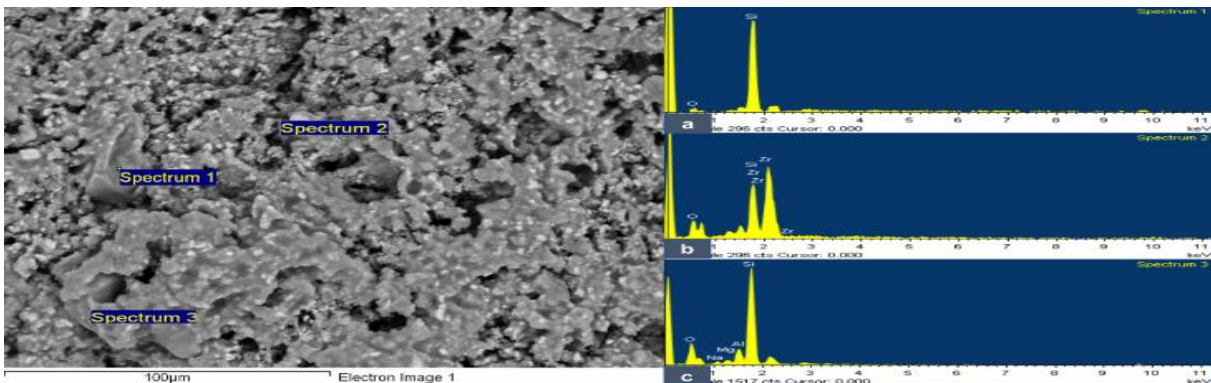

Figure 2 PS1-Std. SEM image of the coded refractory sample and three points selected for EDX analysis on the image; a) Spectrum 1, b) Spectrum 2 and c) Spectrum 3

PS1-Std. whose SEM images are given in Figure 1 a) within the refractory; black areas indicate that the sample has a porous structure. According to the EDX analysis of the points selected according to Table 12; It is seen that there is an elemental distribution forming the corundum, mullite, indialite and quartz phases. PS1-Std in the surface image of the refractory sample, acicular structures are more prominently seen. PS1-Std. XRD phase analysis and EDX analysis results of the sample confirm the formed phases.

Table 12 PS1-Std EDX analyses of selected points on the SEM image of coded refractory samples

	Spectrum1		Spectrum2		Spectrum3	
	Wt.%	A.W %	Wt. %	A.W %	Wt. %	A.W %
Mg	01.17	00.98	00.00	00.00	01.43	01.19
Al	06.23	04.70	00.00	00.00	08.28	06.25
Si	38.50	27.90	46.70	33.30	36.50	26.50
K	03.21	01.67	00.00	00.00	02.51	01.30
O	50.80	64.70	53.20	66.60	50.60	64.40
Ca	00.00	00.00	00.00	00.00	00.54	00.27

Figure 3 PS8. SEM image of the coded refractory sample and three points selected for EDX analysis on the image; a) Spectrum 1, b) Spectrum 2 and c) Spectrum 3

Within the PS8 coded refractory whose SEM images are given in Visual 1.b; black areas indicate that the sample has a porous structure. According to the EDX analysis of the points selected according to Table 12; It is seen that the phases that may occur are the elemental distribution forming the corundum, mullite, indialite, quartz and zircon phases. In Figure 1 b) PS8 in image. The reason why acicular and curved structures supporting primary or secondary mullite formation cannot be seen in the surface image of the refractory sample is due to the fact that zirconium dioxide forms a homogeneous structure on the mullite phases.

In Figure 2, PS1-Std. SEM image of the coded refractory sample is given. EDX analysis results of 3 different points selected on the relevant SEM image are given in Table 12. PS1-Std. When the XRD analysis of the refractory sample is examined; It is observed that indialite, corundum, quartz and mullite phases are formed. It is seen that the indialite phases are homogeneously distributed as small white grains. The structures displayed as blocks between the grains represent the quartz phase. Acicular mullite crystals are observed between quartz grains and indialite structures. In Figure 3, white dots represent ZrO_2, black dark regions represent pores and dark gray regions represent Al_2O_3 (corundum) grains. The XRD phase analysis of the PS8 coded sample confirms the phases formed when it is examined in terms of elemental analysis according to the EDX analysis results. In the patent study of Avedikian and his colleagues named "Sintered refractory product with improved resistance to thermal shocks"; "Mullite-zirconium dioxide grain is understood as a refractory grain in which chemical analysis obtained by sintering or melting reveals the presence of mostly (Al_2O_3), silica (SiO_2) and zirconium dioxide (ZrO_2); silica and alumina are available in the form of $2SiO_2$-$3Al_2O_3$ (mullite). Therefore, alumina (Al_2O_3), silica (SiO_2) and zirconium dioxide (ZrO_2) are the three main components by weight of a mullite – zirconium dioxide particle." have stated [25].

Table 13 PS1-Std. EDX analyses of selected points on the SEM image of coded refractory samples

	Spectrum 1		Spectrum 2		Spectrum 3	
	Wt. %	A.W. %	Wt. %	A.W. %	Wt. %	A.W. %
Si	46.70	33.30	15.10	16.50	39.80	28.40
O	53.30	66.70	35.00	66.72	51.70	64.90
Zr	00.00	00.00	49.90	16.78	00.00	00.00
Na	00.00	00.00	00.00	00.00	01.50	01.39
Mg	00.00	00.00	00.00	00.00	01.61	01.33
Al	00.00	00.00	00.00	00.00	05.39	03.98

4. RESULTS

In the study, in order to prevent deformation during sintering in bone porcelain products, bone porcelain is fired on a refractory carrier called sagar, which has a low thermal expansion coefficient and does not cause shrinkage or deformation problems during firing. In this study, it is aimed to develop a formulation as an alternative to the imported carrier saggars in bone porcelain production. Based on the chemical composition of cordierite, it is very difficult to develop cordierite as a ceramic material using only raw materials.

There are two main reasons for this. The multiplicity of eutectic points and the difficulty of approaching equilibrium. Since the eutectic points are very close to each other, even the slightest deviation from the actual composition causes melting or the formation of unwanted phases. During firing, cordierite compositions show short firing intervals. That is, due to the proximity of various eutectic points, the amount of liquid increases rapidly and it is difficult for the structure to turn into a glassy state. The firing interval can be increased by adding some melting additives to the body.

In this study, PS1-Std. standard refractory recipe and PS2, PS3, PS4, PS5, PS6, PS7 and PS8 coded recipes were prepared. To the prepared prescription suspension; viscosity, thixotropy and 5 min. At the end of the period, wall thickness controls were carried out and rheological properties were determined. At this stage, the problem of sticking to the mold was observed in the PS2, PS3, PS4 and PS5 refractory casting mud suspensions prepared to improve the standard recipe. Therefore, in the continuation of the study, 0.42% bentonite addition was applied in PS6, PS7 and PS8 recipes. In order to determine the mechanical properties of PS6, PS7 and PS8 coded refractory bodies whose rheological properties are accepted within the criteria; shrinkage percentage, strength, deformation and water absorption under vacuum (%) tests were carried out. When comparing the three recipes developed, it was seen that the PS8 recipe was advantageous in terms of its mechanical properties. Dry shrinkage is 2.31%, biscuit shrinkage is 3.65% and baking shrinkage is 6.05%. The strength values obtained in terms of strength values were measured as PS1-Std < PS2 < PS3 < PS4 < PS5 < PS6 < PS7 < PS8. As it is known from the literature, porous refractories have higher thermal properties. For this reason, the high-water absorption value of the PS8 coded refractory sample was evaluated as positive in terms of its thermal properties.

Imported equivalent carrier sagar refractories are used against the PS8 coded carrier refractory body to preserve their mechanical and microstructural properties; The water absorption rate of the equivalent hose under vacuum is between 9.8-17% and its dry strength is specified as 10-15 kg/cm^2. If chemical analyses (XRF) of equivalent products are in charge; It is seen that SiO_2 expanded in the range of 16.82-50.03 percent (%) and Al_2O_3 expanded in the range of 40.41-81.45 percent (%). It is seen that the product of the Al_2O_3/SiO_2 ratio in the composition is called sagar, cordierite or mullite cordierite as superiority in Table 3. It is seen that the dry strength of the PS8 coded final product developed is 15.74 kg/cm^2 according to Table 9.

The water absorption under vacuum was measured as 17%. PS8 coded contents obtained after sintering were designed as 43.06% SiO_2 and 40.56% Al_2O_3 according to Table 11 in the chemical analysis of sagar refractory body bodies. In order to configure the mechanical properties of the cavities in the structure, 8.47% zircon was added to the PS8 coded recipe. In PS7 and PS8 coded prescriptions, improvement in mechanical properties is observed with the addition of zircon. In the study, the improvement in mechanical properties with the addition of zircon was supported by the appearance and microstructure of the mullite phase formed by XRD, SEM and EDX analyses in both structures. The developed refractory body can be shaped according to different bone porcelain product forms and used as a bearing refractory. It has been observed that the bearing refractory products for the bone porcelain firing process developed as a result of the project offer a 10% longer service life compared to the equivalent refractory products that were imported and used in production before the project.

The Declaration of Conflict of Interest/ Common Interest
No conflict of interest or common interest has been declared by the author.

The Declaration of Ethics Committee Approval

The author declares that this document does not require an ethics committee approval or any special permission.

The Declaration of Research and Publication Ethics

The author of the paper declares that he complies with the scientific, ethical, and quotation rules of SAUJS in all processes of the paper and that he does not make any falsification on the data collected. In addition, he declares that Sakarya University Journal of Science and its editorial board have no responsibility for any ethical violations that may be encountered and that this study has not been evaluated in any academic publication environment other than Sakarya University Journal of Science.

REFERENCES

[1] P. Rado, An Introduction to the Technology of Pottery, 2nd edition du., England: Oxford, 1988.

[2] The British Standards Institution, "Domestic and hospitality use ceramic tableware articles intended for contact with foodstuffs." BS8654:2015.

[3] P. Rado, Bone China, Ceramic Monographs Handbook of Ceramics, Verlag Schmid GmbH Freiburg, 1981.

[4] F. Gungor, «Investigation of pyroplastic deformation of whitewares: Effect of cyrstal phases in the "CaO" based glassy matrix,» Ceramics International, vol. 44, no. 11, pp. 13360-13366, 2018.

[5] O. Turkmen, A. Kucuk, S. Akpınar, "Effect of wollastonite addition sintering of hard porcelain" Ceramics International, cilt 41, no. 4, pp. 5505-5512, 2015.

[6] S. Ke, X. Cheng, Y. Wang, Q. Wang, H. Wang, "Dolomite, Wollastonite, and Calcite as Different CaO Sources in Anorthite based Porcelain" Ceramics International, cilt 39, no. 5, pp. 4953-4960, 2013.

[7] S. Kurama, E. Ozel, "The Influence of Different CaO Source in the Production of Anorthite Ceramics" Ceramics International, cilt 35, no. 2, pp. 827-830, 2009.

[8] F. Ceylan, "Anorthite Phase Production and Industrial Applications" Graduate School of Natural and Applied Sciences, Kütahya, 2011.

[9] M. Kosecavus, "Anorthite Synthesis and Characterization from Volcanic Tuff" Graduate School of Natural and Applied Sciences, Ankara, 2007.

[10] S. K. Das, K. Dana, N. Snight, R. Sarkar, "Shrinkage and Strenght Behaviour of Quartzitic and Kaolinitic Clays in Wall Tile Compositions" Applied Clay Science, cilt 29, pp. 137-143, 2005.

[11] J. S. Reed, Introduction to the Principles of Ceramic Processing, Newyork, John Wiley & Sons Inc, 1995, p. 486.

[12] D. Stookey, N. Y. Corning.Patent: U. S. Patent 3241935, 22 March 1966.

[13] H. Soyhan, "Investigation of Shape Changes of Ceramics During the Sintering Process" Graduate School of Natural and Applied Science, İstanbul, 2007.

[14] B. P. Saha, R. Johnson, "Thermal Anisotropy in Sintered Cordierite Monoliths" Materials Chemistry and Physics, no. 67, pp. 145-150, 2001.

[15] T. Bahtlı. Turkey Patent: 2017/10403, 2017.

[16] American Society for Testing and Materials, Standart Test for Drying and

Firing Shrinkages of Ceramics Whiteware Clays.*, ASTM, 2018.

[17] American Society for Testing and Materials, Standart Test for Flexural Properties of Ceramics Whiteware Materials- ASTM-C674*, ASTM, 2018.

[18] The British Standards Institution, Materials and Articles in Contact with Foodstuffs - Test Method for Water Absorption of Ceramics Articles, BSI, 1998.

[19] Mayer and Havas, "Coefficient Expansion of Enamels and Their Chemical Composition" Sprechsaal, 42, 497; 44, 188, 207, 220.

[20] J. P. F. Grilo, H. P. A. Alves, A. J. M. Araujo, R. M. Andrade, R. P. S. Dutra, D. A. Macedo, "Dielectric and electrical properties of a mullite/glass composite from a kaolinite clay/mica-rich kaolin waste mixture" Cerâmica, vol. 65, pp. 117-121, 2019.

[21] E. Gunay, "Sintering Behavior and Properties of a talc-based cordierite composition with boron oxide additions" Journal of Ceramic Processing Research, vol. 11, no. 5, pp. 591-597, 2010.

[22] E. Gunay, "Sintering Behavior and Properties of Sepiolite Based Cordierite Compositions with added Boron Oxide" Turkish Journal of Engineering and Environmental Sciences*, vol. 2, no. 35, pp. 83-92, 2011.

[23] L. J. Trumbulovic, Z. Acimovic, S. Panic, L. J. Andri, "Synthesis and Characterization of Cordierite from Kaolin and Talc for Casting Application" FME Transactions, vol. 31, no.1, pp. 43-47, 2003.

[24] M. S. Kumar, "Processing and Characterization of Pure Cordierite and Zirconia-doped Cordierite Ceramic Composite by Precipitation Technique"" Bulletin of Material Science, vol. 38, no. 3, pp. 679-688, 2015.

[25] R. Avedikian, C. His, T. Champion, M. Bobo. France Patent: EP06808197.5, 2017.

Title: Radon Gas Estimation from Building Materials

Authors: Safa BAŞDEMİR, Caner YALÇIN

Radon Gas Estimation from Building Materials

Safa BAŞDEMİR[1] (iD) Caner YALÇIN*[1] (iD)

Abstract

Radon gas originating from building materials is generally thought to cause low concentration. Investigation and estimation of radon levels originating from building materials are important in terms of public health due to the use of dense concrete in tunnel form type houses, which is a building type widely used in Turkey, even though a significant part of Turkey is an earthquake zone. In this article, the effects of different parameters such as ^{238}U concentration in building materials, diffusion constant of building elements, emanation rate, and ventilation rate on radon gas concentration are investigated. As a result, it is concluded that in some cases (such as high diffusion coefficient and insufficient ventilation rate) in houses built with tunnel form concrete structures, the radon level arising from building materials can reach a level that cannot be neglected.

Keywords: Radon, emanation rate, diffusion coefficient, exhalation rate, concrete

1. INTRODUCTION

Approximately 85% of the radiation that people are exposed to is of natural origin and 15% is artificial. Approximately 50% to 60% of this natural radiation exposure is due to radon gas [1-2]. Radon gas is the radioactive gas resulting from the decay of the ^{238}U isotope. The half-life of radon gas (^{222}Rn) is 3.8235 days [3]. It is a colorless, odorless, tasteless gas that we cannot detect with our senses [4].

Radon gas causes very serious problems for human health. There is strong evidence that lung cancer can occur as a result of exposure to radon and radon decay products in indoor environments, and that it is the second most important cause of cancer after smoking, according to a report published by the International Commission on Radiological Protection (ICRP) and the World Health Organization (WHO) [5-6]. The International Commission on Radiological Protection (ICRP) specified the maximum amount of radon gas that should be present in the indoor environment as 200-300 (Bq m^{-3}) in 2007, while the Turkish Atomic Energy Authority (TAEK) accepted 400 (Bq m^{-3}) as the limit value. In Sweden, the limit value is 200 (Bq m^{-3}) [7]. The United States Environmental Protection Agency (EPA) specified that the amount of radon generated should be below 148 (Bq m^{-3}). It also states that radon levels below this value still pose a risk [8]. The World Health Organization (WHO) recommends a limit level of 100 (Bq m^{-3}) to

* Corresponding author: caner.yalcin@kocaeli.edu.tr (C. YALÇIN)
[1] Kocaeli University
E-mail: safabasdemir@gmail.com
ORCID: https://orcid.org/0009-0009-3599-5785, https://orcid.org/0000-0002-3105-7267

minimize the health hazards caused by radon gas indoors [6].

In 1984, TAEK (Turkish Atomic Energy Authority) started a study to determine radon levels in homes, and as a result of this study (completed in 2004), the average radon level was found to be around 35 ± 12 (Bq m^{-3}) [4]. When the radon activity concentration is compared with the results of the literature reviews, it has been shown that the average radon level of Turkey is 81 (Bq m^{-3}) [9].

When the literature reviews on radon measurements in homes are examined [9-12], it is stated that the ground floors are at risk in general. The reason for this is the high amount of radon gas leaking from the soil to the houses.

However, radon gas is found not only in soil but also in building materials. Studies have shown that there are uranium and thorium isotopes in different building materials such as sand, cement, or brick [13]. However, in the literature reviews, it is stated that the radon concentration originating from the building materials is low in the apartments on the upper floors of the buildings. In this article, in order to test this general opinion, radon gas originating from building materials will be estimated in buildings made with building materials with different radiation levels and properties.

1.1. Radon in Soil and Rocks

Uranium and thorium elements, which are a part of the earth's make-up, are abundant in soil and rocks. Thorium and radium appear during the radioactive decay series of ^{238}U, which is in the soil. Radium diffuses into the upper layers of the soil. ^{226}Ra isotope, which has a half-life of 1600 years, decays continuously in the soil. As a result of this decay, radon atoms are formed, allowing radon to be found freely in the soil [14]. The radon concentration in the soil depends on the radioactivity mass concentration of the radium in the soil, its diffusivity, and the type of soil [15].

1.2. Effect of Radon on Human Health

Radon forms radioactive aerosols by clinging to dust and water droplets in the air. These dust and water droplets are retained by the lungs through respiration. The energy released during the decay of these radioactive particles trapped by the lungs damages the lung tissue. As a result of this damage, it causes cancer [14].

According to the National Radiological Protection Board (NRPB), at least 2500 of the 41,000 lung cancers in the UK annually are attributable to radon. The International Commission on Radiological Protection (ICRP) attributes 10% of total lung cancers to radon [16].

2. MATERIALS AND METHODS

2.1. Sample Room Model

There are many different types of buildings around the world. The tunnel form method is a steel formwork system that allows the load-bearing wall and slabs to be poured at once. When the formwork is removed, the upper concrete slab forms, while the side concretes form reinforced concrete shear walls.

The sample room model shown in Figure 1 was used to investigate the radon concentration from construction materials. It is assumed that all the walls of the room are laid with concrete 10 cm thick. Our sample room is 3x3x2.8 m in size and has a floor area of 9 m^2 and a volume of 25.2 m^3. Calculations were made when the room had a window and a door and no objects in it. In an average house, about 10% of the volume of the room is occupied by furniture. It should be taken into account that this situation will increase the radon concentration at the same rate.
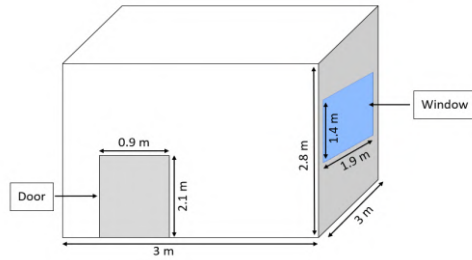
Figure 1 Sample room model made with tunnel form

2.2. Theoretical Framework

2.2.1. Emanation rate

Not all of the radium atoms in porous materials can escape into the space around the pores. Emanation Rate is the rate at which the radium atoms in the material escape into the space of the pores of the material.

The fraction of emanation, f, is equal to the ratio of the rate of emanation and the production rate of Radon. The fraction of emanation is shown in equation (1).

$$f = \frac{E}{A_{Ra}} \tag{1}$$

Where E is the rate of radon production inside the sample and A_{Ra} (Bq kg^{-1}) is the radium activity. The highest fraction of emanation from the soil is 20% [17].

As a result of the studies for concrete, the fraction of emanation produces different results between 0.07 and 0.14. These studies show that the fraction of emanation average value is 0.11 ± 0.02 [18].

2.2.2. Exhalation rate

Exhalation Rate is defined as the number of radon atoms escaping from the sample towards the medium per unit of time.

Radon is transported from the wall into the room by diffusion. Diffusion is the most basic mechanism described by Fick's law. Simplifying the definition in the first theory of Fick's law, it can be considered a one-

dimensional equation. The one-dimensional form of the first theory of Fick's law is given in equation (2).

$$J = -D\frac{\partial C}{\partial Z} \tag{2}$$

Where J is the radon flux (Bq m^{-2} s^{-1}), D is the radon diffusion coefficient (m^2 s^{-1}), $\partial C/\partial Z$ is the concentration gradient (Bq m^{-3}) [19].

The radon diffusion in the material varies depending on factors such as the porosity of the material found and the particle size. It is stated that the diffusion constant of concrete is between 10^{-10} (m^2 s^{-1}) and 10^{-6} (m^2 s^{-1}) [17].

If equation (2) is solved, the exhalation rate can be calculated by equation (3) below.

$$E = \frac{2 \cdot C_{SC} \cdot l \cdot \lambda}{e^{d/l} - e^{(-d/l)}} \tag{3}$$

Where E is the exhalation rate (Bq m^{-2} h^{-1}), C_{SC} is the average concentration in the wall (Bq m^{-3}), l is the radon diffusion length (m), and d (m) is the thickness of the wall.

The radon diffusion length is given in equation (4).

$$l = (D/\lambda_{Rn})^{1/2} \tag{4}$$

Where l is the radon diffusion length (m), D is the radon diffusion coefficient (m^2 s^{-1}), λ_{Rn} is the radon decay constant ($2.11 \cdot 10^{-6}$ s^{-1}) [20].

2.2.3. Radon concentration

When t→∞, the radon concentration in the room is shown in equation (5) [21].

$$C_\infty = \frac{\sum_{i=1}^{6} E_i \cdot A_i}{(\lambda_{Rn} + \lambda_v)V_{room}} \tag{5}$$

Where C_∞ is the radon concentration in the room (Bq m^{-3}), $i = 1, 2, 3, 4, 5, 6$ are surfaces in the room, E$_i$ is the exhalation rate, A_i is the surface area (m^2), λ_{Rn} is the radon decay constant (h^{-1}), λ_v is the ventilation rate (h^{-1}).

In the absence of t→∞, the radon concentration at different time intervals is shown by equation (6) [17].

$$C(t) = C_\infty(1 - e^{-(\lambda_{Rn}+\lambda_v)t})$$ (6)

3. RESULT AND CONCLUSIONS

The given equations show that the radon gas that will accumulate in the room varies depending on factors such as the diffusion coefficient, the radium concentration in the wall concrete, the emanation rate, the wall thickness, the ventilation rate, the volume, and the surface area. According to the different values of these variables, the radon concentration accumulated in the sample room model was calculated. In all calculations, it has been assumed that the radon concentration in the room is zero and the only contribution to the radon concentration that will accumulate in the room comes from the building materials.

As a result of the calculations, it was seen that the changes in the ACH (air changes per hour) value greatly affect the radon concentration that will occur in the environment. Table 1 shows how the radon concentration that will occur in the environment changes under different concentration values of ACH by keeping the diffusion coefficient 10^{-8} ($m^2 s^{-1}$) and the fraction of emanation 0.11.

Table 1 Radon concentration resulting from the change of ACH values

C_{Ra} (Bq/kg)	ACH (h^{-1})				
	0.1	0.2	0.3	0.4	0.5
10	14	9	7	6	5
50	61	33	23	18	15
100	120	63	44	33	27
150	179	94	64	49	40

For figure 2, the diffusion constant 10^{-8} ($m^2 s^{-1}$), and the fraction of emanation 0.11 are kept constant. With this constant value, it is shown how the ACH value changes with time by taking 0, 0.1, 0.2, 0.3, 0.4 and 0.5 respectively.
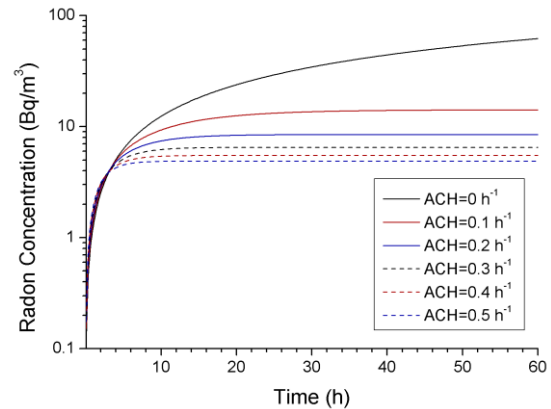

Figure 2 Variation of the effect of different ACH values on radon concentration with time

As seen in Figure 2, the radon concentration reaches its maximum level in a very short time (approximately 10 h).

While keeping diffusion coefficient at 10^{-8} ($m^2 s^{-1}$) and ACH = 0.1 (h^{-1}) rates constant, according to different radium concentration values (10, 20, 30, 40, 50, 75, 100, 125, 150 (Bq kg^{-1}), radon concentrations to accumulate in the room were calculated. As a result of these calculations, radon concentrations were found as, in order, 14.18, 25.18, 37.75, 49.53, 61.31, 90.77, 120.23, 149.68 and 179.14 (Bq m^{-3}).

As mentioned in the fraction of emanation section, the fraction of emanation rate in concrete varies between 0.07 and 0.14 [18]. While keeping the diffusion coefficient constant at 10^{-8} ($m^2 s^{-1}$), radium concentration 50 (Bq kg^{-1}), and ACH = 0.1 (h^{-1}), according to different fractions of emanation 0.07, 0.08, 0.09, 0.10, 0.11, 0.12, 0.13, 0.14 radon concentrations to accumulate in the room were calculated. As a result of these calculations, radon concentrations were found as 39.89, 45.25, 50.60, 55.96, 61.31, 66.67, 72.03, and 77.38 (Bq m^{-3}).

In order to calculate the minimum radon concentration to accumulate in our room model, when we take the diffusion coefficient

as 10^{-9} (m^2 s^{-1}), ACH 0.5 (h^{-1}), fraction of emanation 0.07, and radium concentration 10 (Bq kg^{-1}), the radon concentration was found to be 2.55 (Bq m^{-3}). Similarly, in order to calculate the maximum radon concentration to accumulate in our room model, when we take the diffusion coefficient as 10^{-8} (m^2 s^{-1}), ACH 0.1 (h^{-1}), fraction of emanation 0.14, and radium concentration 150 (Bq kg^{-1}), the radon concentration was found to be 227.34 (Bq m^{-3}).

The radon concentration accumulated in the room varies depending on the diffusion coefficient, ventilation rate, fraction of emanation, and the radium (^{238}U) concentration in the concrete. It has been observed that in some cases, it can contribute to the accumulation of radon gas in houses built with the tunnel form, where the use of concrete is high. It has been observed that radon concentrations above 100 Bq, which is specified as the upper limit by WHO, may occur in the total radon concentration in the room, especially in cases where the ventilation rate is low. In order to minimize this situation, it is important to investigate building materials such as sand, cement, and concrete to be used during the construction of the building, to determine their concentration values and to predict the amount of radon that will contribute to the environment.

Funding
The authors has no received any financial support for the research, authorship or publication of this study.

Authors' Contribution
The authors contributed equally to the study.

The Declaration of Conflict of Interest/ Common Interest
No conflict of interest or common interest has been declared by the authors.

The Declaration of Ethics Committee Approval
This study does not require ethics committee permission or any special permission.

The Declaration of Research and Publication Ethics
The authors of the paper declare that they comply with the scientific, ethical and quotation rules of SAUJS in all processes of the paper and that they do not make any falsification on the data collected. In addition, they declare that Sakarya University Journal of Science and its editorial board have no responsibility for any ethical violations that may be encountered, and that this study has not been evaluated in any academic publication environment other than Sakarya University Journal of Science.

REFERENCES

[1] M. Y. Shoeib, K. M. "Thabayneh, assessment of natural radiation exposure and radon exhalation rate in various samples of Egyptian building materials," Journal of Radiation Research and Applied Sciences, vol. 7, no. 2, pp. 174-181, 2014.

[2] S. U. Duran, B. Küçükömeroğlu, "Karadeniz teknik üniversitesi kanuni kampüsü'nde bazı ofislerde radon gazı ölçümü ve çevrelerindeki topraklarda radyonüklid seviyeleri," BE Fen Bilimleri Dergisi, vol. 9, no.1, pp. 68-77, 2020.

[3] NNDC [Online]. Available: https://www.nndc.bnl.gov/nudat2/

[4] M. E. Kürkçüoğlu, G. Bayraktar, "Süleyman demirel üniversitesi'nde bina içi radon konsantrasyonlarinin nükleer iz dedektörleri kullanilarak belirlenmesi," Süleyman Demirel Üniversitesi Fen Bilimleri Enstitüsü Dergisi, vol. 16, no. 2, pp. 167-183, 2012.

[5] S. Y. Baş, S. A. Selçuk, "Binalarda radon gazi etkisinin azaltilmasina yönelik alinabilecek önlemler üzerine bir değerlendirme," 3rd International Symposium on Innovative Approaches

in Scientific Studies, Ankara, Turkey, 2019, pp. 207-212.

[6] H. Zeeb, F. Shannoun, WHO handbook on indoor radon: a public health perspective. France: World Health Organization, 2009.

[7] Y. Örgün, N. Çelebi, "Radyasyon, radon ve toplum sağliği," TMMOB Jeoloji Mühendisleri Odası, vol. 2016/1, 2016.

[8] United States Environmental Protection Agency. (2016). A citizen's guide to radon [Online]. Available: https://www.epa.gov/sites/default/files/2016-12/documents/2016_a_citizens_guide_to_radon.pdf

[9] N. Celebi, B. Ataksor, H. Taskın, N. A. Bingoldag, "Indoor radon measurements in Turkey dwellings," Radiation Protection Dosimetry, vol. 167, no. 4, pp. 1-7, 2014.

[10] O. Günay, S. Aközcan, F. Kulalı, "Bina içi radon konsantrasyonlarının belirlenmesi," Avrupa Bilim ve Teknoloji Dergisi, vol. 13, pp. 91-97, 2018.

[11] F. Kulalı, O. Günay, S. Aközcan, "Determination of indoor radon levels at campuses of Üsküdar and Okan universities," International Journal of Environmental Science and Technology, vol. 16, no. 9, pp. 5281-5284, 2019.

[12] O. Günay, S. Aközcan, F. Kulalı, "Measurement of indoor radon concentration and annual effective dose estimation for a university campus in Istanbul," Arabian Journal of Geosciences, vol. 12, no. 5, pp. 171, 2019.

[13] N. Sharmar, H. S. Virk, "Exhalation rate study of radon/thoron in some building materials," Radiation Measurements, vol. 34, no. 1-6, pp. 467-469, 2001.

[14] S. S. Ozan, C. E. Ekinci, "Yapılarda radon fenomeni ve radon-sağlık ilişkisi," e-Journal of New World Sciences Academy Engineering Sciences, vol. 6, no. 4, pp. 1590-1602, 2011.

[15] F. Tufaner, "Doğal radon emisyonunun insan sağlığına etkileri ve alınması gereken tedbirler," Graduation Project, Dept. Environ. Eng., Yıldız Teknik Univ., İstanbul, 2015.

[16] E. Dursun, "Rize ilinde akciğer kanserli bireylerin evlerinde radon gazı ölçümleri ve akciğer kanseri radon gazi ilişkisi," Master, Dept. Phys., Recep Tayyip Erdoğan Univ., Rize, 2016.

[17] C. E. Andersen, Radon-222 exhalation from Danish building materials: H + H Industri A/S results. Roskilde, Denmark: Risø National Laboratory, 1999.

[18] B. K. Sahoo, B. K. Sapra, J. J. Gaware, S. D. Kanse, Y. S. Mayya, "A model to predict radon exhalation from walls to indoor air based on the exhalation from building material samples," Science of the Total Environment, vol. 409, no.13, pp. 2635-2641, 2011.

[19] M. İçhedef, "Controlled laboratory experiments on radon diffusion coefficient," Sakarya University Journal of Science, vol. 23, no. 3, pp. 308-312, 2019.

[20] B. Ruvira, B. García-Fayos, B. Juste, J. M. Arnal, G. Verdú, "Experimental estimation of the diffusion coefficient in radon barrier materials based on ISO/TS 11665-13:2017," Radiation

Physics and Chemistry, vol. 193, pp. 109993, 2022

[21] N. Chauhan, R. P. Chauhan, M. Joshi, T. K. Agarwal, P. Aggarwal, B. K. Sahoo, "Study of indoor radon distribution using measurements and CFD modelling," Journal of Environmental Radioactivity, vol. 136, pp. 105-111, 2014.

Title: Potential Health Risks of Chloroacetanilide Herbicides: An In Silico Analysis

Authors: Ahmet Ali BERBER, Şefika Nur DEMİR, Nihan AKINCI KENANOĞLU

Potential Health Risks of Chloroacetanilide Herbicides: An In Silico Analysis

Ahmet Ali BERBER[1] (iD), Şefika Nur DEMİR[*2] (iD), Nihan AKINCI KENANOĞLU[3] (iD)

Abstract

The extensive use of herbicidal products in agriculture and forestry has raised concerns over potential adverse effects on human health and the environment. Chloroacetanilide herbicides are a group of synthetic chemicals used to control weeds in agriculture and forestry. However, so[me of their members have been characterized as possible carcinogens. The genotoxicity and carcinogenicity of two chloroacetanilide herbicides, delachlor and xylachlor, are discussed. This article proposes to use tools to predict their potential toxicities based on their chemical structure. Four software tools, Vega Hub, Toxtree, Lazar, and TEST, are used to predict the potential genotoxic and carcinogenic effects of the herbicides. Vega Hub uses QSAR models, Toxtree uses a decision tree approach, Lazar uses data mining algorithms, and TEST uses QSAR methods to estimate toxicity. The canonical Simplified Molecular Input Line Entry Specification (SMILES) systems of delachlor and xylachlor are entered into each software tool to create a prediction. The study found that delachlor and xylachlor is a class 3 highly toxic compounds with potential mutagenic and carcinogenic effects based on Toxtree and Vega Hub. Meanwhile, Lazar and TEST predicted that delachlor and xylachlor are unlikely to be mutagenic. This study to determine the toxicity of the herbicides delachlor and xylachlor has shown that the possible effects of these herbicides on health and the environment need to be further investigated. The results provide valuable insights into chloroacetanilide herbicide toxicity and help develop safer, more environmentally friendly alternatives.

Keywords: Genotoxicity, carcinogenicity, in silico, chloroacetanilide herbicides

1. INTRODUCTION

The agricultural sector is responsible for producing the food people need to sustain their lives. However, plant diseases, insects, and weeds reduce productivity and quality. Therefore, agrochemicals such as herbicides help farmers to control these adverse effects

* Corresponding author: sefika@stu.comu.edu.tr (Ş. DEMİR)
[1] Vocatioanl School of Health Services, Çanakkale Onsekiz Mart University, Terzioğlu Campus, 17100, Çanakkale, Türkiye
[2] Department of Biology, School of Graduate Studies, Çanakkale Onsekiz Mart University, Terzioğlu Campus, 17100, Çanakkale, Türkiye
[3] Department of Biology, Faculty of Science, Çanakkale Onsekiz Mart University, Terzioğlu Campus, 17100, Çanakkale, Türkiye
E-mail: aberber@comu.edu.tr, nakinci@comu.edu.tr
ORCID: https://orcid.org/0000-0003-3340-598X, https://orcid.org/0000-0002-2036-6929, https://orcid.org/0000-0002-3917-6412

and increase crop yields [1]. However, concerns about potential adverse effects on human health and the environment have arisen from the widespread use of these chemicals. One such concern, which can pose a significant threat to public health and the environment, is the potential genotoxic and carcinogenic effects of herbicides [2, 3].

Chloroacetanilide herbicides are a group of synthetic chemicals that are widely used for the control of weeds in agriculture and forestry. These herbicides are widely used to grow cereals, corn, soybeans, cotton, and many other crops. Due to their effectiveness in controlling weeds that can cause significant yield losses, the use of these herbicides has increased significantly in recent years [4].

Chloroacetanilide herbicides share the 2-chloroacetanilide molecular core, differing only in type and arrangement of substitutions [5]. In spite of the importance of the production of herbicides, there is one aspect that is still dramatic: the carcinogenic potential of the chloroacetanilide herbicides. Some of the members of the chloroacetanilide herbicide family have been characterized by the US Environmental Protection Agency as possible carcinogenic compounds [6]. However, the carcinogenic mechanism of chloroacetanilide compounds remains unclear, although some experiments suggest that the carcinogenic properties are related to the herbicides' ability to nucleophilically react with DNA [7]. Studies have shown that exposure to some of the chloroacetanilide herbicides can cause a range of adverse effects on non-target organisms, including humans [8-11]. These effects include developmental abnormalities, reproductive toxicity, and carcinogenicity. Therefore, it is essential to evaluate the potential toxicity of these herbicides and develop safer alternatives to minimize their environmental and health impacts.

Delachlor and xylachlor are two of the herbicides of the chloroacetanilide group (Figure 1). Delachlor is an herbicide widely used to control weeds in crops such as sugarbeet and cereals. It is also used in combination with other herbicides to control weeds in rice fields. Its chemical formula is $C_{15}H_{22}C_lNO_2$. Xylachlor is an herbicide that has been used for pre-emergence or pre-plant control of annual rgrasses in cereals and other crops. Its chemical formula is $C_{13}H_{18}C_lNO$ [12].
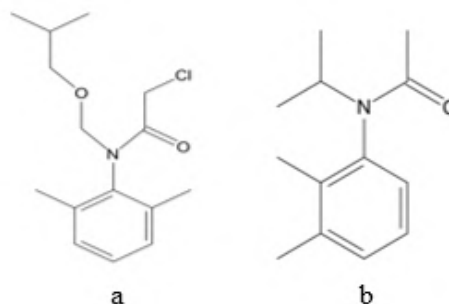

Figure 1 Chemical structures of a) delachlor and b) xylachlor

In silico tools are computer-based methods for predicting chemicals' potential toxicity from their chemical structures. Without the need for animal testing or expensive laboratory equipment, *in silico* toxicity prediction tools may provide an accurate assessment of a xenobiotic's toxicity [13]. This is beneficial because it allows researchers to assess the potential toxicity of a compound or drug quickly and easily without having to incur the cost and time associated with more traditional methods. In addition, by analysing the structure of the molecule and its potential interactions with the system, *in silico* tools can provide a more comprehensive assessment of a compound's toxicity than traditional methods [14].

The study aimed to use four software tools, Vega Hub, Toxtree, Lazar, and TEST, to predict the potential toxicity of these herbicides based on their chemical structures. The findings of this study will provide valuable insights into the toxicity of chloroacetanilide herbicides and aid in the development of safer and more sustainable alternatives.

2. METHODOLOGY

The study used four *in silico* tools to predict the potential genotoxic and carcinogenic effects of delachlor and xylachlor: Vega Hub, Toxtree (Estimation of Toxic Hazard- A Decision Tree Approach), Lazar and TEST (Toxicity Estimation Software Tool). The software tools were selected for their ability to predict the toxicity of chemicals based on their chemical structure. Each of them is open source and free public software.

Vega Hub is a software tool that uses quantitative structure-activity relationship (QSAR) models to predict the toxicity of chemicals based on their physical, chemical and biological properties [15]. QSARs use mathematical models to predict levels of toxicity based on the physical properties of the molecular structure of a chemical, known as molecular descriptors. The tool predicts the toxicity of chemicals based on their similarity to known toxic compounds. It assigns a consensus score to each prediction. This software has an open structure for data sharing and modelling and can be easily used by any user [16].

Toxtree was developed in accordance with the REACH (Registration, Evaluation, Authorisation and Restriction of Chemicals) regulation to assess the toxic effects of chemical substances. It is a software tool that uses a decision tree approach to predict the toxicity of chemicals based on their structural alerts. The tool predicts the toxicity of chemicals by identifying structural features associated with toxicity [17].

Lazar is an open-source web application that uses data mining algorithms to derive predictions for untested compounds from experimental training data, which can be any dataset containing chemical structures and biological activities. Lazar offers researchers a versatile solution by providing both a user-friendly interface and a large database [18].

The Toxicity Estimation Software Tool (TEST) has been developed to facilitate the prediction of chemical toxicity using Quantitative Structure Activity Relationship (QSAR) techniques. TEST analyses the molecular structure of an organic chemical entered by the user to determine toxicity values and physical properties. TEST has no external software requirements and users can enter a chemical to be evaluated via a provided chemical sketch window, a text file of the structure or a database of structures. Various advanced QSAR methods are used within TEST to calculate the necessary molecular descriptors [19].

The canonical Simplified Molecular Input Line Entry Specification (SMILES) systems of delachlor (CC1=C(C(=CC=C1)C)N(COCC(C)C)C(=O)CCl) and xylachlor (CC1=C(C(=CC=C1)N(C(C)C)C(=O)CCl)C) were entered into each software tool to predict their potential toxicity and carcinogenicity [20, 21]. The software tools use a variety of algorithms and models to predict the toxicity and carcinogenicity of chemicals based on their chemical structures.

3. RESULTS

Toxtree predicted that delachlor is a class 3 highly toxic compound with potential mutagenic and carcinogenic properties based on structural alerts. Vega Hub predicted that delachlor is a mutagenic and potentially carcinogenic compound with a consensus score of 0.45, indicating moderate confidence in the prediction. Therefore, Vega Hub predicted that delachlor is not genotoxic, but the model predictions were not in agreement. On the other hand, TEST predicted that delachlor is non-mutagenic with a consensus score of 0.28, while LAZAR predicted that delachlor is non-mutagenic with a probability of 0.419 but cannot predict carcinogenicity.

For xylachlor, toxtree predicted that it is a class 3 highly toxic compound with potential mutagenic and carcinogenic properties based

on structural alerts. Vega hub predicted that xylachlor is a mutagenic and potentially carcinogenic compound with a consensus score of 0.525, indicating a moderate level of confidence in the prediction. However, vega hub also predicted that xylachlor is not genotoxic, indicating that its carcinogenic properties may be due to mechanisms other than dna damage. Test predicted that xylachlor is non-mutagenic with a consensus score of 0.26, while lazar predicted that xylachlor is non-carcinogenic and non-mutagenic with probability scores of 0.217 and 0.213 respectively.

4. DISCUSSION

In silico toxicology prediction tools, also known as computational toxicology, offer several advantages in the field of toxicology. Firstly, they are cost-effective and reduce the need for animal testing, which can be expensive and time-consuming. Secondly, they provide quick and efficient identification of potentially toxic substances, which can be useful in the early stages of drug development. Additionally, they can be used to predict the toxicity of chemicals that have not yet been tested, allowing for more informed decision-making in terms of public health and environmental safety [14]. However, *in silico* toxicology prediction tools do have their limitations. One of the biggest limitations is the lack of complete accuracy, as the predictive models are based on assumptions and extrapolations from existing data. Furthermore, these tools are not yet able to fully replace animal testing, as there are still certain aspects of toxicity that cannot be accurately predicted *in silico* [22].

There have been many studies in the literature on the potential health risks of the chloroacetanilide family of herbicides. The most common chloroacetanilide herbicides are acetochlor, alachlor, butachlor, metolachlor, s-metolachlor, pretilachlor, propachlor and propisochlor. These herbicides may have adverse effects on human health, according to some studies.

These herbicides are classified by the USEPA as Class B2, L2, and C carcinogens and are reported to have moderate to high chronic toxicity [23, 24]. For example, one study has shown that chloroacetanilide herbicides such as alachlor increase the likelihood of developing Parkinson's disease [25]. Ecotoxicological studies suggest that these herbicides are the causal agents for DNA damage and tumor induction in rats, fish, and human lymphocyte cells found in *in vitro* studies [26-29].

This study was conducted using *in silico* analyses to determine the potential toxicity of delachlor and xylachlor herbicides. Analyses through four different software such as Toxtree, Vega Hub, TEST and LAZAR showed that both herbicides exhibited mutagenic and carcinogenic properties in Toxtree and VEGA software. Nonetheless, the results of TEST and LAZAR predicted that delachlor and xylachlor were non-mutagenic, while xylachlor was non-carcinogenic.

Our results suggest that two commonly used herbicides, delachlor and xylachlor, may have potentially harmful effects on human health and the environment. These results emphasize the importance of using *in silico* tools to determine the toxicity of herbicides as well as other chemicals.

5. CONCLUSION

Our study highlights the need for continued research and monitoring of herbicides such as delachlor and xylachlor and underscores the importance of using advanced computational tools to identify and mitigate potential health and environmental risks associated with chemical use in agriculture and forestry. The discrepancies in the predictions among the software tools may be due to the differences in the algorithms and models used, as well as the limitations of the *in silico* approach. *In silico* predictions are based on the chemical structure of the compound and do not take into account the complex interactions and

metabolic processes that occur *in vivo*. Therefore, the *in silico* predictions should be interpreted with caution and confirmed by *in vitro* and *in vivo* experiments. Despite the limitations of the *in silico* approach, it can provide valuable insights into the potential toxicity of chemicals and aid in the development of safer and more sustainable alternatives. By taking a proactive approach to chemical safety, we can ensure that we are protecting human health and the environment for generations to come.

Authors' Contribution
The authors contributed equally to the study.

The Declaration of Conflict of Interest/ Common Interest
No conflict of interest or common interest has been declared by the authors.

The Declaration of Ethics Committee Approval
This study does not require ethics committee permission or any special permission.

The Declaration of Research and Publication Ethics
The authors of the paper declare that they comply with the scientific, ethical and quotation rules of SAUJS in all processes of the paper and that they do not make any falsification on the data collected. In addition, they declare that Sakarya University Journal of Science and its editorial board have no responsibility for any ethical violations that may be encountered, and that this study has not been evaluated in any academic publication environment other than Sakarya University Journal of Science.

REFERENCES

[1] A. De, R. Bose, A. Kumar, S. Mozumdar, "Worldwide Pesticide Use". In: Targeted Delivery of Pesticides Using Biodegradable Polymeric Nanoparticles. SpringerBriefs in Molecular Science. Springer, New Delhi, 5-6, 2014.

[2] B. Alewu, C. Nosiri, "Pesticides and human health," Pesticides in the modern world–effects of pesticides exposure. InTech, pp. 231–50, 2011.

[3] World Health Organization (WHO), "Public health impact of pesticides used in agriculture". World Health Organization, 1990. [Online]. Available: https://apps.who.int/iris/handle/10665/39772

[4] W. Yang, B. A. Holmén, "Relative effects of surfactants and humidity on soil/air desorption of chloroacetanilide and dinitroaniline herbicides," Environmental science & technology, vol. 42, no. 18, pp. 6843–6848, 2008.

[5] W. Liu, J. Gan, S. K. Papiernik, S. R. Yates, "Structural Influences in Relative Sorptivity of Chloroacetanilide Herbicides on Soil," Journal of Agricultural and Food Chemistry, vol. 48, no. 9, pp. 4320–4325, 2000.

[6] K. L. Dearfield, N. E. McCarroll, A. Protzel, H. F. Stack, M. A. Jackson, M. D. Waters, "A survey of EPA/OPP and open literature on selected pesticide chemicals: II. Mutagenicity and carcinogenicity of selected chloroacetanilides and related compounds," Mutation Research/Genetic Toxicology and Environmental Mutagenesis, vol. 443, no. 1–2, pp. 183–221, 1999.

[7] J. D. Coates, R. A. Bruce, J. D. Haddock, "Anoxic bioremediation of hydrocarbons," Nature, vol. 396, no. 6713, pp. 730–730, 1998.

[8] J. Ashby, L. Kier, A. Wilson, T. Green, P. Lefevre, H. Tinwell, G. Willis, W. Heydens, M. Clapp. "Evaluation of the Potential Carcinogenicity and Genetic Toxicity to Humans of the Herbicide Acetochlor." Human & Experimental Toxicology, vol. 15, no. 9: pp. 702–35, 1996.

[9] H. Bian, J. Chen, X. Cai, P. Liu, Y. Wang, L. Huang, X. Qiao, and C. Hao, "Dechlorination of chloroacetanilide herbicides by plant growth regulator sodium bisulfite," Water Research, vol. 43, no. 14, pp. 3566–3574, Aug. 2009.

[10] P. J. Dierickx, "Glutathione- dependent cytotoxicity of the chloroacetanilide herbicides alachlor, metolachlor, and propachlor in rat and human hepatoma- derived cultured cells," Cell biology and toxicology, vol. 15, pp. 325–332, 1999.

[11] S. Furukawa, T. Harada, D. Thake, M. J. Iatropoulos, J. H. Sherman, "Consensus diagnoses and mode of action for the formation of gastric tumors in rats treated with the chloroacetanilide herbicides alachlor and butachlor," Toxicologic Pathology, vol. 42, no. 2, pp. 386–402, 2014.

[12] K. A. Lewis, J. Tzilivakis, D. J. Warner, A. Green, "An international database for pesticide risk assessments and management," Human and Ecological Risk Assessment: An International Journal, vol. 22, no. 4, pp. 1050–1064, 2016.

[13] OECD, "Fundamental and guiding principles for (Q) SAR analysis of chemical carcinogens with mechanistic considerations," Series on testing and assessment. 2015. [Online]. Available: https://one.oecd.org/document/env/jm/mono(2015)46/en/pdf

[14] G. J. Myatt, E. Ahlberg, Y. Akahori, D. Allen, A. Amberg, L. T. Anger, A. Aptula, S. Auerbach, L. Beilke, P. Bellion, R. Benigni, J. Bercu, E. D. Booth, D. Bower, A. Brigo, N. Burden, Z. Cammerer, M. T. D. Cronin, K. P. Cross, L. Custer, M. Dettwiler, K. Dobo, K. A. Ford, M. C. Fortin, S. E. Gad-McDonald, N. Gellatly, V. Gervais, K. P. Glover, S. Glowienke, J. Van Gompel, S. Gutsell, B. Hardy, J. S. Harvey, J. Hillegass, M. Honma, J.-H. Hsieh, C.-W. Hsu, K. Hughes, C. Johnson, R. Jolly, D. Jones, R. Kemper, M. O. Kenyon, M. T. Kim, N. L. Kruhlak, S. A. Kulkarni, K. Kümmerer, P. Leavitt, B. Majer, S. Masten, S. Miller, J. Moser, M. Mumtaz, W. Muster, L. Neilson, T. I. Oprea, G. Patlewicz, A. Paulino, E. Lo Piparo, M. Powley, D. P. Quigley, M. V. Reddy, A.-N. Richarz, P. Ruiz, B. Schilter, R. Serafimova, W. Simpson, L. Stavitskaya, R. Stidl, D. Suarez-Rodriguez, D. T. Szabo, A. Teasdale, A. Trejo-Martin, J.-P. Valentin, A. Vuorinen, B. A. Wall, P. Watts, A. T. White, J. Wichard, K. L. Witt, A. Woolley, D. Woolley, C. Zwickl, and C. Hasselgren, "In silico toxicology protocols," Regulatory Toxicology and Pharmacology, vol. 96, pp. 1–17, 2018.

[15] H.-J. Klimisch, M. Andreae, U. Tillmann, "A Systematic Approach for Evaluating the Quality of Experimental Toxicological and Ecotoxicological Data,"Regulatory Toxicology and Pharmacology, vol. 25, no. 1, pp. 1–5, 1997.

[16] E. Benfenati, A. Manganaro, G. C. Gini, "VEGA-QSAR: AI inside a platform for predictive toxicology.," PAI@ AI* IA, vol. 1107, pp. 21–28, 2013.

[17] G. Patlewicz, N. Jeliazkova, R. J. Safford, A. P. Worth, B. Aleksiev, "An evaluation of the implementation of the Cramer classification scheme in the

Toxtree software," SAR and QSAR in Environmental Research, vol. 19, no. 5–6, pp. 495–524, 2008.

[18] A. Maunz, M. Gütlein, M. Rautenberg, D. Vorgrimmler, D. Gebele, C. Helma, "Lazar: a modular predictive toxicology framework". Frontiers in pharmacology, 4, 38, 2013.

[19] T. M. Martin, "User's Guide for T.E.S.T. (Toxicity Estimation Software Tool)", 2020.

[20] PubChem, "Delachlor." https://pubchem.ncbi.nlm.nih.gov/com pound/32321 (accessed Apr. 02, 2023).

[21] PubChem, "Xylachlor." https://pubchem.ncbi.nlm.nih.gov/com pound/162992 (accessed Apr. 02, 2023).

[22] T. Tralau, M. Oelgeschläger, R. Gürtler, G. Heinemeyer, M. Herzler, T. Höfer, H. Itter, T. Kuhl, N. Lange, N. Lorenz, C. Müller-Graf, U. Pabel, R. Pirow, V. Ritz, H. Schafft, H. Schneider, T. Schulz, D. Schumacher, S. Zellmer, G. Fleur-Böl, M. Greiner, M. Lahrssen-Wiederholt, A. Lampen, A. Luch, G. Schönfelder, R. Solecki, R. Wittkowski, A. Hensel, "Regulatory toxicology in the twenty-first century: challenges, perspectives and possible solutions". Archives of Toxicology, vol. 89, 823–850, 2015.

[23] USEPA, "Inventory of US greenhouse gas emissions and sinks: 1990–2011. EPA-430-R-13-001," 2013.

[24] M. Cheng, Q. Meng, Y. Yang, C. Chu, Q. Chen, Y. Li, D. Cheng, Q. Hong, X. Yan, J. He, "The Two-Component Monooxygenase MeaXY Initiates the Downstream Pathway of Chloroacetanilide Herbicide Catabolism in Sphingomonads".

Applied and Environmental Microbiology, 83, 2017.

[25] N. Wan, G. Lin, "Parkinson's disease and pesticides exposure: new findings from a comprehensive study in Nebraska, USA," The Journal of Rural Health, vol. 32, no. 3, pp. 303–313, 2016.

[26] B. Hill, P. R. Jefferies, G. B. Quistad, J. E. Casida, "Dialkylquinoneimine metabolites of chloroacetanilide herbicides induce sister chromatid exchanges in cultured human lymphocytes," Mutation Research/Genetic Toxicology and Environmental Mutagenesis, vol. 395, no. 2–3, pp. 159–171, 1997.

[27] T. Green, R. Lee, R. B. Moore, J. Ashby, G. A. Willis, V. J. Lund, M. J. L. Clapp, "Acetochlor-induced rat nasal tumors: further studies on the mode of action and relevance to humans". Regulatory Toxicology and Pharmacology, vol. 32, no. 1, 127-133, 2000.

[28] B. Ateeq, M. A. Farah, W. Ahmad, "Detection of DNA damage by alkaline single cell gel electrophoresis in 2, 4-dichlorophenoxyacetic-acid-and butachlor-exposed erythrocytes of Clarias batrachus," Ecotoxicology and environmental safety, vol. 62, no. 3, pp. 348–354, 2005.

[29] C. D. Nwani, U. I. Ama, F. Okoh, U. O. Oji, R. C. Ogbonyealu, A. A. Ibiam, O. Udu-Ibiam, "Acute toxicity of the chloroacetanilide herbicide butachlor and its effects on the behavior of the freshwater fish Tilapia zillii". African journal of biotechnology, vol. 12, no. 5, 2013.

Title: A Novel Machine Learning-based Diagnostic Algorithm for Detection of Onychomycosis through Nail Appearance

Authors: Serkan DÜZAYAK, Muhammed Kürşad UÇAR

A Novel Machine Learning-based Diagnostic Algorithm for Detection of Onychomycosis through Nail Appearance

Serkan DÜZAYAK [1] ID, Muhammed Kürşad UÇAR*[2] ID

Abstract

Onychomycosis is the most common nail fungus disease in clinical practice worldwide, caused by the localization of various fungal agents, including dermatophytes, on the nail. The tests traditionally used for diagnosing onychomycosis are native examination, histopathological examination with periodic acid Schiff (PAS) staining, and nail culture. There is no gold standard method for diagnosing the disease, and the diagnosis process is time-consuming, costly, and quite laborious. Today, new technologies are needed to detect onychomycosis via AI-based ML to reduce the clinician and laboratory-induced error rate and increase diagnostic sensitivity and reliability. The present study aimed to design a decision support system to help the specialist doctor detect toenail fungus with artificial intelligence-based image processing techniques. The toenail images were taken by any camera initially from the individuals referred to the clinic. The image is divided into 12 RGB channels. Three hundred features were removed from each channel as 25 in the time domain. The best features were selected through feature selection algorithms in the next step to increase the performance and reduce the number of features, and models were created by algorithm classification. The average performance values of all proposed models, accuracy, sensitivity, and specificity, are 89.65, 0.9, and 0.89, respectively. The performance values of the most successful model-created accuracy, sensitivity, and specificity are 97.25, 0.96, and 0.98, respectively. Although the proposed method, according to the findings obtained in the study, has many advantages compared to the literature, it can be used as a decision support system for clinician diagnosis.

Keywords: Onychomycosis, nail fungus, image processing, artificial intelligence, machine learning

1. INTRODUCTION

Onychomycosis is the most common nail fungus disease in clinical practice in the world caused by the localization of various fungal agents including dermatophytes on the nail [1], [2]. The risk of onychomycosis increased by aging. Furthermore, tinea pedis history, trauma, obesity, diabetes mellitus are other risk factors [3]. The condition constitutes a public health problem because it is transmitted from person to person and through direct contact with contaminated surfaces. Furthermore, the quality of life of

* Corresponding author: mucar@sakarya.edu.tr (M.K. UÇAR)
[1] Adıyaman University, Faculty of Medicine, Department of Dermatology and Veneral Diseases, Adıyaman, Türkiye
[2] Sakarya University, Faculty of Engineering, Electrical and Electronics Engineering, Serdivan, Sakarya, Türkiye
E-mail: sduzayak@adiyaman.edu.tr
ORCID: https://orcid.org/ 0000-0002-4853-9860, https://orcid.org/ 0000-0002-0636-8645

Serkan DÜZAYAK, Muhammed Kürşad UÇAR

A Novel Machine Learning-based Diagnostic Algorithm for Detection of Onychomycosis through Nail Appea...

patients is impaired due to aesthetic problems caused by deformities in the nails, localized pain in dystrophic nails that may affect the daily life [4].

The tests which are traditionally used for the diagnosis of onychomycosis are native examination (microscopic KOH test), histopathological examination with periodic acid schiff (PAS) staining, and nail culture. None of these tests are considered a stand-alone standard test. The combined use of the tests may increase the sensitivity and specificity. However, there is not any consensus on the most appropriate test combination. The most important disadvantage is that the nail culture which is another diagnostic method may provide a result after 3 weeks at least, and the culture procedure bears the risk of contamination. Another diagnostic test is histopathological examination with PAS staining; however, this test poses a disadvantage because it cannot be applied to all patients and is expensive [5]. The KOH analysis is more practical and cheaper than other methods. However, limitations of this test include variable sensitivity between 44% and 100%, the possibility of being affected by experience of the clinician, and average testing period between 30 and 60 minutes.

Since the visual diagnosis is at the forefront, dermatology is increasingly involved in artificial intelligence (AI) studies. Machine learning (ML) is a component of AI which recognizes models synthesized from data and automatically teaches the tasks to the machines [6]. Although AI and ML have been developed in dermatology mostly for the diagnosis of melanoma and non-melanoma cutaneous tumors, they are also used for evaluation of psoriasis, atopic dermatitis, cutaneous ulcers and detection of onychomycosis [7-11]. Today, new technologies are needed for the detection of onychomycosis via AI-based ML in order to reduce the clinician and laboratory-induced error rate and increase diagnostic sensitivity and reliability.

The artificial intelligence algorithms have been used frequently in the field of dermatology in the recent years [12-14]. These applications include skin cancer detection [13, 15]. It is possible to create artificial intelligence-based decision support systems with every image taken from the skin, such as psoriasis, onychomycosis and acne [12]. Artificial intelligence methods have started to be preferred frequently in the dermatological oncology [12]. Deep learning artificial intelligence algorithms are preferred since applications with image processing frequently have higher performance value [16-19]. The most significant disadvantage of deep learning is requirement of much when compared to classical machine learning algorithms [18].

Onychomycosis is one of the diseases that is frequently studied in dermatology. The disease may be diagnosed with microscopic images as well as artificial intelligence-based diagnosis with skin images [14]. The model offered in this study works with microscopic images with a achievement rate of 95.9% based on artificial intelligence. It was stated in the aforesaid study that the clinician may diagnose with an accuracy rate of 72.8%. Microscopic images are needed for diagnosis in the relevant study. The present study offers a method that diagnosis may be established with clinical images of nails without the need for microscopic images. The diagnosis period thereby may become shorter.

The accuracy rate of a proposed model based on artificial intelligence for the diagnosis of onychomycosis has been reported to be 84.58% [20]. Disease diagnosis in dermatology is based on tissue and color analysis [21]. The color and tissue changes appear in the course of onychomycosis. In this case, diagnosis can be made by using color analysis with the help of image processing techniques [22, 23]. The mainstay of artificial intelligence and image processing studies is color analysis and the perception of this color difference by the artificial intelligence.

Serkan DÜZAYAK, Muhammed Kürşad UÇAR

A Novel Machine Learning-based Diagnostic Algorithm for Detection of Onychomycosis through Nail Appea...

In two different studies, the accuracy rates of the deep learning-based diagnostic system were reported as 65% with the nail images obtained from Kaggle [24, 25]. The accuracy rates ıf both studies are quite lower. A previous study conducted by Han et al. in 2018 developed a diagnostic model through a data set of approximately 50 thousand nail images with deep learning-based methods such as CNN, R-CNN, ResNet-152, and VGG-19 [8]. The sensitivity of model performance values ranged between 87.2 and 96.7, the specificity was between 69.3 and 96.7, and AUC value ranged between 0.82 and 0.98. These high-performance values are an indication that artificial intelligence may be used in dermatology. Kim et al. offered CNN deep learning model in a different study [26]. The sensitivity and specificity values of the model performance were 70.2 and 72.7, respectively. The sensitivity and specificity of labeling done by 5 dermatologists were 73 and 49.7 in the aforesaid study. It is noteworthy that the artificial intelligence model has a higher achievement rate than dermatologists.

Unlike the literature, the aim of the present study was to detect Onychomycosis with a high achievement rate with the help of classical machine learning algorithms instead of deep learning methods. This study aims to design a decision support system that would help the specialist doctor for the detection of toenail fungus with artificial intelligence-based image processing techniques. The procedures are carried out as follows in a referring individual in the study. In the first step, toenail images are taken from the individual with the help of any camera. The noise is removed from the captured images with the help of digital filters. The clarified images are split into 12 RGB channels for more information extraction. Twenty-five (25) features are extracted in the time domain from each channel information. A total of 300 extracted features become parameters representing images. The best features were selected through feature selection algorithms in the next step in order to increase the

performance and reduce the number of features. After this stage, classification models are created through data sets created with selected features. The created models are ready for use in the clinic.

2. MATERIAL AND METHOD

The present research was carried out within the frame of the steps shown in Figure 1. The aim of the study is to detect nail fungus based on artificial intelligence with nail fungus images. Within this context, the data were collected from individuals to create an artificial intelligence model. The images were then cleared through digital filters and separated into RGB channels. Different images were obtained during the filtering. Feature extraction was performed from the obtained image channel information. Relevant features are selected with the help of feature selection algorithm. The artificial intelligence trainings were carried out through different machine learning algorithms at the last stage. The detailed additional information for the process steps is given in the sub-titles.

2.1. Data Collection

This research includes sick and healthy nail images collected from 76 individuals who have referred to dermatology and venereal diseases polyclinic of Sakarya Karasu Public hospital between 02/01/2020 and 02/01/2021 (Table 1.).

Table 1 The distribution of gender-based age individual count

	Male	Female	Total
n	39	37	76
Mean	37.18	33.30	35.29
Std	13.85	13.34	13.65
Min	18	18	18
Max	67	60	67

n: number of individuals

Serkan DÜZAYAK, Muhammed Kürşad UÇAR

A Novel Machine Learning-based Diagnostic Algorithm for Detection of Onychomycosis through Nail Appea...
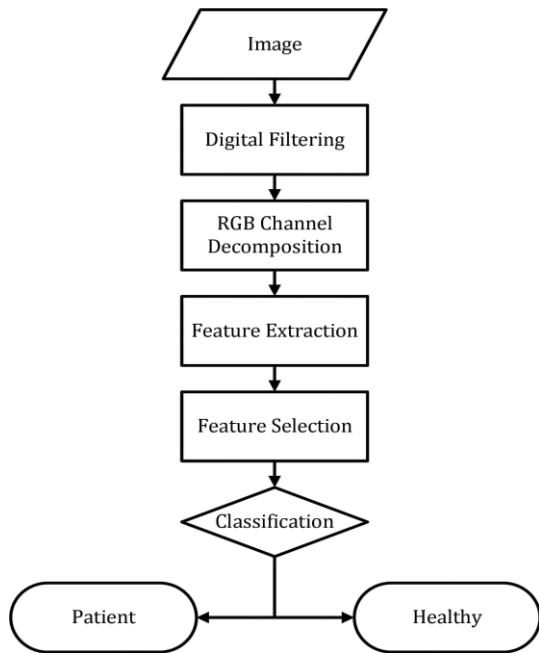
Figure 1 Study implementation process

Nail images collected from a total of 76 individuals including 39 males and 37 females were classified as fungal disease or healthy by the specialist within the framework of examinations (Table 2.). In other words, more than one image was taken from an individual.

Table 2 Distribution of the images as sick, healthy, and gender-based

	Male	Female	Total
Patient	155	87	242
Healthy	139	307	446
Total	294	394	688

2.2. Image Preprocessing

Totally 688 nail images collected from individuals were preprocessed (Figure 2.). As a first step, the nail image on each finger was trimmed rawly. Manual segmentation was performed on the trimmed image. A mask was created for each image. Image smoothing was performed by applying an average filter to the segmented image. The Hue Saturation Value (HSV) image of both filtered and unfiltered image was obtained. As a result of this process, four images including the original,

the original mean filtered, the original HSV and the filtered HSV image appeared. The RGB channels of each image are separated and the image is rendered processable. After this stage, the feature will be extracted from each RGB channel.
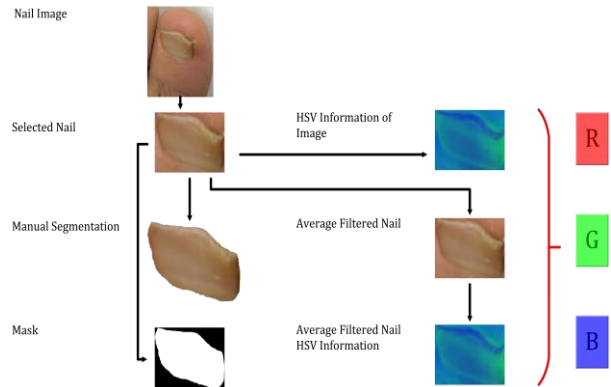
Figure 2 Detailed visual representation of the signal processing process

The steps and step outputs related to the process of filtering the original image and obtaining the HSV information are shown in detail in Figure 3.

2.3. Feature Extraction

After the processing steps of the images, four images (Orginal Image, Average Filtered İmage, Original Image HSV Information And Average Filtered Nail HSV Information, Figure 3.) and their 12 RBG channel information were obtained for each nail image. A total of 300 features were extracted from each channel, including 25 statistical features in the time domain (Table 3.).

Figure 3 The change of the images after filtering.

Serkan DÜZAYAK, Muhammed Kürşad UÇAR

A Novel Machine Learning-based Diagnostic Algorithm for Detection of Onychomycosis through Nail Appea...

The features were released in the MATLAB environment and the MATLAB library was used for some features. Özellik çıkarma oldukça önemli bir süreçtir. Feature extraction is a very important process. The extracted features should describe the signal well. It is known that statistical-based feature extraction processes, which are thought to describe data sets well in previous studies, affect performance quite well. For this reason, the study was carried out using the features used in the literature before [27-31].
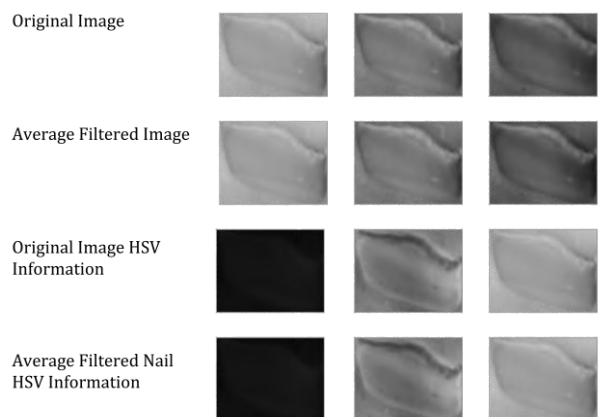
2.4. Feature Selection

Three hundred (300) features were extracted from four images and 12 RGB channels for a nail image until this stage. The aim of the feature selection step is to improve the performance of machine learning by weeding out irrelevant features.

A previous study in which the Eta feature selection algorithm was compared with other algorithms states that it could be more efficient than existing algorithms in terms of performance [27].

Eta feature selection algorithm is used to select features to increase model performance.

The feature selection algorithm based on the eta correlation coefficient performs the selection process between the unordered qualitative (Sick/ Healthy) variables and the continuous numerical variables (the average pixel value of the image) according to the level of the correlation coefficient.

Table 3 Mathematical equations for the features [27]

No.	Feature	Equation
1	Kurtosis	$x_{kur} = \sum_{i=1}^{n} (x(i) - \bar{x})^4 / (n-1)S^4$
2	Skewness	$x_{ske} = \sum_{i=1}^{n} (x_i - \bar{x})^3 / (n-1)S^3$
3	* IQR	$IQR = iqr(x)$
4	DK	$DK = (S / \bar{x})100$
5	Geometric Mean	$G = \sqrt[n]{x_1 + \cdots + x_n}$
6	Harmonic Mean	$H = n / \left(\frac{1}{x_1} + \cdots + \frac{1}{x_n} \right)$
7	Activity - Hjort Parameters	$A = S^2$
8	Mobility - Hjort Parameters	$M = S_1^2 / S^2$
9	Complexity - Hjort Parameters	$C = \sqrt{(S_2^2 / S_1^2)^2 - (S_1^2 / S^2)^2}$
10	* Maximum	$x_{max} = max(x_i)$
11	Median	$\tilde{x} = \begin{cases} x_{\frac{n+1}{2}} & : x \text{ odd} \\ \frac{1}{2}(x_{\frac{n}{2}} + x_{\frac{n}{2}+1}) & : x \text{ even} \end{cases}$
12	* Mean Absolute Deviation	$MAD = mad(x)$
13	* Minimum	$x_{min} = min(x_i)$
14	* Central Moments	$CM = moment(x,10)$
15	Mean	$\bar{x} = \frac{1}{n} \sum_{i=1}^{n} = \frac{1}{n}(x_1 + \cdots + x_n)$
16	Average Curve Length	$CL = \frac{1}{n} \sum_{i=2}^{n} |x_i - x_{i-1}|$
17	Average Energy	$E = \frac{1}{n} \sum_{i=1}^{n} x_i^2$
18	Root Mean Squared	$X_{rms} = \sqrt{\frac{1}{n} \sum_{i=1}^{n} |x_i|^2}$
19	Standard Error	$S_{\bar{x}} = S / \sqrt{n}$
20	Standard Deviation	$S = \sqrt{\frac{1}{n} \sum_{i=1}^{n} (x_i - \bar{x})}$
21	Shape Factor	$SF = X_{rms} / \left(\frac{1}{n} \sum_{i=1}^{n} \sqrt{|x_i|} \right)$
22	* Singular Value Decomposition	$SVD = svd(x)$
23	* 25% Trimmed Mean	$T25 = trimmean(x, 25)$
24	* 50% Trimmed Mean	$T50 = trimmean(x, 50)$
25	Average Teager Energy	$TE = \frac{1}{n} \sum_{i=3}^{n} (x_{i-1}^2 - x_i x_{i-2})$

* The feature was computed using MATLAB
IQR Interquartile Range, DK Coefficient of Variation

Serkan DÜZAYAK, Muhammed Kürşad UÇAR

A Novel Machine Learning-based Diagnostic Algorithm for Detection of Onychomycosis through Nail Appea...

The algorithm calculates a correlation coefficient between each feature of the image and the image tag (r) [32]. The r coefficient is called the inter-correlation coefficient Eta. Calculated correlation coefficients are rated between 0 and 1, with 1 indicating the best correlation. The features are arranged in order of relevance by arranging the r values from the largest to the smallest. After this stage, models are created by selecting the best X% features in order to determine how many features would affect the performance. The X indicates the percentage quantity that is wanted to be selected. In this study, 20 different values were determined by increasing the X value between 5 and 100 with 5 step intervals. The models created with each value are called levels. As the feature selection level is increased, in other words, as the X value is increased, new datasets are created. Twenty feature groups were created at the end of this process.

2.5. Machine Learning

In this research, three basic machine learning methods were preferred due to their higher performance. The first of these is artificial neural networks (ANN) which are the basis of deep learning [33, 34]. ANN is an algorithm that has higher performance as classical machine learning algorithms and fast deep learning. The performance could be made quite higher depending on the type of problem. The deep learning models are the right choice, especially for problems where direct processing of images is required; however, ANN can remain at the basic level. However, as the complexity of the problem decreases, preferring ANN models may be the right choice. The biggest challenge during ANN trainings is performing the parameter optimization depending on the data set. Therefore, many trials should be done by changing the ANN parameters for different datasets during the training. This number of trials may be up to millions. Some parameters may be kept constant in order to reduce the number of trials. For example, trainlm is one of the most optimized structures among ANN

training algorithms. Therefore, keeping such parameters constant will reduce the number of trial variances.

Another algorithm is the Support Vector Machine (SVM) used in classical machine learning [35, 36]. SVM is one of the classical machine learning algorithms with higher adaptability to datasets, higher performance and shorter training time in general. The aim of the algorithm is to create an n-dimensional plane that will divide the dataset into two classes. The dataset is sized depending on the number of features. The algorithm has two basic working structures including linear and non-linear. Depending on the suitability of the data set, this structure may be preferred by the user.

The last method is Ensemble Decision Trees (EDT) containing a hybrid structure [37, 39]. Ensemble structures are generally hybrid structures created by combining more than one algorithm. These hybrid structures take the average of decisions given by all algorithms in the structure and reflects to the output. The output may be found by the average or weighted grading. This means that the effect of each machine learning on the output is determined by proportioning it between 0 and 1. The algorithm with the highest performance would be more effective. In this type of structures, it is often preferred because the error rate decreases, and single classifiers come together to create models with higher performance.

CNN is a new artificial intelligence algorithm that is frequently used today. However, high performance computers or servers are required for its use. Since high-performance computers are costly, classical machine learning algorithms are preferred in this study. In order for the success rate to be at the same level with deep learning methods, innovations have been made in the signal processing process [8, 9, 26].

Serkan DÜZAYAK, Muhammed Kürşad UÇAR

A Novel Machine Learning-based Diagnostic Algorithm for Detection of Onychomycosis through Nail Appea...

2.6. Performance Assessment Criteria

In this study, six performance evaluation criteria which are frequently used in the literature were preferred. These include accuracy, sensitivity, specificity, F-Measure, Kappa coefficient, and AUC value. The equations of the parameters may be accessed via relevant reference [40]. The models were divided into two as training by 80%, and test by 20% (Table 4.).

Table 4 The data distribution for training and test process

The dataset	Training (80%)	Test (20%)	Total
Patient:	193	49	242
Healthy	244	60	304

3. RESULTS

The aim of the study is to detect nail fungus with artificial intelligence-based nail images. The data collected in the polyclinic were obtained from 688 nail images of 76 individuals with 242 sick and 446 healthy nail images. A total of 12 images were obtained by preprocessing each image (Figure 2.). After preprocessing, 25 features were extracted from each image and 300 features were extracted from 12 images in total (Table 3.). Eta feature selection algorithm is used to improve machine learning models.

The features are selected with a certain amount through the feature selection algorithm, and models at different levels are created (Table 5.). The best result in the table is marked in red. The level 1 model was created by selecting the best 5% features. The models were created with three machine learning at this level. A total of 15 features were selected with 5% features. Thirty features were selected with the best 10% features for the level. Tree models were created with three machine learning at this level. The achievement rate reaches its maximum when the amount of features increases and reaches by 90%. The achievement rate was 79.82 at 5%, and 97.25% at 90%. Balance and higher levels are expected in other parameters as well as accuracy rate. The sensitivity and specificity values of the model created with 5% feature are 0.84 and 0.83. Such values are 0.96 and 0.97 with a feature by 90%. The closeness of these ratios indicates that the model is stable and balanced. In the graphical representation of the performances, it has been determined that the performance increases when the number of features increases (Figure 4.) . Different performance values are compared on the spider chart for the best performance Level 10 and 18 (Figure 5.). Different performance values are compared on the spider chart for the best performance Level 10 and 18. It was determined that the EDT model for level 18 and the SVMS model for level 10 were the most efficient.

The model performance values proposed in this study were compared with the results of the studies in the literature (Table 6, 7.). The reason for the proposed model being better than others stated in the literature may be the steps in the image processing processes. The difference here is the methods chosen in the feature extraction, feature selection, and classification stages.

Serkan DÜZAYAK, Muhammed Kürşad UÇAR

A Novel Machine Learning-based Diagnostic Algorithm for Detection of Onychomycosis through Nail Appea...

Table 5 Model performances

Info	Performance Evaluation Criteria					
L=1, NF=15, FP=5						
Model	Acc	Sen	Spe	F-O	Kappa	AUC
CNet	83.49	0.84	0.83	0.84	0.67	0.84
EDT	80.73	0.84	0.78	0.81	0.61	0.81
SVMs	79.82	0.88	0.73	0.80	0.60	0.81
L=2, NF=30, FP=10						
Model	Acc	Sen	Spe	F-O	Kappa	AUC
CNet	83.49	0.82	0.85	0.83	0.67	0.83
EDT	84.40	0.86	0.83	0.85	0.69	0.85
SVMs	86.24	0.90	0.83	0.86	0.72	0.87
L=3, NF=45, FP=15						
Model	Acc	Sen	Spe	F-O	Kappa	AUC
CNet	87.16	0.86	0.88	0.87	0.74	0.87
EDT	87.16	0.88	0.87	0.87	0.74	0.87
SVMs	79.82	0.80	0.80	0.80	0.59	0.80
L=4, NF=60, FP=20						
Model	Acc	Sen	Spe	F-O	Kappa	AUC
CNet	83.49	0.84	0.83	0.84	0.67	0.84
EDT	88.99	0.90	0.88	0.89	0.78	0.89
SVMs	82.57	0.82	0.83	0.82	0.65	0.82
L=5, NF=75, FP=25						
Model	Acc	Sen	Spe	F-O	Kappa	AUC
CNet	88.07	0.88	0.88	0.88	0.76	0.88
EDT	89.91	0.90	0.90	0.90	0.80	0.90
SVMs	88.99	0.90	0.88	0.89	0.78	0.89
L=6, NF=90, FP=30						
Model	Acc	Sen	Spe	F-O	Kappa	AUC
CNet	92.66	0.90	0.95	0.92	0.85	0.92
EDT	93.58	0.94	0.93	0.94	0.87	0.94
SVMs	90.83	0.90	0.92	0.91	0.81	0.91
L=7, NF=105, FP=35						
Model	Acc	Sen	Spe	F-O	Kappa	AUC
CNet	89.91	0.86	0.93	0.89	0.79	0.90
EDT	92.66	0.90	0.95	0.92	0.85	0.92
SVMs	89.91	0.92	0.88	0.90	0.80	0.90
L=8, NF=120, FP=40						
Model	Acc	Sen	Spe	F-O	Kappa	AUC
CNet	92.66	0.90	0.95	0.92	0.85	0.92
EDT	91.74	0.90	0.93	0.92	0.83	0.92
SVMs	88.99	0.86	0.92	0.89	0.78	0.89
L=9, NF=135, FP=45						
Model	Acc	Sen	Spe	F-O	Kappa	AUC
CNet	90.83	0.90	0.92	0.91	0.81	0.91
EDT	89.91	0.92	0.88	0.90	0.80	0.90
SVMs	90.83	0.90	0.92	0.91	0.81	0.91
L=10, NF=150, FP=5						
Model	Acc	Sen	Spe	F-O	Kappa	AUC
CNet	**92.66**	**0.92**	**0.93**	**0.93**	**0.85**	**0.93**
EDT	**93.58**	**0.96**	**0.92**	**0.94**	**0.87**	**0.94**
SVMs	**93.58**	**0.96**	**0.92**	**0.94**	**0.87**	**0.94**

L: Level, NF: Number of Feature, FP: Percentage of Feature

Table 5 Model performances (continuance)

Info	Performance Evaluation Criteria					
L=11, NF=165, FP=50						
Model	Acc	Sen	Spe	F-O	Kappa	AUC
CNet	88.07	0.88	0.88	0.88	0.76	0.88
EDT	96.33	0.94	0.98	0.96	0.93	0.96
SVMs	88.07	0.90	0.87	0.88	0.76	0.88
L=12, NF=180, FP=60						
Model	Acc	Sen	Spe	F-O	Kappa	AUC
CNet	91.74	0.92	0.92	0.92	0.83	0.92
EDT	96.33	0.96	0.97	0.96	0.93	0.96
SVMs	88.99	0.94	0.85	0.89	0.78	0.89
L=13, NF=195, FP=65						
Model	Acc	Sen	Spe	F-O	Kappa	AUC
CNet	86.24	0.88	0.85	0.86	0.72	0.86
EDT	91.74	0.92	0.92	0.92	0.83	0.92
SVMs	90.83	0.92	0.90	0.91	0.82	0.91
L=14, NF=210, FP=70						
Model	Acc	Sen	Spe	F-O	Kappa	AUC
CNet	93.58	0.92	0.95	0.93	0.87	0.93
EDT	96.33	0.94	0.98	0.96	0.93	0.96
SVMs	89.91	0.88	0.92	0.90	0.80	0.90
L=15, NF=225, FP=75						
Model	Acc	Sen	Spe	F-O	Kappa	AUC
CNet	89.91	0.92	0.88	0.90	0.80	0.90
EDT	89.91	0.94	0.87	0.90	0.80	0.90
SVMs	86.24	0.84	0.88	0.86	0.72	0.86
L=16, NF=240, FP=80						
Model	Acc	Sen	Spe	F-O	Kappa	AUC
CNet	69.72	1.00	0.45	0.62	0.42	0.73
EDT	94.50	0.92	0.97	0.94	0.89	0.94
SVMs	91.74	0.88	0.95	0.91	0.83	0.91
L=17, NF=255, FP=85						
Model	Acc	Sen	Spe	F-O	Kappa	AUC
CNet	93.58	0.94	0.93	0.94	0.87	0.94
EDT	96.33	0.94	0.98	0.96	0.93	0.96
SVMs	88.99	0.86	0.92	0.89	0.78	0.89
L=18, NF=270, FP=90						
Model	Acc	Sen	Spe	F-O	Kappa	AUC
CNet	**92.66**	**0.96**	**0.90**	**0.93**	**0.85**	**0.93**
EDT	**97.25**	**0.96**	**0.98**	**0.97**	**0.94**	**0.97**
SVMs	**92.66**	**0.94**	**0.92**	**0.93**	**0.85**	**0.93**
L=19, NF=285, FP=95						
Model	Acc	Sen	Spe	F-O	Kappa	AUC
CNet	90.83	0.92	0.90	0.91	0.82	0.91
EDT	97.25	0.96	0.98	0.97	0.94	0.97
SVMs	83.49	0.84	0.83	0.84	0.67	0.84
L=20, NF=300, FP=100						
Model	Acc	Sen	Spe	F-O	Kappa	AUC
CNet	91.74	0.92	0.92	0.92	0.83	0.92
EDT	93.58	0.92	0.95	0.93	0.87	0.93
SVMs	91.74	0.90	0.93	0.92	0.83	0.92

L: Level, NF: Number of Feature, FP: Percentage of Feature

Serkan DÜZAYAK, Muhammed Kürşad UÇAR

A Novel Machine Learning-based Diagnostic Algorithm for Detection of Onychomycosis through Nail Appea...
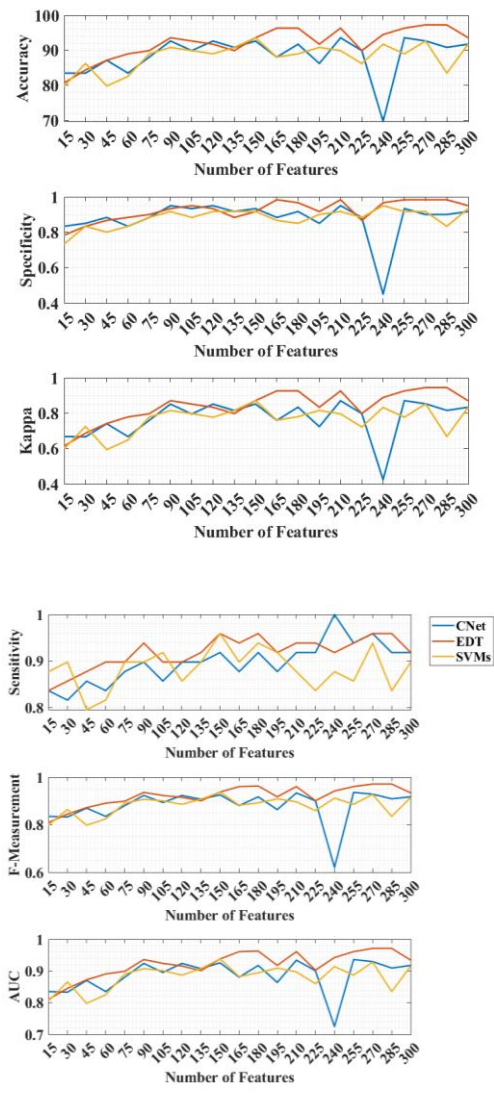
Figure 4 Graphical representation of model performances

Figure 5 Spider graphical representation of model performances for levels 10 and 18

4. DISCUSSION AND CONCLUSION

Early diagnosis in dermatology is of vital importance for improving the quality of life. There is a need for new, reliable and fast decision support systems that will shorten the diagnostic processes for early diagnosis. New artificial intelligence-based diagnostic techniques that meet the specifications may be developed today. The aim of this study was to develop a fast and reliable decision support system based on artificial intelligence for the detection of Onychomycosis. There are guidelines suggested for image processing processes in the literature [41].

These outlines consist of image, feature extraction, feature selection, and classification steps. The system performance here is directly dependent on the process developed. It has been recently discovered that performances may be increased very well with deep learning methods [33]. With all these developments, interest in the use of deep learning methods has increased. However, the need for high-performance computers for the training of deep learning algorithms is increasing day by day. The interest in classical machine learning still continues due to this disadvantage. In this study, classical machine learning algorithms were preferred considering hardware inadequacies. Considering the applicability of the systems, it is obvious that high-capacity computers cannot exist in every clinic. All image processing processes are done by algorithm in deep learning when classical machine learning algorithms are preferred, deepening should be applied in image processing processes. Digital filters are used to process

Serkan DÜZAYAK, Muhammed Kürşad UÇAR

A Novel Machine Learning-based Diagnostic Algorithm for Detection of Onychomycosis through Nail Appea...

images in this study. The noise on the image is cleared. In addition to the filters, the images were separated into channel information and different information was produced. Revealing different information that defines the image is thereby aimed. However, having a lot of information does not mean that they are meaningful. Therefore, feature selection algorithms are used to highlight useful information. It is seen in the results that the selected features increase the performance (Table 5.). This increase is an indication of the efficient implementation of the process. The results obtained are compatible with the literature. In addition, the feature selection algorithm helped to increase the performance.

There are studies recommended for the diagnosis of Onychomycosis in the literature [8, 9, 26]. The common feature of these studies is performing deep learning-based classification. Image preprocessing is relatively very less. Images are integrated into the system with their tags. The image processing process is driven by deep learning. Although this process seems relatively adequate, it is quite time consuming for training time. Furthermore, it has a different disadvantage that requiring high level hardware. The most significant advantage of these systems is their high-performance value. The compactness of the model provides a great advantage to the developers [42, 43]. However, non-model development of deep learning processes is possible by an expert developer, like this study.

The performance value of the model proposed in this study is higher than the model results made with deep learning in the literature (Table 6, 7.) [5, 8, 14, 26]. This may be associated with the feature extraction and selection process in image processing. In this study, unlike the literature, high performance is achieved with the help of classical machine learning algorithms instead of deep learning methods. The results obtained are quite good compared to the literature. The image processing process has greatly increased the performance.

Table 6 Comparison of literature results

No	References	Method	Image
1	[14] Yılmaz 2022	Deep Learning	Microscopic Image
2	[14] Yılmaz 2022	Specialist Clinician	Microscopic Image
3	[20] Nijhawan 2017	Deep Learning	Nail Image
4	[24] Indi 2016	Deep Learning	Nail Image
5	[25] Kanchna 2021	Deep Learning	Nail Image
6	[5] Velasquez-Agudelo 2017	KOH-Systematic Compilation	
7	[5] Velasquez-Agudelo 2017	Histopathology	
8	[26] Kim 2020	Deep Learning	
9	[26] Kim 2020	Five Specialist Clinicians	
10	[13] Han 2018	Deep Learning	
11	**Model Offered**	**Ensemble Decision Tree**	**Nail Image**

Table 7 Comparison of literature results 2

No	Acc	Sen	Spe	F-M	K	AUC	F1	Pre
1	95.90	95.5	97.5			0.991	95.5	95.58
2	72.8	61	95			0.87	74.69	96.3
3	85.11	89.8	89.1		0.848			
4	65							
5	65							
6		61 (44-100)	95 (75-100)					
7		84 (61-93)	89 (44-100)					
8		70.2	72.7					
9		73	49.7					
10		87.2-96.7	69.3-96.7			0.82-0.98		
11	97.25	96	98	0.97	0.94	0.97		

: F-Measurement, AUC: Area Under the Receiver Operating Characteristic (ROC) Curve, Acc Accuracy, Sen Sensitivity, Spe Specificity, Pre Precision, K Kappa, F1 F1-Score

After onychomycosis formation on the nail, pigments of different colors begin to form in the nail. This an important point for diagnosis. A study conducted in 2022 developed an onychomycosis diagnosis algorithm with deep learning methods based on changes in nail pigments [40]. The achievement rate of the system was evaluated over the pigment-based estimation. The most important limitation of the study is that the performance values given are not comparable with other

Serkan DÜZAYAK, Muhammed Kürşad UÇAR

A Novel Machine Learning-based Diagnostic Algorithm for Detection of Onychomycosis through Nail Appea...

studies in the literature. All the results given in this study have been evaluated from different perspectives so that they can be compared with the literature. The results obtained are better than the literature. This may be because the image processing process is done effectively.

Researches on artificial intelligence in different methods continue for the diagnosis of onychomycosis [44, 45]. Methods considered as new research topics are Nail Dermoscopy (Onychoscopy), Reflectance Confocal Microscopy and Molecular Assays. The developed methods are still being investigated in the literature and their sensitivity varies between 52.9% and 100%. This change in sensitivity still indicates that research needs to continue.

It is an inevitable fact that the development of artificial intelligence-supported diagnostic processes in dermatology will facilitate the work of dermatologists. As the society, dermatologists and developers may adapt to this process faster, the diagnosis and treatment times will be shorter. Therefore, artificial intelligence studies in dermatology have started to have a vital importance. Further studies are important building blocks needed for systems to become perfect.

This study is one of the artificial intelligence applications in dermatology. The proposed method for the detection of Onychomycosis in the study is different and better than the literature in terms of performance and procedure steps. The significant advantages of the study may be listed as follows. 1. Conventional machine learning algorithms were preferred instead of deep learning, and the training period was shortened. 2. More detailed information about the images is revealed along with the advanced image processing process. 3. The relevant information of the images is selected through the help of feature selection algorithms. Significant improvements were thereby achieved in training duration and performance. 4. The performance value of the

models proposed in this study has a higher accuracy rate compared to the literature. 5. The model developed is adequate to work on all kinds of platforms. When all these advantages are considered in general, it is evaluated that the proposed model may help the dermatologist as a decision support system in the clinic.

Funding
The authors has no received any financial support for the research, authorship or publication of this study.

Authors' Contribution
The authors contributed equally to the study.

The Declaration of Conflict of Interest/ Common Interest
No conflict of interest or common interest has been declared by the authors.

The Declaration of Ethics Committee Approval
Ethics Committee approval was obtained to conduct this study. Sakarya University, Faculty of Medicine, Date and Number: 06/11/2019 E.13973 - 71522473/050.01.04/148

The Declaration of Research and Publication Ethics
The authors of the paper declare that they comply with the scientific, ethical and quotation rules of SAUJS in all processes of the paper and that they do not make any falsification on the data collected. In addition, they declare that Sakarya University Journal of Science and its editorial board have no responsibility for any ethical violations that may be encountered, and that this study has not been evaluated in any academic publication environment other than Sakarya University Journal of Science.

REFERENCES

[1]   A. K. Gupta, G. Gupta, H. C. Jain, C. W. Lynde, K. A. Foley, D. Daigle, E. A. Cooper, R. C. Summerbell., "The

Serkan DÜZAYAK, Muhammed Kürşad UÇAR

A Novel Machine Learning-based Diagnostic Algorithm for Detection of Onychomycosis through Nail Appea...

prevalence of unsuspected onychomycosis and its causative organisms in a multicentre Canadian sample of 30 000 patients visiting physicians' offices," Journal of the European Academy of Dermatology and Venereology, vol. 30, no. 9, pp. 1567–1572, Sep. 2016.

[2] A. K. Gupta, R. R. Mays, S. G. Versteeg, B. M. Piraccini, A. Takwale, A. Shemer, M. Babaev, C. Grover, N. G. Di Chiacchio, P. R. O. Taborda, V. B. A. Taborda, Neil H. Shear, V. Piguet, A. Tosti, "Global perspectives for the management of onychomycosis," International Journal of Dermatology, vol. 58, no. 10, pp. 1118–1129, Oct. 2019.

[3] M. Papini, B. M. Piraccini, E. Difonzo, A. Brunoro, "Epidemiology of onychomycosis in Italy: prevalence data and risk factor identification," Mycoses, vol. 58, no. 11, pp. 659–664, Nov. 2015.

[4] C. R. Stewart, , L. Algu, R. Kamran, C. F. Leveille, K. Abid, C. Rae, S. R. Lipner, "Effect of onychomycosis and treatment on patient-reported quality-of-life outcomes: A systematic review," Journal of the American Academy of Dermatology, vol. 85, no. 5, pp. 1227–1239, Nov. 2021.

[5] V. Velasquez-Agudelo, J. A. Cardona-Arias, "Meta-analysis of the utility of culture, biopsy, and direct KOH examination for the diagnosis of onychomycosis," BMC Infectious Diseases, vol. 17, no. 1, pp. 1–11, Feb. 2017.

[6] S. B. Lunge, N. S. Shetty, V. R. Sardesai, P. Karagaiah, P. S. Yamauchi, J. M. Weinberg, L. Kircik, M. Giulini, M. Goldust, "Therapeutic application of machine learning in psoriasis: A Prisma systematic review," Journal of Cosmetic Dermatology, 2022.

[7] D. T. Hogarty, J. C. Su, K. Phan, M. Attia, M. Hossny, S. Nahavandi, P. Lenane, F. J. Moloney, A. Yazdabadi, "Artificial Intelligence in Dermatology—Where We Are and the Way to the Future: A Review," American Journal of Clinical Dermatology 2019 21:1, vol. 21, no. 1, pp. 41–47, Jul. 2019.

[8] S. S. Han, G. H. Park, W. Lim, M. S. Kim, J. I. Na, I. Park, S. E. Chang, "Deep neural networks show an equivalent and often superior performance to dermatologists in onychomycosis diagnosis: Automatic construction of onychomycosis datasets by region-based convolutional deep neural network," PLoS One, vol. 13, no. 1, p. e0191493, Jan. 2018.

[9] X. Zhu, B. Zheng, W. Cai, J. Zhang, S. Lu, X. Li, L. Xi, Y. Kong, "Deep learning-based diagnosis models for onychomycosis in dermoscopy," Mycoses, vol. 65, no. 4, pp. 466–472, Apr. 2022.

[10] A. De, A. Sarda, S. Gupta, S. Das, "Use of artificial intelligence in dermatology," Indian Journal of Dermatology, vol. 65, no. 5, p. 352, 2020.

[11] E. Gustafson, J. Pacheco, F. Wehbe, J. Silverberg, W. Thompson, "A Machine Learning Algorithm for Identifying Atopic Dermatitis in Adults from Electronic Health Records," Proceedings - 2017 IEEE International Conference on Healthcare Informatics, ICHI 2017, pp. 83–90, Sep. 2017.

[12] A. Martorell, A. Martin-Gorgojo, E. Ríos-Viñuela, J. M. Rueda-Carnero, F. Alfageme, R. Taberner, "Artificial Intelligence in Dermatology: A Threat

Serkan DÜZAYAK, Muhammed Kürşad UÇAR

A Novel Machine Learning-based Diagnostic Algorithm for Detection of Onychomycosis through Nail Appea...

or an Opportunity?," Actas Dermosifiliogr, vol. 113, no. 1, pp. 30–46, Jan. 2022.

[13] S. S. Han, M. S. Kim, W. Lim, G. H. Park, I. Park, S. E. Chang, "Classification of the Clinical Images for Benign and Malignant Cutaneous Tumors Using a Deep Learning Algorithm," Journal of Investigative Dermatology, vol. 138, no. 7, pp. 1529–1538, Jul. 2018.

[14] A. Yilmaz, R. Varol, F. Goktay, G. Gencoglan, A. A. Demircali, B. Dilsizoglu, H. Uvet, "Deep Convolutional Neural Networks for Onychomycosis Detection," Jun. 2021.

[15] J. Shaikh, R. Khan, Y. Ingle, N. Shaikh, "Improved skin cancer detection using CNN," International journal of health sciences (Qassim), pp. 14347–14360, Jun. 2022.

[16] P. Puri, N. Comfere, L. A. Drage, H. Shamim, S. A. Bezalel, M. R. Pittelkow, M. D. P. Davis, M. Wang, A. R. Mangold, M. M. Tollefson, J. S. Lehman, A. Meves, J. A. Yiannias, C. C. Otley, R. E. Carter, O. Sokumbi, M. R. Hall, A. G. Bridges, D. H. Murphree, "Deep learning for dermatologists: Part II. Current applications," Journal of the American Academy of Dermatology, vol. 0, no. 0, 2020.

[17] F. Lussier, V. Thibault, B. Charron, G. Q. Wallace, J. F. Masson, "Deep learning and artificial intelligence methods for Raman and surface-enhanced Raman scattering," TrAC Trends in Analytical Chemistry, vol. 124, p. 115796, Mar. 2020.

[18] A. Nogales, Á. J. García-Tejedor, D. Monge, J. S. Vara, C. Antón, "A survey of deep learning models in medical therapeutic areas," Artificial Intelligence in Medicine, vol. 112, p. 102020, Feb. 2021.

[19] X. Liu, L. Faes, A. U. Kale, S. K. Wagner, D. J. Fu, A. Bruynseels, T. Mahendiran, G. Moraes, M. Shamdas, C. Kern, J. R. Ledsam, M. K. Schmid, K. Balaskas, E. J. Topol, L. M. Bachmann, P. A. Keane, A. K. Denniston, "A comparison of deep learning performance against health-care professionals in detecting diseases from medical imaging: a systematic review and meta-analysis," The Lancet Digital Health, vol. 1, no. 6, pp. e271–e297, Oct. 2019.

[20] R. Nijhawan, R. Verma, Ayushi, S. Bhushan, R. Dua, A. Mittal, "An integrated deep learning framework approach for nail disease identification," in Proceedings - 13th International Conference on Signal-Image Technology and Internet-Based Systems, SITIS 2017, Apr. 2018, vol. 2018-January, pp. 197–202.

[21] J. Shaikh, R. Khan, Y. Ingle, N. Shaikh, "Improved skin cancer detection using CNN," International journal of health sciences (Qassim), pp. 14347–14360, Jun. 2022.

[22] R. Regin, Reddy G, K. C. S. G., J. CVN, "Nail Disease Detection and Classification Using Deep Learning," Central Asian Journal of Medical And Natural Science, vol. 3, no. 3, pp. 574–594, 2022.

[23] R. H. Chen, M. Snorrason, S. M. Enger, E. Mostafa, J. M. Ko, V. Aoki, J. Bowling, "Validation of a Skin-Lesion Image-Matching Algorithm Based on Computer Vision Technology," Telemedicine and e-Health, vol. 22, no. 1, pp. 45–50, Jan. 2016.

[24] T. S. Indi, Y. A. Gunge, "Early Stage Disease Diagnosis System Using

Serkan DÜZAYAK, Muhammed Kürşad UÇAR

A Novel Machine Learning-based Diagnostic Algorithm for Detection of Onychomycosis through Nail Appea...

Human Nail Image Processing," International Journal of Information Technology and Computer Science, vol. 8, no. 7, pp. 30–35, Jul. 2016.

[25] A. Kanchna, D. Navanisha, V. Pavithra, D. Reshika, U. G. Scholar, "Early Stage Diseases Diagnosis using Human Nail in Image Processing," International Journal of Information Technology and Computer Science, 2021.

[26] Y. J. Kim, S. S. Han, H. J. Yang, S. E. Chang, "Prospective, comparative evaluation of a deep neural network and dermoscopy in the diagnosis of onychomycosis," PLoS One, vol. 15, no. 6, p. e0234334, Jun. 2020.

[27] M. K. Uçar, "Eta Correlation Coefficient Based Feature Selection Algorithm for Machine Learning: E-Score Feature Selection Algorithm," Journal of Intelligent Systems: Theory and Applications, vol. 2, no. 1, pp. 7–12, Jul. 2019.

[28] E. Melekoglu, U. Kocabicak, M. K. Uçar, C. Bilgin, M. R. Bozkurt, M. Cunkas, "A new diagnostic method for chronic obstructive pulmonary disease using the photoplethysmography signal and hybrid artificial intelligence," PeerJ Computer Science, vol. 8, p. e1188, Dec. 2022.

[29] M. Nour, D. Kandaz, M. K. Ucar, K. Polat, A. Alhudhaif, "Machine Learning and Electrocardiography Signal-Based Minimum Calculation Time Detection for Blood Pressure Detection," Computational and Mathematical Methods in Medicine, vol. 2022, 2022.

[30] M. Akman, M. K. Uçar, Z. Uçar, K. Uçar, B. Baraklı, M. R. Bozkurt, "Determination of Body Fat Percentage by Gender Based with Photoplethysmography Signal Using

Machine Learning Algorithm," IRBM, vol. 43, no. 3, pp. 169–186, Jun. 2022.

[31] M. K. Uçar, K. Uçar, Z. Uçar, M. R. Bozkurt, "Determination gender-based hybrid artificial intelligence of body muscle percentage by photoplethysmography signal," Computational and Mathematical Methods in Medicine, vol. 224, p. 107010, Sep. 2022.

[32] R. Alpar, Spor, Applied Statistic and Validation – Reliability, Detay Publisher, 2016

[33] K. He, X. Zhang, S. Ren, J. Sun, "Delving Deep into Rectifiers: Surpassing Human-Level Performance on ImageNet Classification," in 2015 IEEE International Conference on Computer Vision (ICCV), Dec. 2015, pp. 1026–1034.

[34] X. Glorot, Y. Bengio, "Understanding the difficulty of training deep feedforward neural networks." JMLR Workshop and Conference Proceedings, pp. 249–256, Mar. 31, 2010.

[35] C. Cortes, V. Vapnik, "Support-Vector Networks," Machine Learning, vol. 20, pp. 273–297, 1995.

[36] M. Vogt, V. Kecman, "Active-Set Methods for Support Vector Machines," in Support Vector Machines: Theory and Applications, vol. 177, Berlin, Heidelberg: Springer, 2005, pp. 133–158.

[37] P. Bühlmann, "Bagging, Boosting and Ensemble Learning," in Handbook of Computational Statistics: Concepts and Methods, J. E. Gentle, W. K. Härdle, and Y. Mori, Eds. Springer-Verlag Berlin Heidelberg, 2012, pp. 1–38.

Serkan DÜZAYAK, Muhammed Kürşad UÇAR

A Novel Machine Learning-based Diagnostic Algorithm for Detection of Onychomycosis through Nail Appea...

[38] T. G. Dietterich, "Ensemble Methods in Machine Learning," International Workshop on Multiple Classifier Systems MCS 2000: Multiple Classifier Systems. Springer, pp. 1–15, 2000.

[39] L. Rokach, A. Schclar, E. Itach, "Ensemble methods for multi-label classification," Expert Systems with Applications, vol. 41, no. 16, pp. 7507–7523, Nov. 2014.

[40] I. Topal, M. K. Ucar, "Hybrid Artificial Intelligence Based Automatic Determination of Travel Preferences of Chinese Tourists," IEEE Access, vol. 7, 2019.

[41] X. Zhang, W. Dahu, "Application of artificial intelligence algorithms in image processing," Journal of Visual Communication and Image Representation, vol. 61, pp. 42–49, May 2019.

[42] P. Mamoshina, A. Vieira, E. Putin, A. Zhavoronkov, "Applications of Deep Learning in Biomedicine," Molecular Pharmaceutics, vol. 13, no. 5, pp. 1445–1454, May 2016.

[43] C. Shen, D. Nguyen, Z. Zhou, S. B. Jiang, B. Dong, X. Jia, "An introduction to deep learning in medical physics: advantages, potential, and challenges," Physics in Medicine & Biology, vol. 65, no. 5, p. 05TR01, Mar. 2020.

[44] Y. Chen, H. Liu, Z. Liu, Y. Xie, Y. Yao, X. Xing, H. Ma, "Development and validation of the interpretability analysis system based on deep learning model for smart image follow-up of nail pigmentation," Annals of Translational Medicine, vol. 10, no. 10, pp. 551–551, May 2022.

[45] S. S. Lim, J. Ohn, J. H. Mun, "Diagnosis of Onychomycosis: From Conventional Techniques and Dermoscopy to Artificial Intelligence," Frontiers in Medicine (Lausanne), vol. 8, p. 460, Apr. 2021.

FEN BİLİMLERİ ENSTİTÜSÜ
DERGİSİ

Sakarya University Journal of Science
SAUJS

Title: Characterization of Polyphenol Oxidase from Eruca sativa

Authors: Negin SHABNAM, Sibel KAHRAMAN

Characterization of Polyphenol Oxidase from *Eruca sativa*

Negin SHABNAM[1] 🆔, Sibel KAHRAMAN[*1] 🆔

Abstract

Enzymatic browning reactions by polyphenol oxidases cause alteration of appearance, flavor and nutritive value of vegetables and fruits. It is one of the important problems for vegetables used as salads and causes lots of economic losses. In this study, polyphenol oxidase (PPO) from *Eruca sativa* was extracted and characterization studies were carried out. Substrate specificity for variable substrates, optimum pH, optimum temperature, effect of different metal ions were assayed. K_m and V_{max} values were determined as for pyrocatechol $K_m = 10.24$ mM, $V_{max} = 0.0018$ U min^{-1}, catechin; $K_m = 12.57$ mM, $V_{max} = 0.0012$ U min^{-1}, gallic acid; $K_m = 23.07$ mM, $V_{max} = 0.0001$ U min^{-1}. Optimum pH and temperature were determined as pH:7.0 and 20 ºC respectively. Effect of various metal ions such as, K^+, Fe^{2+}, Mg^{2+}, Zn^{2+}, Cu^{2+} and Hg^{2+} on enzyme activity were measured. K^+, Mg^{2+}, Zn^{2+}, Cu^{2+} ions inhibited PPO activity significantly. However Fe^{2+} ion did not inhibit PPO activity.

Keywords: Characterization, *Eruca sativa*, enzyme, polyphenol oxidase

1. INTRODUCTION

Polyphenol oxidases (PPO, EC 1.14.18.1) are a group of copper-containing enzymes which catalyses two basic reactions, in the presence of molecular oxygen, the o-hydroxylation of monophenols to give o-diphenols and the subsequent oxidation of o-diphenols to o-quinones [1, 2]. O-quinones are the precursors of the browning products [3]. Enzymatic browning reaction is one of the important problems for vegetables especially for salads and causes lots of economic loss. Because, enzymatic browning poses a significant issue for vegetables used in salads since it can lead to undesirable changes in their appearance, flavor, and nutritive value, which can directly affect consumer acceptance and marketability.

Purification and characterization studies were carried out for many different plants, vegetables and fruits because of the role of PPO in enzymatic browning reactions. Since many studies aimed to suppress the activity of PPO for protecting its quality.

Eruca sativa is an edible annual plant, also known as salad rocket, roquette [4]. *Eruca sativa*, which is widely popular as salad, is one of the species of *Eruca* native to the Mediterranean region; Morocco, Portugal, Syria, Lebanon and Turkey [5, 6]. It is a good source of vitamin A, vitamin C, calcium, iron and minerals and antioxidants like flavonoids.

* Corresponding author: sibelkahraman@aydin.edu.tr (S.KAHRAMAN)
[1] İstanbul Aydın University
E-mail: neginshabnam@gmail.com
ORCID: https://orcid.org/0000-0002-5272-8664, https://orcid.org/0000-0002-8625-5471

Hydroxycinnamic and kaempferol derivatives are the main phenolic compounds in *Eruca sativa* [7]. After harvesting the plant these phenolics are subjected to oxidation which leads to enzymatic browning. This affects nutritive values and also organoleptic properties of the plant like appearance, flavor and acceptance of the consumers. Browning reactions are also sign for injury.

In our study, biochemical characterization of *Eruca sativa* PPO was aimed by determining pH and temperature effect on enzyme activity, substrate specificity, effect of metal ions and inhibitors and also kinetic determinations like K_m and V_{max} values for different substrates. The novelty and benefit of this study lie in the detailed analysis of the PPO enzyme in *Eruca sativa*, for which limited research has been previously conducted. We determined the optimum conditions for enzyme activity, such as pH, temperature, substrate specificity, and the effect of metal ions and inhibitors. This in-depth analysis offers valuable insights into the factors affecting PPO activity, which may potentially lead to innovative strategies for the prevention of enzymatic browning in *Eruca sativa* and the enhancement of its overall quality and consumer acceptance. These findings could contribute to developing strategies for preventing quality loss in *Eruca sativa*, in terms of appearance, taste, and nutritional value.

2. EXPERIMENTAL

2.1. Materials

Pyrocatechol, catechin and gallic acid were obtained from Sigma Aldrich, Merck (St. Louis, MO, USA). All the chemicals used in the study were analytical grade.

2.2. Plant Material

The identified *Eruca sativa* seeds were used from İstanbul tohumculuk. They had been cultivated in Ulus Organic Garden (İstanbul) between March and June 2015. They were stored at +4 ℃ until further use. All of the studies were performed within 24 hours after the plants were collected.

2.3. Preparation of Crude Enzyme Extract

E. sativa (5 g) was homogenized by using Waring blender (Waring commercial, USA) in 40 mL of 50 mM phosphate buffer (pH=7.0). The homogenate was filtered before centrifugation with a NF 400R centrifuge at 4100 rpm for 20 min at 4 ℃. The supernatant was used as the enzyme extract.

2.4. Enzyme Activity Assay

PPO activity was determined with spectrophotometer (Optizen POP, KLAB, Daejeon, Republic of Korea) by using pyrocatechol as substrate, measuring the increase in absorbance at 420 nm [8]. The reaction mixture contained 1.9 mL of 50 mM substrate solution prepared in 50 mM phosphate buffer at pH: 7.0 and 0.1 mL of enzyme solution. For enzyme activity, one unit was described as change 0.001 in absorbance per minute.

2.5. Evaluation of Enzyme Properties

2.5.1. Substrate specificity

Substrate specificity was tested by using 50 mM solutions of pyrocatechol, catechin and gallic acid. The reaction of substrates with PPO was measured spectrophotometrically at the particular wavelength of each substrate in 50 mM phosphate buffer (pH 7.0).

2.5.2. Effect of pH on PPO activity

Optimum pH for *E. sativa* PPO activity was assayed by monitoring its activity at pH range of 4.0-10.0 with 50 mM buffer solutions. Acetate buffer (pH 4.0–5.0), phosphate buffer (pH 6.0–7.0), and Tris-HCl buffer (pH 8.0–9.0) were used for different pH degrees. PPO activity was determined under the standard assay condition.

2.5.3. Effect of temperature on PPO activity

Optimum temperature for *E. sativa* PPO activity was assayed by measuring the enzyme activity at different temperatures. Enzyme was incubated at water bath for 45 min at the temperatures from 20 to 70 °C with 10 °C increases, prior to the addition of substrate. PPO activity was determined with pyrocatechol substrate.

2.5.4. Enzyme kinetic parameters

The specificity of *E. sativa* PPO activity was distinguished by mixing the crude extract with three different substrates: pyrocatechol, catechin and gallic acid at 420 nm at various concentrations; 5, 10, 15, 20, 25 and 30 mM. The kinetic data was plotted as $1/V$ versus $1/[S]$. The Michaelis-Menten constant (K_m) and maximum velocity (V_{max}) parameters were obtained with variable substrate concentrations in the standard reaction mixture. Substrate specificity (V_{max}/K_m) was determined by using Lineweaver-Burk plot [9].

2.5.5. Effect of metal ions on PPO activity

The effect of 5 mM solution of each metal ions such as K^+, Fe^{2+}, Mg^{2+}, Zn^{2+}, Cu^{2+} and Hg^{2+} on enzyme activity was evaluated and then percentage residual activities were found out in comparison with standard assay mixture in the absence of metal ion.

3. CONCLUSIONS AND DISCUSSION

3.1. Substrate Specificity

The varied number of phenolic compounds were reported as substrates for PPO. In this study, pyrocatechol, catechin and gallic acid were used for comparing substrate specificity. Pyrocatechol was used as main substrate because the enzyme showed high affinity (Table 1). It was followed by gallic acid and catechin respectively. The relative activities of the other substrates calculated regarding

the pyrocatechol activity. *E. sativa* PPO showed low affinity towards catechin and gallic acid. The affinity order of the enzyme towards the substrates pyrocatechol > catechin> gallic acid. In a separate study on lentil sprout PPOs [10], it was demonstrated that the enzyme had the greatest affinity for catechol (K_m = 1.32, 1.76, and 0.94 mM, respectively), which is consistent with our findings.

Table 1 Substrate specificity of *Eruca sativa* PPO

Substrates (50 mM)	Relative activity (%)
Pyrocatechol	100
Catechin	14
Gallic acid	21

3.2. Kinetic Parameters

K_m value is showing the affinity of the enzyme towards the tested substrate. Lower values are indicatives of high affinity, however higher values are indicatives of low affinity. For *E. sativa* PPO activity, Michaelis-Menten constant (K_m), the maximum reaction velocity (V_{max}), and V_{max}/K_m values were calculated using Lineweaver and Burk [9] method (Table 2). K_m and V_{max} values for pyrocatechol, catechin and gallic acid substrates were calculated and can be seen from the Table 2. *E. sativa* PPO had the highest affinity to pyrocatechol substrate due to smallest K_m value (10.24 mM). All the determination studies were done using same substrate concentrations. K_m value was reported for mamey fruit PPO K_m = 44 mM [11], 682.5 mM in cabbage [12] and 20 mM in Stanley plum [13] for catechol substrate. The blueberry PPO exhibited a K_m of 15 mM and V_{max} of 2.57 DA420 nm/min [14], for blackberry PPO, K_m of 17 mM and V_{max} of 2.02 DA420nm/min, with catechol [15]. Zhao et al., [16] reported 10.17 mM K_m value with catechol for sugar cane similar to our findings. Catechin was reported as the best substrate with a K_m of 0.49 mM for Indian tea leaf PPO [17].

Table 2 K_m and V_{max} values of *E. sativa* PPO for different substrates

Substrates (50 mM)	K_m (mM)	V_{max} (μM min^{-1})	V_{max}/K_m
Pyrocatechol	10.24	18×10^{-5}	1×10^{-5}
Catechin	46.84	32×10^{-5}	6.8×10^{-6}
Gallic acid	23.07	1×10^{-4}	4.3×10^{-6}

These differences for K_m value caused by substrate, type of extraction, purity fold of the enzyme, and location of the enzyme [18].

3.2.1. Effect of pH

The activity of *E. sativa* PPO was determined at different pH values, changing from 4.0 to 10, using pyrocatechol as substrate. All procedure was done at room temperature.

The results show that highest activity peak was obtained at pH 7.0 (Figure 1). When the pH of the media changes, also the charge of the enzyme's surface which affecting the solubility and conformation of it. That also affects the binding of the enzyme with various substrates and inhibitors [19]. Generally, PPO enzyme from different sources like plants, vegetables and fruits show its maximum activity near to neutral pHs [1, 5] therefore our result is consistent with the literature. It is worth noting that PPO reached its maximum activity near pH 7.5 for *Acetes chinensis* [20]. Altunkaya [5] found out optimum pH as 6.0 for fresh cut rocket PPO. It was also reported that optimum pH was 7.0 for borage PPO [21], red chard PPO [22], mamey fruit PPO [11].
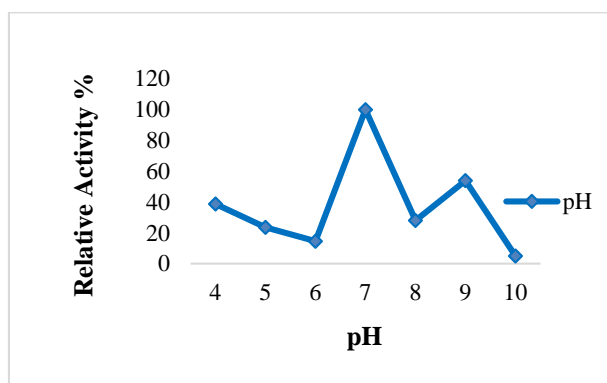
Figure 1 pH stability of *E. sativa* PPO

E. sativa PPO activity was decreased either alkaline or acidic pH's. Enzyme was almost fully inactivated at extreme alkaline conditions like pH:10 and also activity loss was observed for acidic pH's (4.0-6.0). *E. sativa* PPO activity at pH: 5.0 was lost 80%.

3.2.2. Effect of temperature
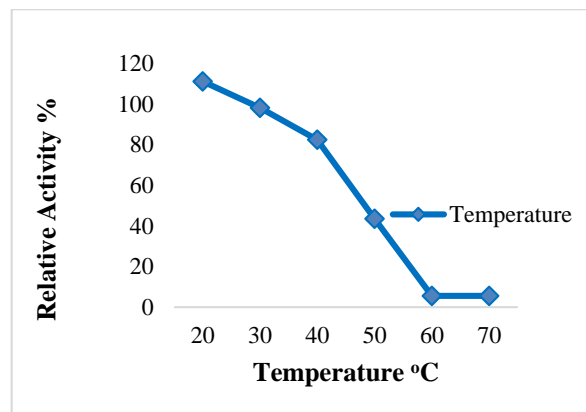
Figure 2 Temperature effect on *E. sativa* PPO

The effect of temperature between 20 and 70 ^{o}C were determined using pyrocatechol as substrate (Figure 2). Enzyme was incubated prior to the substrate addition. The results show that optimum temperature for *E. sativa* PPO was 20 ^{o}C. The enzyme activity was decreased in significant proportions higher than 50 ^{o}C. Moreover when the enzyme incubated at higher temperatures like 50-70 ^{o}C it was almost totally inactivated (5.5% residual activity).

Temperature is one of the parameters which modulate the catalytic activity of enzymes either increasing or decreasing the activity. Optimum temperature for PPO was reported as 10 °C to 60 °C for different sources and substrates [23]. Moreover PPO was known as stable at lower temperatures but unstable at higher temperatures [5]. *E. sativa* PPO activity was decreased with increasing temperatures and its activity almost completely lost when the assay temperature reached 60 ^{o}C. Palma-Orozco et al. [11] found that the mamey PPO activity decreased between 50–60 ^{o}C and after 65 ^{o}C no activity remained. Optimum temperature was reported as 30 ^{o}C for fresh cut rocket PPO [5].

Sikora *et al.* [10] reported the maximum activity of PPO from lentil sprouts occured at 35 ºC when using catechol as the substrate.

3.2.3. Effect of metal ions

The effects of various metal ions on the *E. sativa* PPO activity were studied at a concentration of 5 mM using pyrocatechol substrate at standard assay conditions. The results are presented as percentages of residual activity of PPO in Table 3.

Table 3 Effect of metal ions on *E. sativa* PPO activity

Metal ions	Relative activity (%)
K^+	21.78
Fe^{2+}	100
Mg^{2+}	24.81
Zn^{2+}	23.48
Cu^{2+}	32.57
Hg^{2+}	62.50

K^+, Mg^{2+}, Zn^{2+}, Cu^{2+}, Hg^{2+} ions decreased the PPO activity. The minimum residual activity was calculated as 21.78 % in the presence of K^+ ions. However, enzyme kept its activity in 100% after the addition of Fe^{2+} ion. Zhao et al. [16] reported inhibitory effect of K^+, $Mg^{2+,}$ Zn^{2+}, Cu^{2+} ions on sugar cane PPO. In contrast to that Mg^{2+} and Cu^{2+} increased Thomson seedless grape PPO activity, while Zn^{2+} and K^+ had an inhibitory effect [24]. Jang et al. [25] found out that PPO activity was inhibited by Mg^{2+} and Cu^{2+} and activated by Fe^{2+} and Zn^{2+} for *Solanum tuberosum* Jasim. Metal ions play important roles in maintaining substrate binding in the active site of metalloenzymes and in controlling the redox activity of metalloenzymes in enzymatic reaction [26], and the influence of metal ions on the activity of PPO is more complicated, with the degree of influence varying across different sources [27]. For instance, the activity of PPOs from flower buds of *Lonicera japonica* increased in the presence of Zn^{2+} and Mg^{2+} (10 mM) [28].

4. CONCLUSION

In this study, we aimed to provide a comprehensive investigation of PPO in *Eruca sativa*, focusing on its biochemical properties and the effects of different factors on its activity. Our findings revealed the enzyme's highest affinity for pyrocatechol ($K_m = 10.24$ mM) among the three tested substrates. The optimal pH for enzyme activity was found to be 7.0, with a decline observed at acidic pH values between 4.0 and 6.0 and alkaline pH values between 8.0 and 10.0. The optimal temperature was determined to be 20 °C, and the enzyme was found to be unstable at high temperatures.

Among the tested metal ions, the maximum decrease in enzyme activity occurred in the presence of K^+, while enzyme activity remained intact in the presence of Fe^{2+}. These findings contribute to our understanding of the optimal conditions for *Eruca sativa* PPO activity and the potential use of inhibitors for preventing quality loss. This study presents valuable insights into the potential applications of *Eruca sativa* PPO and paves the way for future research on preserving the appearance, taste, and nutritional value of the plant.

The Declaration of Research and Publication Ethics

The authors of the paper declare that they comply with the scientific, ethical and quotation rules of SAUJS in all processes of the paper and that they do not make any falsification on the data collected. In addition, they declare that Sakarya University Journal of Science and its editorial board have no responsibility for any ethical violations that may be encountered, and that this study has not been evaluated in any academic publication environment other than Sakarya University Journal of Science.

REFERENCES

[1]   A. Altunkaya, V. Gökmen, "Partial purification and characterization of polyphenoloxidase from durum wheat (*Triticum durum* L.)", Journal of Cereal Science, vol. 55, no. 3, pp. 300–304, 2012.

[2]   R. Yoruk, M. R. Marshall, "Physicochemical properties and function of plant polyphenol oxidase: a review 1", Journal of Food Biochemistry, vol. 27, no. 5, pp. 361-422, 2003.

[3]   A. M Mayer, E. Harel, "Phenoloxidases and their significance in fruit and vegetables" Food Enzymology, vol. 1, pp. 373-398, 1991.

[4]   J. Ahmed, F. Al-Salman, A. S. Almusallam, "Effect of blanching on thermal color degradation kinetics and rheological behavior of rocket (*Eruca sativa*) puree", Journal of Food Engineering, vol. 119, no. 3, pp. 660–667, 2013.

[5]   A. Altunkaya, "Effect of Various Inhibitors on Enzymatic Browning, Antioxidant Activity and Total Phenol Content of Fresh-Cut Rocket Salad (*Eruca Sativa* Mill.)", Hacettepe Journal of Biology & Chemistry, vol. 49, no. 4, pp. 345-354, 2021.

[6]   M. Blamey, C. Grey-Wilson, "Illustrated flora of Britain and Northern Europe. Hodder and Stroughton, 1989.

[7]   E. Degl`Innocenti, A. Pardossi, F. Tattini, L. Guidi, "Phenolic compounds and antioxidant power in minimally processed salad", Journal of Food Biochemistry, vol. 32, pp. 642-653, 2008.

[8]   U. Gawlik-Dziki, "Effect of hydrothermal treatment on the antioxidant properties of broccoli (*Brassica oleracea* var. botrytis italica) florets", Food Chemistry, vol. 109, no. 2, pp. 393–401, 2008.

[9]   H. Lineweaver, D. Burk, "The determination of enzyme dissociation constants", Journal of American Chemical Society, vol. 56, pp. 658-666, 1934.

[10]   M. Sikora, M. Świeca, M. Franczyk, A. Jakubczyk, J. Bochnak, & U. Złotek, "Biochemical properties of polyphenol oxidases from ready-to-eat lentil (Lens culinaris Medik.) sprouts and factors affecting their activities: A search for potent tools limiting enzymatic browning", Foods, vol. 8, no. 5, pp. 154, 2019.

[11]   G. Palma-Orozco, A. Ortiz-Moreno, L. Dorantes-Álvarez, J. G. Sampedro, H. Nájera, "Purification and partial biochemical characterization of polyphenol oxidase from mamey (*Pouteria sapota*)", Phytochemistry, vol. 72, no. 1, pp. 82-88, 2011.

[12]   T. Nagai, N. Suzuki, "Partial purification of polyphenol oxidase from Chinese cabbage *Brassica rapa*

L", Journal of Agricultural Food Chemistry, vol. 49, pp. 3922–3926, 2001.

[13] M. Siddiq, N. K. Sinha, J. N. Cash, "Characterization of polyphenol oxidase from Stanley plums", Journal of Food Science, vol. 57, pp. 1177–1179, 1992.

[14] M. Siddiq, K. D. Dolan, "Characterization of polyphenol oxidase from blueberry (*Vaccinium corymbosum* L.)", Food Chemistry, vol. 218, pp. 216-220, 2017.

[15] E. M. Gonzalez, B. de Ancos, & M. Pilar-Cano, "Partial characterization of peroxidase and polyphenol oxidase activities in blackberry fruits", Journal of Agricultural Food Chemistry, vol. 48, pp. 5459–5464, 2000.

[16] Z. G. Zhao, L. C. Zhu, S. J. Yu, M. Saska, "Partial purification and characterization of polyphenol oxidase from sugarcane (*Saccharum officinarum* L.)", Zuckerin-dustrie, vol. 136, pp. 296–301, 2011.

[17] J. Halder, P. Tamuli, A. N. Bhaduri, "Isolation and characterization of polyphenol oxidase from Indian tea leaf (*Camellia sinensis*)", Journal of Nutritional Biochemistry, vol. 9, no. 2, pp. 75-80, 1998.

[18] P. Montero, A. Avalos, M. Perez-Mateos, "Characterization of polyphenoloxidase of prawns (*Penaeus japonicus*), Alternatives to inhibition: additives and high-pressure treatment", Food Chemistry, vol. 75, no. 3, pp. 317-324, 2001.

[19] A. M. Mayer, "Polyphenol oxidases in plants and fungi: going places? A review", Phytochemistry, vol. 67, pp. 2318–2331, 2006.

[20] J. Zhang, G. Zhou, L. Fei, L. Chen, L. Sun, F . Lyu, Y. Ding, "Study on Purification and Characterization of Polyphenol Oxidase from *Acetes chinensis*", Molecules. vol. 26, no. 24, pp. 7545, 2021.

[21] E. H. Alici, G. Arabaci, "Purification of polyphenol oxidase from borage (*Trachystemon orientalis* L.) by using three-phase partitioning and investigation of kinetic properties", International Journal of Biological Macromolecules, vol. 93, pp. 1051–1056, 2016.

[22] G. Zhao-Jian, H. Xiao-Hong, X. Xing-Guo, "Purification and characterisation of polyphenol oxidase from red swiss chard (*Beta vulgaris* subspecies cicla) leaves", Food Chemistry, vol. 117, pp. 342-348, 2009.

[23] D. Panadare, V. K. Rathod, "Extraction and purification of polyphenol oxidase: A review", Biocatalysis and Agricultural Bio-technnology, vol. 14, pp. 431–443, 2018.

[24] Y. Zheng, J. Shi, Z. Pan, "Biochemical characteristics and thermal inhibition kinetics of polyphenol oxidase extracted from Thompson seedless grape", European Food Research and Technology, vol. 234, pp. 607–616, 2012.

[25] J. W. Jang, Y. Y Ma, J. M. Shin, K. B. Song, "Characterization of polyphenol oxidase extracted from *Solanum tuberosum* Jasim", Food Science and Biotechnology, vol. 14, pp. 117–122, 2005.

[26] D. K. Yadav, A. Prasad, J. Kruk, P. Pospisil, "Evidence for the involvement of loosely bound plastosemiquinones in superoxide anion radical production in photosystem II", PLoS ONE , vol. 9, no.12, pp. e115466, 2014.

[27] K.Saby John, S. G. Bhat, U. J. S. Prasada Rao, "Isolation and partial characterization of phenol oxidases from *Mangifera indica* L. sap (latex) ", Journal of Molecular Catalysis B: Enzymatic, vol. 68, no. 1, pp. 30–36, 2011.

[28] N. Liu, W. Liu, D. Wang, Y. Zhou, X. Lin, X. Wang, S. Li, "Purification and partial characterization of polyphenol oxidase from the flower buds of *Lonicera japonica* Thunb.", Food Chemistry, vol. 138, no. 1, pp. 478–483, 2013.

Title: Experimental and Numerical Investigation of Flexural Properties of Solid Wood Materials Reinforced with Various FRP

Authors: Şemsettin KILINÇARSLAN, Yasemin ŞİMŞEK TÜRKER

Experimental and Numerical Investigation of Flexural Properties of Solid Wood Materials Reinforced with Various FRP

Şemsettin KILINÇARSLAN [*1] iD , Yasemin ŞİMŞEK TÜRKER[1] iD

Abstract

Wood material is destroyed over time by biotic and abiotic factors. Many of the historical buildings are made of wooden materials and these materials can degrade over time with the effect of environmental conditions. In order to ensure the sustainability of these buildings with historical value, they need to be repaired and strengthened over time. In this study, 20x20x360 mm wood specimens of Ash tree species were strengthened with carbon, basalt and glass based FRP materials. The flexural properties of the reference sample without wrapping and the samples reinforced with carbon, basalt and glass based FRP material were examined. For this purpose, at first three-point bending test has been performed, and then obtained results are compared with the numerical ones found from finite element analysis software ANSYS. As result, a good agreement has been found between experimental and numerical results. As a result of the flexural tests, the load-displacement curves, values of flexural strength and values of modulus of elasticity the samples were determined. In this study, it was determined that the highest load carrying capacity value belongs to the sample reinforced with carbon-based FRP polymers.

Keywords: Reinforcement, wood structures, wood materials, numerical, ANSYS

1. INTRODUCTION

Wood is a construction, aesthetic and engineering material with a wide range of uses, its many positive properties [1, 2]. Its biological structure, physical and mechanical properties and chemical composition allow wood to be used in many different products. The fact that wood is a good insulation material and its resistance high values compare to its density are among the reasons for preference [3-7].

In addition to its many positive features, wood also has some undesirable features that limit the areas of use or cause problems during its use. With these inconvenient features, the wooden element requires maintenance, repair and reinforcement over time. There are many studies on those improvements of wooden materials and it is important to strengthen these structures. Wooden structures have traditionally been reinforced with pieces of steel and wood material [8]. It was stated that the investigation of the effect of reinforcement

* Corresponding author: semsettinkilincarslan@sdu.edu.tr (Ş:KILINÇARSLAN)
1 Suleyman Demirel University
E-Mail: yaseminturker@sdu.edu.tr
ORCID: https://orcid.org/0000-0001-8253-9357, https://orcid.org/0000-0002-3080-0215

Şemsettin KILINÇARSLAN, Yasemin ŞİMŞEK TÜRKER

Experimental and Numerical Investigation of Flexural Properties of Solid Wood Materials Reinforced wi...

with fiber-reinforced polymers (FRP) on different properties of wooden elements dates back to the 60s [9].

Fiber reinforced polymer (FRP) composites consist of fibers embedded in a polymer component matrix. Composite material, which consists of a combination of fiber and this polymer component matrix, has superior properties than its original components. In recent years, various studies have been carried out on the strengthening of wood materials with FRP polymers [10-14]. Spaun (1981) [15] examined the increase in stiffness and tensile strength by performing the bending test of reinforced beams using glass fiber reinforcement. In later studies, carbon fiber started to be used as a reinforcement material for the reinforcement of beams [9]. Garcia et al., (2013) [16] stated in their study that if the lower surface of a beam subjected to bending is reinforced with FRP (carbon and basalt-based fabrics) composite materials, there will be an increase in bearing capacity as well as an increase in ductility.

Kilincarslan and Simsek Türker (2021) [17], are aimed to strengthen the joints of carbon fiber reinforced polymer and glulam column-beam joints. For this purpose, using WV90080 and ALUMIDI 160, WV90110 and ALUMIDI 200 connection elements, they produced 2 column-beam connection samples of each connection type. They prepared one of the samples produced in each connection as a reference and the other as a reinforced sample. They subjected the produced column-beam joint samples to the load-displacement test within the framework of the experiment.

It was determined that the load carrying capacity, energy dissipation capacity and rigidity values of the samples whose column-beam connections were strengthened were high. It has been stated that reinforcement with carbon-based FRP fabric increases the strength and durability of the column-beam connection area.

Karagöz Isleyen and Kesik (2021) [18] 22 used carbon fiber reinforced polymer to improve the mechanical behavior of old wood samples that were damaged over time due to various environmental and biological factors. They investigated the effect of FRP reinforcement on the strength values of old and new wood specimens under bending and compression loads. They found that the values of flexural strength for new wood, reinforced old wood and reinforced new wood increased by 28%, 34% and 59%, respectively, compared to the old unreinforced wood material. They determined that the values of elasticity modulus of new wood, reinforced old wood and reinforced new wood were 15%, 19% and 34% higher than the old wood, respectively.

In this study, it was aimed to investigate the effect of reinforcement with carbon, glass and basalt-based polymer fabric on the flexural properties of Ash beams.

2. MATERIAL AND METHODS

In this study, Ash (*Fraxinus excelsior L.*) wood species, which is widely used in the production of wood composites and especially for structural purposes, is studied. The Ash beam samples used in the study have been supplied from Nasreddin Forest Products (Naswood) Ltd. in the Antalya region. The wooden beams are manufactured from smooth, knot-free, flawless timber with dimensions of 20x20x360 mm. Before the beams are tested, all samples have been kept at temperature 20 ºC (±2) ºC and relative humidity 65% (±5) conditions until they reached the same equilibrium humidity. After the samples were kept in the air-conditioning cabinet, the humidity levels were checked with an electric humidity meter.

Fiber reinforced polymer fabric based on carbon, glass and basalt is used for reinforcement in the study. The technical properties of the FRP fabrics used are given in Table 1.

Şemsettin KILINÇARSLAN, Yasemin ŞİMŞEK TÜRKER

Experimental and Numerical Investigation of Flexural Properties of Solid Wood Materials Reinforced wi...

Table 1 The technical properties of carbon, glass and basalt fabrics (BASF, 2020)

Structure of the Material	Carbon	Glass	Basalt
Weight (g/m^2)	300	300	200
Modulus of Elasticity (GPa)	230	72	82
Tensile strength (N/mm^2)	4900	3900	3200
Design Section Thickness (mm)	0.166	1.162	0.167
Elongation at Break (%)	2.1	4.8	3.5
Width (mm)	500	500	500

In this study, at least two layers of wrapping are used for the strengthened samples with fiber-reinforced polymer fabrics, due to two layers of wrapping is proposed in the practical use of industry. Roll priming is performed to form a thin film layer (0.1 -0.2 mm) with an epoxy-based primer developed for the MasterBrace® FRP (MasterBrace® P 3500) System. After the priming process, Developed Epoxy adhesive for MasterBrace® FRP (MasterBrace® SAT 4500) Fibrous Polymer System is used. Epoxy adhesive is applied to the primed surfaces with a roller to achieve a thickness of 1 mm. As seen in Figure 1, the wrapping process of wooden beams with FRP composites has been performed in a U-shaped reinforcement in three regions of the beam. After the epoxy adhesive is applied, fibrous polymer fabrics cut in appropriate sizes are stretched in the direction of their fibers and adhered to the surface, immediately. Then, it is ensured that the epoxy is absorbed into the fabric and there is not any gap between it and the surface by pressing in the direction of the fibers of the fibrous polymer fabrics with a roller. After the first layer of adhesive is completed, the same operations have been repeated once again, the second layer is wrapped and the wrapping process is completed.

The wrapped beams are kept for 1 week before being subjected to the three-point bending test. Flexural strength tests are carried out on 20x20x360 mm specimens prepared in accordance with TS 2474 (2005). In the bending tests, the loading speed is set as 6 mm/min constant speed and the experiments

are carried out. The span of the support points is taken as 300 mm in the experiments.

Figure 1 Image of the wrapping process with FRP polymers, A: Preparing the beams for wrapping after the priming process B: Wrapping the beams with FRP polymer fabric

The flexural strength and modulus of elasticity are determined as follows, respectively.

$$\sigma_E = \frac{aP_{max}l}{2bh^2} \tag{1}$$

$$E = \frac{\Delta Pl^3}{4bh^2\Delta f} \tag{2}$$

where σ_E is the flexural strength (N/mm^2), P_{max} is the breaking load (N), l is the space between the support points (mm), b is the width of the specimens (mm) and h is the height of the specimens (mm), $\Delta P = P_2 - P_1$ is the increase of force in the loading/ deflection curve linear section [N], $\Delta f = f_2 - f_1$ is the deflection increase in the middle of the test specimen's length.

The flexural strength and modulus of elasticity values of the beams are determined, and the effect of reinforcement with carbon, glass and basalt-based FRP fabric polymers on the flexural properties of Ash beams are investigated.

The wooden beams are modeled and numerically analyzed in the finite element analysis software ANSYS. Due to wood is an anisotropic material owing to the presence of

Şemsettin KILINÇARSLAN, Yasemin ŞİMŞEK TÜRKER

Experimental and Numerical Investigation of Flexural Properties of Solid Wood Materials Reinforced wi...

knots and defects, it is generally modeled as orthotropic material in numerical analysis. The behaviors of wood behaviors are described using the engineering constants such as the modulus of elasticity (MOE) in the longitudinal, radial, and tangential directions (Ex; Ey; Ez), shear modulus (Gxy, Gxz, Gyz), and Poisson's ratio.

After the material definition, the loads and supports are also defined and meshed. The thickness values of the FRP fabrics are taken as 0.166 mm during the modeling. Figure 2, shows A) Reference beam, B) 360 mm long beam reinforced with various FRP fabrics.
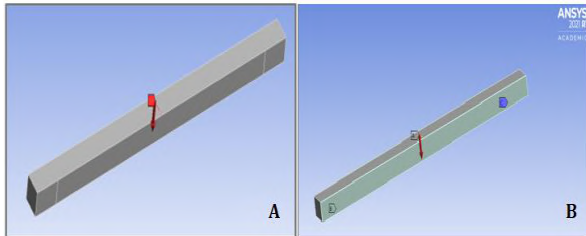
Figure 2 Modeling of beams in ANSYS Software A: Reference sample B: Reinforcement with FRP polymers in 360 mm length

As a result of the analyzes made in the ANSYS Software program, the results are given in Figure 3.
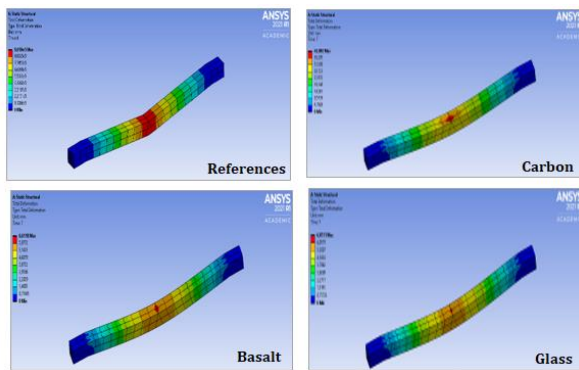
Figure 3 Finite element analysis images of Iroko samples reinforced with Carbon, Basalt, and Glass FRP polymers

After performing the analyzes with ANSYS, the finite element results and the static analysis results are compared.

3. RESULTS AND DISCUSSION

In this study, Ash beams are reinforced with carbon, glass and basalt based FRP fabrics. Reference beams and reinforced beams are subjected to the bending test. Load-displacement graphs and values of flexural strength-modulus of elasticity obtained in the study are given in Figure 4, Figure 5 and Figure 6.
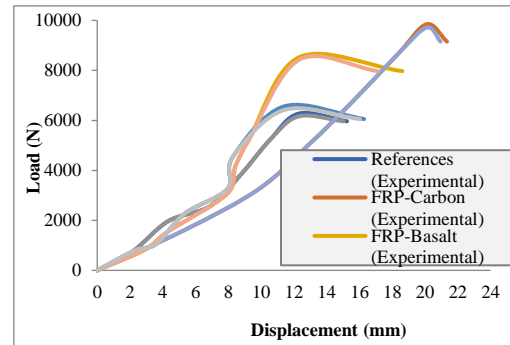

Figure 4 Load-displacement graphs of beams

It was determined that the load bearing capacities of the beams reinforced with carbon, basalt and glass-based FRP polymers increased by 56.95%, 36.00% and 4.57%, respectively, compared to the reference sample. It was determined that the displacement amounts of the reinforced beams increased by 40.02%, 3.37% and 1.04%, respectively, in carbon, basalt and glass-based fabrics compared to the reference beams.
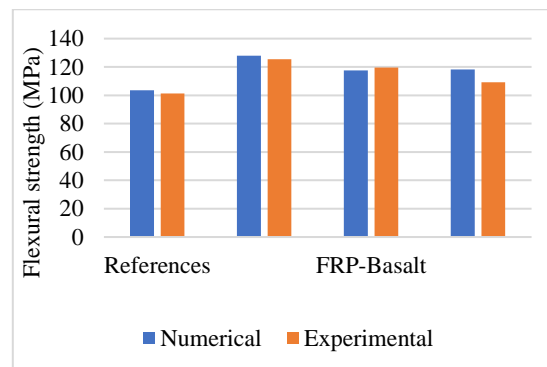

Figure 5 Flexural strength of reference and reinforced beams

Şemsettin KILINÇARSLAN, Yasemin ŞİMŞEK TÜRKER

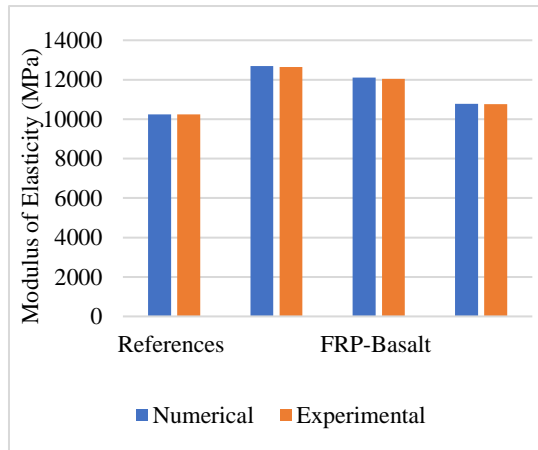Experimental and Numerical Investigation of Flexural Properties of Solid Wood Materials Reinforced wi...

Figure 6 Modulus of elasticity of reference and reinforced beams

When Figure 4 and Figure 5 are examined, the values of flexural strength of the beams reinforced with carbon, basalt and glass-based polymer fabrics increased by 23.68%, 18.10% and 7.71%, respectively, compared to the reference beams. The values of modulus of elasticity increased by 23.36%, 17.48% and 5.02%, respectively. Results of the static bending test were compared with those for numerical ones, it was observed that both results are in good agreement.

4. CONCLUSION

In this study, the effect of reinforcement with carbon, basalt and glass-based fiber reinforced polymer fabric on the bending properties of ash beams was investigated. It has been determined that strengthening with FRP polymers increases the load carrying capacity, displacement amount, flexural strength values and modulus of elasticity of wood materials. When the test results obtained from the experiments and the values obtained by numerical modeling were compared, it was seen that both results gave almost the same values. Compared with the reference samples, it was determined that the highest flexural strength and modulus of elasticity were obtained by carbon-based FRP polymers, and the lowest load-carrying capacity was obtained by glass-based FRP polymers. It has been determined that this change is compatible with the modulus of elasticity values of FRP fabrics. It has been concluded that the FRP polymer fabrics used can be used to strengthen wooden structures.

The Declaration of Conflict of Interest/ Common Interest
No conflict of interest or common interest has been declared by the authors.

Authors' Contribution
The authors contributed equally to the study

The Declaration of Ethics Committee Approval
This study does not require ethics committee permission or any special permission

The Declaration of Research and Publication Ethics
The authors of the paper declare that they comply with the scientific, ethical and quotation rules of SAUJS in all processes of the paper and that they do not make any falsification on the data collected. In addition, they declare that Sakarya University Journal of Science and its editorial board have no responsibility for any ethical violations that may be encountered, and that this study has not been evaluated in any academic publication environment other than Sakarya University Journal of Science.

REFERENCES

[1] K. Akgün, "The effects of tannin and heat treatment on some physical and mechanical properties of laminated

Şemsettin KILINÇARSLAN, Yasemin ŞİMŞEK TÜRKER

Experimental and Numerical Investigation of Flexural Properties of Solid Wood Materials Reinforced wi...

chestnut (*castanea sativa* mill.) wood", Zonguldak Karaelmas University, Graduate School of Natural and Applied Sciences, Ph.D. Thesis, p. 98, 2008.

[2] H. T. Sahin, M. B. Arslan Korkut, S., C. Sahin, ''Colour changes of heat-treated woods of red-bud maple, European hophornbeam and oak.'' Color Research & Application, 36(6), 462-466, 2011.

[3] C. K. Sahin, B. Onay. ''Alternative wood species for playgrounds wood from fruit trees.'' Wood Research, 65(1), 149-160, 2020.

[4] C. K. Sahin, M. Topay, A. A. Var, ''A study on suitability of some wood species for landscape applications: surface color, hardness and roughness changes at outdoor conditions.'' Wood Research, 65(3), 395-404, 2020.

[5] C. Sahin, B. Onay, E. Mirza, ''A Natural Sustainable Material for Urban Design: Wood, In: "Theories, Techniques, Strategies" for Spatial Planners & Designers Planning,'' Design, Applications, Murat Ozyavuz (ed.), Peter Lang GmbH. Berlin 221-234, 2021.

[6] Y. Bozkurt, Y. Göker, "Utilization of forest products textbook", Istanbul University Faculty of Forestry Publications, İstanbul, 1981.

[7] S. Yıldız, "Physical, mechanical, technological and chemical properties of heat treated eastern beech and eastern spruce woods", Karadeniz Technical University, Graduate School of Natural and Applied Sciences Doctoral Thesis, p. 285, Trabzon, 2002.

[8] C. González Bravo, "Recuperación de la capacidad mecánica en piezas de madera solicitadas a flexión en estructuras tradicionales operando por

la cara superior mediante refuerzos y prótesis metálicas". PhD Thesis. E.T.S. of Architecture, Polytechnic University of Madrid, p. 265, 2007.

[9] F. H. Theakston, "A feasibility study for strengthening timber beams with fibreglass", Canadian Agricultural Engineering, vol. 17, 1965.

[10] J. Fiorelli, A.A. Dias, "Analysis of the strength and stiffness of timber beams reinforced with carbon fiber and glass fiber", Materials Research, vol. 6, pp. 193–202, 2003.

[11] M. Fossetti, G. Minafò, M. Papia, "Flexural behaviour of glulam timber beams reinforced with FRP cords", Construction and Building Materials, vol. 95, pp. 54-64, 2015.

[12] S. Kilincarslan, Y. Şimşek Türker, ''The Effect of Strengthening With Fıber Reinforced Polymers on Strength Propertıes of Wood Beams'', 2nd International Turkish World Engineering and Science Congress, pp. 8-14, 2019.

[13] F. J. Rescalvo, C. Abarkane, E. Suárez, Valverde- I. Palacios and A. Gallego, "Pine beams retrofitted with FRP and poplar planks: mechanical behavior". Materials, vol. 12, no. 19, 2019.

[14] B. F. Donadon, N. T. Mascia, Vilela, R. L., M. Trautwein, "Experimental investigation of glued-laminated timber beams with Vectran-FRP reinforcement". Engineering Structures, vol. 202, 109818, 2020.

[15] F. D. Spaun, "Reinforcement of wood with fibreglass". Forest Product Journal, vol. 31, no.4, pp. 26–33, 1981.

[16] P. De La Rosa García, A. C. Escamilla, M., N. G. García, "Bending reinforcement of timber beams with

Şemsettin KILINÇARSLAN, Yasemin ŞİMŞEK TÜRKER

Experimental and Numerical Investigation of Flexural Properties of Solid Wood Materials Reinforced wi...

composite carbon fiber and basalt fiber materials". Composites Part B: Engineering, vol. 55, pp. 528-536, 2013.

[17] S. Kilincarslan, Y. Şimşek Türker, "Experimental investigation of the rotational behaviour of glulam column-beam joints reinforced with fiber reinforced polymer composites". Composite Structures, vol. 262, 2021.

[18] Ü. K. Işleyen, H. İ. Kesik, "Experimental and numerical analysis of compression and bending strength of old wood reinforced with CFRP strips", Structures, vol. 33, pp. 259-271, 2021.

Title: Bibliometric Profile of Global Scientific Research on Monitoring and Assessment of Aquatic Toxicology (2015-2019)

Authors: Ayşen Nil BERBER, V. Zülal SÖNMEZ, Ceyhun AKARSU, Nüket SİVRİ

Bibliometric Profile of Global Scientific Research on Monitoring and Assessment of Aquatic Toxicology (2015-2019)

Ayşen Nil BERBER[1] , V. Zülal SÖNMEZ*[1] , Ceyhun AKARSU[1] , Nüket SİVRİ[1]

Abstract

In recent decades, extensive research has been conducted to explore toxicity in the aquatic environment. In spite of the extensive research conducted on toxicity in the aquatic environment, there is a need for a comprehensive analysis that integrates various aspects of the research landscape. This study focused on: i) providing characteristics of research areas of publications, ii) assessing productive countries and institutions, iii) identifying research topics based on certain keywords and defining research hotspots, and iv) assisting in the perspective of current hot topics, future trends, and challenges. A systematic review and analysis of studies on natural water and wastewater toxicology from the Scopus database were conducted, covering the period from 2015 to 2019. This study presents a temporal distribution of publications considering several factors, such as materials, types of toxicity, test organisms, journals, and country. By conducting a comprehensive search on Scopus, our study identified a total of 7,043 articles on acute (62%) and chronic toxicity (38%). Freshwater environments accounted for the majority of acute and chronic toxicity studies, while studies on wastewater environments were relatively scarce. *Daphnia magna* emerged as the most used organism, representing 41% of acute toxicity studies and 27% of chronic toxicity studies. The results show that China is the most productive country with 330 articles. The study has made it possible to visualise an effective contribution to science by filling the existing gaps. It has provided some perspectives and insights for the development of further research on this topic.

Keywords: Ecotoxicity, acute, chronic, aquatic systems, bibliometric analysis

1. INTRODUCTION

Examining the studies of each branch of science shows the stages of development in the field. It is also important to determine which topics have been the focus over time [1]. Bibliometric analyses are important tools to assess and measure the growth of the literature on a particular topic. Recently, the bibliometric method has been used in various contexts to identify research gaps for future studies and to show trends in research activity [2-7]. Therefore, bibliometric analysis is nowadays a promising alternative approach for assessing research on water and wastewater toxicity.

* Corresponding author: zulal.sonmez@iuc.edu.tr (V.Z. SÖNMEZ)
[1] Istanbul University-Cerrahpasa, Engineering Faculty, Environmental Engineering Department, Istanbul, Türkiye
E-mail: aysennil34@gmail.com, ceyhunakarsu@iuc.edu.tr, nuket@iuc.edu.tr
ORCID: https://orcid.org/0000-0001-8779-2183, https://orcid.org/0000-0002-7488-2996 , https://orcid.org/0000-0002-0168-9941 , https://orcid.org/0000-0002-4269-5950

BERBER et al.

Bibliometric Profile of Global Scientific Research on Monitoring and Assessment of Aquatic Toxicology...

Aquatic toxicology is the scientific field that examines the impact of substances and physicochemical conditions on plants and animals residing in water ecosystems. It encompasses the investigation of mechanisms through which alterations in water quality or food availability influence the growth, reproduction, behavior, and survival of aquatic organisms. The discipline of aquatic toxicology delves into the effects of both synthetic chemicals and naturally occurring substances, as well as human-induced and natural activities, on aquatic organisms at various levels of organization. These levels range from subcellular and individual organisms to communities and ecosystems [5].

The most effective way to protect aquatic ecosystems is to measure and monitor changes in the area of concern [8]. Toxicity testing is important for monitoring water quality and discharge areas, protecting organisms in the food chain and determining the stimulatory effects of toxic substances on organisms [9-11]. Toxicity tests conducted for this purpose attempt to determine the toxic effect on the selected organism (acute/chronic) based on exposure [12]. Factors such as organism types, trophic levels (producers, primary and secondary consumers, decomposers), taxonomic groups, organism species and strains, age, sex, temperature, body mass index, maturity, and experimental environmental conditions affecting the quality of life of the organism are effective in determining the endpoint of toxicity [13]. By conducting bioanalysis studies, ecotoxicity can be demonstrated in environmental risk assessment and water quality/pollution control [14]. Pollutants originating from industrial, domestic and agricultural activities first flow into rivers and enter lakes and oceans through them. Pollution of water bodies not only affects the creatures they harbour, but also reaches humans through the food chain [15-18].

Zooplankton are frequently utilized in ecotoxicological tests due to their high sensitivity to toxic chemicals and their crucial role in the lentic food chain. These organisms can provide valuable insights into their responses to toxicity and the overall effects on the ecosystem [19-20]. However, not every organism that meets the requirements of a toxicity test may be suitable. For instance, in environments with lower toxicity, such as surface waters, it is more appropriate to employ more sensitive test organisms.

Despite the considerable research efforts dedicated to the study of toxicity in the aquatic environment, there remains a need for a comprehensive analysis encompassing the various facets of the research landscape [5]. The aim of this study is, therefore, to evaluate the studies on toxicity in water and wastewater from the Scopus database (Elsevier), in order to address the existing research gaps comprehensively. This study focuses on several objectives: i) providing characteristics of the research areas covered in the publications, ii) assessing productive countries and institutions, iii) identifying research topics based on specific keywords and defining research hotspots, and iv) offering insights into current hot topics, future trends, and challenges.

2. MATERIALS AND METHODS

2.1. Keywords Used in Literature Search

This study utilized the Scopus search engine to identify acute and chronic toxicity studies in the field of environmental sciences conducted between 2015 and 2019. The identification of toxicity studies was performed in two steps using predefined keywords, encompassing research on both acute and chronic toxicity. In the first step, a general search was conducted using keywords such as "toxicity," "acute/chronic," "journal," "environmental science," "article," and "years" to identify relevant publications. The second step involved a focused search using the keywords "toxicity" and "acute" or "chronic" or "freshwater (FW)" for freshwater environments, "marine water (MW)/seawater (SW)" for seawater environments, and "wastewater (WW)" for wastewater

BERBER et al.

Bibliometric Profile of Global Scientific Research on Monitoring and Assessment of Aquatic Toxicology...

environments. Additionally, the years "2015," "2016," "2017," "2018," and "2019" were selected to assess changes over time, applying the restriction to both the first and second search criteria.

2.2. Limitations of the Study

The identified search was limited to the research field of environmental science. In this way, study areas such as medicine, chemistry and pharmacology, or any other departments of toxicology were excluded.

Publications were searched for the words "article" or "original research" to identify original studies. Articles published in book chapters, reviews, opinion pieces and conference papers were excluded from the analysis for reasons of scientific acceptability. In addition, publications that did not contain multiple research informants such as organism, environment and/or substance were not included in this study. These studies were included in the group "Other".

2.3. Analysis and Visualization of Data in the Study

Microsoft Excel® and VOSviewer® (version 1.6.16) were used for the visual representation of the data. The data obtained on organisms, countries and journals were transferred to the VOSviewer® programme and displayed visually, as the VOS analysis tool shows the best performance among the other techniques [21]. VOSviewer® supports the visual representation and verification of bibliometric networks by providing easy access to the VOS mapping method [21]. The interpretation of the images, the size of the circles on the map, the font used, and the number of classes are indicated by colour clusters. The interpretation of the similarity and relationship between the circles is indicated by the distance between the circles [22].

3. RESULTS AND DISCUSSION

To interpret the results of the study, each article identified in the Scopus search tool between 2015 and 2019 was categorised by research environment (freshwater, seawater, and wastewater), toxicity (acute/chronic), authors, organism, article title, journal name and years. The data are presented and interpreted in subheadings by toxicity exposure, research setting, years, test organism, countries, and published journals.

3.1. Distrubution by Exposure

Based on the Scopus search, 7043 articles were found on acute and chronic toxicity between 2015 and 2019 in the first search. Of these, 62% were acute, while 38% of them were chronic studies. The second search revealed 1162 articles on acute toxicity and 613 articles on chronic toxicity. 5268 articles identified out of 7043 products are included in the "others" category (see subtitle 2.2). Of the articles in the "Others" category, 3186 of them were related to acute toxicity and 2082 to chronic toxicity (Figure 1).

The first search found a large number of articles because there was no restriction of "FW, WW, SW and MW" in the search field. In the second search, the keywords "FW, WW, SW and MW" were used to restrict the research environment in aquatic areas. However, despite the use of keywords to restrict the research environment, it was found that there are also studies where the search field is not aquatic areas. The present study is based on literature searches where samples were taken from aquatic environments for toxicity testing.
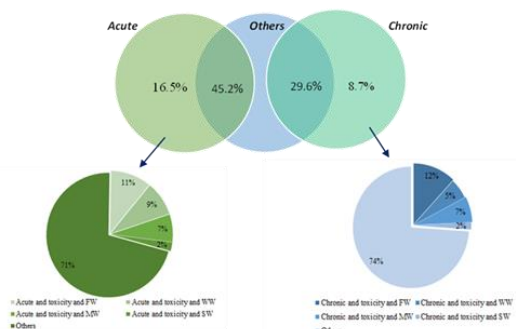
BERBER et al.

Bibliometric Profile of Global Scientific Research on Monitoring and Assessment of Aquatic Toxicology...

Figure 1 Distribution by exposure ("Others" category considered)

No search criteria were used to identify studies involving organisms. For this reason, each of the articles was examined individually, and the articles that did not contain organism species were excluded. In this way, the types of organisms were determined. However, the limitation of the search field is not the only factor here. Although the keywords "toxicity, acute, chronic, FW, WW, SW and MW" and the limiting criteria "journal, article, environmental science, 2015, 2016, 2017, 2018 and 2019" were used, it was found that some studies did not meet these criteria. When the articles found in the second search were examined individually, studies that were not related to environmental science were excluded to ensure that publications from different disciplines were not encountered as science. For this reason, the importance of examining the content of the articles became apparent. All these identified studies were included in the category "Other".

The results indicated a higher number of acute toxicity studies compared to chronic toxicity studies. This difference can be attributed to the fact that acute toxicity tests provide faster results for researchers compared to chronic toxicity tests. Furthermore, chronic toxicity studies tend to be more costly and time-consuming [23]. Acute toxicity tests are often preferred in emergency situations or when there is a need for a quicker assessment of chemicals, wastewater, or water samples. However, combining acute toxicity studies with chronic toxicity studies enables a more

comprehensive toxicological evaluation, allowing for the consideration of various risk scenarios.

3.2. Distrubution by Environment

The second search, limited to the research setting, found 1775 articles, of which 682 were in FW, 596 in SW and 497 on WW. Most studies on acute toxicity were found in FW with a rate of 36% and the fewest in WW environments with a rate of 31%. On the other hand, most chronic toxicity studies were in FW (46%) and the fewest in WW (22%) (Figure 2).
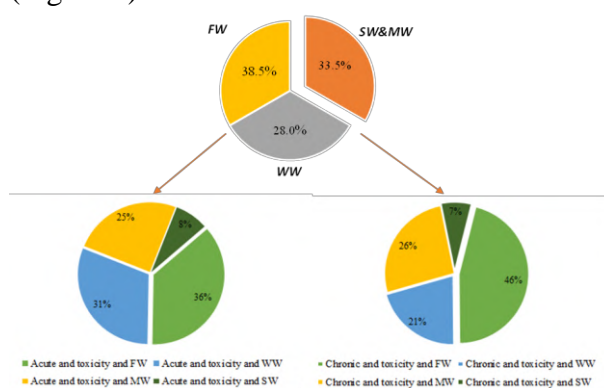

Figure 2 Intersection of acute and chronic toxicity studies across different research environments (2015-2019)

In some studies, both acute and chronic cues were included together. In total, there are 311 articles containing both acute and chronic toxicity studies. The overlap of acute and chronic toxicity studies included 147 FW, 87 SW and 69 WW studies.

Given the geographical locations of countries, freshwater ecosystems tend to be more widespread and accessible compared to seawater ecosystems. Freshwater resources encompass a variety of water bodies, including lakes, rivers, and streams, whereas seawater ecosystems are limited to seas and oceans. Considering that freshwater ecosystems play a crucial role in sectors such as agriculture, drinking water supply, energy production, and industry, addressing water resource conservation and human health becomes of greater importance. Consequently, researchers may be inclined to

BERBER et al.

Bibliometric Profile of Global Scientific Research on Monitoring and Assessment of Aquatic Toxicology...

focus more on understanding the toxic effects within freshwater ecosystems. However, it is important to acknowledge that the choice of test organisms used can also be considered as another contributing factor. *Daphnia magna*, a small planktonic crustacean, is commonly used for toxicity tests that provide rapid results. For this reason, "freshwater" was the most commonly studied medium in both acute and chronic toxicity studies, while seawater was the least studied environment.

3.3. Distrubiton by Years

Studies on acute and chronic toxicity were categorized as FW, WW, and MW-SW to analyze their distribution over the years. In terms of acute toxicity, there were 232 studies, while chronic toxicity studies numbered 122, as depicted in Figure 3. The figure clearly illustrates the numerical dominance of acute toxicity studies over chronic toxicity studies. In the case of acute toxicity, the highest number of studies (102 articles) was observed in FW in 2018, whereas the lowest number (48 articles) was recorded in SW in 2015. Regarding chronic toxicity, the most studies were conducted in FW, totaling 70 articles in 2018, whereas the fewest studies (22 articles) were carried out in WW between 2015 and 2017.

In Figure 3, a regression line was added to the graph to better observe the changes in the acute and chronic toxicity studies. The regression analysis resulted in R^2 values of 0.825 for acute toxicity studies and 0.705 for chronic toxicity studies, indicating a moderately strong fit between the regression line and the data. Although an R^2 value approaching 1 would indicate a closer fit, the obtained values still suggest a significant relationship between the variables. From 2015 to 2019, there was a general increase in acute toxicity studies, with relatively small increases observed in 2017 and 2019. On the other hand, no definite increase was observed in the chronic toxicity studies. The growing importance of environmental awareness and management in recent years has contributed

to the increasing number of studies in the field of ecotoxicology, highlighting the need for further investigation.
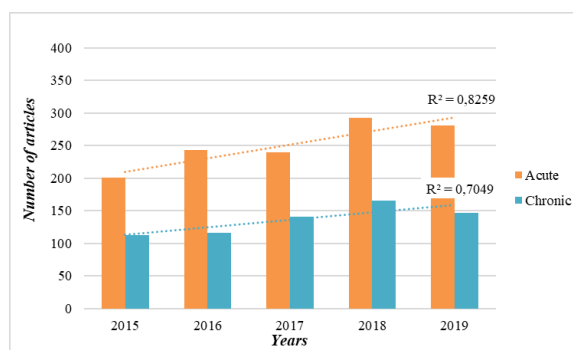

Figure 3 Change in acute and chronic toxicity studies over the years

3.4. Distribution By Test Organisms

Daphnia magna emerges as the predominant organism, accounting for 41% in acute toxicity studies and 27% in chronic toxicity studies. Among the standardized test protocols, toxicology tests involving *Daphnia magna* take precedence due to its easy availability, low cost, ease of cultivation and maintenance, reproducibility, and extensive scientific data available for this organism.

In addition to *Daphnia magna*, other frequently employed organisms in acute toxicity studies include *Aliivibrio fischeri*, *Danio rerio*, and *Artemia salina*, while chronic toxicity studies commonly utilize *Ceriodaphnia dubia*, *Aliivibrio fischeri*, and *Hyalella azteca* (Figure 4). *Aliivibrio fischeri* has gained popularity in recent years among laboratories and researchers due to its heightened sensitivity and significantly faster testing durations (5, 15, and 30-minute exposures) compared to toxicity tests conducted with *Daphnia magna* [24, 25].
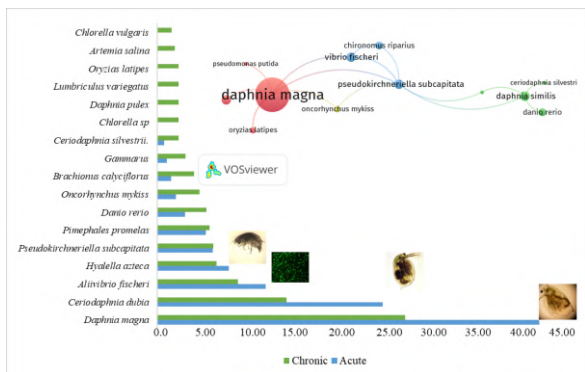
BERBER et al.

Bibliometric Profile of Global Scientific Research on Monitoring and Assessment of Aquatic Toxicology...

Figure 4 Representation of the organisms most commonly used in acute and chronic toxicity studies

3.5. Distribution By Country

When examining the distribution and collaborations among countries regarding acute and chronic toxicity, it becomes evident that 64 countries were identified for acute toxicity and 54 countries for chronic toxicity between 2015 and 2019 (Figure 5-a). Notably, there are distinct clusters represented by nine different colors. However, the presence of Japan (14 publications) and Sweden (15 publications) in relatively smaller clusters suggests a comparatively lower emphasis on toxicity studies in these countries compared to the USA and China, among others.

Figure 5-b and Figure 5-c provide a more detailed analysis of acute toxicity and chronic toxicity, respectively. In the realm of acute toxicity studies, China takes the lead with 243 articles, followed by Brazil with 122 articles and the USA with 111 articles. When assessing the aquatic areas where these studies were conducted in China, it is observed that 60 articles focused on freshwater (FW), 77 articles on seawater (SW), and 106 articles on wastewater (WW).

Regarding chronic toxicity studies, the USA tops the list with 93 articles, closely followed by China with 87 articles. Other countries with a notable number of studies include Brazil (51 articles) and Australia (42 articles) (Figure 5-c). In terms of specific aquatic areas, the number of published studies in FW, SW, and WW were 43, 40, and 17, respectively. Overall, China, the USA, and

Brazil emerge as the top three countries in both acute and chronic toxicity studies. These findings highlight that the focus of scientific research may vary depending on factors such as a country's level of development, proximity to the sea, or abundance of water resources.
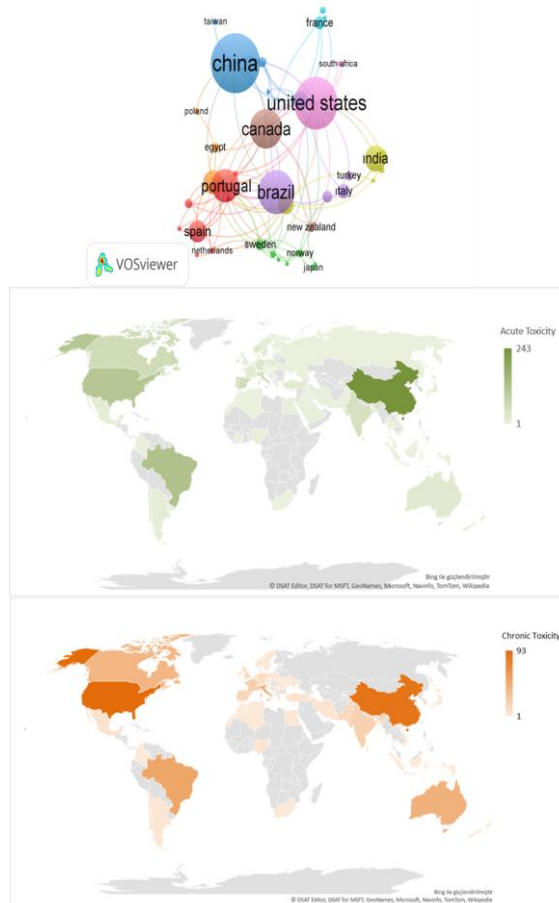

Figure 5 a) Network analysis of the publishing density of countries. b) Countries studying on acute toxicity c) countries studying on chronic toxicity

3.6. Distribution of Studies By Journals Published

Figure 6 presents a visual representation of the prominent journals in the field of acute and chronic toxicity studies. The journals are grouped based on their publication frequency, resulting in multiple clusters. The larger red circles in the center indicate the journals with the highest number of published studies. Among these leading journals, Environmental Toxicology and Chemistry stands out as the largest circle. Other influential journals in this field include Ecotoxicology and

BERBER et al.

Bibliometric Profile of Global Scientific Research on Monitoring and Assessment of Aquatic Toxicology...

Environmental Safety, Chemosphere, Environmental Science and Pollution Research, and Science of the Total Environment.
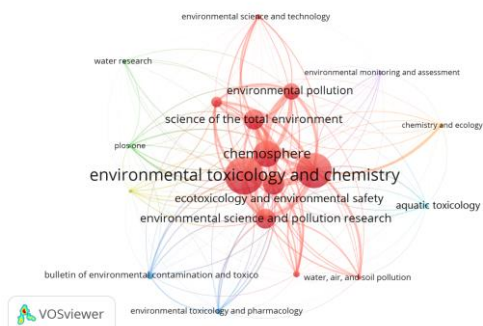

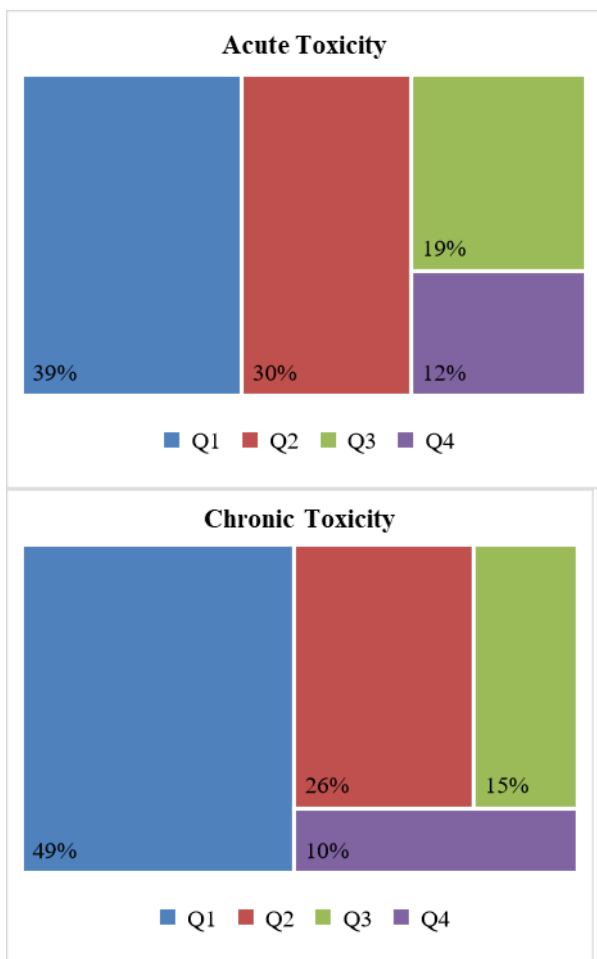Figure 6 Network analysis of journals in which most acute and chronic toxicity studies were published

Figure 7 Q factor of journals in which acute and chronic toxicity studies were published

Figure 7 illustrates the classification of journals that published acute and chronic toxicity studies based on their Q-factors.

Among the 155 journals publishing acute toxicity studies, the majority (Q1 category) accounted for 78 journals. Similarly, 78 journals in the chronic toxicity studies category fell into the Q1 category. Consequently, there is a linear increase in the number of journals from the Q4 category to the Q1 category. It is notable that the majority of publications in both acute and chronic toxicity studies appear in Q1 category journals, while the fewest publications are found in Q4 category journals.

4. CONCLUSIONS

This study presents a comprehensive bibliometric analysis of acute and chronic toxicity studies in water and wastewater, utilizing data from the Scopus database. The analysis provides valuable insights into research trends, key characteristics, knowledge structures, and hotspots in this field.

The findings of the performance analysis indicate a consistent upward trend in the number of publications addressing acute and chronic toxicity. Among the total studies, 62% focused on acute toxicity, with a significant portion of these studies conducted in freshwater environments. *Daphnia magna* emerged as the most commonly used organism, accounting for 41% of acute toxicity studies and 27% of chronic toxicity studies. Notably, China, the USA, and Brazil emerge as the top three countries contributing to both acute and chronic toxicity research.

To safeguard the ecological balance in water ecosystems, it is crucial to enhance studies that focus on the characterization of water areas, examine the relationship between pollution levels and toxicity, implement robust toxicity monitoring methods, and promote scientific research in these domains. Among the countries engaged in environmental toxicology, Turkey demonstrates a commendable research output, surpassing the efforts of many other nations. This emphasizes the importance for

BERBER et al.

Bibliometric Profile of Global Scientific Research on Monitoring and Assessment of Aquatic Toxicology...

countries to prioritize acute and chronic toxicity studies as a means to protect and preserve the ecosystem.

Authors' Contribution

ANB: Data collection, literature research, writing - analysis - original draft; VZS: Writing - original draft, visualization; CA: Writing - original draft, comprehensive analysis; NS: Writing - original draft, supervision.

The Declaration of Conflict of Interest/ Common Interest

No conflict of interest or common interest has been declared by the authors.

The Declaration of Ethics Committee Approval

This study does not require ethics committee permission or any special permission.

The Declaration of Research and Publication Ethics

The authors of the paper declare that they comply with the scientific, ethical and quotation rules of SAUJS in all processes of the paper and that they do not make any falsification on the data collected. In addition, they declare that Sakarya University Journal of Science and its editorial board have no responsibility for any ethical violations that may be encountered, and that this study has not been evaluated in any academic publication environment other than Sakarya University Journal of Science.

REFERENCES

[1] M. Hotamışlı, I. Erem, " Bibliometric Analysis of the Articles Published in Journal of Accounting and Finance," The Journal of Accounting and Finance, no. 63, pp. 1-20, 2014.

[2] R. Kumaresan, K. Vinitha, K. Kannan, "Bibliometric analysis of aquatic microbial ecology from 2000–2014", International Journal of Research in Library Science, vol. 3, no. 2, 1-14, 2017.

[3] J. A. Wallin, "Bibliometric Methods: Pitfalls and Possibilities," Basic & Clinical Pharmacology & Toxicology, vol. 97, no 5, pp. 261-75, 2005.

[4] T. Van Raan, "Advances in bibliometric analysis: Research performance assessment and science mapping, Bibliometrics: Use and Abuse in the Review of Research Performance", vol. 87, 17-28, 2014.

[5] R. Kumaresan, K. Vinitha, K. Kannan, "Aquatic Toxicology (2005–2014): a bibliometric study." Research trends in library and information science: a festschrift volume in honour of Prof. V. Geetha, T. Muruganantham, Ed.. Tiruchirappalli: Alumni Association of Library and Information and PG & Research Department of Library and Information Science, Bishop Heber College (Autonomous), 95-106, 2016.

[6] K., Mendis, J. Baileyi, R. G., Mclean, "Tracking Australian health and medical research expenditure with a

BERBER et al.

Bibliometric Profile of Global Scientific Research on Monitoring and Assessment of Aquatic Toxicology...

PubMed bibliometric method", Australian and New Zeland Journal of Public Health, vol. 39, no 3, pp. 203-298, 2015.

[7] U. Al, R. Coştur, "Bibliometric Profile of Turkish Journal of Psychology," Turkish Librarianship, vol. 21, no 2, pp. 142-163, 2007.

[8] A. D. Canning, R. G. Death, "Ecosystem Health Indicators," Freshwater Environments Encyclopedia of Ecology (Second Edition), vol. 1, pp. 46-60, 2019.

[9] H. Arnold, H. J. Pluta, T. Braunbeck, T. "Cytological alterations in the liver of rainbow trout (*Oncorhynchus mykiss*) after prolonged exposure to low concentrations of waterborne endosulfan," Diseases of Aquatic Organisms, vol. 25, pp. 39-52, 1996.

[10] J. E. Klauning, "Pesticide Toxicology, Evaluating Safety and Risk," Purdue Pesticide Programs. Purdue University Cooperative Extension Service, P-40, Indiana University School of Medicine, 2000.

[11] V. S. Leblond, M. Bisson, A. Hontela, "Inhibition of cortisol secretion in dispersed head kidney cells of rainbow trout (*O. mykiss*) by endosulfan, an organochlorine pesticide" General and Comparative Endocrinology, vol. 121, no 1, pp. 48-56, 2001.

[12] D. Arome, E. Chinedu, "The importance of toxicity testing" Journal of Pharmaceutical and BioSciences, vol. 4, pp. 146-148, 2013.

[13] G. Hanrahan, Çevre Kimyasında Temel Kavramlar (Ed. İsmail Toröz), Nobel Akademik Yayıncılık, 2013, Ankara. (in Turkish).

[14] M. A. Aydın, S. Yıldız, S. Özcan, G. Kara, "Atıksuların toksisitesinin belirlenmesinde farklı biyotest yöntemlerinin uygulanması," 7. Ulusal Çevre Mühendisliği Kongresi, İzmir, Turkey, 2000, pp. 683-700. (in Turkish).

[15] F. Yılmaz, "Physico-Chemical Features of Mumcular Dam Lake (Mugla-Bodrum)" Ecology, vol. 14 no 50, pp. 10-17, 2004.

[16] H. Kalyoncu, M. Barlas M, B. Yorulmaz, "The Relationship between the Physicochemical Structure and the Epilithic Algae Diversity of Aksu River (Isparta-Antalya)", Ecology, vol. 17, no 66, 15-22, 2008.

[17] M. Akbulut, H. Kaya, E. S. Celik, D. A. Odabasi, S. S. Odabasi, K. Selvi, "Assessment of Surface Water Quality in the Atikhisar Reservoir and Saricay Creek," Ecology, vol. 19, no 74, pp. 139-149, 2010.

[18] M. Ayvaz, E. Tenekecioğlu, E. Koru, "Determination of trophic status of Afşar (Manisa-Turkey) dam lake," Ecology, vol. 20, no 81, pp. 37-47, 2011.

[19] T. Hanazato, "Pesticide effects on freshwater zooplankton: An ecological perspective," Environmental Pollution, vol. 112, no 1, pp. 1-10, 2001.

[20] A. N. Berber, "Bibliometric profile of global scientific research on monitoring and assessment of aquatic and wastewater toxicology (2015-2019)", MSc Thesis, Institute of Graduate Education, Istanbul University-Cerrahpasa, Turkey, 2021.

[21] N. J. Van Eck, L. Waltman, R. Dekker, J. Van den Berg, "A comparison of two techniques for bibliometric mapping: Multidimensional scaling and VOS,"

BERBER et al.

Bibliometric Profile of Global Scientific Research on Monitoring and Assessment of Aquatic Toxicology...

Journal of the American Society for Information Science and Technology, vol. 61, no 12, pp. 2405-2416, 2010.

[22] G. M. Khalil, C. A. G. Crawford, "A Bibliometric Analysis of Us-Based Research on the Behavioral Risk Factor Surveillance System," American Journal of Preventive Medicine, vol. 48 no 1, pp. 50-57, 2015.

[23] J. M. Parnis, D. Mackay, "Multimedia environmental models: The fugacity approach," CRC Press, 3rd Ed., 2019, pp 301.

[24] S. Parvez, C. Venkataraman, "A review on advantages of implementing luminescence inhibition test (*Vibrio fischeri*) for acute toxicity prediction of chemicals" Environment International, vol 32, no 2, 265-268, 2006.

[25] A. Białk-Bielińska, L. Grabarczyk, E. Mulkiewicz, A. Puckowski, S. Stolte, P. Stepnowski "Mixture toxicity of six pharmaceuticals towards *Aliivibrio fischeri, Daphnia magna*, and *Lemna minor*" Environmental Science and Pollution Research, vol 29, 26977-26991, 2022.

Title: The Effect of Royal Jelly on Irisin in Experimentally Diabetic Rats

Authors: Selcen ÇAKIR

The Effect of Royal Jelly on Irisin in Experimentally Diabetic Rats

Selcen ÇAKIR *1 ID

Abstract

Diabetes Mellitus (DM) is considered a very common health problem today. It causes many acute and chronic complications and negatively affects the quality of life of patients. It is known that diabetes has an impact on many biochemical processes. This study aimed to evaluate the interaction between royal jelly (RJ) and diabetes with irisin, a parameter that has not been investigated before. The study was planned with 3 groups: control group, DM group, DM+350 mg/kg RJ group. In the experiments, 18 female Wistar albino rats were studied. Irisin levels in rat blood serum were determined using the ELISA (Enzyme-Linked Immuno Sorbent Assay) method. Glucose levels in blood taken from the tail vein were determined with a glucometer. As a result of the experimental study, a statistically significant difference was found in the DM+350 mg/kg RJ group compared to the control group ($p<0.05$). The selected dose reduced serum irisin levels in RJ applications. With diabetes, a statistically significant increase was observed in blood glucose levels ($p<0.05$). Although the RJ application caused a numerical decrease, it was not statistically significant. Previous studies have emphasized the effect of RJ on DM and blood biochemical parameters; however, the observation that the relevant dose of RJ reduces irisin levels is recent. The relationship of irisin with energy metabolism is still being investigated. Further studies are required to explain the relationship between irisin and RJ.

Keywords: Diabetes mellitus, Irisin, Royal jelly

1. INTRODUCTION

Diabetes mellitus (DM) is a metabolic disease that is characterized by high fasting blood glucose and causes damage to carbohydrate, lipid, and protein metabolism. In patients with DM, the high level of blood glucose brings the problem of energy homeostasis along [1]. As a concept, energy homeostasis includes energy expenditure, digestion, and energy storage in adipose tissue. Peptide hormones, also known as adipokines, are involved in this hemostasis [2].

Irisin was recently identified by Boström et al. (2012) and is a peptide with 112 amino acids and a weight of 12,587 kDa [2]. Irisin was recognized as an adipokine due to its contribution to the mechanism that causes the browning of white adipose tissue [3-5]. It is also a myokine that is secreted from muscles and is associated with exercise. The presence

---

* Corresponding author: selcencakir@comu.edu.tr (S. ÇAKIR)

1 Çanakkale Onsekiz Mart University, Vocational School of Health Services, Çanakkale, Türkiye

E-mail: selcencakir@gmail.com

ORCID: https://orcid.org/0000-0002-6474-9032

of irisin has been demonstrated in adipose tissue, muscles, cerebrospinal fluid, breast milk, saliva, and Purkinje cells in the cerebellum. Irisin is an anti-diabetic and anti-obesity hormone and achieves this effect by affecting adipose tissue metabolism and maintaining glucose homeostasis [2].

Irisin regulates energy metabolism by inducing the browning of white adipose tissue. It is mainly expressed in muscles as fibronectin type III domain-containing 5 (FNDC5), a type I membrane precursor protein, and then secreted into the circulatory system [4]. The extracellular part of FNDC5 is cleaved and secreted as irisin. FNDC5 is one of the target proteins of the peroxisome proliferator-activated receptor gamma co-activator 1α (PGC-1α) [2,6]. Therefore, irisin has drawn great attention as an attractive target in the fight against obesity and type 2 diabetes mellitus (T2DM). Irisin levels can be increased by PGC-1α overexpression and aerobic exercise training [7]. Irisin modulates glucose metabolism and insulin sensitivity in skeletal muscles and participates in neuroplasticity and satiety in the central nervous system. It also regulates the remodeling of the pancreas, bone tissue, and adipose tissue [3]. It is stated that irisin levels increase in obesity and decrease in T2DM patients. Clinical studies have indicated that irisin may be a predictive marker for insulin resistance, T2DM, or metabolic syndrome [8].

Royal jelly (RJ) is an important food that ensures the development of the queen bee [9]. The unique protein structure of RJ has been subject to many studies. Thanks to its content, this product has positive effects, especially on blood sugar, obesity, and diabetes [10]. RJ is a rich food consisting of proteins, fatty acids, vitamins, carbohydrates, and minerals such as iron, calcium, copper, potassium, magnesium, zinc, and sulfur [11]. Besides hypoglycemic [10], hypotensive [12], and antihypercholesterolemic [13], activities, it has been shown to have high antioxidative and free radical scavenging activity [14].

The drugs used in the treatment of diabetes have high side effects; therefore, alternative treatments have begun to be investigated. For this reason, interest in natural products that lower blood sugar has increased. In a healthy diet, in addition to carbohydrates, macronutrients such as lipids, proteins, and water, micronutrients, vitamins, and minerals are needed. RJ is considered a promising therapeutic product thanks to its rich biological content, but there are not enough studies on it. This study aimed to test the effect of RJ on the irisin parameter, which changes in DM.

2. METHODS

The number of subjects in the study was determined in G*Power 3.1 program. The total sample size was determined as 18 with an effect size of 0.85, an α error of 0.05, and a Power(1-β) of 0.80. Eighteen female Wistar albino rats weighing 200-250 g were divided into 3 groups, resulting in 6 rats in each group. Experiments were carried out in Çanakkale Onsekiz Mart University, Experimental Research Application and Research Center under a temperature of 21 ± 2 °C, a humidity of $50\% \pm 5\%$, and a cycle of 12 hours light and 12 hours dark. Groups were formed as in Table 1. To induce diabetes, 50 mg/kg of STZ was administered by intraperitoneal injection. Three days later, blood glucose levels were measured with a glucometer. Rats with a level of 250 mg/dl and above were considered diabetic. RJ was administered by gavage 5 days a week under conditions approved by the ethics committee. Throughout the experiment, animals were given water and pellets ad-libitum.

2.1. Biochemical Analysis

At the end of the experiment, the animals were fasted for 10 hours and anesthetized by administering 70 mg/kg Ketamine and 10 mg/kg Xylazine intraperitoneally (ip). After 30 minutes, blood was taken from their hearts by puncture and the blood was transferred to anticoagulant-free tubes for serum. After the tubes were centrifuged at 1400 g at 4 °C for

10 minutes, the serum was separated and stored in labeled tubes at -80 °C. In the study, Rat Irisin ELISA Kit Cat. No: Elabscience (E-EL-R2514), Biotek ELx800 ELISA Reader, and Biotek ELx50 washer were used. Glucose levels in blood taken from the tail vein were determined with a glucometer.

2.2. Statistical Analysis

The SPSS 23.0 program for Microsoft was used for the statistical evaluation. The difference between the groups was determined by a one-way analysis of variance (ANOVA) ($p < 0.05$). The evaluation was made using mean and standard deviation values ($M \pm SD$). The difference between the groups was evaluated with the Tukey post hoc test.

Table 1 Design of groups

Experimental and control groups	Number of animals per group
Control group	6
Diabetes group (DM)	6
Diabetes + 350 mg/kg Royal jelly (DM+RJ)	6

3. RESULTS AND DISCUSSION

Figure 1 shows serum irisin levels. According to the results, there was no statistical difference between the control group and the DM group. After RJ application, serum irisin levels decreased. A statistical difference was found between the control group and the DM-RJ group ($p < 0.05$).

Figure 2 shows blood glucose levels. There was a statistically significant increase between the control group and DM and DM+RJ groups ($p < 0.05$) whereas no statistically significant difference was determined between the DM and DM+RJ groups.
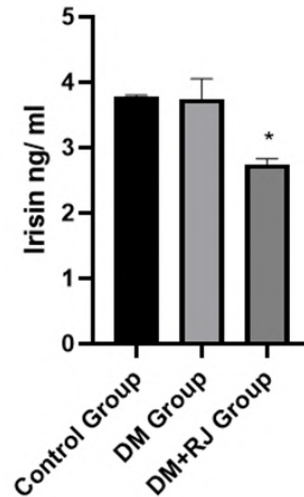

Figure 1 Blood serum irisin ng/ ml. "*" indicates a statistical difference compared to the control group ($P < 0.05$, $M \pm SD$)
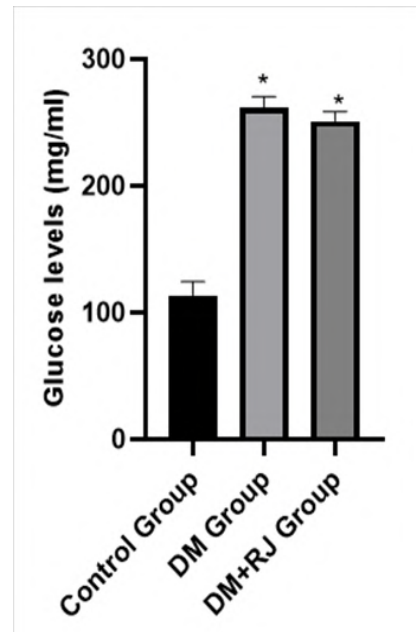

Figure 2 Blood Glucose levels mg/ ml. "*" indicates a statistical difference compared to the control group ($P < 0.05$, $M \pm SD$)

Studies on irisin, a recently identified peptide, have mostly focused on exercise, obesity, T2DM, and metabolic syndrome [15, 16]. No sufficient number of studies has examined the relationship between STZ-induced experimental diabetes and irisin. STZ-induced experimental diabetes reduces insulin secretion by causing the destruction of β-cells. It also causes significant body weight loss due to dehydration caused by polyuria [1]. STZ-induced DM causes impairment in

glucose metabolism and also poses a serious risk for energy metabolism.

In the study conducted by Malfitano et al., in which experimental diabetes was induced with 50 mg/kg STZ, it was emphasized that blood glucose level increased whereas body weight and serum insulin level decreased [17]. Moreover, in experimentally diabetic rats induced by 65 mg/kg STZ, firstly the activation of gluconeogenesis for energy production and then the over-mobilization of muscle proteins and lipids were emphasized [18]. Similar to previous studies, in this study, it was observed that STZ-induced DM increased glucose levels.

Although irisin is a member of energy metabolism that has just begun to be investigated, it is emphasized that it may have anti-obesity and anti-hyperglycemic effects [3]. Jiang et al. (2021) investigated the relationship between irisin and FNDC5 in diabetic mice and reported low plasma irisin levels [19]. It was shown that STZ-induced mice have significantly reduced plasma irisin levels as well as low FNDC5 expression in different tissues compared to controls. It was also concluded that the increase in glucose uptake resulted from irisin which induces the expression of Glucose transporter type 4 (GLUT4) in adipocytes [1]. Expression of genes encoding GLUT4 proteins, carnitine palmitoyl transferase, and hormone-sensitive lipase is reported to be significantly increased in adipocyte tissues of irisin-treated individuals [20, 21]. In a study conducted on individuals with normal glucose tolerance who had been newly diagnosed with T2DM, serum irisin levels of individuals with T2DM were found to be lower compared to the control group [21]. Irisin increases glucose uptake and glycogenolysis while decreasing lipid accumulation, adipogenesis, and gluconeogenesis [20]. It is also stated that irisin reduces diabetes-related insulin resistance [22,23]. In addition to studies showing that the irisin level decreases in DM, there are data emphasizing an increase. Norheim et al. (2014) reported that the plasma irisin levels of the prediabetes group were higher compared to the control group [24]. Al-Daghri et al. (2015) similarly reported higher irisin levels in subjects with T2DM than in healthy controls [25]. According to some views, the first increase seen in serum irisin occurs in the obese and diabetic groups. In the second stage, this mechanism is depleted or acclimated, possibly resulting in lower irisin secretion. This can be considered the reason for the contradictory results in the studies [26,27]. In this study, no statistically significant difference was determined between irisin levels in the diabetes group and the control group. The reason for this can be considered as the completion of this study in 4 weeks. Moreover, it has been emphasized that measurement is difficult due to the short half-life of irisin [5].

In a study conducted on serum fasting blood glucose and serum glycosylated hemoglobin levels in women with T2DM, it was reported that RJ significantly decreased serum fasting blood glucose and increased insulin concentration [28]. Furthermore, RJ significantly reduced serum fasting blood glucose, while increasing insulin, albumin, and total protein levels in STZ-induced diabetic rats [9]. In a study conducted with long-term RJ administration, it was reported that irisin inhibited a key enzyme, glucose-6-phosphatase by inducing the expression of protein kinase activated by adiponectin receptor-1 mRNA and phosphorylated AMP in abdominal fat and thus, cured hyperglycemia [10]. 10-hydroxy decanoic acid, the active agent of RJ, has a healing effect on hyperglycemia and insulin resistance [10]. After RJ administration in STZ-induced diabetic rats, there was an improvement in serum biochemical changes and oxidative stress of the liver and pancreas, and an increase in serum insulin level [14]. In this study, serum irisin levels decreased after RJ administration compared to the control group. Due to the antihyperglycemic effect of both RJ and irisin [8,20,29], it has been evaluated that RJ may reduce irisin expression in STZ-induced DM.

It has been reported that irisin is extremely difficult to monitor. Evaluating the data with different techniques will enable us to achieve more comprehensive results. In future studies, the aim is to overcome this limitation with advanced techniques and more studies on dosing for longer periods.

4. CONCLUSION

Recent studies have shown that irisin, an adipomyokine, may play a role in the regulation of thermogenesis, total body energy metabolism, and glucose homeostasis. Therefore, some studies are focusing on the evaluation of irisin as a therapeutic agent. Although studies have shown that recombinant irisin can be given externally, it is possible to try different substances and combinations that balance the circulating irisin level. Especially the short half-life of irisin complicates the external use of this peptide for therapeutic purposes. However, the determination of the auxiliary dose of a product that increases the secretion of this peptide and also supports the treatment of diabetes will contribute to the literature. In this study, it was observed that the relevant dose of RJ decreased blood glucose but did not significantly increase irisin levels. The reason for this may be associated with the selected RJ dose or the duration of administration. Further studies are required to better elucidate the mechanisms of action of both irisin and RJ.

Authors' Contribution
S.Ç: Conceptualization, literature review, laboratory analysis, data collection, design, and writing, reviewing, and editing.

The Declaration of Conflict of Interest/ Common Interest
No conflict of interest or common interest has been declared by the author.

The Declaration of Ethics Committee Approval
The study was approved by Animal Experiments Local Ethics Committee of Çanakkale Onsekiz Mart University (ÇOMÜ HADYEK 30.06.2020; 2020/06-06).

The Declaration of Research and Publication Ethics
The authors of the paper declare that they comply with the scientific, ethical and quotation rules of SAUJS in all processes of the paper and that they do not make any falsification on the data collected. In addition, they declare that Sakarya University Journal of Science and its editorial board have no responsibility for any ethical violations that may be encountered, and that this study has not been evaluated in any academic publication environment other than Sakarya University Journal of Science.

REFERENCES

[1]   H. Duan, B. Ma, X. Ma, H. Wang, Ni Z, Wang B, Li X, Jiang P, Umar M, M. Li, "Anti-diabetic activity of recombinant irisin in STZ-induced insulin-deficient diabetic mice," International Journal of Biological Macromolecules, vol.84, pp 457-63, 2016.

[2]   P, Boström, J. Wu, MP. Jedrychowski, A. Korde, L. Ye, JC. Lo, KA. Rasbach, Boström EA, JH. Choi, JZ. Long, Kajimura S, Zingaretti MC, Vind BF, Tu H, Cinti S, Højlund K, SP. Gygi, BM. Spiegelman, "PGC1-α-dependent myokine that drives brown-fat-like development of white fat and thermogenesis," Nature, vol. 481, pp 463-8, 2012.

[3]   S. Shen, Q. Liao, X.Chen, C. Peng, Lin L, "The role of irisin in metabolic flexibility: Beyond adipose tissue browning. Drug Discovery Today,"vol. 27, no. 8, pp 2261-7, 2022.

[4] A. Roca-Rivada,C. Castelao, LL. Senin, MO. Landrove, J. Baltar, AB Crujeiras, LM. Seoane, FF. Casanueva, M. Pardo, "FNDC5/Irisin Is Not Only a Myokine but Also an Adipokine," PLoS One,vol. 8, no. 4, pp 1-10, 2013.

[5] HP. Erickson, "Irisin and FNDC5 in retrospect," Adipocyte,vol. 2, no.4, pp 289-93, 2013.

[6] L. Huang, S. Yan, L. Luo, L. Yang, "Irisin regulates the expression of BDNF and glycometabolism in diabetic rats," Molecular Medicine Reports, vol. 19, no. 2, pp 1074-82, 2019.

[7] Liu Y, F. Xu, P. Jiang, "Effect of sitagliptin on expression of skeletal muscle peroxisome proliferator-activated receptor γ coactivator-1α and irisin in a rat model of type 2 diabetes mellitus," Journal of International Medical Research, vol. 48, no.5, 2020.

[8] N. Perakakis, GA. Triantafyllou, JM. Fernández-Real, JY. Huh, KH. Park, J. Seufert, CS. Mantzoros, "Physiology and role of irisin in glucose homeostasis," Nature Reviews Endocrinology, vol. 13, no. 6, pp 324-37, 2017.

[9] E. Ghanbari, V. Nejati, M. Khazaei, "Antioxidant and protective effects of Royal jelly on histopathological changes in testis of diabetic rats," International Journal of Reproductive BioMedicine, vol. 14, no. 8, pp 511-8, 2016.

[10] M. Yoshida, K. Hayashi, R. Watadani, Y. Okano, K. Tanimura, J. Kotoh, D. Sasaki, K. Matsumoto, A. Maeda, "Royal jelly improves hyperglycemia in obese/diabetic KK-Ay mice," Journal of Veterinary Medical Science, vol. 79, no. 2, pp 299-307, 2017.

[11] A. Stocker, P. Schramel, A. Kettrup, E. Bengsch, "Trace and mineral elements in royal jelly and homeostatic effects," Journal of Trace Elements in Medicine and Biology, pp 183-9, 2005.

[12] K. Tokunaga hiko, C. Yoshida, Suzuki K michi, H. Maruyama, Y. Futamura, Y. Araki, S. Mishima, "Antihypertensive effect of peptides from Royal Jelly in spontaneously hypertensive rats," Biological and Pharmaceutical Bulletin, vol. 27, no. 2, pp 189-92, 2004.

[13] H. Guo, A. Saiga, M. Sato, I. Miyazawa, M. Shibata, Y. Takahata, F. Morimatsu, "Royal jelly supplementation improves lipoprotein metabolism in humans," Journal of Nutritional Science and Vitaminology, vol. 53, no. 4, pp 345-8, 2007.

[14] E. Ghanbari, V. Nejati, M, Khazaei, "Improvement in serum biochemical alterations and oxidative stress of liver and pancreas following use of royal jelly in streptozotocin-induced diabetic rats," Cell Journal, vol. 18, no. 3, pp 362-70, 2016.

[15] N. Marrano, G. Biondi, A. Borrelli, A. Cignarelli, S. Perrini, L. Laviola, F. Giorgino, A. Natalicchio. "Irisin and incretin hormones: Similarities, differences, and implications in type 2 diabetes and obesity," Biomolecules, vol. 11, pp 1-23, 2021.

[16] H. Li, F. Wang, M. Yang, J. Sun, Y. Zhao, D. Tang. "The Effect of Irisin as a Metabolic Regulator and Its Therapeutic Potential for Obesity," International Journal of Endocrinology, 2021.

[17] C. Malfitano, A.L. de Souza Junior, M. Carbonaro, A. Bolsoni-Lopes, D. Figueroa, L.E. de Souza, K.A.S. Silva, F. Consolim-Colombo, R. Curi, M.C.

Irigoyen, "Glucose and fatty acid metabolism in infarcted heart from streptozotocin-induced diabetic rats after 2weeks of tissue remodeling," Cardiovascular Diabetology, vol. 14, pp 1-10, 2015.

[18] M.R. Alezandro, D. Granato, M.I. Genovese, "Jaboticaba (Myrciaria jaboticaba (Vell.) Berg), a Brazilian grape-like fruit, improves plasma lipid profile in streptozotocin-mediated oxidative stress in diabetic rats," Food Research International, vol. 54, pp 650-659, 2013.

[19] S. Jiang, L. Piao, E.B. Ma, H. Ha, J.Y. Huh, "Associations of circulating irisin with fndc5 expression in fat and muscle in type 1 and type 2 diabetic mice," Biomolecules, vol. 11, pp 1-14, 2021.

[20] X.Q. Xiong, D. Chen, H.J. Sun, L. Ding, J.J. Wang, Q. Chen, Y.H. Li, Y.B. Zhou, Y. Han, F. Zhang, X.Y. Gao, Y.M. Kang, G.Q. Zhu, "FNDC5 overexpression and irisin ameliorate glucose/lipid metabolic derangements and enhance lipolysis in obesity," Biochimica et Biophysica Acta - Molecular Basis of Disease, vol. 1852 pp 1867-1875, 2015.

[21] Y.K. Choi, M.K. Kim, K.H. Bae, H.A. Seo, J.Y. Jeong, W.K. Lee, J.G. Kim, I.K. Lee, K.G. Park, "Serum irisin levels in new-onset type 2 diabetes, Diabetes Res," Diabetes Research and Clinical Practice, vol. 100, pp 96-101, 2013.

[22] J.M. Moreno-Navarrete, F. Ortega, M. Serrano, E. Guerra, G. Pardo, F. Tinahones, W. Ricart, J.M. Fernández-Real, "Irisin is expressed and produced by human muscle and adipose tissue in association with obesity and insulin resistance," Journal of Clinical Endocrinology and Metabolism, vol.

98, no. 4, pp 769-778, 2013.

[23] M.G. Hekim, M.M. Kelestemur, F.G. Bulmus, B. Bilgin, F. Bulut, E. Gokdere, M.R. Ozdede, H. Kelestimur, S. Canpolat, M. Ozcan, "Asprosin, a novel glucogenic adipokine: a potential therapeutic implication in diabetes mellitus," Arch. Physiol. Biochem, pp 1-7, 2021.

[24] F. Norheim, T.M. Langleite, M. Hjorth, T. Holen, A. Kielland, H.K. Stadheim, H.L. Gulseth, K.I. Birkeland, J. Jensen, C.A. Drevon, "The effects of acute and chronic exercise on PGC-1α, irisin and browning of subcutaneous adipose tissue in humans," FEBS Journal, vol. 281, no. 3, pp 739-749, 2014.

[25] N.M. Al-Daghri, M.S. Alokail, S. Rahman, O.E. Amer, O.S. Al-Attas, H. Alfawaz, G. Tripathi, S. Sabico, G.P. Chrousos, P.G. Mcternan, M.K. Piya, "Habitual physical activity is associated with circulating irisin in healthy controls but not in subjects with diabetes mellitus type 2," European Journal of Clinical Investigation, vol. 45, no. 8, pp 775-781, 2015.

[26] D. Zhu, H. Wang, J. Zhang, X. Zhang, C. Xin, F. Zhang, Y. Lee, L. Zhang, K. Lian, W. Yan, X. Ma, Y. Liu, L. Tao, "Irisin improves endothelial function in type 2 diabetes through reducing oxidative/nitrative stresses," Journal of Molecular and Cellular Cardiology, vol. 87, pp 138-147, 2015.

[27] T. Kurdiova, M. Balaz, M. Vician, D. Maderova, M. Vlcek, L. Valkovic, M. Srbecky, R. Imrich, O. Kyselovicova, V. Belan, I. Jelok, C. Wolfrum, I. Klimes, M. Krssak, E. Zemkova, D. Gasperikova, J. Ukropec, B. "Ukropcova, Effects of obesity, diabetes and exercise on Fndc5 gene

expression and irisin release in human skeletal muscle and adipose tissue: In vivo and in vitro studies," Journal of Physiology, vol. 592, no. 5, pp 1091-1107, 2014.

[28] S. Pourmoradian, R. Mahdavi, M. Mobasseri, E. Faramarzi, M. Mobasseri, "Effects of royal jelly supplementation on glycemic control and oxidative stress factors in type 2 diabetic female: A randomized clinical trial," Chinese Journal of Integrative Medicine, vol. 20, pp 347-352, 2014.

[29] P. Irandoost, N. Mesri Alamdari, A. Saidpour, F. Shidfar, N. Roshanravan, M. Asghari Jafarabadi, F. Farsi, N. Asghari Hanjani, M. Vafa, "The effects of royal jelly and tocotrienol-rich fraction on impaired glycemic control and inflammation through irisin in obese rats," Journal of Food Biochemistry, vol. 44, no. 12, pp 1-10, 2020.

Title: Survay Study of Antimicrobial Activities of Different Region Honeys in Turkey

Authors: Mehtap USTA

Survay Study of Antimicrobial Activities of Different Region Honeys in Turkey

Mehtap USTA [*1]

Abstract

Honey is a functional food with high nutritional properties and rich in bioactive components. The fact that the biological activity of honey differs according to botanical origin, geography and climatic characteristics necessitates a comprehensive consideration of monofloral and multifloral honeys produced in Turkey. The adoption of the understanding of replacing natural preservatives with synthetic products enables the search for alternative uses of honey. For this purpose, the antimicrobial activities of linden, rhododendron, chestnut and multifloral honeys were determined in this study and their antimicrobial activities were compared. Obtained zone diameters were statistically compared with the IBM SPSS version 22.0 statistical program. According to the results, it was determined that in general, multifloral honey has higher antimicrobial activity than monofloral honey, rhododendron honey from monofloral honeys shows strong inhibition against the tested microorganisms, and Yalova linden honey has the weakest antibacterial effect. It was determined that the antimicrobial activity in all honey varieties was generally bacteria > yeast > mold respectively.

Keywords: Antimicrobial activity, honey, microbiology, monofloral, multifloral

1. INTRODUCTION

Honey is a highly nutritious food produced by bees using pollen and plant secretions. Although it varies depending on the variety of plants obtained, it is known that there are over 200 compounds in honey. While sugars constitute 95% of the dry matter as the basic component, the rest is composed of proteins, free amino acids, phenolic compounds, vitamins, minerals and organic acids. It has been stated that the amount and variety of minor components also vary according to bee species, seasonal and environmental factors [1-5].

Scientific studies have reported that honey has antioxidant, antidiabetic, antimicrobial, anti-inflammatory, antiproliferative, anticancer and antimetastatic effects, which are important for human health, thanks to its many bioactive components [6-17]. It is stated that its antimicrobial activity is due to its biological properties, hydrogen peroxide, osmolarity, acidity, aromatic acids and phenolic compounds [18, 19].

In studies examining the antibacterial effect, it has been reported that honey has an inhibitory effect on approximately 60 species of Gram-negative and Gram-positive bacteria with aerobic/anaerobic properties [20].

* Corresponding author: mehtapyakupoglu@trabzon.edu.tr (M. USTA)
[1] Trabzon University, Tonya Vocational School
ORCID: https://orcid.org/0000-0001-7656-5655

Among the reported bacterial species, it was determined that it showed broad-spectrum activity on antibiotic-resistant strains, and honey had a bactericidal effect, especially on methicillin-resistant *Staphylococcus aureus* (MRSA). It has also been reported to be effective on clinical strains of biofilm-forming *Staphylococcus aureus* and *Pseudomonas aeruginosa* [21]. However, many *Candida* spp., *Trichosoporon* spp. and antifungal activity against mold species (*Fusarium oxysporum*, *Cladosporium herbarum*, *Botrytis cinerea*, *Aspergillus flavus*) [22-24].

Honeys are named according to the plant source from which they are obtained and its diversity, geography and production methods. Generally, it is divided into two as flower and secretion honey according to the way the nectar is obtained. Flower honeys are called monofloral and multifloral according to the floral sources they contain. Monofloral honeys are preferred by today's consumers because of their different tastes and the biological benefits they provide. Since minor components such as aromatic and phenolic compounds, to which antimicrobial activity and other biological benefits are attributed, vary according to the floral source, different monofloral honeys are available for various uses [25].

Turkey is extremely suitable for the production of different kinds of monofloral honeys due to its favorable ecology, rich vegetation and faunistic diversity. Among these, chestnut, linden, rhododendron, thyme, lavender and citrus honeys are among the honeys whose production has become increasingly widespread from past to present [26]. When the studies on this subject are examined, the determination of the inhibition zone and the Minimum Inhibition Concentration (MIC) is generally focused on determining the antimicrobial activities of multifloral and monofloral honeys.

In this study, it was aimed to determine the antimicrobial activities of monofloral honeys such as rhododendron, chestnut, linden and multifloral honey, which are known to be widely produced in Turkey, as well as the inhibition zone and MIC value, as well as the Minimum Bacterial/Fungicidal Honeys that have a killing effect on microorganisms. Concentrations (MBK/MFK) were also determined.

2. MATERIALS AND METHODS

2.1. Materials

In this study, 25 different flower honey and chestnut honey from 5 different regions were used. The flower and chestnut honeys used in the experiment were obtained from beekeepers in different regions of Turkey (Gümüşhane, Artvin, Ordu, Rize, Isparta, Bingöl, Bursa, Erzincan, Aydın, Ardahan, Kars, Yalova). It has been confirmed by beekeepers that flower honeys are linden, rhododendron and multifloral. Honey samples were stored in the dark and at room temperature until the beginning of the analysis.

2.2. Methods

2.2.1. Test microorganisms and Inoculums Preparation

The antimicrobial properties of honey were tested on the bacteria and yeast given in Table 1. Bacteria (Mueller Hinton Broth) and yeast (Sabouraud Dextrose Broth) was adjusted to 0.5 McFarland turbidity with appropriate medium after 24 hours of incubation at 37°C and 25°C, respectively.

2.2.2. Agar well diffusion method

100 µL of set inoculum; Mueller Hinton Agar (MHA) for bacteria and SDA medium for yeast were transferred to the surface and spread with a drigalski spatula. 50 µL of 70% (v/v) honey sample was added to the wells opened sterilely with a 5 mm diameter tip

(Magaldi et al. 2004, Valgas et al. 2007). Bacteria were incubated at 37°C for 24 hours and yeast at 25°C for 48 hours for 3 to 5 days. The inhibition zone diameters (mm) formed

were measured. Sterile water was used as negative control. Kanamycin was used as a positive control.

Table 1 Test microorganisms used for the antimicrobial activity

Microorganism	Bacteria/Fungus/Yeast
Bacillus subtilis ATCC 6051-U	Bacteria
Enterobacter cloacae ATCC 2468	Bacteria
Enterococcus feacalis ATCC 51299	Bacteria
Escherichia coli ATCC 2471	Bacteria
Klepsiella pneumonia ATCC 700603	Bacteria
Proteus vulgaris ATCC 6896	Bacteria
Salmonella typhimurium ATCC 13311	Bacteria
Serretia marcescens ATCC 13880	Bacteria
Staphylococcus epidermis ATCC 14990	Bacteria
Candida albicans ATCC 10351	Yeast
Penicillium italicum ATCC 10454	Fungus

2.2.3. Liquid microdilution method

Each honey sample was adjusted to nine different doses in the range of 10-90% (v/v) with sterile water and 180 μL sample was transferred to the microplate. Inoculum prepared in 0.5 McFarland turbidity standard was diluted 1:20 and added to the microplate with 20 μL of inoculum [27, 28]. Bacteria were incubated for 18-24 hours at 37°C, yeast and fungus were incubated for 46-72 hours, and the microorganism density was measured at 600 nm with a microplate reader.

2.2.4. Statistical analysis

Zone diameters are given as mean ± standard deviation. The obtained zone diameters were statistically compared with the IBM SPSS version 22.0 statistical program. First of all, it was tested whether the data fit the normal distribution (Shapiro-Wilk Test), then the

statistical difference in the data conforming to the normal distribution was determined by applying the one-way ANOVA analysis, which is a parametric test, and the Duncan multiple comparison test. The Kruskall Wallis H test was used for data that did not fit the normal distribution, and the Mann Whitney U test was used to determine the difference between the groups.

3. RESULTS AND DISCUSSION

Inhibition zones formed by honey samples on bacteria, yeast and fungus are given in Table 2. Accordingly, it was seen that all honey samples exhibited antibacterial and antifungal activity on the selected microorganisms, and the results of both methods used were consistent with each other. It was determined that the effects of honey varieties on different microorganisms were statistically different ($p < 0.001$).

In this study, the antimicrobial effect of 11 different microorganisms against 25 different types of honey were tested. Microorganisms *Bacillus subtilis* ATCC 6051-U, *Enterobacter cloacae* ATCC 2468, *Enterococcus feacalis* ATCC 51299, *Escherichia coli* ATCC 2471, *Klepsiella pneumonia* ATCC 700603, *Proteus vulgaris* ATCC 6896, *Salmonella typhimurium* ATCC 133113880 *Staphylococcus epidermis*, ATCC 10351 and *Penicillium italicum* ATCC 10454. Honey samples, obtained from the regions where the beekeeping industry is developed, representing different regions of Turkey. These honey samples are multifloral, chestnut, rhododendron from Gümüşhane, multifloral and chestnut from Artvin, multifloral and rhododendron from Ordu, chestnut and linden from Rize, linden and multifloral from Isparta, multifloral and linden from Bingöl, Chestnut and linden from Bursa, multifloral and chestnut from Erzincan, linden and multifloral from Aydın, linden and multifloral from Ardahan, linden and chestnut from Kars and multifloral and linden from Yalova. In particular, the same type of honey was tried to be selected. It is aimed to see the differences of the same type of honey according to the region. Considering these results, the highest rate for Bacillus subtilis seems to be for G. Rhododendron. For Enterobacter cloacea, the highest rate was seen for G. Rhododendron again. Enterecoccus feacalis gave the highest rate for G. Multifloral. Escherichia coli gave the highest rate for G. Rhododendron. Klepsiella pneumonia gave the highest rate for O. Rhododendron. Pretous vulgaris gave the highest rate for G. Multifloral. Salmonella typhium gave the highest rate in R. Linden honey. Serretia marcescens gave the highest rate in O. Multifloral honey. Staphylococcus epidermis bacteria gave the highest rate in O. Multifloral honey. Candida albicans yeast gave the highest rate for O. Rhododendron honey. Penicillium italicum gave the highest rate for I. Linden honey. It was determined that antibacterial properties between honeys did not cause a significant difference between gram properties of bacteria ($p<0.001$).

The abbreviations of the honey names in the table are as follows: G. Multifloral: Gümüşhane Multifloral, G. Chestnut: Gümüşhane Chestnut, G. Rhododendron: Gümüşhane Rhododendron, Art. Multifloral: Artvin Multifloral, Art. Chestnut: Artvin Chestnut, O. Multifloral: Ordu Multifloral, O. Rhododendron: Ordu Rhododendron, R. Chestnut: Rize Chestnut, R. Linden: Rize Linden, I. Linden: Isparta Linden, I. Multifloral: Isparta Multifloral, B. Multifloral: Bingöl Multifloral, B. Linden: Bingol Linden, Bu. Chestnut: Bursa Chestnut, Bu. Linden: Bursa Linden, E. Multifloral: Erzincan Multifloral, E. Chestnut: Erzincan Chestnut, Ay. Linden: Aydin Linden, Ay. Multifloral: Aydın Multifloral, Ar. Linden: Ardahan Linden, Ar. Multifloral: Ardahan Multifloral, K. Linden: Kars Linden, K. Chestnut: Kars Linden, Y. Multifloral: Yalova Multifloral, Y. Linden: Yalova Linden.

Among the honeys used in this study, except for multifloral honey, the antimicrobial effect was found to be bacteria > yeast > mold, respectively ($p<0.001$). In this respect, it can be said that the antibacterial activity of monofloral honey is higher than its antifungal property. MIC, MBK and MFK values of honey are given in Table 3. It was observed that 10-60% (v/v) concentrations of honey samples were sufficient to inhibit all bacteria. These results emphasize that it is similar to the agar well diffusion method. According to the results of the liquid microdilution analysis, MIC values were listed as mold > yeast > bacteria, and molds were seen to be the most resistant group of microorganisms. This result supports the agar well diffusion method. As a result of both antimicrobial and MIC tests, it is seen that the most effective samples are those obtained from Gümüşhane.

Table 2 Inhibition zone diameter of honey samples on test microorganisms (mm)

	Bacillus subtilis ATCC6051U	Enterobacter cloacae ATCC2468v	Enterococcus feacalis ATCC51299	Escherichia coli ATCC2471	Klepsiella pneumonia ATCC700603	Proteus vulgaris ATCC6896	Salmonella typhimurium ATCC13311	Serretia marcescens ATCC13880	Staphylococcus epidermis ATCC14990	Candida albicans ATCC10351	Penicillium italicum ATCC10454
G. Multifloral	15.46±0.66[ab]	17.26±0.61[bc]	22.30±0.55[e]	20.20±0.58[d]	16.36±0.57[b]	23.26±0.54[ef]	18.23±0.60[c]	17.10±0.40[bc]	19.00±0.75	14.26±0.54[ab]	15.03±0.17[ab]
G. Chestnut	18.10±0.78[c]	17.30±0.51[bc]	19.10±0.56[dc]	22.33±0.54[e]	18.20±0.51[c]	18.10±1.19[c]	18.00±0.57[c]	18.10±0.41[c]	20.06±0.52	15.16±0.61[ab]	17.00±0.57[bc]
G. Rhododendron	22.03±0.53[e]	24.90±0.49[f]	23.20±0.60[ef]	24.33±0.57[f]	20.33±0.33[d]	18.26±0.55[c]	19.10±0.62[dc]	17.33±0.75[bc]	17.96±0.57[bc]	16.30±0.47[b]	14.26±0.40[ab]
Art. Multifloral	14.06±0.67[ab]	14.96±0.50[ab]	17.00±0.69[bc]	16.00±0.57[d]	20.26±0.37[d]	21.43±0.29[de]	19.00±0.72[dc]	19.20±0.55[dc]	21.43±0.29[de]	13.90±0.45[a]	13.43±0.29[a]
Art. Chestnut.	20.53±0.24[d]	21.83±0.44[de]	22.90±0.45[e]	19.03±0.17[dc]	21.63±0.28[de]	17.26±0.08[bc]	16.96±0.24[b]	19.36±0.31[dc]	20.26±0.08[d]	16.10±0.15[b]	14.70±0.86[ab]
O. Multifloral	17.33±0.12[bc]	17.30±0.26[bc]	16.80±0.11[b]	16.86±0.28[b]	20.93±0.27[d]	19.23±0.08[dc]	21.43±0.29[de]	24.33±0.08[f]	22.63±0.32[e]	15.60±0.25[ab]	15.46±0.32[ab]
O. Rhododendron	21.70±0.35[de]	22.80±0.36[e]	20.80±0.36[d]	23.60±0.40[ef]	22.46±0.27[e]	19.46±0.27[dc]	19.30±0.05[dc]	18.66±0.33[c]	16.96±0.28[b]	17.76±0.27[bc]	15.73±0.54[ab]
R. Chestnut	16.40±0.25[b]	17.60±0.11[bc]	20.53±0.29[d]	18.33±0.33[c]	18.60±0.11[c]	22.63±0.24[e]	21.86±0.33[dc]	19.80±0.30[d]	19.33±0.33[d]	15.06±0.67[ab]	14.93±0.58[ab]
R. Linden	14.50±0.25[ab]	17.30±0.05[bc]	17.83±0.08[bc]	17.96±0.57[bc]	19.26±0.37[dc]	21.83±0.41[de]	22.40±0.05[e]	20.96±0.08[d]	16.26±0.08[b]	14.93±0.27[ab]	16.20±0.20[b]
I. Linden	17.06±0.18[bc]	17.36±0.14[bc]	17.00±0.11[bc]	15.93±0.18[ab]	19.46±0.12[dc]	20.80±0.11[d]	17.60±0.40[bc]	18.33±0.33[c]	17.83±0.08[bc]	15.00±0.11[ab]	17.20±0.36[bc]
I. Multifloral	21.06±0.18[de]	19.10±0.47[dc]	16.56±0.23[b]	17.63±0.20[bc]	18.76±0.38[c]	18.70±0.17[c]	15.83±0.32[ab]	16.03±0.27[b]	14.30±0.25[ab]	13.73±0.14[a]	13.50±0.25[a]
B. Multifloral	19.33±0.23[dc]	17.90±0.11[bc]	15.90±0.32[ab]	16.43±0.28[b]	16.40±0.34[b]	14.33±0.37[ab]	17.50±0.36[bc]	16.33±0.37[b]	18.36±0.38[c]	14.53±0.44[ab]	16.33±0.43[b]
B. Linden	15.33±0.35[ab]	14.40±0.34[ab]	16.33±0.40[b]	13.43±0.34[a]	17.40±0.32[bc]	17.33±0.37[bc]	15.33±0.37[b]	15.40±0.32[ab]	14.36±0.40[a]	13.36±0.41[a]	11.20±0.46[a]
Bu. Chestnut	15.36±0.34[ab]	14.40±0.34[ab]	15.36±0.40[ab]	14.33±0.37[ab]	14.43±0.44[ab]	13.33±0.40[a]	16.33±0.35[b]	17.50±0.36[bc]	16.33±0.4[b]	11.50±0.32[a]	12.37±0.34[a]
Bu. Linden	17.53±0.40[bc]	17.36±0.34[bc]	19.60±0.61[dc]	21.66±0.33[de]	15.53±0.24[ab]	14.50±0.36[ab]	17.46±0.35[bc]	16.60±0.20[b]	17.33±0.35[bc]	15.73±0.14[ab]	14.13±0.24[ab]
E. Multifloral	16.36±0.34[b]	15.33±0.35[ab]	15.33±0.37[ab]	17.30±0.35[bc]	17.46±0.40[bc]	18.46±0.40[c]	19.36±0.58[dc]	22.00±0.15[e]	17.36±0.37[bc]	16.33±0.35[b]	16.43±0.35[b]
E. Chestnut	16.36±0.41[b]	15.46±0.40[ab]	17.56±0.43[bc]	16.50±0.40[b]	18.40±0.32[c]	18.46±0.39[c]	15.70±0.20[ab]	16.70±0.17[b]	17.53±0.2[bc]	15.70±0.20[ab]	16.53±0.41[b]
Ay. Linden	18.23±0.46[c]	19.86±0.43[dc]	16.56±0.21[b]	15.66±0.20[ab]	17.40±0.34[bc]	20.63±0.18[d]	22.83±0.08[e]	21.66±0.33[de]	16.93±0.17[c]	16.76±0.14[b]	14.40±0.32[ab]
Ay. Multifloral	17.26±0.31[bc]	17.93±0.06[bc]	15.53±0.44[ab]	17.70±0.37[bc]	16.56±0.53[b]	16.23±0.28[b]	16.03±0.14[b]	18.83±0.08[c]	20.00±0.17[d]	15.80±0.11[ab]	16.93±0.47[b]
Ar. Linden	18.33±0.88[c]	19.80±0.11[dc]	16.46±0.47[b]	17.53±0.37[bc]	17.36±0.32[bc]	16.23±0.31[b]	16.00±0.20[b]	16.76±0.26[b]	18.33±0.35[c]	14.23±0.39[ab]	15.00±0.57[ab]
Ar. Multifloral	14.46±0.35[ab]	15.63±0.42[ab]	15.56±0.38[ab]	16.93±0.63[b]	16.36±0.34[b]	18.36±0.34[c]	19.70±0.51[dc]	17.40±0.37[bc]	16.36±0.37[b]	14.70±0.17[ab]	14.43±0.31[ab]
K. Linden	18.90±0.20[c]	17.80±0.11[bc]	19.00±0.11[dc]	19.96±0.14[dc]	13.40±0.34[a]	15.46±0.35[ab]	17.43±0.31[bc]	18.93±0.21[c]	14.50±0.36[ab]	13.83±0.08[a]	16.26±0.37[b]
K. Chestnut	17.33±0.33[bc]	18.96±0.14[c]	16.36±0.34[b]	17.30±0.65[bc]	15.40±0.32[ab]	14.83±0.41[ab]	16.40±0.34[b]	17.33±0.35[bc]	18.40±0.34[c]	15.46±0.40[ab]	14.80±0.50[ab]
Y. Multifloral	15.80±0.11[ab]	15.50±0.36[ab]	16.40±0.36[b]	14.50±0.36[ab]	17.53±0.41[bc]	16.23±0.39[b]	14.70±0.17[ab]	18.33±0.35[c]	16.50±0.25[b]	11.46±0.43[a]	13.80±0.11[a]
Y. Linden	11.06±0.54[a]	15.46±0.35[ab]	14.36±0.34[ab]	13.36±0.37[a]	16.40±0.34[b]	17.43±0.43[bc]	14.33±0.35[ab]	15.33±0.33[ab]	16.66±0.3[b]	13.33±0.33[a]	13.33±0.33[a]

In this study, the antimicrobial effect of 11 different microorganisms against 25 different types of honey were tested. Microorganisms *Bacillus subtilis* ATCC 6051-U, *Enterobacter cloacae* ATCC 2468, *Enterococcus feacalis* ATCC 51299, *Escherichia coli* ATCC 2471, *Klepsiella pneumonia* ATCC 700603, *Proteus vulgaris* ATCC 6896, *Salmonella typhimurium* ATCC 133113880 *Staphylococcus epidermis*, ATCC 10351 and *Penicillium italicum* ATCC 10454. When the antimicrobial results are examined, it is observed that the effects of rhododendron, linden and multifloral honeys obtained from Gümüşhane are high. When all the results are examined, it is seen that the activity of honey from the Black Sea region is high. Of course, it can be said that this is related to the flora of this region.

The antimicrobial activity of honey depends on its acidity, pH, osmotic pressure, and enzymatic hydrogen peroxide production via glucose oxidase. As additional honey components, aromatic acids or phenolic compounds may contribute to the overall antimicrobial activity. The reason for the antibacterial activity observed in various honey samples was classified as four factors. These; inhibition due to high sugar concentration (low water activity), hydrogen peroxide formation, presence of proteinaceous antimicrobial components and unidentified components [29].

It is known that honey has a broad spectrum antimicrobial effect against bacteria and many yeast/mold species [30-33]. In a study examining the antimicrobial activity and mechanism of action of multifloral and monofloral honeys, all bacteria except *P. aeruginosa* ATCC 27853 were found in all honey samples. Antibacterial effects were observed at different concentrations on however, it has been determined that 100% (v/v) concentrations of some multifloral honeys and monofloral honeys provide inhibition on bacteria such as *L. monocytogenes* ATCC 15313, *B. cereus* ATCC 9634 and *Streptococcus mutans*

ATCC 25175 [34]. It is thought that hydrogen peroxide and high sugar concentration in the structure of honey are the main factors in providing antimicrobial activity, while phenolic compounds and other component diversity cause honey to show activity in a wide spectrum [1, 35, 36].

In this study, antibacterial and antifungal activity of multifloral honey was found to be higher compared to other honey samples. It is predicted that the diversity of components in multifloral flower honey contributes to the antimicrobial activity and thus has an inhibitory effect on more microorganisms. In the study evaluating the antifungal activities of honeys with different floral sources (multifloral, eucalyptus, orange and rhododendron) on forty different yeast strains including *C.albicans*, *Candida krusei*, *Candida glabrata* and *Trichosoporon*, the MIC value on multifloral flower honey *C. albicans* was 35%. While it was 56 (v/v), MIC values in rhododendron, orange and eucalyptus honeys were reported as 40.00%, 62.22% and 44.44%, respectively [22]. These findings support that the multifloral flower honey in the study showed high antifungal activity compared to other honeys.

Mundo et al., in their microbiological analysis on 27 honey samples from different flora and geographical regions; 7 food spoilage microorganisms (*Alcaligenes faecalis*, *Aspergillus niger*, *Bacillus stearothermophilus*, *Geotrichum candidum*, *Lactobacillus acidophilus*, *Penicillium expansum*, *Pseudomonas fluorescens*) and 5 pathogens that cause food poisoning (*Bacillus cereus*, *Escherichia coli* O157:H7, *Listeria monocytogenes*, *Salmonella enterica*, *Ser. typhimurium*, and *Staphylococcus aureus*) They found that they showed inhibitory properties on staph. Inhibition effect was observed in the samples on aureus. None of the samples inhibited mold growth [29].

Table 3 MIC, MBC and MFC of honey samples (% v/v)

Microorganisms	Bacillus subtilis ATCC 6051U	Enterobacter cloacae ATCC2468v	Enterococcus feacalis ATCC51299	Escherichia coli ATCC2471	Klepsiella pneumonia ATCC700603	Proteus vulgaris ATCC6896	Salmonella typhimurium ATCC13311	Serretia marcescens ATCC13880	Staphylococcus epidermis ATCC14990	Candida albicans ATCC10351	Penicillium italicum ATCC10454
G. Multifloral	30	50	40	30	40	50	20	40	50	60	70
G. Chestnut	40	40	30	50	60	30	30	40	50	70	80
G. Rhododendron	50	30	50	60	50	40	40	50	60	60	70
Art. Multifloral	30	40	20	40	30	50	30	40	50	70	90
Art. Chestnut.	20	30	40	50	30	40	50	40	30	50	60
O. Multifloral	20	20	30	40	30	50	30	20	40	60	70
O. Rhododendron	50	40	50	50	60	40	30	20	40	50	60
R. Chestnut	30	20	40	20	30	40	50	40	30	60	70
R. Linden	30	40	20	40	40	30	20	50	60	70	80
I. Linden	40	20	30	50	30	20	50	40	30	60	50
I. Multifloral	20	60	30	40	30	50	20	30	40	50	60
B. Multifloral	30	40	20	40	30	50	40	30	60	70	60
B. Linden	20	10	40	30	50	40	30	20	50	50	60
Bu. Chestnut	20	30	40	30	20	50	40	30	60	60	70
Bu. Linden	20	40	30	30	40	50	60	40	30	50	60
E. Multifloral	20	50	40	30	20	40	30	50	60	50	70
E. Chestnut	50	20	40	40	30	30	20	40	40	60	70
Ay. Linden	30	20	40	40	20	50	40	40	50	60	60
Ay. Multifloral	30	50	20	40	20	40	50	40	50	60	80
Ar. Linden	40	10	30	20	30	40	30	50	30	60	70
Ar. Multifloral	20	40	30	30	40	30	50	50	60	70	80
K. Linden	30	20	40	20	30	40	40	50	50	70	60
K. Chestnut	20	30	50	30	40	10	40	30	50	60	50
Y. Multifloral	20	20	30	40	30	50	40	30	10	50	70
Y. Linden	20	20	30	30	20	40	50	30	60	50	40

4. CONCLUSION

In this study, the highest antimicrobial activity was observed against rhododendron honey obtained from Gümüşhane of *E. coli* with a ratio of 24.33±0.57. The lowest antimicrobial activity was the activity of linden honey obtained from Yalova against *Bacillus subtilis* with a ratio of 11.06±0.54. As it is known, rhododendron honeys are unique to the Black Sea Region and should be consumed in a controlled manner due to their toxic effects. Antibacterial activity is significantly related to the acidity of honey, but is not pH dependent. The antibacterial activity of honey varies depending on the plants from which it is produced rather than the genus of the bee [1].

According to the findings, as stated in the literature, the characteristics of honey, the environment in which it is grown, and the obtained plants are important. In terms of content and medicinal properties, the properties of honey differ according to the obtained plants.

REFERENCES

[1] S. Bogdanov, K. Ruoff, L. Persano Oddo. "Physico-chemical methods for the characterisation of unifloral honeys: A review," Apidologie, vol. 35, no. 1, pp. 4-17, 2004.

[2] E. Mahmoodi-Khaledi, J. Lozano-Sánchez, A. Bakhouche, M. Habibi-Rezaei, I. Sadeghian, A. Segura-Carretero. "Physicochemical properties and biological activities of honeys from different geographical and botanical origins in Iran," European Food Research and Technology, vol. 243, no. 6, pp. 1019-1030, 2017.

[3] S. Samarghandian, T. Farkhondeh, F. Samini. "Honey and Health: A Review of Recent Clinical Research," Pharmacognosy Research, Vol. 9, no. 2, pp. 121-127, 2017.

[4] F. J. Leyva-Jimenez, J. Lozano-Sanchez, I. BorrasLinares, M. L. Cadiz-Gurrea, E. MahmoodiKhaledi. "Potential antimicrobial activity of honey phenolic compounds against Gram positive and Gram negative bacteria," LWT- Food Science and Technology, vol. 101, pp. 236-245, 2018.

[5] E. I. Ramsay, S. Rao, L. Madathil, S. K. Hegde, M. P. Baliga-Rao, T. George, M. S. Baliga. "Honey in oral health and care: A mini review," Journal of Oral Biosciences, vol. 61, pp. 32- 36, 2019.

[6] N. Gheldof, X. H. Wang, N. J. Engeseth. "Buckwheat honey increases serum antioxidant capacity in humans," Journal of Agricultural Food Chemistry, vol. 51, no. 5, pp. 1500-1505, 2003.

[7] R. A. Pérez, M. T. Iglesias, E. Pueyo, M. Gonzalez, C. de Lorenzo. "Amino acid composition and antioxidant capacity of Spanish honeys," Journal of Agricultural Food Chemistry, Vol. 55, no. 2, pp.360-365, 2007.

[8] S. K. Jaganathan, M. Mandal. "Honey constituents and their apoptotic effect in colon cancer cells," Journal of ApiProduct ApiMedical Science, vol. 1, no. 2, pp. 29–36, 2009.

[9] A. N. Fauzi, M. N. Norazmi, N. S. Yaacob. "Tualang honey induces apoptosis and disrupts the mitochondrial membrane potential of human breast and cervical cancer cell lines," Food and Chemical Toxicology, Vol. 49, no. 4, pp. 871- 878, 2011.

[10] R. B. Pimentel, C. A. de Q., da Costa, P. M. Albuquerque, S. D. Junior. "Antimicrobial activity and rutin identification of honey produced by the stingless bee Melipona compressipes manaosensis and commercial honey," BMC Complementary and Alternative Medicine, vol. 13, no. 1, pp. 1-14, 2013.

[11] D. M. Borsato, A. S. Prudente, P. M. Döll-Boscardin, A. V. Borsato, C. F. P. Luz, B. H. L. N. S. Maia, O. G. Miguel. "Topical anti-Inflammatory activity of a monofloral honey of *Mimosa scabrella* provided by *Melipona marginata* during winter in Southern Brazil," Journal of Medicinal Food., vol. 17, no. 7, pp. 817–825, 2014.

[12] O. O. Erejuwa, S. A. Sulaiman, M. S. Wahab. "Effects of honey and its mechanisms of action on the development and progression of cancer," Molecules, vol. 19, no. 2, pp. 2497-522, 2014.

[13] P. M. Kustiawan, S. Puthong, E. T. Arung, C. Chanchao. "In vitro cytotoxicity of Indonesian stingless bee products against human cancer cell lines," Asian Pacific Journal of Tropical Biomedicine, vol. 4, no. 7, pp. 549–556, 2014.

[14] P. V. Rao, K. T. Krishnan, N. Salleh, S. H. Gan. "Biological and therapeutic effects of honey produced by honey bees and stingless bees: A comparative review," Brazilian Journal of Pharmacognosy, vol. 26, no. 5, pp. 657–664, 2016.

[15] M. S. A. Aziz, N. Giribabu, P. V. Rao, N. Salleh. "Pancreatoprotective effects of Geniotrigona thoracica stingless bee honey in streptozotocin-nicotinamide-induced male diabetic rats," Biomedicine & Pharmacotherapy, vol. 89, 135–145, 2017.

[16] P. Saranraj, S. Sivasakthi. "Comprehensive Review on Honey: Biochemical and Medicinal Properties," Journal of Academia and Industrial Research, vol. 6, pp. 165–181, 2018.

[17] V. C. Nolan, J. Harrison, J. A. G. Cox. "Dissecting the Antimicrobial Composition of Honey," Antibiotics, vol. 8, no. 4, pp. 251, 2019.

[18] P. C. Molan. "The antibacterial activity of honey: 1. The nature of the antibacterial activity," Bee World, vol. 73, no. 1, pp. 5-28, 1992.

[19] S. Anand, M. Deighton, G. Livanos, P. D. Morrison, E. C. K. Pang, N. Mantri. "Antimicrobial activity of Agastache Honey and characterization of its bioactive compounds in comparison with important commercial honeys," Frontiers in Microbiology, vol. 10, pp. 269- 285, 2019.

[20] V. Bansal, B. Medhi, P. Pandhi. "Honey–a remedy rediscovered and its therapeutic utility," Kathmandu University Medical Journal, vol. 3, no. 3, pp. 305–309, 2005.

[21] R. Wang, M. Starkey, R. Hazan, L. G. Rahme. "Honey's ability to counter bacterial infections arises from both bactericidal compounds and QS inhibition," Frontiers in Microbiology, vol. 3, pp. 144-150, 2012.

[22] A. N. Koc, S. Silici, B. D. Ercal, F. Kasap, H. T. Hörmet- Öz, H. Mavus-Buldu. "Antifungal activity of Turkish honey against *Candida* spp. and *Trichosporon* spp: an in vitro evaluation," Sabouraudia, vol. 47, no. 7, pp. 707-712, 2009.

[23] M. Candiracci, B. Citterio, E. Piatti. "Antifungal activity of the honey flavonoid extract against *Candida*

albicans," Food Chemistry, vol. 131, no. 2, pp. 493 – 499, 2012.

[24] H. Zafar, M. S. Israili. "Antimicrobial Properties of Honey," American Journal of Therapeutics, vol. 21, no. 4, pp. 304-323, 2014.

[25] J. M. Alvarez-Suarez, S. Tulipani, S. Diaz, Y. Estevez, S. Romandini, F. Giampieri, P. Damiani, S. Astolfi, S. Bompadre, M. Batting. "Antioxidant and antimicrobial capacity of several monofloral Cuban honeys and their correlation with colour, polyphenol content and others chemical compounds," Food and Chemical Toxicology, vol. 48, pp. 2490- 2499, 2010.

[26] Ö. Seçmen, Y. Gemici, G. Görk, L. Bekat, E. Leblebici. "Systematic of seeded plants," Bornova, İzmir: Ege Üniversitesi, Faculty of Science Publications, vol. 116. pp. 396, 2000.

[27] M. Balouiri, M. Sadiki, S. K. Ibnsouda. "Methods for *in vitro* evaluating antimicrobial activity: A review," Journal of Pharmaceutical Analysis, vol. 6, no. 2, pp. 71-79, 2016.

[28] I. Wiegand, K. Hilpert, R. E. Hancock. "Agar and broth dilution methods to determine the minimal inhibitory concentration (MIC) of antimicrobial substances," Nature Protocols., vol. 3, no. 2, pp. 163-175, 2008.

[29] M. M. Mundo, O. I. Padılla-Zakour, R. W. Worobo. "Growth inhibition of foodborne pathogens and food spoilage organisms by select raw honeys," International Journal of Food Microbiology, vol. 97, pp. 1–8, 2004.

[30] Ö. Ertürk, H. Şahin, S. Kolaylı, M. Ç. Ayvaz. "Antioxidant and antimicrobial activity of East Black Sea Region honeys," Turkish Journal of Biochemistry/Turk Biyokimya Dergisi, vol. 39, no. 1, pp. 99-106, 2014.

[31] J. Irish, D. A. Carter, T. Shokohi, S. E. Blair. Honey has an antifungal effect against *Candida* species," Medical Mycology, vol. 44, no. 3, pp. 289-291, 2006.

[32] M. D. Mandal, S. Mandal. Honey: its medicinal property and antibacterial activity," Asian Pacific Journal of Tropical Biomedicine, vol. 1, no. 2, pp. 154-160, 2011.

[33] P. J. Taormina, B. A. Niemira, L. R. Beuchat. "Inhibitory activity of honey against foodborne pathogens as influenced by the presence of hydrogen peroxide and level of antioxidant power," International Journal of Food Microbiology, vol. 69, no. 3, pp. 217-225, 2001.

[34] J. J. Gallardo-Chacón, M. Caselles, M. IzquierdoPulido, N. Rius. "Inhibitory activity of monofloral and multifloral honeys against bacterial pathogens," Journal of Apicultural Research, vol. 47, no. 2, pp. 131-136, 2008.

[35] K. L. Allen, P. C. Molan, G. M. Reid. "A survey of the antibacterial activity of some New Zealand honeys," Journal of Pharmacy and Pharmacology,vol. 43, no. 12, pp. 817-822, 1991.

[36] Jr. J. W. White, M. H. Subers, A. I. Schepartz. "The identification of inhibine, the antibacterial factor in honey, as hydrogen peroxide and its origin in a honey glucose-oxidase system," Biochimica et Biophysica Acta (BBA)- Specialized Section on Enzymological Subjects, vol. 73, no. 1, pp. 57-70, 1963.